AFRL-AFOSR-UK-TR-2018-0032

Non-Foster Source-load Networks and Metasurfaces

Silvio Hrabar
FAKULTET ELEKTROTEHNIKE I RACUNARSTVA
UNSKA 3
ZAGREB, 10000
HR

08/09/2018
Final Report

Air Force Research Laboratory
Air Force Office of Scientific Research
European Office of Aerospace Research and Development
Unit 4515 Box 14, APO AE 09421

REPORT DOCUMENTATION PAGE

Form Approved
OMB No. 0704-0188

1. REPORT DATE *(DD-MM-YYYY)*	2. REPORT TYPE	3. DATES COVERED *(From - To)*
09-08-2018	Final	01 Jun 2015 to 28 Feb 2018

4. TITLE AND SUBTITLE
Non-Foster Source-load Networks and Metasurfaces

5a. CONTRACT NUMBER

5b. GRANT NUMBER
FA9550-15-1-0120

5c. PROGRAM ELEMENT NUMBER
61102F

6. AUTHOR(S)
Silvio Hrabar

5d. PROJECT NUMBER

5e. TASK NUMBER

5f. WORK UNIT NUMBER

7. PERFORMING ORGANIZATION NAME(S) AND ADDRESS(ES)
FAKULTET ELEKTROTEHNIKE I RACUNARSTVA
UNSKA 3
ZAGREB, 10000 HR

8. PERFORMING ORGANIZATION REPORT NUMBER

9. SPONSORING/MONITORING AGENCY NAME(S) AND ADDRESS(ES)
EOARD
Unit 4515
APO AE 09421-4515

10. SPONSOR/MONITOR'S ACRONYM(S)
AFRL/AFOSR IOE

11. SPONSOR/MONITOR'S REPORT NUMBER(S)
AFRL-AFOSR-UK-TR-2018-0032

12. DISTRIBUTION/AVAILABILITY STATEMENT
A DISTRIBUTION UNLIMITED: PB Public Release

13. SUPPLEMENTARY NOTES

14. ABSTRACT
This study reports on a 24-month research effort undertaken towards two basic goals: (1) significantly suppress stability problems in the most common applications of non-Foster elements (the non-Foster metamaterials and the non-Foster matching) by novel design of non-Foster elements and/or applying concept of all-negative stable networks, and (2) propose a novel concept of non-Foster source that turns instability of non-Foster network into a useful feature, convenient for use in transmitting applications. All achieved results clearly show that a novel concept of improving the stability properties of generalized non-Foster networks, as well as a novel concept of a non-Foster source and associated non-Foster antenna transmitter are correct. Finally, we have argued that these new concepts could be extended into microwave regime and pave a way towards manufacturing of stable non-Foster metasurfaces for manipulation of electromagnetic waves. Yet another future application would be non-Foster-based self-oscillating metasurfaces with a tuning bandwidth ten times larger than the existing transmitting systems.

15. SUBJECT TERMS
EOARD, Metamaterials

16. SECURITY CLASSIFICATION OF:			17. LIMITATION OF ABSTRACT	18. NUMBER OF PAGES	19a. NAME OF RESPONSIBLE PERSON
a. REPORT	b. ABSTRACT	c. THIS PAGE			FOLEY, JASON
Unclassified	Unclassified	Unclassified	SAR		19b. TELEPHONE NUMBER *(Include area code)* 011-44-1895-616036

Standard Form 298 (Rev. 8/98)
Prescribed by ANSI Std. Z39.18

FINAL REPORT FOR CONTRACT **FA9550-15-1-0120**

Non-Foster Source-load Networks and Metasurfaces

by

Silvio Hrabar
Igor Krois
Josip Loncar
Leo Vincelj

SUBMITTED BY: Prof. Silvio Hrabar
Faculty of Electrical Engineering and Computing
University of Zagreb
Unska 3
Zagreb, HR-10000, Croatia

31st May 2018

TABLE OF CONTENTS

Chapter 1 INTRODUCTION: GENERALIZED NON-FOSTER MTM STRUCTURES

Introduction: Generalized non-Foster metamaterial structures

1.1. Constraints of passive metamaterial structures

Electromagnetic properties of all materials (except vacuum) change with frequency, thus, all materials are dispersive [1,2]. The dispersion is associated with inevitable resonant behavior of electric/magnetic polarization. The simplest physical picture deals with mechanical inertia of polarized particles (electrons or molecules), caused by their finite mass. Due to inertia, the particles cannot respond instantaneously to an external electromagnetic field. Thus, there will be a phase lag/lead between particle movement and applied field, resulted by mechanical oscillations [2]. Clearly, this effect causes change of induced electric/magnetic dipoles and, therefore, the change of relative permittivity/permeability with frequency (i.e. dispersion). The electrical engineering analogue of a mechanical harmonic oscillator is a simple RLC resonant circuit, in which energy re-distribution between electric and magnetic fields takes place [2]. The energy redistribution is described by a familiar Lorentz dispersion curve with 'parallel' (f_p) and 'series' (f_s) resonant frequency [1,2], (Fig. 1). It describes electromagnetic properties of most passive materials (more precisely, the most passive materials can be modelled as a collection of finite number of Lorentz oscillators with different resonant frequencies, which all together form the actual dispersion curve).

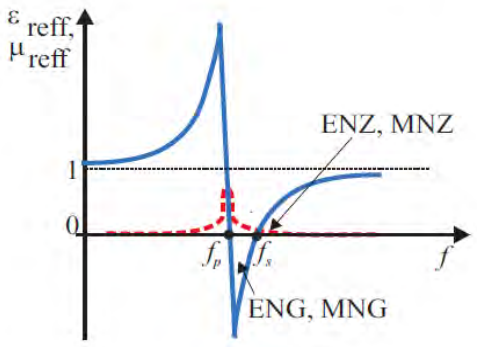

Figure 1-1 Lorentz dispersion model. Solid (blue): Real part of relative permittivity/permeability, Dashed (red): Imaginary part of relative permittivity/permeability

A quick inspection of the Lorentz curve reveals that the dispersion is negligible if a material is used far below its first resonant frequency (f_p). This is the case of most ordinary dielectrics in radiofrequency and microwave regime.

On the contrary, there are several unusual effects based on phase lead of the signal and the occurrence of negative or less-than-unity effective constitutive parameters

(**E**psilon**N**e**G**ative, **M**u**N**e**G**ative, **E**psilon**N**ear**Z**ero, and **M**u**N**ear**Z**ero), which occur in the vicinity of resonant frequencies. These exotic effects usually occur at very high frequencies (above microwave and millimeter regimes) and they are quite weak. Most importantly, these effects are *always accompanied with pronounced dispersion,* caused be resonant energy exchange between electric and magnetic fields [1,2,3].

One concludes that every passive material with negative or less-than-unity effective parameters is *inevitably* narrowband. This fact is mathematically expressed in the form of well-known energy-dispersion constraints [1,2,3]:

$$\frac{\partial[\varepsilon(\omega)]}{\partial\omega}>0,\ \frac{\partial[\mu(\omega)]}{\partial\omega}>0. \tag{1.1}$$

Very similar equations apply for any reactive element in circuit-theory (Foster's reactance theorem) [3,4]:

$$\frac{\partial[X(\omega)]}{\partial\omega}>0,\ \frac{\partial[B(\omega)]}{\partial\omega}>0. \tag{1.2}$$

Here ε and μ stand for permittivity and permeability while X and B are reactance and susceptance, respectively, Symbol ω represents angular frequency.

Negative or less-than-unity effective parameters have been known in physics for many years [1,4-7]. However, they were mostly considered as an academic curiosity while the development of engineering applications started with the introduction of metamaterials [1,4-18].

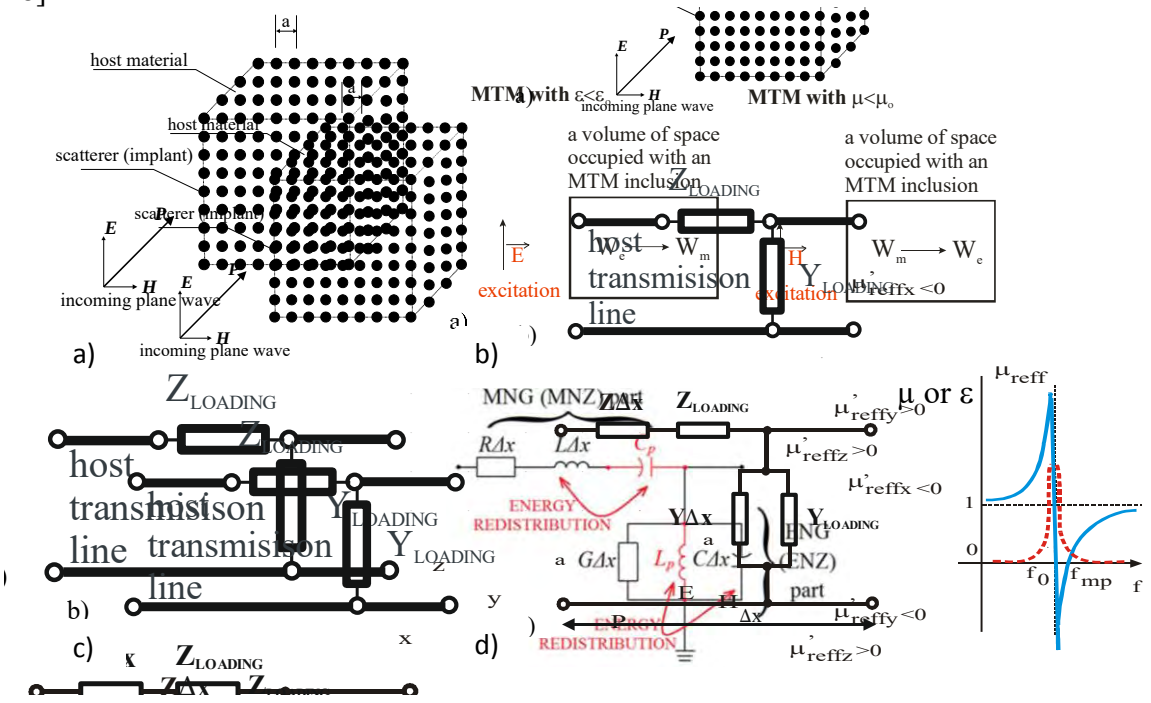

Figure 1-2 a) Concept of a volumetric metamaterial, b) Energy redistribution in a general passive metamaterial, c) Transmission line periodically loaded with lumped elements, d) A subwavelength segment of transmission line loaded with lumped elements – concept of a transmission-line-based metamaterial

Metamaterials (MTM) are artificial structures, electromagnetic properties of which (permittivity and permeability) cannot be found in (macroscopically) continuous, naturally

occurring materials [4]. Historically, early designs used a volumetric ensemble (Figure 1-2, (a) of electrically small electromagnetic inclusions with a mutual distance that is a small fraction of the wavelength [2, 4]. When an electromagnetic (EM) wave impinges on this structure, the field scattered from the inclusions modifies the original field distribution in a way similar to the mechanism of polarization (and magnetization) in continuous materials. Therefore, the structure behaves as a hypothetical continuous material with new (homogenized) values of constitutive parameters (permittivity ε and permeability μ). In this way, it is possible to 'engineer' exotic values of permittivity and permeability that are either rare in nature (such as ENG, MNG, ENZ, MNZ), or not available at all (**D**ouble**N**e**G**ative).

Metamaterials have brought some novel intriguing physical phenomena such as negative refraction, sub-wavelength propagation, resolution-free imaging, just to mention a few [1,2,4-7,9-18]. Unfortunately, the practical real-word engineering applications are still *very rare and limited* due to two basic *connected* problems: pronounced losses and a narrow operating bandwidth.

Where do these problems come from? As detailed in [2], the inclusions in (Figure 1-2), (a) always behave as some kind of a resonator, in which the energy redistribution *always* takes place (Figure 1-2, (b)). The energy redistribution from the electric field into magnetic field causes the lowering of effective permittivity to less-than-one or negative value. Similarly, the energy redistribution from the magnetic field into electric field causes the lowering of effective permeability to less-than-zero or negative value. This energy distribution is a time-dependent resonant process. Therefore, the 'negative' or 'near-zero' behavior is always narrowband, irrespectively of the internal structure of a given passive metamaterial.

There is a second approach for construction of metamaterials that uses an ordinary transmission line periodically loaded with series and/or shunt lumped reactive elements (Figure 1-2, (c)). It is very well-known that this periodic structure shows alternating pass-bands and stop-bands [4-6,19]. If the mutual distance between the loading elements is much smaller than the wavelength (Figure 1-2, (d)), the structure operates in the lowest pass-band. In this case, it can be said that the additional reactive elements simply modify the distributed impedance and admittance (and therefore, the effective permeability and effective permittivity). This main idea of so-called transmission-line metamaterials is explained in Figure 1-3 [2,4-6,20].

Briefly, a standard transmission-line model comprises a series *RL* branch (impedance

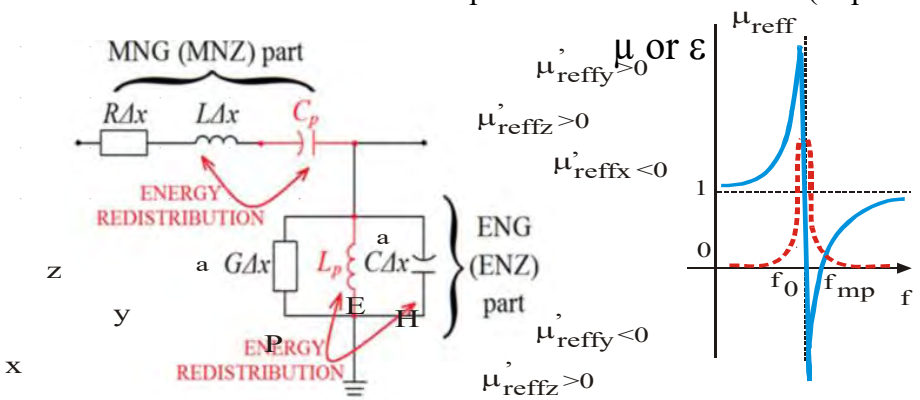

Figure 1-3 Transmission-line-based model of a general passive metamaterial and explanation of resonant energy flow

of which is proportional to the complex permeability) and a shunt *GC* branch (admittance of which is proportional to the complex permittivity) (the black elements in Figure 1-3). Here *L*, *C*, *R* and *G* stand for distributed inductance, capacitance, resistance, and conductance, respectively. In the case of ordinary passive MNZ or MNG metamaterials, one includes an

additional lumped capacitor into the series branch (series red element in Figure 1-3). This causes a resonant redistribution of energy from the magnetic field (previously stored in the series distributed inductance) into the electric field (within additional lumped capacitor). Mathematically, a new series combination possesses either near-zero impedance (μ_r~0, the MNZ effect at the resonant frequency) or a capacitive impedance (μ_r<0, the MNG effect below the resonant frequency).

Similarly, one can include additional inductance into the shunt branch (the red inductor in Figure 1-3) and achieve either the ENZ (ε_r~0) or the ENG (ε_r<0) behavior. Of course, if both series and shunt branches are loaded (with series capacitor and shunt inductor, respectively), it is possible to achieve **D**ouble-**N**ear-**Z**ero (ε_r~0, μ_r~0) or DNG (ε_r<0, μ_r<0) behavior. This simple approach can be extended to various 2D metamaterials [4-6].

At first sight, it seems that the circuit in Figure 1-3 should lead to a single-resonance Drude dispersion model (the Lorentz model with f_p=0). However, as detailed in [2], the inevitable 'parasitic' capacitance of a realistic inductor and 'parasitic' inductance of a realistic capacitor introduce additional resonance(s). Thus, the circuit (and the whole metamaterial) obeys the Lorentz dispersion. Since the frequency of 'parallel' resonance is rather low, the dispersion in transmission-line-based metamaterials is less pronounced than one in inclusion-based volumetric metamaterials. Thus, the main drawback of transmission-line-based metamaterials is again inevitable inherent dispersion.

Simply stating, it is clear that the host material and inclusions of volumetric metamaterials (Figure 1-2, (a)) as well as the host transmission line and associated loading lumped elements (Figure 1-2, (d)) are made out of ordinary materials constrained by the energy-dispersion constraints (1.1) (or Foster theorem (1.2)). The same applies for all other passive electromagnetic metamaterials such as plasmonic, terahertz and optical metamaterials. Hence, inevitably *all passive metamaterials* are always dispersive, i.e. narrowband.

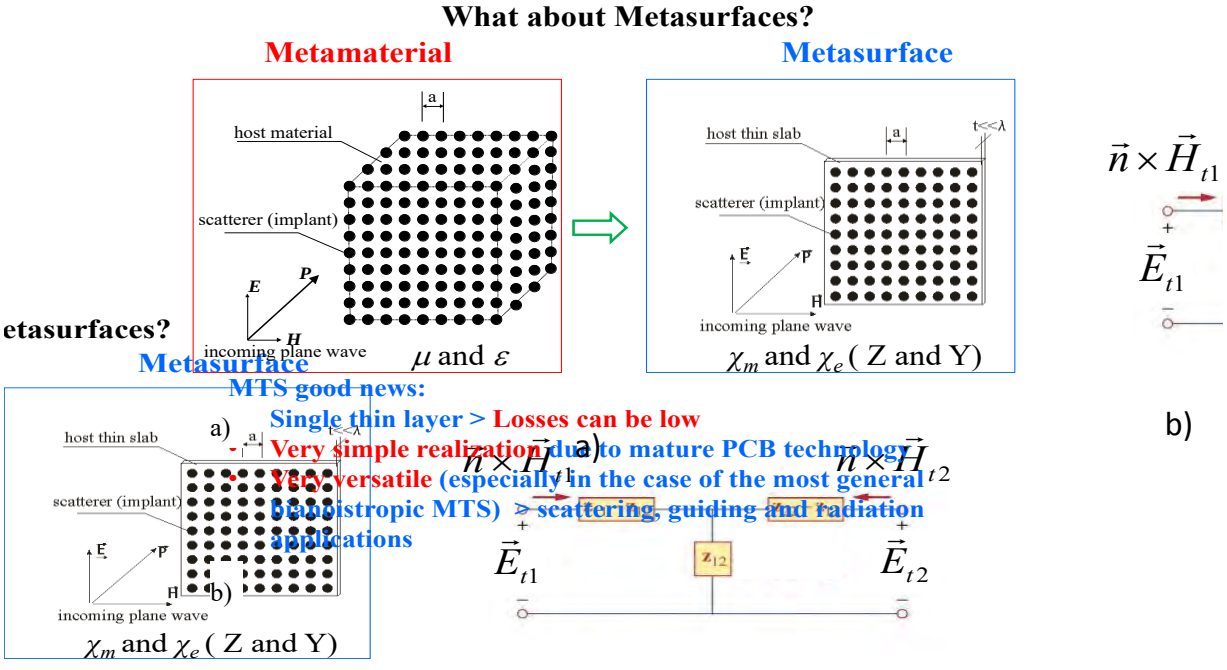

Figure 1-4 a) Evolution of metasurface from volumetric metamaterial b) Metasurface lumped-element equivalent circuit

In recent years, the whole electromagnetic community has focused their research efforts on thin artificial sheets (so-called metasurfaces, MTS, [21]), which are 2D equivalents of metamaterials (Figure 1-4, (a).

Here, the bulk constitutive parameters (permittivity and permeability) are replaced with so-called surface admittance and impedance parameters associated with equivalent electric and magnetic surface currents. An obvious practical advantage of this approach is a smaller number of unit cells (that results with lower losses) and very simple fabrication that uses printed-circuit-board technology. In addition, it was shown possible to apply different forms of patterning that lead to polarization conversion, beam refraction, surface wave manipulation, and many other interesting properties [21-23].

The great versatility of metasurfaces caused common (incorrect) opinion that they can solve some main problems of metamaterials, including intrinsic dispersion and narrow operating bandwidth. However, the metasurface comprises ordinary passive materials (a thin dielectric slab with metallic pattern) that are again, constrained by energy-dispersion relations (1.1). Moreover, due to its small thickness, the MTS can usually be modelled as a simple lumped-element circuit (Figure 1-4, (b)). In the first approximation of lossless structure, the elements of equivalent circuit are of pure reactive type (some network that comprises capacitors and inductors), for which the Foster theorem must be obeyed. Thus, the basic physical constraints of metamaterials apply for the metasurfaces, as well [22, 23].

1.1. Non-Foster and generalized Non-Foster elements

In the previous paragraph, it was shown that the main drawback of a (classical) passive metamaterial is a pronounced inherent dispersion, accompanied with narrowband operation. From the circuit theory point of view, one may say that this dispersion occurs due to the basic difference in the frequency behavior of a capacitor and an inductor (solid curves in Figure 1-5).

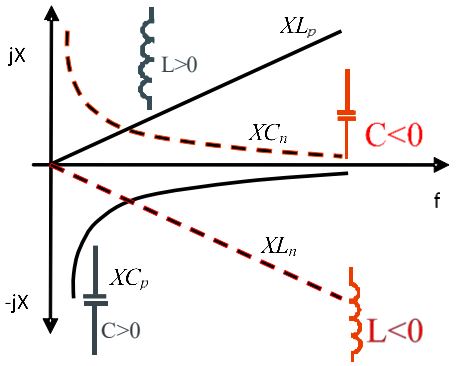

Figure 1-5 Comparison of dispersion properties of ordinary positive (Foster) reactance (solid) and negative (non-Foster) reactance (dashed)

This difference is not a surprise, since it is a direct consequence of a fact that ordinary reactive circuit elements (capacitors and inductors) obey Foster's theorem (1.2). However, one might (hypothetically) define new 'negative' (or 'non-Foster') elements: negative capacitor (C_n<0) and negative inductor (L_n<0) (Figure 1-5) [2,3,19,24-43].

Due to negative capacitance/inductance, the terminal current of these elements is negative (it flows outward from the positive terminal). Thus, a negative capacitor and a negative inductor behave as (reactive) *sources*, i.e. they are inevitably *active devices* [2,40,41].

It is important to notice that energy-dispersion constraints (and Foster's theorem) have been derived assuming that there are no losses present [1,3,19,24]. So, strictly speaking, hypothetical negative resistor (an active element that delivers real power [19]) should not be termed as a 'non-Foster element'. However, one might say that a negative capacitor, a negative inductor, together with a negative resistor form a complete group of (hypothetical) 'Generalized non-Foster elements'. These ideal elements are *postulated* to be linear and dispersionless (Figure 1-6) [20].

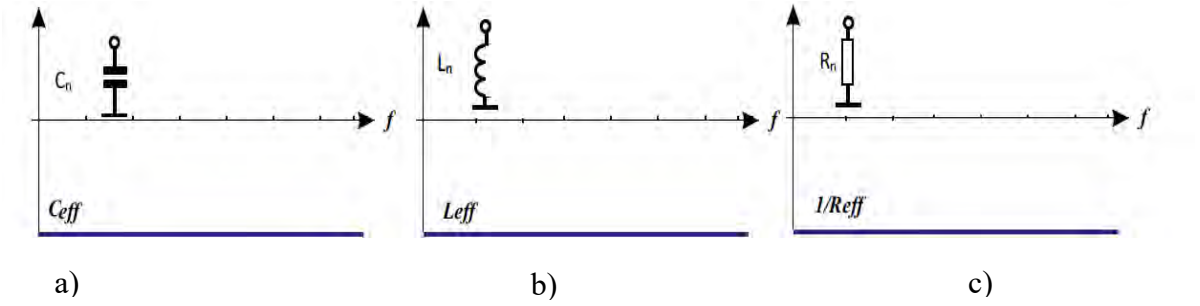

Figure 1-6 Linear models of ideal generalized non-Foster elements.
a) Negative capacitor, b) Negative inductor, c) Negative resistor

In practice, 'negative' elements are mimicked by appropriate electronic circuitry, so called '**N**egative **I**mpedance **C**onverters', [2,25-28,34-57] and '**N**egative **I**mpedance **I**nverters, [27,28], proposed more than 60 years ago. In essence, these are specially designed amplifiers with positive feedback.

1.2. Principle of dispersion cancellation and related applications

The first potential application of negative capacitors and inductors (that has been investigated for many years and it is still active nowadays) is broadband matching of small antennas [29,58-66]. Briefly, this matching relies on the compensation of frequency dispersion of an ordinary reactive network with the 'inverse' dispersion of a 'negative' non-Foster network. This compensation yields (theoretically) infinite bandwidth. Apart from matching, several (mostly theoretical) studies, that investigated the use of active elements in periodic structures for various microwave applications such as manipulation of bianisotropy [30] and emulation of perfectly matched layers (ideal absorbers) [31,32], were published in the past.

The first paper that theoretically discussed a possible use of active non-Foster elements for 'dispersion compensation' in metamaterials was published in 2001 [34]. It analyzed the equations for polarizability of metamaterials based on an ensemble of short loaded dipoles and small loaded loops. In [34] it was shown analytically that a loading of a short dipole with a *negative capacitance* (instead of ordinary, positive inductance) should lead to the wideband dispersionless ENG behavior. Similarly, the loading of a small loop with a *negative inductance* (instead of ordinary, positive capacitance) should lead to the wideband dispersionless MNG behavior. In this case, the bandwidth would be limited only by the bandwidth of the realized non-Foster element itself. Thus, the inherent energy-dispersion constraints (1.1) would be bypassed.

In our recent report (Broadband Epsilon-Near-Zero (ENZ) and Mu-Near-Zero (MNZ) Active Metamaterial, FA 8655-10-1-3030, EOARD and AFRL, August 2011 [2]) we showed that it is possible to overcome the basic dispersion-energy constraints (and, therefore, to overcome the inherent narrowband operation) of passive metamaterials by incorporation of the so-called non-Foster elements into standard transmission-line-based structures. The basic principle of non-Foster metamaterial from [2,35-43,46,50] is briefly explained in Figure 1-7.

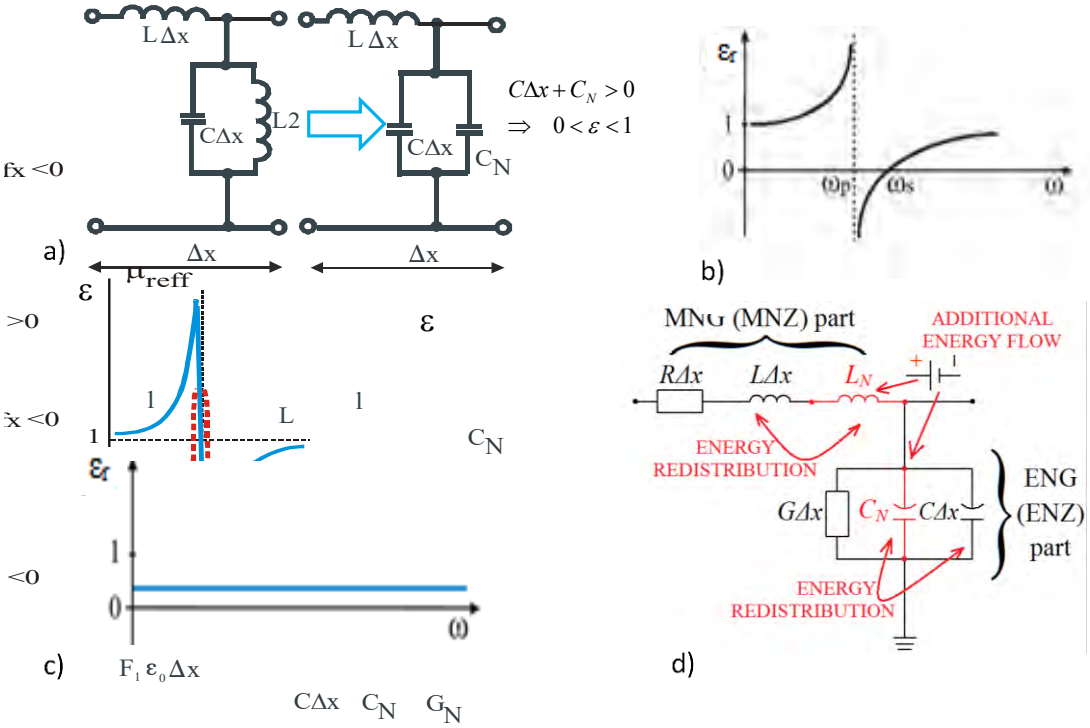

Figure 1-7 a) Evolution of active ENZ metamaterial from passive ENZ metamaterial b) Lorentz dispersion model of passive ENZ metamaterial, c) Dispersion model of active ENZ metamaterial, d) Energy flow in active ENZ metamaterial

A typical one-dimensional (1D) implementation of an ENZ (or ENG) metamaterial uses a transmission line periodically loaded with lumped inductances (Figure 1-7(a)). This equivalent circuit describes a well-known wire medium [7]. The resonator in Figure 1-7 (a) is actually a tank circuit formed by the line shunt capacitance $C\Delta x$ (C being the distributed capacitance and Δx being the line segment length) and the lumped inductor L_2. This circuit (with neglected 'parasitics') obeys the Drude dispersion model (i.e. Lorentz model with ω_p=0, Figure 1-7, (b)):

$$\varepsilon_r(\omega)=\left[\frac{1}{\varepsilon_0}\left(C-\frac{1}{\omega^2 L_2\Delta x}\right)\right]. \qquad (1.3)$$

Within the narrow band above the resonant frequency, the expression in square brackets in (1.3) has a value smaller than one, which shows the ENZ behavior ($0<\varepsilon_r<1$). As stressed before, all known passive metamaterials behave very similarly and, inevitably, also exhibit dispersion.

In [39,51] we proposed a novel equivalent circuit of an active non-Foster metamaterial (Figure 1-7 (a), right part). It is rather similar to that of a passive metamaterial (Figure 1-7 (a), left part). The important difference is that the lumped inductor L_2 is replaced with an artificial

negative capacitor C_N (C_N<0) (as mentioned before, this is actually an electronic circuit that employs positive feedback and generates negative capacitance [26]). A new CC_N 'tank circuit' in Figure 1-7 (b) does not have the usual resonant behavior and the equivalent permittivity is *not dependent* on the frequency:

$$\varepsilon_r(\omega)=\left[\frac{1}{\varepsilon_0}\left(C-\frac{|C_N|}{\Delta x}\right)\right]. \tag{1.4}$$

Thus, if ($|C_N|/\Delta$x)<C, the equivalent permittivity will show an ENZ behavior (0<ε_r<1) that is entirely dispersionless.

Clearly, very similar expression can be derived for the equivalent permeability in the case of added series negative inductor (Figure 1-7, (d)), [36-39]

$$\mu_r(\omega)=\left[\frac{1}{\mu_0}\left(L-\frac{|L_N|}{\Delta x}\right)\right]. \tag{1.5}$$

Thus, if the negative capacitor (or negative inductor) are ideal, the real parts of effective permittivity (or permeability) will be 'flat' with frequency (Figure 1-7, (c)). Actually, the negative capacitor and negative inductor behave as frequency-dependent controlled sources [40,41] that supply additional currents to the positive elements. For instance, there is an additional current in the shunt branch (Figure 1-7, (d)). This current causes faster charging of the distributed capacitance and, therefore, it decreases the overall effective capacitance (and effective permittivity). Instead of an energy redistribution from the electric field into magnetic field (or vice versa) used in passive metamaterial, here one introduces an additional energy flow from the active device (that has its own DC power supply (Figure 1-7, (d))).

In [2] we have developed several negative capacitors in 2-40 MHZ RF range, in 50-100 MHz RF range and in 1-2 GHz microwave range with appropriate 1D and 2D ENZ unit cells, extracted effective permittivity and verified broadband operation. We have also developed an entire three-cell 1D active ENZ metamaterial that has a fractional dispersion bandwidth of 200% (more than four octaves) (Figure 1-8). In addition, this line supports counter-intuitive superluminal phase and group velocities [42,43,51]. All of the prototypes were 'hand-crafted' and based on low-cost FET, BJT and OPAMP components. Achieved bandwidth varied from one octave (1-2 GHz) to more than four octaves (2-40 MHZ). This is significantly better than the bandwidth of *any* passive metamaterial available at present and, to the best of our knowledge, this is the first experimental demonstration of a non-Foster broadband, dispersion-less ENZ metamaterial.

In [2], we have also proposed a possible extension to, both the isotropic and the anisotropic, 2D non-Foster metamaterials. The unit cells of such metamaterials are based on two orthogonal branches with series inductances. By varying these inductances one can adjust needed values of the (positive) permeability in the x and y directions, respectively. Similarly, the shunt susceptance contains a negative capacitor (connected in parallel with a distributed capacitance of the transmission line assuring ENZ behavior).

After initial efforts reported in (Broadband Epsilon-Near-Zero (ENZ) and Mu-Near-Zero (MNZ) Active Metamaterial, FA 8655-10-1-3030, EOARD and AFRL, August 2011 [2]) they were several unclear points left. At first, it was noted that idealistic dispersion-free linear models of generalized non-Foster element are not physical [2,41,90]. Occasionally, it may predict (qualitative) behavior of a specific network but only in the steady state conditions and only within some finite bandwidth. However, there are many cases, in which the behavior predicted using an ideal negative capacitor is entirely non-physical. Thus, a better, physically sound model of a realistic negative capacitor, which always predicts correct behaviour was needed. In addition, it was not clear if it is possible to develop a negative inductance needed for

proposed anisotropic MNZ and MENZ metamaterials and enhance them with tunability and re-configurability features. Finally, the question of possible increase of the operating frequency into the microwave region has remained open.

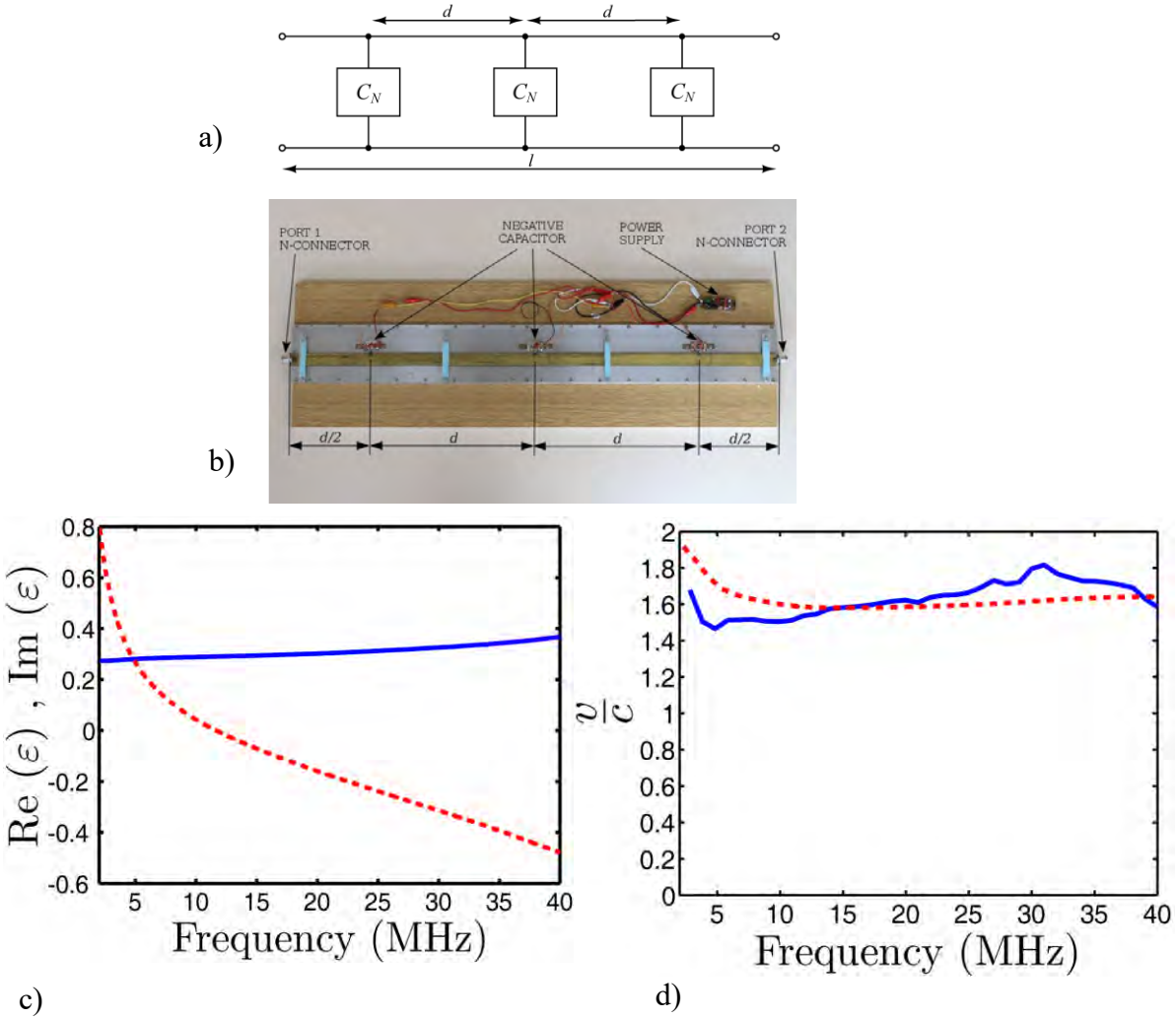

Figure 1-8 An example of a non-Foster ENZ transmission line (1D non-Foster metamaterial) (taken from [2,42,43]).

a) Basic block-diagram
b) A photo of manufactured prototype
c) Measured effective permittivity, solid blue –real part, dashed red – imaginary part
d) Measured signal velocities, solid blue – group velocity, dashed red- phase velocity

All aforementioned issues were investigated in our next effort reported in 'Active Reconfigurable Metamaterial Unit Cell Based on Non-Foster Elements', EOARD/AFRL, Contract FA8655-12-1-2081, October 2013 [51].

Specifically, we have developed a more realistic one-pole, two-pole and three-pole models of a dispersive negative capacitor [51]. Developed model showed very good agreement with both SPICE-based simulations and the measurements on the manufactured prototypes across the whole operating bandwidth. That analysis showed that generated negative reactance is always accompanied by occurrence of unwanted resistance (either positive or negative). Similarly, that generated negative resistance is always accompanied by occurrence of unwanted

reactance (either positive or negative), Figure 1-9. This fact may be interpreted as a special case of Kramers-Kronig relations (or, in a broader sense, of causality [1]).

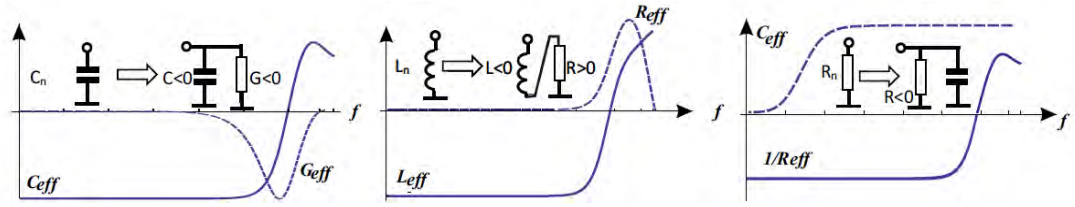

Figure 1-9 Linear models of realistic generalized non-Foster elements.
a) Negative capacitor
b) Negative inductor
c) Negative resistor

In addition, in [51] we analyzed the feasibility of increase of the highest operating frequency of a non-Foster ENZ metamaterial towards UHF and microwave parts of the EM spectrum. We designed, simulated and built the prototypes of the active ultra-broadband non-Foster ENZ unit cells that operate from 1 MHz to 700 MHz. This bandwidth (1:700 or more than 9 octaves) surpasses the bandwidth of all passive and active metamaterials available at the present state of the art.

Furthermore, in [51] we analyzed the feasibility of construction of a stable RF negative inductor that would enable development of non-Foster MNZ metamaterials [2], and constructed a prototype based on OPamp that generates effective inductance of –10 nH within the bandwidth 100 kHz–700 MHz.

Finally, in [51] we analyzed a feasibility of adding tunability/reconfigurability features to the developed negative capacitors/inductors and the associated unit cells of ENZ/MNZ metamaterials. We managed to achieve direct tuning of the effective negative capacitance (by applying an external DC voltage on the embedded varactor, Figure 1-10, (a)).

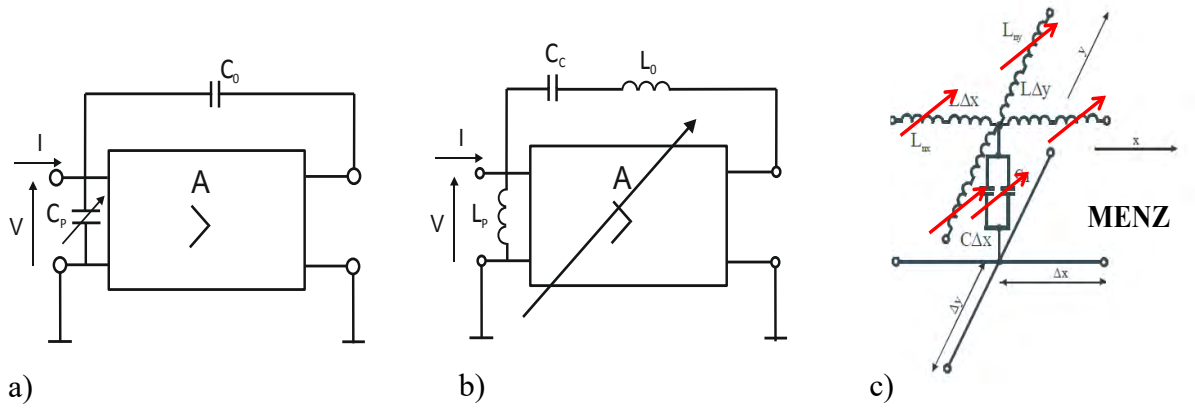

Figure 1-10 Examples of tunability in non-Foster metamaterials a) tunable capacitor b) tunable inductor c) tunable anisotropic non-Foster MENZ unit cell (taken from [51])

Achieved capacitance was between -1 pF to -3 pF within the bandwidth 100 kHz-700 MHz. In the case of the negative inductor, we used a PIN diode configured as a variable resistor that controlled the gain and, therefore, the value of generated effective inductance (Figure 1-10, (b)). Achieved effective inductance was between -5 nH and -9 nH, within the bandwidth 100

kHz-700 MHz. These two approaches were merged together into an anistropic ENZ/MNZ unit cell with tunable relative permittivity from 0.2 to 0.8, and tunable relative permeability from 0.2 to 0.5, within the bandwidth 100 kHz – 700 MHz Figure 1-10, (c). Using the approach developed in [51], the same unit cell could be inserted into various transmission-line-based structures and (depending on its configuration) enable different applications such as: cloaking, squint-free leaky-wave antennas, metasurfaces, and broadband phase shifters in antenna arrays.

1.3. Stability issue, open questions and future trends

Nowadays, the research of metamaterial and metamaterial-inspired structures based on generalized non-Foster elements is very active [37,44-49,52-54,57,63-85]. However, this technology has also some drawbacks.

The most important problem that still prevents widespread application of metamaterial structures with negative elements is the stability management [2,77-79,86-94]. All generalized non-Foster elements (both non-Foster capacitors and inductors as well as negative resistors) employ some kind of a positive feedback, which in some case leads to instability. This issue is still not well understood, which makes a design of stable non-Foster circuits extremely challenging.

Many methods of stability prediction that are routinely used in microwave engineering fail in the case of non-Foster networks. A detailed review of this problem is given in [86-89]. Briefly, only the methods that use Laplace domain (or time domain) and take into account all the meshes and nodes of the analyzed network (analysis of system determinant [87,88], **N**ormalized **D**eterminant **F**unction [91], Nyquist method [88], etc.) are always reliable and cannot result with incorrect stability prediction.

Another important fact is that stability does not depend only on the non-Foster element but also on the other elements in a given network [2,86-89]. Usually, it is believed that it is enough to fulfill widely accepted stability criterion that the overall 'mesh' capacitance or inductance must be positive number. This criterion was discussed in details in [60,93]. A common way of achieving this 'compensation' is the insertion of an additional positive element (the so-called 'swamping element') in series or in parallel to negative element. Therefore, a new equivalent element (a combination of positive and negative element) behaves as an ordinary positive element. This approach has (at least) two unclear points.

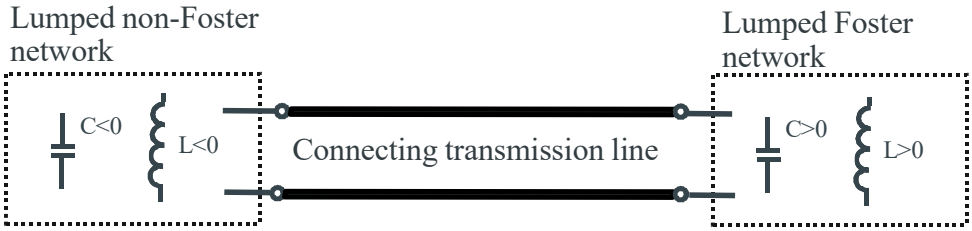

Figure 1-11 Example of 'mixed' lumped-distributed Foster/non-Foster network

Firstly, it is based on lumped elements, while in some applications (antenna matching [60,61], active non-Foster metamaterials ([35-46,50,51,95], active non-Foster metasurfaces and absorbers [67-69,96,97], active non-Foster leaky-wave antennas [71-73] etc.) positive and negative elements are connected via a segment of transmission line, forming some kind of

'mixed' lumped-distributed network. This problem is very important and needs additional investigations due to the fact that some of the reports with mixed networks in the literature are inconsistent. For example, some experimental studies reported stable operation [38,39,42,43] although the associated theoretical analysis (based on numerical simulations with transmission line and ideal generalized negative elements) predicted instability [92].

Let us go back to the basic stability criteria of positive mesh inductance, capacitance, and resistance [60, 93]. According to it, one concludes that is possible to build the structures with ENZ/MNZ properties (as we did in [2,51]) but the structures with SNG/DNG properties *appear to be always unstable*, i.e. *they appear not to be feasible in practice*. On the other hand, the theoretical findings in [51] show that a network comprising *solely negative ideal elements* is inherently stable (as it is an ordinary network that contains solely positive elements). A very preliminary experimental confirmation of this counter-intuitive phenomenon was provided in [51, 77] by successful prototyping and testing of a stable negative RLC circuit. Following those initial efforts, one may think of including negative resistors into a lumped non-Foster network obtaining 'entirely negative metasurface' (Figure 1-12, (Δx stands for metasurface thickness)). Providing that the net resistance is negative, this system will be inherently stable. It would enable the construction of *stable broadband inclusions for active metasurfaces* such as in broadband polarization-manipulation metasurface [21], DB metasurface [23], Omega metasurfaces [98], Parity-time metasurfaces [84, 85] etc.

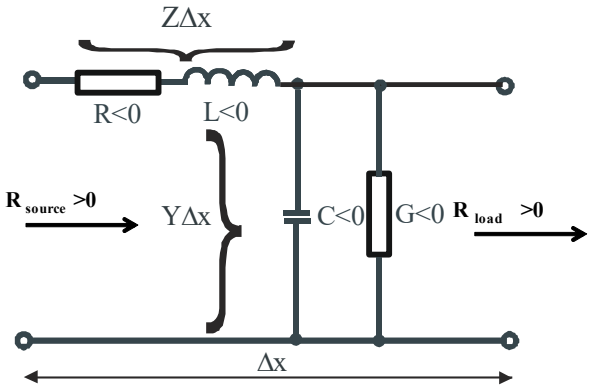

Figure 1-12 An idea of 'all-negative' stable network for metasurface unit cell

Furthermore, the basic principle of non-Foster metamaterials [51] is, in the sense, similar to the long-standing efforts in a wideband matching of a general load with complex impedance to the source (i.e. the broadband matching of an antenna) [60,61]. Again, the most difficult issue in this application is the inherent instability of non-Foster elements. It can be shown that it is impossible (even theoretically) to perfectly match an antenna to the load using non-Foster elements without introducing instability (this problem is conceptually identical to the problem of instability in non-Foster SNG/DNG metamaterial, which was discussed above). Additional, well-known problem in non-Foster matching is the implementation of this approach in transmitting applications, which requires operation at high-power levels. It is interesting that these similarities between non-Foster metamaterials and non-Foster matching have not been investigated so far in the literature available in public.

The similarity between non-Foster metamaterials and wideband non-Foster matching led us to the novel concept of non-Foster source, i.e. the source with negative internal reactance

that assures direct matching to the antenna [82,83]. Let us suppose that the load (the antenna) consists of a reactance that is equal to the non-Foster internal reactance (but with the opposite sign) and the associated radiation resistance is equal to the absolute value of effective negative resistance. In this case, this whole system will be reflection-free. Thus, the non-Foster source is a nearly perfectly matched oscillator (a transmitter) that actually turns the instability into a very useful feature. Such a method drops out classical matching, in which a transmitter, a matching network, and an antenna are different blocks. Here, a transmitter and a single radiator or an antenna array become a nearly dispersionless and inherently broadband non-Foster-based source-antenna system. This approach could enable manufacturing of nearly perfectly matched transmitter-antenna systems with a bandwidth ten times larger than existing designs.

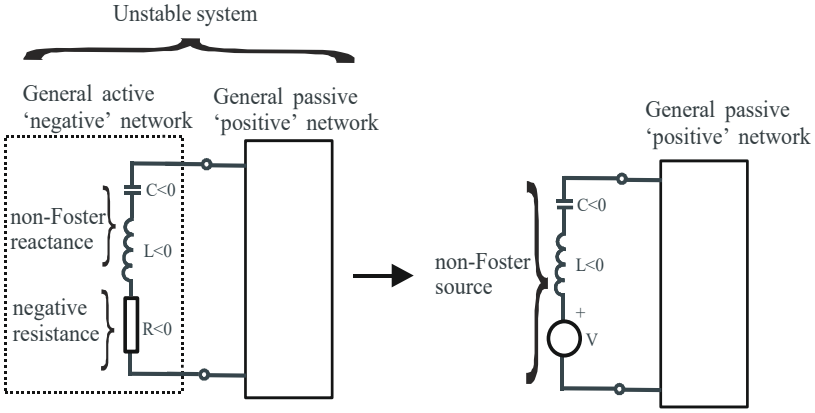

Figure 1-13 An Idea of a non-Foster source

1.4. Summary

Previous AFRL/EOARD-funded efforts (Broadband Epsilon-Near-Zero (ENZ) and Mu-Near-Zero (MNZ) Active Metamaterial, FA 8655-10-1-3030, EOARD and AFRL, August 2011 [2], 'Active Reconfigurable Metamaterial Unit Cell Based on Non-Foster Elements', EOARD/AFRL, Contract FA8655-12-1-2081, October 2013 [51]) yielded several novel and promising results but a few important questions remain opened:

1. Is it possible to develop an analytical model that could predict stability of 'mixed' lumped-distributed Foster/non-Foster networks and give the 'recipe' for novel non-Foster structures that are more robust to instability?
2. Is it possible to apply an idea of 'all-negative' stable Foster/non-Foster lumped network for real engineering applications based on SNG (or DNG) metamaterials and metasurfaces?
3. Is it possible to apply an idea of a 'non-Foster source' for construction of nearly-perfectly-matched and broadly tunable antenna-transmitter system?
4. Is it possible to extend the ideas of 'all-negative' stable Foster/non-Foster lumped network and broadly tunable antenna-transmitter system towards active metasurfaces for applications in antenna technology?

The purpose of the project is, therefore, to provide further insight into issues presented above by analytical, numerical and experimental investigation. The most important goal is the development of an experimental demonstrator of widely tunable antenna-transmitter system

operating in the lower RF band (the choice of the frequency band is constrained by the technology available at University of Zagreb).

Chapter 2 PROJECT OBJECTIVE AND REALIZED OUTCOMES

Project objective and realized outcomes

Almost twenty years have passed from the introduction of the field of RF electromagnetic metamaterials [8]. These are artificial structures, electromagnetic properties of which (permittivity and permeability) are not found in (macroscopically) continuous, naturally occurring materials. Metamaterials have brought some novel intriguing physical phenomena such as negative refraction, sub-wavelength propagation, resolution-free imaging, just to mention a few [1,4-7,9-18]. Unfortunately, the practical real-word engineering applications are still *very rare and limited* due to two basic problems: pronounced losses and a narrow operating bandwidth.

A few years back, a very interesting idea that might work around this inherent limitation was proposed [35]. It is based on so-called non-Foster elements. These are active electronic circuits, which behave as negative capacitors or negative inductors, violating the energy-dispersion constraints and Foster's reactance theorem. Negative capacitors and negative inductors have dispersion curves that are the exact inverse of the dispersion curves of ordinary 'positive' elements. Therefore, one could expect that the dispersion of ordinary passive metamaterials can be compensated for with the 'inverse' dispersion of non-Foster elements, resulting in an extremely broadband behavior.

In our EOARD/AFRL-funded project (FA 8655-10-1-3030, August 2011 [2]), it was shown possible to go around inherent dispersion limitations by inclusion of non-Foster elements into the passive metamaterial structures. Specifically, the investigation in [2] yielded active ENZ metamaterials with operating bandwidth of more than four octaves (1 MHz to 40 MHz). This bandwidth is considerably wider than the bandwidth of *all passive ENZ metamaterials available at present* and this clearly proved the correctness of the proposed novel concept. Most experiments in [2] were limited to a maximal operating frequency in low RF range (up to 100 MHz) due to available fabrication facilities at University of Zagreb.

Therefore, in the follow-up EOARD/AFRL-funded project (FA8655-12-1-2081, October 2013 [51]), the maximal frequency of operation was pushed into the UHF region and the operating bandwidth was extended to *1:700 or more than 9 octaves* (1MHz to 700 MHz) using cheap of-the-shelf discrete components. At the same time, the versatility of non-Foster-element-based metamaterials was increased by the development of specially designed reconfigurable unit cell. This unit cell is in-situ reconfigurable (by external DC control signal) and able to achieve either DPS-ENZ or DPS-MNZ behavior. Using this approach, the same unit cell could be inserted into various transmission-line-based structures and (depending on its configuration) enable different applications such as: cloaking, squint-free leaky-wave antennas, metasurfaces, and broadband phase shifters in antenna arrays.

Previous AFRL/EOARD-funded efforts [2,51] have brought several very encouraging results and real-word prototypes with stable operations, together with a clear 'recipe' of choosing appropriate methods for stability prediction. In spite of this, the stability management is still an extremely challenging engineering task.

Specifically, there are neither studies of the networks that contain ordinary elements and generalized non-Foster elements connected via a transmission line (‘mixed lumped-distributed networks’). This problem is very important from a practical point of view. Firstly, there are several applications such as antenna matching [60,61] and active non-Foster metamaterials [2], in which the positive and negative elements are connected via a segment of transmission line. Secondly, some reports on mixed networks in the literature are not consistent. There are reports on stable operation of practical prototypes [38,39,42,43] while the associated theoretical analysis predicts instability [92].

Yet another very important issue is a recently presented idea of ‘all-negative’ stable Foster/non-Foster lumped network [51]. It is based on a preliminary experimental demonstration of a counter-intuitive stable negative RLC circuit. It is not clear whether this idea can be used in real-world engineering applications based on SNG (or DNG) metamaterials and metasurfaces.

The third issue deals with ‘non-Foster source’ and ‘non-Foster antenna-transmitter’ [82,83]. This is a network that comprises the load (the antenna), the reactance of which is equal to the non-Foster internal reactance (but with the opposite sign) and the associated radiation resistance is equal to the absolute value of effective negative resistance. Thus it is actually a nearly perfectly matched ‘active transmitting antenna‘, which actually turns instability into a very useful feature. It is not clear whether this interesting idea can be demonstrated in practice.

Therefore, the purpose of this 24-month research effort is to significantly suppress stability problems in *the most common applications* of non-Foster elements (*the non-Foster metamaterials and the non-Foster matching*).

Proposed research is novel and unique since so far it has been believed that the construction of stable non-Foster SNG/DNG transmission lines/metamaterials/metasurfaces is not feasible. In addition, the idea of turning the instability of non-Foster element into a useful feature in the form of non-Foster source and source-antenna system has not been presented yet. To the best of our knowledge, there are no papers available in the public literature that deal with these approaches.

If successful, the proposed efforts could pave a way towards manufacturing of non-Foster-based matched transmitter-antenna systems and metasurfaces with a bandwidth ten times larger than the existing designs.

The work in the project has been divided in the following tasks:

1. Re-examination of fundamental stability issues of both ideal and realistic non-Foster reactive elements (negative capacitors and negative inductors) complemented with negative resistors (‘generalized non-Foster elements’). Extension of the analysis to the case of ‘mixed lumped-distributed networks’. Development of the stability criterion.

2. Development of the design strategy that would improve stability of practical general non-Foster network. Verification of developed design strategy by SPICE-based numerical simulations and the measurements on specially designed laboratory prototype-demonstrator operating in low RF range.

3. Analytical investigation of counterintuitive physics of ‘all-negative’ stable Foster/non-Foster lumped network with ‘reversed power flow’. Extension of lumped ‘all-negative’ network to ‘all-negative’ active unit cell and numerical verification with the help of commercial SPICE-based circuit simulator.

4. Analysis of basic non-intuitive physical phenomena of non-resonant active matching. Development of mathematical model of non-Foster source and study of the direction of power flow and effective matching. Derivation of the criteria for stability/instability of source-antenna and investigation of the influence of non-linearity of realistic non-Foster network. Determination of optimal design parameters constrained by the tradeoff between achieved return loss and the operation bandwidth. Verification using SPICE-based circuit simulator

5. Development of a prototype-demonstrator of a non-Foster source based on negative series RC circuit, operating in low RF range. This circuit should behave as a Thevenin's source with negative internal impedance. Development of dedicated passive network that emulates an antenna and testing of self-oscillation phenomenon. Extension of this simple demonstrator to real 'antenna-transmitter' by connecting the non-Foster source to a simple short dipole antenna and measurements of the spectrum of radiated signal and tuning range.

The main realized outcomes of the project are:

- We have shown that the widely accepted stability criterion of positive 'mesh' capacitance fails for parallel combination of positive and ideal negative capacitor with connecting transmission line. Such a network is always unstable, regardless of the line length and capacitance values of positive and negative capacitor. However, the inherent dispersion of a realistic negative capacitor (usually considered as a drawback) can be tailored in a way that assures stable operation. Very similar conclusion applies for a series combination of positive and ideal negative inductor with connecting transmission line. We have also shown a rather surprising fact that in some cases of lumped and mixed networks with a realistic model of negative capacitor, stable operation is feasible even if overall capacitance is negative. We have verified all observed phenomena by ADS^{TM} simulations based on realistic negative capacitor with simple one-pole model of OPamp, as well as by simulations that used realistic SPICE model of commercial OPamp.

- We have found that a concept of unstable 'mixed lumped-distributed network' can be used in active self-oscillating non-Foster Fabry-Pérot antenna. Theoretical investigation predicted increase of 1 dB bandwidth for ten times (compared with ordinary passive Fabry-Pérot antenna). One dimensional model of such a system was analyzed using both simple linear model and SPICE-based non-linear model. An RF experimental demonstrator operating in 10 MHz range was constructed and measured. Experimental results proved the correctness of basic idea of a broadband active self-oscillating FP antenna (antenna-transmitter system). This system has -1 dB bandwidth of 20% and it can be tuned at any frequency within this band.

- We have developed a novel topology of 'bandpass' non-Foster capacitor intended for use in active metamaterials/metasurfaces and antennas. Analytical and numerical results have shown that the stability properties of a 'bandpass' negative capacitor are significantly better than those from classic designs. We have developed appropriate experimental demonstrator based on high-speed OPamp, operating in low RF range (< 100 MHz). Measurements have shown stable operation although the overall capacitance

is negative and the results match analysis and simulations very well. We believe that this is the first demonstration of a stable 'bandpass' negative capacitor.

- We have performed analytical and numerical investigation of counterintuitive physics of 'all-negative' stable lumped network with 'reversed power flow' and found that such a network is indeed stable if equivalent 'mesh elements' are negative. It is interesting that stable operation is possible for realistic generalized non-Foster elements (of course, for some restricted set of design parameters). It was found possible to design active RC, RL, And RLC networks that might find application as unit cells of active metasurfaces. All analytical results were verified by circuit simulations that used a realistic SPICE model of commercial OPamp and measurements on negative RLC RF demonstrator.

- We have investigated an idea of non-Foster source ('non-Foster antenna-transmitter') based on negative series RC circuit and found that it indeed offers (theoretically) infinite tuning bandwidth. In practice, the tuning bandwidth is constrained by used NIC circuit and properties of tuning network. We constructed an experimental demonstrator operating in a lower RF range (300 kHz – 10 MHz). Demonstrator comprised an OP-amp based negative RC circuits connected to a simple, short top-loaded monopole (the length of $\lambda/15$ at the highest frequency). Measurements revealed stable oscillations with amplitude flatness of approximately +- 2 dB, within the range 1MHz – 10 MHz.

- We have extended the concept of 'non-Foster antenna-transmitter' to 'non-Foster antenna-transmitter array. Comparing to the previous design based on a self-oscillating single short dipole, proposed approach offers much broader (theoretically infinite) tuning and matching bandwidth, it enables use of any type of small antenna, and it has up to 3 dB higher radiated power. The simulation results and associated proof-of-concept demonstrator verified correctness of the proposed approach. We have constructed an experimental demonstrator based on two crossed dipoles and verified oscillations that can be tuned within 16 – 32 MHz bandwidth. It is important to stress that this tuning bandwidth was constrained only by available tuning elements. The simulations showed that the tuning bandwidth larger than 1:10 can be achieved by using different tuning elements.

Chapter 3 IMPROVING STABILITY OF GENERALIZED NON-FOSTER NETWORKS

Improving Stability of Negative-element-based RF Networks

3.1. Previous work

As briefly discussed in Chapter 1, stability management is a difficult problem that still prevents widespread engineering applications of generalized non-Foster networks [2].

Firstly, it is clear that the stability depends not only on the generalized non-Foster elements (the NIC circuitry) but also on the topology of the external loading network [2,20,51]. Even if one had ideal negative elements, many proposed circuits would never be stable due to the chosen topology of an external circuit. Unfortunately, this important issue is often overlooked.

Furthermore, practical systems that contain general non-Foster networks are rather complicated and some degree of simplification during stability predictions is inevitable. These systems (almost always) contain both the 'network' part (for example, an active matching network or transmission line loaded with active elements) and an 'electromagnetic' part (for example, an antenna or the host metasurface). In order to make the stability prediction as simple as possible, a very common approach is to replace the electromagnetic part by its circuit-theory (or transmission-line-theory) equivalent. In simple configuration it is usually done using available models from standard textbooks or, in more complicated cases, using extraction of scattering parameters from full-wave simulations and fitting values of equivalent network elements. Once the electromagnetic part is 'converted' to the equivalent circuit-level model it is combined with the 'network' part for stability prediction. Several different approaches are used at this point.

There is a traditional approach that examines stability properties of the NIC circuitry itself and gives a 'recipe' which kind of NIC should be used for some particular type of 'external' passive network [61,87]. This is well-known OCS/SCS approach, which classifies the NIC circuits into "open-circuit stable" (OCS) and "short-circuit stable" (SCS) types). It is interesting that limitations of this approach are still not clear, although it was originally introduced in the sixties of previous century [99-101].

The second approach uses ideal (linear) dispersionless generalized non-Foster elements (Figure 1-6) and applies some method of stability analysis of a given linear network [2,86-90]. As stressed in Chapter 1, it is clear that idealistic dispersion-free linear models of generalized non-Foster element are not physical. Thus, there are many cases, in which the behavior predicted using the ideal generalized negative elements is non-physical. In spite of this flaw, the approach based on ideal generalized non-Foster elements is still very common.

The third approach includes inherent dispersion of active elements in NIC circuitry and it is physically sound (within the limits of linear circuit theory). Although the basics of this approach were introduced a long time ago [26,29], it has been revisited and expanded just recently [20,41,51].

All three approaches presume linearity of generalized non-Foster networks. Obviously, it is only an approximation since generalized non-Foster elements (just as all active circuits) inevitably enter non-linear regime at high levels of input signal. However, linear stability analysis is acceptable if it is enough to predict whether the system is stable or not. Indeed, every non-linear effect 'begins' with linear instability (unbounded signal growth). When the signal amplitude reaches some level, the non-linear effects occur. On the other hand, if the application of non-Foster generalized network is inherently non-linear and it is important to know the details of the transient state (for example, in oscillating circuits) the linear stability analysis of generalized non-Foster network may not be acceptable (this case is discussed in Chapter 4).

3.1.1. Stability analysis based on OCS/SCS approach

It is well-known that generalized non-Foster elements are realized by terminating a NIC two-port in the corresponding positive element (load impedance Z_L, Figure 3-1). It is, by analogy, a form of an ideal transformer with a ratio of an impedance transformation of –k. This impedance transformation operates in both directions (bilateral behavior).

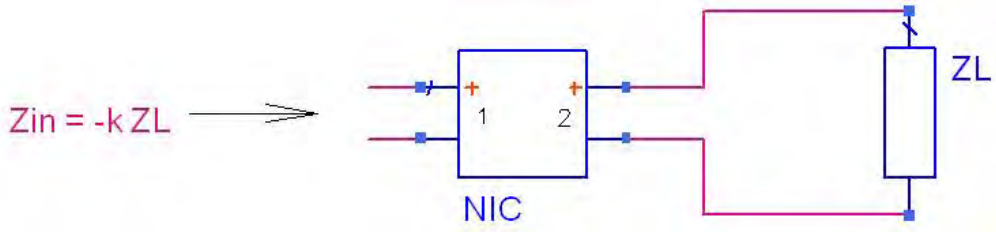

Figure 3-1 Definition of input impedance of a NIC terminated with arbitrary load

As explained in [2,29] the input impedance (seen into the port 1) reads as:

$$Z_{in} = \frac{V_1}{I_1} = h_{11} - \frac{k \cdot Z_1}{1 + h_{22} \cdot Z_1}, \quad k = h_{12} \cdot h_{21}. \tag{3.1}$$

Here, k stands for the conversion ratio [29]. An ideal NIC should have k=1. Inspection of (3.1) shows that this will be achieved if the following conditions are satisfied:

$$h_{11} = h_{22} = 0, \tag{3.2}$$

$$h_{12} \cdot h_{21} = 1. \tag{3.3}$$

Of course, using the same methodology one can easily calculate the input impedance (seen into port 2) if port 1 is terminated with an arbitrary impedance. So, one can think of a simple system that comprises an external network connected to the input impedance at port 1 (or port 2) (for some particular termination at port 2 (or port 1) and investigate the stability properties.

Choosing the short-circuit or open-circuit as a load impedance leads to the SCS/OCS analysis. Historically, it was observed that a practical NIC is always SCS at one port, and OCS at the other port (and vice versa). For instance if the port 1 of a NIC (terminated with some load

impedance at port 2) is short-circuited and the whole network is stable, it means that the port 1 is SCS. If so, according to above experimental observation, if the port 2 of the same NIC (terminated with some load impedance at the port 1) is left open, the whole network will be stable. Thus, the port 2 is OCS.

Brownlie [99], Hoskins [100], and Schwarz [101] offered three separate proofs to justify this stability phenomenon by considering the existence of poles or zeros in the RHS of the complex plane. All three authors introduced some prerequisite conditions. Brownlie [99] assumed the existence of 'parasitic' parameters in the NIC h-matrix. Hoskins [100] assumed the existence of time delay in the NIC circuit. Schwarz [101] assumed that either right-half-plane poles or zeros are introduced during the conversion process. In other words, in all three approaches, the NIC is not considered ideal anymore ((3.2, 3.3) are not satisfied).The introduction of a prerequisite condition in the discussion of the NIC stability problem is some kind of a mathematical 'trick'. It is necessary because without such an assumption an ideal NIC does not have any transient behavior and the stability problem does not arise at all.

Deeper physical explanation, based on two different approaches, was given in [102]. The first approach analyzed the NIC and its terminating networks as a linear frequency dependent system. In order to prove that the practical NIC is SCS at one port, and OCS at the other port it was found necessary to prove that the input impedance at one port has no right-half-plane pole but has right-half-plane zero and that the input admittance at the other port has no right-half-plane pole but has right-half-plane zero. The second approach analyzed the practical NIC, when terminated in resistors, as a nonlinear system. More precisely, the saturation region of used active elements (bipolar transistors or FETs) was taken into account. To prove that the practical NIC is SCS at one port and OCS at the other port it was necessary to prove that the negative input resistance of the NIC was voltage-controlled ('N' type of non-linearity) at one port and current-controlled ('S type of non-linearity) at the other port.

It is very important to stress that whether a practical NIC will remain stable or not in a system depends on the properties of *networks that are connected to the NIC*. To investigate the stability of the NIC, it is necessary to consider the NIC and its terminating networks (or the system) as a whole. Usually it is assumed that (practically speaking) OCS means, that if a very large resistance terminates the port 1 on NIC, then the overall network will be stable. Similarly, it is usually considered that SCS means that overall network will be stable if a very large conductance is placed across the input. Originally, Linvill [26] suggested that OCS versions should be used only as series elements, while SCS versions should be used as shunt elements. This 'recipe' based on the selection of SCS/OCS type is widely used in many studies [47-49,53,60,61,67,96,97].

However, one should be very careful in interpretation of above common assumptions. Firstly, it comes from the analysis of purely resistive (conductive) loads and nothing is said about the reactive parts (it is similar to the fact that common colloquial terms such as 'high impedance' and 'low impedance' are not strictly correct since the impedance is a complex number). Indeed, even a pure negative (non-Foster) reactance when connected to a positive resistance leads to instability [41,90,93]. Secondly, if some system is SCS (or OCS) *it does not necessary mean* that it will be stable for some very low resistance (or some very low conductance). For instance, there are two very interesting examples presented in [87]. The first example deals with a one-port network that is SCS but unstable for any resistance between 0.5Ω and 1Ω. The second example presented in [87] shows a two-port network with SCS/OCS ports that is unstable if either port is terminated with 1Ω resistor.

One concludes that, although widely used for the first selection of NIC circuit type, the SCS/OCS method is strictly valid only for short-circuit and open circuit termination. As it is

stated in [87], 'The SCS/OCS property is uninformative about the stability of general non-Foster circuits having terminated NICs'

3.1.2. Stability analysis based on ideal (dispersionless) lumped negative elements

The SCS/OCS method discussed in the previous paragraph usually does not analyze the generalized non-Foster network *per se*. Instead, it deals with the NIC circuit terminated with networks that contain ordinary positive lumped elements. Many authors use the next level of abstraction and analyze the lumped networks that contain ordinary (positive) elements and ideal generalized non-Foster elements (ideal negative resistor, ideal negative capacitor, and ideal negative resistor). Is this a physically correct approach? Clearly, idealized dispersion-free models of negative elements are not physical. Several examples of predicted non-physical behavior can be found in the literature [2,41,90]. Thus, the answer to the question above is surely 'no'. However, the question 'Can the analysis based on idealized dispersionless elements give any useful information?' is more complex and the answer is not so clear. Let us discuss this point in some more details.

There are two groups of non-physical behavior observed in stability analysis: the unbounded signal growth associated with the infinite energy and incompatibility of predicted signal with causality. The unbounded signal growth neglects inherent saturation i.e. the non-linearity that is inevitably present in every practical active element. Nevertheless (as mentioned in the introduction of Section 3.1.) every non-linear instability effect started as a linear effect (for early time and small signal levels), so *the occurrence of instability* will be predicted correctly. Of course, since the gain compression and saturation effects are neglected, the waveform of predicted signal will be incorrect. As far as the causality problems concern, they are inevitable connected to networks with delay (transmission lines). Unfortunately, available public literature is sparse of such studies (An example of analysis of 'mixed' lumped-distributed network is presented in Section 3.2).

It is important that the use of idealized dispersionless elements may (sometimes) predict behavior that is *physical* (within the limits given by linear stability analysis) and compatible with causality, but *still incorrect*. ([93], this report - Section 3.2.). This happens due to the unwanted ('parasitic') conductance and reactance of realistic generalized non-Foster elements (Figure 1-9). Thus, the issue of usefulness of stability prediction using idealized dispersion-free models of negative elements can be summarized as follows. If the network does not contain transmission lines and it is only important to predict whether it is stable or not, the analysis with ideal elements *might* give a correct answer and *might* help in identifying the 'problematic' parts. However, this result should be cross-checked by realistic models of negative elements (such as models developed in [51], which will be briefly reviewed in the next paragraph). Alternatively, one may use the 'subnetworks' comprising both ideal negative elements and ideal positive elements that together give behavior similar to behavior of a realistic dispersive negative element [92,103].

The widely accepted stability criterion in networks with ideal elements is that *the overall 'mesh'* capacitance or inductance must be a positive number [60,93]. A very thorough instigation reported in [2] confirmed this assumption for many simple combinations that contained not only reactive (L, C) elements but also resistive (R) elements. Thus, above criterion is extended *to overall 'mesh' resistance*, which should also be a positive number. Counter-intuitively, the same analysis showed stable behavior if the overall 'mesh' capacitance, inductance, and resistance *is negative.* Such all-negative network has reversed power flow [51,77], which is discussed in Section 3.3.4.

Very recently, it was shown that the criterion that requires positive (or negative) overall mesh capacitance, inductance and resistance of ideal dispersionless elements is not complete

[104]. The correct criterion was stated as 'Circuits are stable *if and only if every* negative capacitor and negative inductor has an adjacent series or shunt positive capacitor or positive inductor that "swamps" its reactance'. Of course this criterion can be extended to include the resistance and 'swamping 'of both positive and negative values is possible.

Finally, let us briefly review some of the methods of stability analysis and their connection to ideality (or non-ideality) of negative elements. Every negative element contains some kind of a controlled source (in practice, it is usually some active element such as BJT, FET or OPamp that acts as an amplifier). If an ideal amplifier with infinite bandwidth existed, a generated negative capacitance, inductance or resistance would also be ideal (i.e. dispersionless). However, the gain of every realistic amplifier (regardless of used technology) will always be band-limited and its amplitude and phase transfer functions must be connected via Hilbert transform (Kramers-Kronig relations). One may argue that a phase shift is negligible for practical purposes if the operating frequency is far below the frequency of the first pole of active element [39]. This may be true *but it does not mean* that one could use some method of stability analysis in frequency domain within this limited bandwidth. The stability prediction in phasor domain (steady-state analysis with real frequencies) should not be used at all. This approach neglects the transient response that is (as discussed in previous paragraph) crucial in generalized non-Foster circuits. This is connected to commonly used incorrect saying like 'This circuit is stable within frequency band of …'. Thus, stability analysis in the Laplace domain (with complex frequency $s = \sigma + j\omega$) or in the time domain is a first prerequisite (necessary, but not always sufficient!) for a reliable stability prediction. The methods that reduce the network to the equivalent 'black box' and then look at the properties of the 'black box' input port impedance (or reflection coefficient) may fail [2,87-89]. This happens due to the inherent poles located in the RHS of a complex plane, the existence of which cannot be inferred just from the analysis of the 'black box' input port reflection coefficient (the existence of so-called 'hidden modes') [87-89]). In order to avoid problems with hidden modes one should use the method (either in the Laplace domain or in the time domain) that takes into account *all the meshes and nodes* of the analyzed network.

3.1.3. Stability analysis based on realistic (dispersive) negative elements

In discussion in previous paragraph, it was stressed that commonly used 'mathematical' dispersionless model of an ideal non-Foster negative capacitor is nonphysical and it might be used only for the crude prediction of the qualitative behavior within a finite bandwidth. Outside this band, the model should not be used at all (even for qualitative analysis) because it gives unphysical behavior [51].

A simple, more realistic three-pole model of a dispersive negative capacitor was proposed in [51]. Indeed, a realistic negative capacitor can always be modelled as a dispersive voltage-controlled source, internal impedance of which is an ordinary positive capacitor. This model is capable of prediction of both basic physical phenomena and accurate dispersion characteristics.

Moreover, as shown in subsequent publication [41], this equivalent circuit clearly explains the origin of negative conductance that always accompanies negative capacitance, as well as the background physics of previously reported counter-intuitive phenomena in non-Foster metamaterials. Theoretical analysis was verified by simulations and measurements on an experimental low frequency (100 Hz – 25 kHz) demonstrator. The same strategy can be used for modelling negative inductance and negative resistance. This investigation silently indicated that, for realistic generalized non-Foster elements, the criterion which requires that each

element is 'swapped' with its neighbor *might not be always* valid. If this indication were true, it would open possibility for ENG/MNG/DNG –based applications.

Very recent findings on stability of 'mixed' lumped-distributed networks [84,93], which will be discussed in Section 3.2, confirm validity of above indication.

3.2. Stability of mixed lumped-distributed non-Foster networks

So far, stability of only lumped generalized non-Foster network (i.e. a network consisted of lumped negative capacitors, lumped negative inductors, and lumped negative resistors) has been reviewed. Presuming that a network comprises only ideal dispersionless elements it will be stable *if and only if every* negative capacitor, negative inductor, and negative resistor has an adjacent series or shunt positive capacitor or positive inductor that "swamps" its reactance (resistance) to positive or negative value. In other words, all 'effective' elements (the networks that comprises original and swamping elements) must have *the same sign*. It is instructive to revise the above statement using example of (probably) the most frequently used generalized non-Foster element: a negative capacitor.

A parallel combination of a positive resistor (R_{G}), a positive capacitor (C_{P}) and a negative capacitor (C_{N}) may be taken as a basic example of a non-Foster network (Figure 3-2).

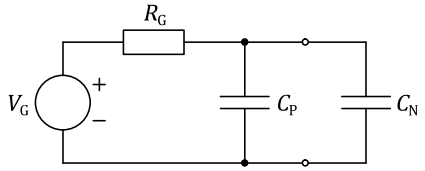

Figure 3-2 Basic lumped network with a parallel combination of positive and negative capacitor.

Here, one defines the transfer function as a ratio between the voltage drop across capacitors C_{P} and C_{N}, and a voltage across a 'disturbing generator' V_{G}. The complex frequencies ($s = \sigma + \mathrm{j}\omega$), for which the denominator of the transfer function becomes zero represent the system poles:

$$s = -\frac{1}{R_{\mathrm{G}} C_{\mathrm{EQ}}}, \quad C_{\mathrm{EQ}} = C_{\mathrm{P}} + C_{\mathrm{N}}, \tag{3.4}$$

where C_{EQ} is the equivalent (overall) capacitance of the parallel combination. The stability requires that all the system poles must be located in the LHS (left hand side) of a complex plain, which yields the following stability criterion:

$$C_{\mathrm{EQ}} > 0 \quad \rightarrow \quad |C_{\mathrm{P}}| > |C_{\mathrm{N}}|. \tag{3.5}$$

Thus, the circuit from Figure 3-2 is stable if the capacitance of a positive capacitor is greater than an absolute value of the capacitance of a negative capacitor.

In the case of a series combination of a resistor and positive and negative capacitor, the stability condition is exactly opposite ($|C_{\mathrm{P}}| < |C_{\mathrm{N}}|$) (though the overall capacitance of a series

combination again has to be positive). Of course, this simple analysis presumed that the network contains only ideal (i.e. dispersionless) positive and negative lumped elements [86,88].

As already mentioned in Chapter I, a number of practical circuits (both in antenna matching technology [71,105,106] and in active metamaterials [42,43]) are of mixed nature, i.e. they contain both lumped and distributed elements (transmission lines).

Unfortunately, there are only a few papers in the literature that deal with the influence of a transmission line on stability of non-Foster elements. Again, as already stressed before, some of them predict serious stability problems [92,107], while the other ones report successful practical realizations [42,43,105,106]. Thus, neither a clear physical picture of stability nor appropriate stability criteria are available for mixed generalized non-Foster networks.

In the next section, we discuss the simplest mixed network that comprises ordinary positive element and generalized non-Foster element (negative capacitor, negative inductor, or negative resistor) mutually connected via a segment of transmission line. This topology is present in many applications, particularly for the scenario with positive and negative capacitor. In the case of non-Foster matching [105,106] there may be a piece of transmission line connecting antenna feeding point and matching network. In the case of non-Foster metamaterial [42,43,71] (and non-Foster distributed amplifier [108]), there is a transmission line periodically loaded with non-Foster elements. Thus, the basic 'building element' is again a network that comprises two impedances mutually connected via a segment of transmission line. Actually, every practical generalized non-Foster element is always connected to some other impedance using leads that act as a segment of transmission line.

3.2.1. Basic concepts

Let us start with the analysis of a generic mixed network (Figure 3-3).

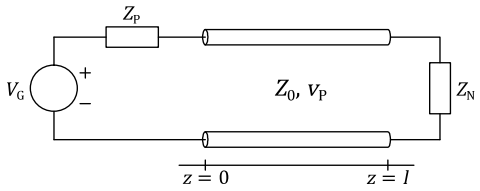

Figure 3-3 Generic mixed network with two impedances connected via an ideal lossless transmission line.

It comprises one positive (Z_P) and one negative impedance (Z_N), connected via a segment of an ideal transmission line described by its length (l), characteristic impedance (Z_0), and phase velocity (v_P). Using a standard transmission-line theory [109] one finds the voltage (in the Laplace domain), at the arbitrary observation point z on the transmission line (3.6).

$$V(z,s) = V_G \frac{Z_0}{Z_0 + Z_P} \cdot \left[e^{-\frac{sz}{v_P}} \sum_{n=0}^{\infty} \Gamma_N^n \Gamma_P^n e^{-\frac{s(2n)l}{v_P}} + e^{\frac{sz}{v_P}} \sum_{n=0}^{\infty} \Gamma_N^{n+1} \Gamma_P^n e^{-\frac{s(2n+2)l}{v_P}} \right] \tag{3.6}$$

The reflection coefficients Γ_{P} and Γ_{N} are defined at the input and output of the transmission line, respectively:

$$\Gamma_{\mathrm{P}}(s) = \frac{Z_{\mathrm{P}} - Z_0}{Z_{\mathrm{p}} + Z_0}, \quad \Gamma_{\mathrm{N}}(s) = \frac{Z_{\mathrm{N}} - Z_0}{Z_{\mathrm{N}} + Z_0} \tag{3.7}$$

Using (3.6) and (3.7) one derives the transfer function (defined as a ratio between the voltage at the transmission line observation point and the voltage of the disturbing source):

$$H(z,s) = Z_0 \frac{Z_0 \tanh\left(s\frac{l-z}{v_{\mathrm{P}}}\right) + Z_N}{\tanh\left(\frac{sl}{v_{\mathrm{P}}}\right) + \frac{Z_{\mathrm{N}}Z_0 + Z_{\mathrm{P}}Z_0}{Z_{\mathrm{N}}Z_{\mathrm{P}} + Z_0^2}}. \tag{3.8}$$

By equating the denominator of a transfer function (3.8) to zero, one derives the basic stability equation [110]:

$$\tanh\left(\frac{sl}{v_{\mathrm{P}}}\right) + \frac{Z_{\mathrm{N}}Z_0 + Z_{\mathrm{P}}Z_0}{Z_{\mathrm{N}}Z_{\mathrm{P}} + Z_0^2} = 0. \tag{3.9}$$

The solution of (3.9) gives the system poles for any mixed network that can be represented by Figure 3-3 (a transmission line inserted between any parallel or series combinations of positive/negative capacitors, inductors or resistors). In the most general case, (3.9) is a transcendental equation that cannot be solved analytically. Thus, a graphical method has been implemented in the Wolfram Mathematica™ programing environment. The method finds those complex frequencies s, for which the absolute value of LHS (left hand side) of (3.9) is less than arbitrary positive real number ε (required numerical precision):

$$\left|\tanh\left(\frac{sl}{v_{\mathrm{P}}}\right) + \frac{Z_{\mathrm{N}}Z_0 + Z_{\mathrm{P}}Z_0}{Z_{\mathrm{N}}Z_{\mathrm{P}} + Z_0^2}\right| < \varepsilon. \tag{3.10}$$

The solutions of (3.10) can be interpreted as closed areas in the complex plane, which contain the system poles. By decreasing the parameter ε, the solution area becomes smaller.

3.2.2. Transmission line with positive and negative resistor

The first and the simplest form of a generic 'mixed' network from Figure 3-3 is a transmission line that connects pure resistors (Figure 3-4). In the most general case, these resistors can have both positive and negative signs.

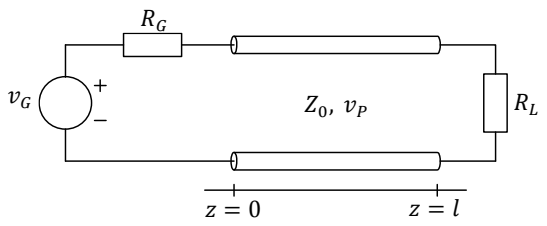

Figure 3-4 Mixed network containing a series combination of positive and negative resistor, connected via an ideal lossless transmission line.

Thus, Z_P and Z_N impedances are replaced with resistors R_G and R_L, respectively., Mathematically speaking, R_G and R_L are now real numbers ($R_G,\ R_L \in \mathbb{R}$).

This leads to an analytical expression for pole locations:

$$s = \frac{v_P}{l}\operatorname{artanh}\left(-\frac{R_L Z_0 + R_G Z_0}{R_L R_G + Z_0^2}\right). \tag{3.11}$$

Taking into account logarithmic definition of inverse hyperbolic tangent function, expression (3.11) can be written in different, simpler form:

$$s = \frac{v_P}{2l}\ln(\Gamma_G \Gamma_L). \tag{3.12}$$

Equation (3.12) leads directly to the stability criterion (3.13) of the network shown in Figure 3-4.

$$|\Gamma_G \Gamma_L| < 1 \tag{3.13}$$

Since the negative resistance can be interpreted as the energy source (a generator), (3.13) can be interpreted as follows: the network is stable if, and only if, the amount of energy dissipated on the positive resistance is greater than the amount of energy introduced by the negative resistance. It is important to stress that (3.13) is similar to the equations routinely used in design of microwave oscillators [19]. In Figure 3-5 it is shown which values of the resistance can be chosen in order for the network to be stable. Both resistances are normalized to the transmission line characteristic impedance.

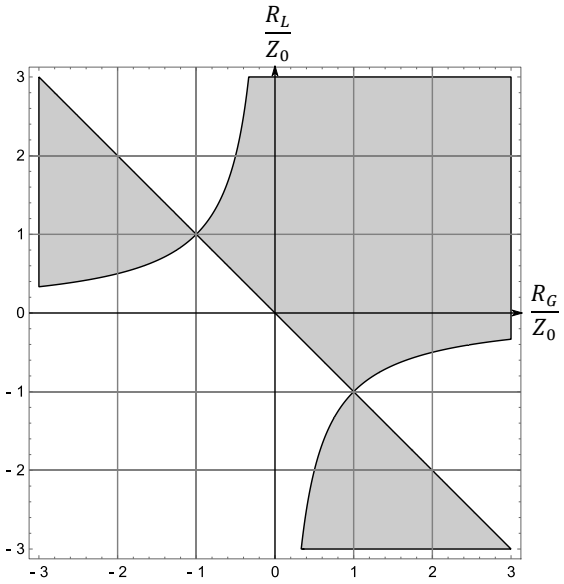

Figure 3-5 Graphical representation of stability criterion for networks with general resistors. Shaded areas represent resistance values that assure stabile operation.

It can be seen that the stability criterion of lumped networks ($R_G + R_L > 0$) is not valid any more. Mathematical explanation of this fact is that the connecting transmission line (at some complex frequency *s*) transforms resistance in such a way that the above inequality is not fulfilled.

Based on the equations (3.12) and (3.13), four different types of network impulse response can be determined:

- Stable exponential response ($0 < \Gamma_G\Gamma_L < 1$),
- Stable oscillatory response ($-1 < \Gamma_G\Gamma_L < 0$),
- Unstable exponential response ($\Gamma_G\Gamma_L > 1$),
- Unstable oscillatory response ($\Gamma_G\Gamma_L < -1$).

Finally, it can be noted that above analysis can be applied to so-called PT symmetry networks that are gaining popularity in electromagnetic community [84,85].

3.2.3. Transmission line with positive and negative capacitor

The next mixed network is shown in Figure 3-6.

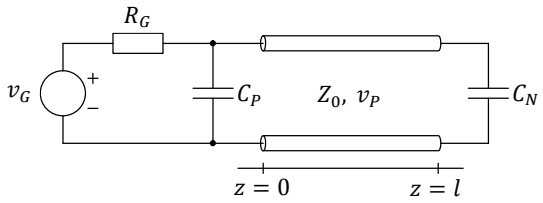

Figure 3-6 Mixed network containing a parallel combination of positive and negative capacitor, connected via an ideal lossless transmission line.

It comprises a positive capacitor C_P and a negative capacitor C_N, connected as a 'parallel' circuit via a segment of a transmission line. In this example, both capacitors are assumed to be ideal (i.e. dispersionless). By applying Thévenin theorem, this network is transformed to a generic network from Figure 3-3:

$$Z_\mathrm{N} = \frac{1}{sC_\mathrm{N}}, \quad Z_\mathrm{P} = \frac{R_\mathrm{G}}{1 + sR_\mathrm{G}C_\mathrm{P}}. \tag{3.14}$$

When all the elements of the generic network (Figure 3-3) are known, (3.10) is solved graphically (Figure 3-7 (a)). Please note that the capacitances were chosen to satisfy (3.5). If this were the case of a simple parallel combination of two capacitors (Figure 3-2), one would have stable behavior (3.4), (3.5). However, the inclusion of a transmission line fundamentally changes the stability issue (Figure 3-7 (a)).

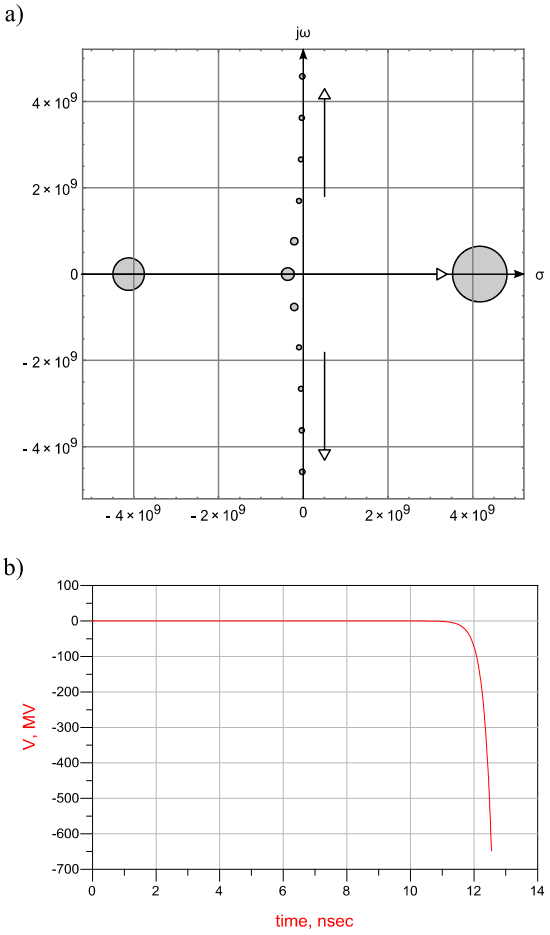

Figure 3-7 a) Pole locations of the network containing an ideal positive capacitor and an ideal negative capacitor, connected via a lossless transmission line (Fig. 3-6 (c). Parameters used in calculation: $l = 1$ m, $v_{\mathrm{P}} = 3 \cdot 10^8$ m/s, $Z_0 = 50\ \Omega$, $R_{\mathrm{G}} = 50\ \Omega$, $C_{\mathrm{P}} = 15$ pF, $C_{\mathrm{N}} = -5$ pF, $\varepsilon = 0.25$. b) Voltage across negative capacitor obtained by ADS$^{\mathrm{TM}}$ transient simulation (excitation was single-pulse voltage source (amplitude of 1V, the width of 3 ns and 1 ns rise and fall time)).

It should be noted that the initial value of a transmission line length (1m) was chosen completely arbitrary. It can be seen that there is a stable system pole located on the real axis in LHS of the complex plane. But, there is also another real pole in RHS (right hand side) of the complex plane, associated with unbounded exponential growth of the DC signal (a signal of $\mathrm{e}^{\sigma t}$ form). Now, let us assume than the length of the connecting transmission line (l) is decreased. On the first sight, one might expect that this shortening contributes to the stability, since a circuit with shorter transmission line becomes more similar to a simple lumped circuit with two capacitors (Figure 3-2). However, the pole locus in Figure 3-7 (a) reveals unexpected behavior. If the length of the line (l) is decreased, the unstable RHS real pole shifts towards $+\infty$ (it is denoted by the horizontal arrow in Figure 3-7 (a)). This movement causes steeper exponential growth of the DC signal (parameter σ in $\mathrm{e}^{\sigma t}$ becomes larger) i.e. the instability of a network is more pronounced. Surprisingly, the network is unstable for any finite line length. However, when the length becomes zero, the real pole 'jumps' from $+\infty$ to $-\infty$, and the network suddenly

becomes stable (a network reduces to a stable lumped network from Figure 3-2). This is certainly a counter-intuitive behavior.

It may seem that this effect has serious consequences on the realization of stable practical devices based on negative capacitors and transmission lines (antenna matching circuits [29,105,106], metamaterials [42,43,71,111] etc.). Fortunately, (as it will be shown later) the unavoidable band-limited operation of realistic negative capacitor may assure stability in practice. Mathematically, the function that describes real RHS pole position has discontinuity at $l = 0$ with different left-sided and right-sided limits (as l approaches zero). Physical explanation is much more subtle and peculiar. An ideal negative capacitor has the same capacitance for all the complex frequencies ($s = \sigma + \mathrm{j}\omega$) i.e. the negative capacitance is dispersionelss across the whole complex plane. It means that the ideal negative capacitor can operate with all possible signal waveforms. Among others, these include steady-state sinusoidal signals (signals of the $\mathrm{e}^{\mathrm{j}\omega t}$ form, associated with $j\omega$ axis and defined for every angular frequency ω), but also zero-frequency exponentially growing signals (signals of the $\mathrm{e}^{\sigma t}$ form, associated with σ axis and defined for every signal 'stiffness' σ). This exponential signal satisfies time-domain wave equation, so it is a physically valid excitation signal. As all other time-varying signals, it does propagate along a transmission line, it does experience reflection, it does build up a standing wave and it does transform the load impedance. Thus, for a particular value of σ, the reactance of negative capacitance ($1/(\sigma C_{\mathrm{N}})$) will be transformed into a new input reactance that does not satisfy the ordinary stability criterion (3.5). Since the maximal value of σ is not bounded in any way, this transformation will occur for every length of the transmission line (including arbitrary short line with $l \neq 0$). Formally, this effect is similar to the well-known impedance transformation along a transmission line for angular frequencies ω (steady-state $\mathrm{e}^{\mathrm{j}\omega t}$ signals). Going back to Figure 3-7 (a), there is also an infinite number of poles located along the imaginary ($\mathrm{j}\omega$) axis. These poles primarily depend on ω (angular frequency) and describe the 'periodic' behavior of a transmission line (well-known impedance transformation). The shortening of a transmission line increases the mutual distance between neighboring poles (denoted by vertical arrows in Figure 3-7 (a)).

Locations of all the poles in Figure 3-7 (a) have been cross-checked numerically. In addition, the stability of the network was verified by transient simulations in a commercial circuit-theory simulator Advanced Design System (ADS$^{\mathrm{TM}}$). Briefly, the 'disturbing generator' was modeled as a single-pulse voltage source while the response signal (voltage) was monitored (at the input of negative capacitor). Results (Figure 3-7 (b)) revealed expected unbounded exponential growth associated with the RHS real pole. Of course, in practice, the maximal voltage will be limited by the DC power supply of the amplifier.

A 'series' case (a mixed network containing a series combination of positive and negative capacitor, connected via an ideal lossless transmission line), was analyzed, as well (results not shown due to brevity). Briefly, this case shows intuitive behavior: a shortening of the connecting transmission line shifts unstable pole towards the origin and the network becomes more and more similar to a lumped network.

3.2.4. Transmission line with positive and negative inductor

Stability analysis of the network containing series of ideal positive and negative inductor, with an ideal lossless transmission line is based on the network shown in Figure 3-8.

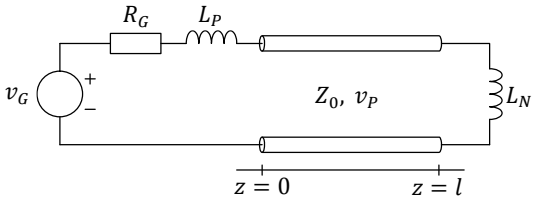

Figure 3-8 Mixed network containing a series combination of positive and negative inductor, connected via an ideal lossless transmission line.

According to the figure, Z_N and Z_P in (3.9) can be replaced with the expression from (3.15). Those expression are used in the following stability analysis.

$$Z_G = R_G + sL_P, \quad Z_L = sL_N \tag{3.15}$$

Again, in analysis of the lumped network ($l = 0$), one can analytically find the location of a network pole in a complex plane using (3.9) and (3.16).

$$s = -\frac{R_G}{L_{EQ}}, \quad L_{EQ} = L_P + L_N \tag{3.16}$$

According to (3.16), there is only one pole placed at the real axis of complex plane, just like in the previously analyzed cases. Here L_{EQ} represents the equivalent inductance of a series L_P-L_N combination, composed of positive (L_P) and negative (L_N) inductor. Since R_G is a positive real number, L_{EQ} must also be positive in order the network to be stable. This leads to the stability criterion (3.17) of the lumped series inductors shown in Figure 3-8.

$$|L_P| > |L_N| \tag{3.17}$$

For the analysis of the series inductor topology network with the transmission line, length of which defers from zero, a graphical method is used. This analysis is also based on equations (3.9) and (3.15) and performed in the *Wolfram Mathematica* environment. Approximate pole locations are shown in Figure 3-9. As expected, there is a single pole placed at the real axes in RHP of complex plane, which makes the network unstable. All pole shifts caused by shortening of the transmission line length are indicated by arrows. The same network behavior is observed as in the case of the networks with parallel combination of ideal positive and negative capacitors. Since L_G and L_L are chosen to satisfy (3.17), it is expected that the shortening of the transmission line length contributes to the stability of the network, but again, this is not the case. There is a counterintuitive shift of the critical unstable pole along the real axes toward infinity, which makes series inductors network inherently unstable for any $l \neq 0$.

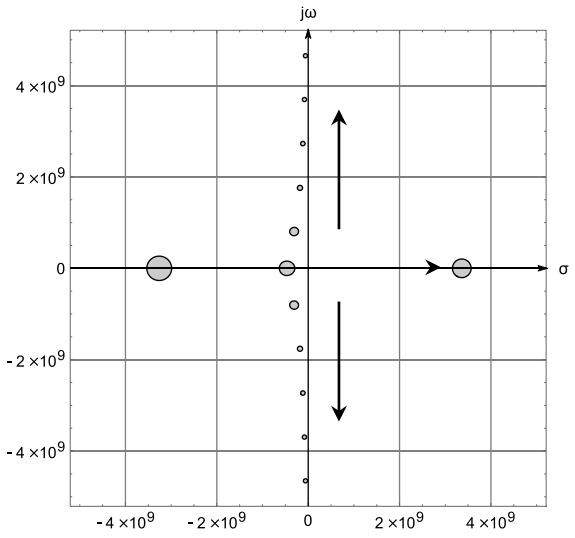

Figure 3-9 Approximate pole location of the network containing series of ideal positive and negative inductors

A 'parallel' case (a mixed network containing a parallel combination of positive and negative inductor, connected via an ideal lossless transmission line), was also analyzed (results not shown due to brevity). Briefly, this case shows intuitive behavior: shortening of the connecting transmission line shifts unstable pole towards the origin and the network becomes more and more similar to a lumped network.

It would be interesting to analyze all previous examples with realistic dispersive elements. Due to brevity, only the case of realistic negative capacitor (which is most common in practice) is presented in the next paragraph.

3.2.5. Networks with realistic negative capacitor

Analysis presented so far dealt with a negative capacitor as a simple mathematical dual of an ordinary positive capacitor. One of the possible practical implementations is sketched in Figure 3-10. Here, a positive capacitor C_{F} is placed inside of a positive feedback loop of a voltage amplifier, excited by the input voltage V_{IN}.

If the voltage gain of the amplifier is larger than unity ($A > 1$), the voltage drop across the capacitor C_{F} will become negative ($V_{\mathrm{CF}} = V_{\mathrm{IN}} - V_{\mathrm{OUT}} = (1 - A)V_{\mathrm{IN}}$). The input current I_{IN} will also be negative, which generates negative input impedance (and, therefore, the negative input capacitance C_{IN}):

$$Z_{\mathrm{IN}}(s) = \frac{V_{\mathrm{IN}}(s)}{I_{\mathrm{IN}}(s)} = \frac{1}{1 - A(s)} \frac{1}{sC_{\mathrm{F}}} = \frac{1}{sC_{\mathrm{IN}}},$$
$$C_{\mathrm{IN}} = [1 - A(s)]C_{\mathrm{F}}. \tag{3.18}$$

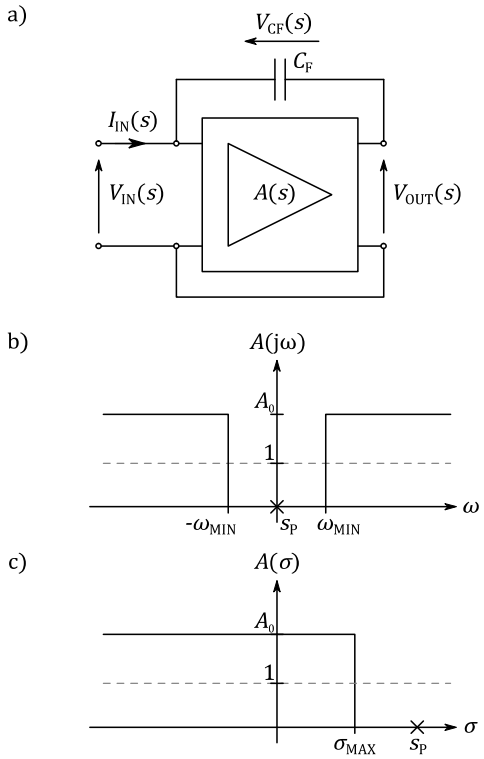

Figure 3-10 a) Realization of negative capacitor using voltage amplifier, b) Stability enforcement by limiting the gain bandwidth in $\boldsymbol{j\omega}$ domain, c) Stability enforcement by limiting the gain bandwidth in $\boldsymbol{\sigma}$ domain.

If the amplifier gain $A(s)$ in (3.18) were a constant (an ideal zero-delay amplifier with infinite bandwidth), generated negative capacitance would also be ideal (i.e. dispersionless). However, the gain of every realistic amplifier (regardless of used technology) will always be band-limited. In other words, realistic negative capacitor will always be band-limited and dispersive device. On the other hand, as shown earlier, the instability primarily occurs due to an unwanted transformation of negative capacitance along the transmission line, for exponential signals of $e^{\sigma t}$ form. Now, let us suppose that the inherent dispersion is tailored in a way that does not allow a negative capacitance phenomenon in the areas of complex plane, within which the RHS pole is expected (Figure 3-10, (b)) and Figure 3-10, (c)). In the first concept (Figure 3-10,(b)), the gain drops below unity for signals with $\omega < \omega_{MIN}$. Please note that this includes the DC signals ($\omega = 0$). Since gain is lower than one, neither the negative capacitance effect can exist (3.18) for DC signals, nor can the RHS pole be located on real axis. This 'high-pass' design of non-Foster capacitor 'avoids' the occurrence of the RHS real pole and assures stability. Alternatively, it is possible to limit the bandwidth for exponential signals (i.e. to limit the bandwidth in σ domain). Indeed, there is no realistic amplifier that can respond to step excitation instantaneously. There is always a finite 'slew rate' given by some maximal value of σ_{MAX}. If $\sigma_{MAX} < s_P$ (s_P is a real RHS pole in the case of ideal dispersionless negative capacitor) the system will be stable. Physically, the system cannot respond fast enough to excite the instability.

It is clear that the idealized rectangular gain functions in Figure 3-10, (b) and Figure 3-10, (c) are not possible in practice since their impulse responses are not causal. Realistic gain function has more complicated shape. It is a complex function, real and imaginary parts of which are inevitably mutually connected via Hilbert transform (Kramers-Kronig relations). In spite of this, the basic principle of tailoring the operation bandwidth is still feasible. Application of this principle turns the (usually disadvantageous) inherent dispersion of realistic negative

capacitors into a very useful feature that assures stable operation. In order to analyze a realistic non-Foster capacitor, the amplifier in Figure 3-10, (a) is modeled using a one-pole gain function:

$$A(s) = \frac{A_0}{1 + s\tau}, \quad \omega_{\mathrm{P}} = \frac{1}{\tau}. \tag{3.19}$$

Here τ stands for the amplifier time constant, associated with pole frequency ω_{P} (cut-off frequency of an amplifier). If $\tau = 0$, the model reduces to the ideal non-dispersive case with infinite bandwidth. Using (3.18), (3.19) one finds the input impedance:

$$Z_{\mathrm{IN}} = \frac{1 + s\tau}{1 + s\tau - A_0} \frac{1}{sC_{\mathrm{F}}}. \tag{3.20}$$

In steady-state ($\sigma = 0$) it is more convenient to think of the equivalent input admittance ($\overline{Y_{\mathrm{IN}}}(\omega) = G_{\mathrm{IN}}(\omega) + \mathrm{j}\omega C_{\mathrm{IN}}(\omega)$), which consists of a parallel combination of a dispersive capacitance $C_{\mathrm{IN}}(\omega)$ and a dispersive conductance $G_{\mathrm{IN}}(\omega)$:

$$C_{\mathrm{IN}} = C_{\mathrm{F}}\left[1 - \frac{A_0}{1 + \omega^2\tau^2}\right], \quad G_{\mathrm{IN}} = -\frac{A_0 C_{\mathrm{F}}\omega^2\tau}{1 + \omega^2\tau^2}. \tag{3.21}$$

At some particular frequency gain drops to unity and generated capacitance becomes zero. By further increase of the frequency, input capacitance approaches (positive) capacitance C_{F}. On the other hand, the delay of the amplifier causes the occurrence of dispersive negative input conductance (3.21), which becomes more and more pronounced with the increase of the frequency. Of course, this negative conductance degrades the performance of a negative capacitor. Using (3.21) it can be shown that the 'Q factor' decreases with frequency and it reaches value of 10 at the frequency equal to approximately one tenth of the pole frequency ($\omega \approx 0.1/\tau$).

In order to investigate the influence of aforementioned imperfections on stability, a new variant of the network in Figure 3-2 (a lumped network with two capacitors connected as parallel combination and driven by a voltage source with internal resistance) has been analyzed.

Here it is assumed that a negative capacitor has realistic behavior, given by (3.18) and (3.19). It leads to the quadratic equation, roots of which represent the system poles:

$$s = \frac{-b \pm \sqrt{b^2 - 4ac}}{2a} \tag{3.22}$$

$$\begin{gathered} a = \tau R_{\mathrm{G}}(C_{\mathrm{P}} + C_{\mathrm{F}}), \\ b = \tau + R_{\mathrm{G}}[C_{\mathrm{P}} + (1 - A_0)C_{\mathrm{F}}], \\ c = 1. \end{gathered} \tag{3.23}$$

Analysis of (3.22) and (3.23) reveals that the network with a realistic negative capacitor has two complex poles in the most general case. By enforcing the requirement ($\mathcal{R}e\{s\} < 0$), one gets the new stability criterion:

$$|C_{\mathrm{F}}(1 - A_0)| < C_{\mathrm{P}} + \frac{\tau}{R_{\mathrm{G}}}. \tag{3.24}$$

In some sense, (3.22) resembles (3.5) from the ideal lumped-element case. The LHS of (3.15) represents the absolute value of minimal input negative capacitance (negative capacitance at $\omega = 0$). However, the RHS of (3.24) contains not only the capacitance of the positive capacitor, but also an additional term (τ/R_{G}). This 'effective capacitance' is caused by one-pole low-pass

behavior of the used amplifier and it (as it will be shown later) fundamentally changes the stability issue. Using (3.22) and (3.23) one finds different stability regions for different values of $|C_{\mathrm{IN}}|$ (at $\omega = 0$) and C_{P} (Figure 3-11, (a), solid curves).

In region 1, the network has stable exponential impulse response (real LHS pole, signal of $\mathrm{e}^{\sigma t}$ form, $\sigma < 0$) and the positive capacitance is always larger than the negative capacitance. Thus, this region is convenient for applications in antenna matching systems, active broadband ENZ metamaterials and related devices [29,42,43,71,105,106,108,111]. With the decrease of the time constant τ, region 1 becomes larger (the system is more similar to ideal dispersionless case). In region 2, the network has stable response with damped diminishing oscillations (complex LHS poles, signal of $\mathrm{e}^{(\sigma+\mathrm{j}\omega)t}$ form, $\sigma < 0$).

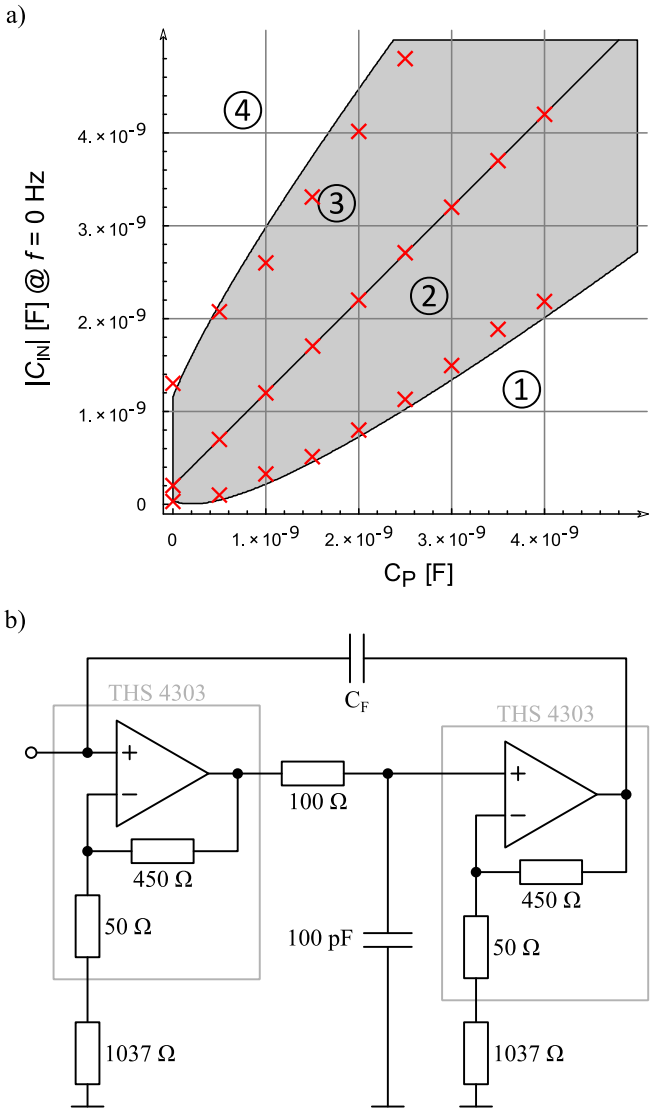

Figure 3-11 a) Stability regions for lumped network (Fig. 3-2 (a)) containing parallel combination of an ideal positive and a realistic negative capacitor. Solid curves: Results obtained using analytical expressions (3.22, 3.23) and one-pole amplifier model, ($R_{\mathrm{G}} = 50\ \Omega$, $\tau = 10$ ns, $A_0 = 2$, parameters C_{P} and C_{F} are varied). Crosses: Results obtained by ADS-SPICE simulation of negative capacitor based on operation amplifier THS 4303. b) Schematic diagram of negative capacitor based on operation amplifier THS 4303 and used in ADS-SPICE simulation. The biasing (±2.5 V) is not shown.

Surprisingly, the overall capacitance over here can be negative (for some values of C_{P} and C_{F}). This is an *entirely new and striking property* that might open up possibility of construction of stable non-Foster Epsilon-NeGative metamaterials (so far, this was considered as non-feasible [42]) Of course, with the decrease of time constant τ region 2 becomes smaller. The boundary between region 2 and region 3 is associated with loss-free oscillatory behavior (purely imaginary poles, signal of $\mathrm{e}^{\mathrm{j}\omega t}$ form, $\sigma = 0$). Above this boundary there are two unstable regions. Region 3 causes unstable growing oscillatory response (complex RHS poles, signal of $\mathrm{e}^{(\sigma+\mathrm{j}\omega)t}$ form, $\sigma > 0$). Region 4 supports unstable exponential response (real RHS pole, signal of $\mathrm{e}^{\sigma t}$ form, $\sigma > 0$).

Although predicted phenomena have strong physical background, one may wonder whether this simple model can be applied in the case of a practical negative capacitor. Practical devices are based on amplifiers that have many properties not included in the above simple model (more complicated frequency characteristic, finite input and output impedances, finite slew-rate etc.). In order to investigate this important issue, we repeated the whole analysis with a negative capacitor designed using commercial active elements. This negative capacitor is based on two high-speed operational amplifiers THS 4303 (Figure 3-11, (b)). It is configured as a non-inverting chain with $A \approx 2$ and the dominant pole defined with a RC time constant $\tau = 10$ ns). Positive feedback loop is connected across the whole chain and it contains an 'inverting' capacitor C_{F} (value of which is varied in this example). In this way, the circuit from Figure 3-11, (b) is a practical implementation of basic idea from Figure 3-10, (a). The SPICE model of THS 4303 (provided by manufacturer [112]) was imported into ADS™ and the case from Figure 3-2 was simulated again. Obtained results are given in the form of 'cross' markers in Figure 3-11, (a). It can be seen that four stability regions are still present and the boundaries are similar to those obtained by simple one-pole model. This simulation, which includes all non-idealities of the used amplifier, is an independent validation of analytically predicted phenomena.

In the last step, the transmission line was inserted between an ideal positive capacitor and a realistic negative capacitor modeled with a 1-pole amplifier (a network from Figure 3-6, with the negative capacitor model from (3.10)). Again, the network was reduced to a generic network (Figure 3-3, (b)) using the following substitutions:

$$Z_{\mathrm{N}} = Z_{\mathrm{IN}} = \frac{1+s\tau}{1+s\tau-A_0}\,\frac{1}{sC_{\mathrm{F}}}, \quad Z_{\mathrm{P}} = \frac{R_{\mathrm{G}}}{1+sR_{\mathrm{G}}C_{\mathrm{P}}}. \tag{3.25}$$

Here Z_{N} is the impedance of a realistic capacitor (Z_{IN}) and Z_{P} represents a parallel combination of R_{G} and C_{P} (Thévenin impedance). The sample of pole loci (obtained by a graphical method) is shown in Figure 3-12.

The capacitors C_{P} and C_{F} were chosen in a way that yields $|C_{\mathrm{P}}| > |C_{\mathrm{IN}}|$ (at $\omega = 0$). In other words, the capacitances satisfy traditional stability criterion for the ideal dispersionless case. It was shown earlier that the network in Figure 3-6 is always unstable, for every finite length of the transmission line different than zero. However, in this case with a realistic capacitor, there is no RHP pole and the network is stable (for the set of parameters given in Figure 3-12). The shortening of a transmission line again increases the mutual distance between neighboring 'periodic' poles (denoted by vertical arrows in Figure 3-12). During this process, there are no poles that enter the RHS of a complex plane, thus, the network remains stable. The analysis was repeated for many different values of design parameters and it was found that the amplifier time constant (τ) has the largest impact on stability. If this constant is chosen properly, the influence of the length of transmission line on stability is negligible. As in the previous case, this behavior was cross-checked by ADS™ transient simulations using both simple one-pole model and a full SPICE model of practical negative capacitor from Figure 3-11 (in this example,

$C_F = 5$ pF). The results from both approaches match pretty well (Figure 3-12). It can be seen that the response diminishes with time, so the network is indeed stable. This is unexpected but, at the same time, rather convenient behavior that has not been observed so far. This might be the explanation why some experimental studies reported stable operation [42,43,105,106] although theoretical analysis with ideal dispersionless elements predicts instability. Moreover, it was found that (for properly chosen time constant τ), the absolute value of maximal negative input capacitance (capacitance at $\omega = 0$) can be larger than the positive capacitance. This is an important property that could find applications in future broadband ENG metamaterials.

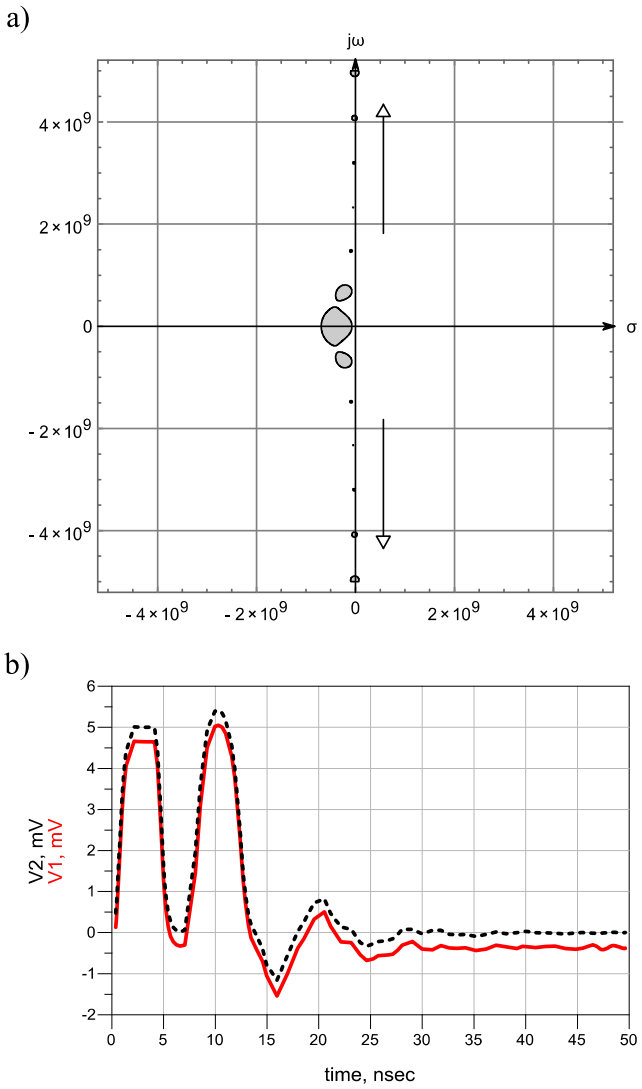

Figure 3-12 a) Pole locations of the network containing an ideal positive capacitor and a realistic negative capacitor, connected via a lossless transmission line (Figure 3-6). Parameters used in calculation: $l = 1$ m,$v_P = 3 \cdot 10^8$ m/s, $Z_0 = 50\ \Omega$, $R_G = 50\ \Omega$, $C_P = 15$ pF, $C_F = 5$ pF, $A_0 = 2, \tau = 10$ ns, $\varepsilon = 0.7$. b) Voltage across negative capacitor obtained by ADS^{TM} transient simulation. Excitation was a single-pulse voltage source with the amplitude of 10 mV, the width of 3 ns and the rise and fall time of 1 ns. Dashed curve: A negative capacitor was modeled using one-pole amplifier model with parameters stated above. Solid curve: A negative capacitor was modeled using SPICE model of operational amplifier THS 4303 (Figure 3-11).

One concludes that the widely accepted stability criterion of positive 'mesh' capacitance fails for parallel combination of positive and ideal negative capacitor with connecting transmission line. Such a network is always unstable, regardless of the line length and capacitance values of positive and negative capacitor. However, the inherent dispersion of a realistic negative capacitor (usually considered as a drawback) can be tailored in a way that assures stable operation. Surprisingly, in some cases of lumped and mixed networks with realistic model of negative capacitor, stable operation is feasible even if overall capacitance is negative.

3.3. Band-limited non-Foster networks for metasurface unit cell

One of the hot research topics in artificial EM structures is surely the field of metasurfaces [21]). If one compares a metasurface with a volumetric metamaterial, he will probably find that a smaller number of unit cells (that results with lower losses) and a very simple fabrication are the main advantages. Thinking of active non-Foster metasurfaces, one recognizes yet another advantage: Significantly better robustness to instability. Indeed, it is reasonable to expect that a smaller number of active unit cells decreases the possibility of mutual electromagnetic interactions that could lead to instability. In addition, for normal incidence of an electromagnetic wave, the active metasurface behaves very similarly to a pure lumped circuit (Figure 3-13). The equivalent circuit of interaction is essentially a transmission line loaded with one shunt admittance. Of course, the value of this shunt admittance changes for oblique incidence of an impinging wave. In spite of that, the unwanted instability problems associated with 'mixed network' (detailed in Section 3.2) are less pronounced. Therefore, it would be very convenient to design a simple *lumped* metasurface unit cell that could lead to metasurfaces with negative inductive, negative capacitive, or negative resistive surface reactance (i.e. a surface equivalent of MNG/ENG effects). Thus, one needs a stable, band-limited non-Foster network that would act as a negative capacitance/inductance/resistance loading of a small dipole or loop antenna, usually used in metasurface inclusion.

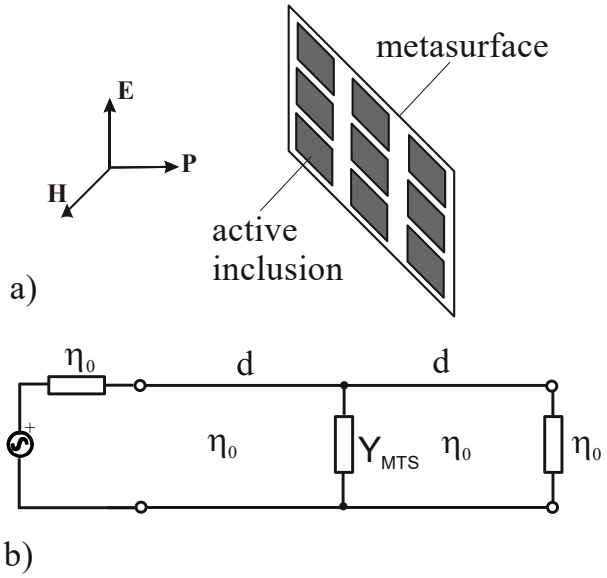

Figure 3-13 a) An EM wave impinging on active metasurface, b) transmission-line-based equivalent circuit

3.3.1. Band-pass negative capacitor: basic concepts

The analysis presented in Section 3.2. revealed that the presence of a transmission line within a (generalized) non-Foster network has very significant impact on its stability. This inconvenient fact can be attributed to a real pole that resides in RHP of a complex plane. Occurrence of a real RHS pole is associated to the generalized impedance transformation properties of the transmission line, which vary with a complex frequency *s*. If *all negative elements were ideal* (dispersionless), there would *always* be some critical complex frequencies. At these frequencies, a value of passive termination (resistance, capacitance, or inductance) is transformed to the new impedance (at the input of a transmission line (Figure 3-3) in a way that the system becomes unstable. However, if a given negative element is not ideal, it is in principle possible to 'limit' operation complex frequencies to those at which generalized impedance cannot yield unwanted impedance value. Simply stating, one should somehow limit the operating region in a complex plane in a way that does not allow occurrence of a real RHS pole. As detailed in the previous paragraph, this procedure actually limits the bandwidth for exponential signals.

Clearly, the σ and ω domains are always bound to each other. This is a direct consequence of the properties of Hilbert transform (Kramers-Kronig equations [8]). Therefore, if a response of an amplifier is limited in ω domain (for sinusoidal excitation), it will inevitably be limited in σ domain (for exponential signal excitation). Generalized bandwidth, used in [93], can be defined as a range of complex frequencies, for which the amplifier has voltage gain higher or equal to one (for this range of complex frequencies, the generation of negative capacitance is possible). With the help of (3.19) one finds the following inequality:

$$|A(s)| \geq 1 \rightarrow \left|\frac{A_0}{1+s\tau}\right| \geq 1 \tag{3.26}$$

Having in mind that $s = \sigma + j\omega$, a region of complex frequencies, for which previously defined condition is satisfied, can be found:

$$(\sigma + \omega_{\mathrm{P}})^2 + (\omega)^2 \leq (A_0\omega_{\mathrm{P}})^2. \tag{3.27}$$

By inspection of the expression (3.27) one concludes that the defined region is a circle shifted to the left by the amplifier pole frequency ω_P. The example of such a circle is shown in Figure 3-14. Radius of the circle is defined as a product of DC gain A_0 and the pole frequency ω_P. In the case of an ideal amplifier the time constant is zero (infinite pole frequency). This makes the radius of the circle infinite, which corresponds to infinite bandwidth. Introduction of a one-pole amplifier with finite pole frequency shrinks the generalized bandwidth circle.

It is clear that gain exists not only for sinusoidal signals, but also for exponential signals, and of course for their combination. It is interesting that the bandwidth is symmetric in ω, and asymmetric in σ domain.

To limit the bandwidth of an amplifier means to reduce the gain of an amplifier used for non-Foster element realization (in other words, limit the radius of previously described circle) in a way to make sure that amplifier's gain is lower than unity at the frequency at which the RHS pole is expected. The generalized bandwidth circle should not 'cover' the region of a complex plane in which the RHS pole is expected (a part of σ axis).

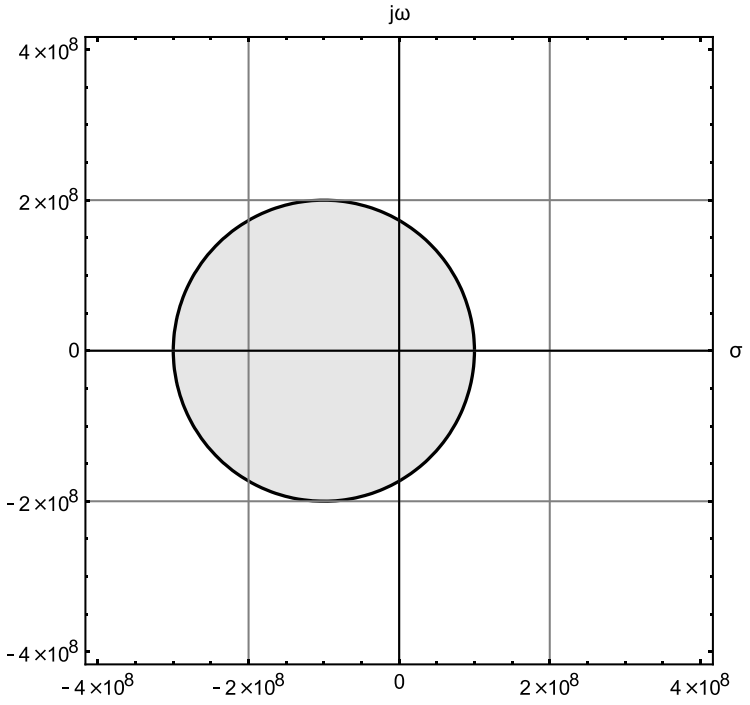

Figure 3-14 An example of generalized bandwidth circle in complex s-plane ($A_0 = 2$ and $\tau = 10$ ns).

There is a strong physical 'intuition' that complements aforementioned mathematical explanation. Let us suppose that an ideal dispersionless negative (non-Foster) element is indeed a physically feasible device. Due to infinite bandwidth, such an element would respond to every excitation instantaneously. Thus, equivalent 'continuous building material' of this element would not support any form of 'electric' or 'magnetic polarization' accompanied with mechanical inertia. In other words, the 'continuous building material' would behave as vacuum, which is a contradiction to the hypothesis of the existence of ideal non-Foster element. One may argue that this is nothing more than a narrative form of Kramers-Kronig equations but please note that the perquisite of stability (no poles residing in RHS of a complex plane) is not mentioned at all.

Since it is clear that any practical implementation of negative element must be band-limited one could *deliberately* incorporate limited bandwidth into the design process. This should improve stability properties substantially. Apart from above discussion that indicates that unstable 'DC pole' can be avoided by limiting the bandwidth (either for real or imaginary frequencies) of an amplifier used for construction of non-Foster element, there is another theoretical study [81] that introduced hypothetical lossless 'bandpass' non-Foster elements. They possess negative capacitance (or negative inductance) within a finite frequency band and positive inductance (or positive capacitance) outside of it.

3.3.2. Band-pass negative capacitor: theoretical investigation

(*The part of the results presented in sections 3.3.2. and 3.3.3 were achieved with the help of Dominik Zanic, who is a graduate student at University of Zagreb, Faculty of Electrical Engineering and Computing).

The block-diagram of a band-pass negative capacitor is sketched in Figure 3-15.

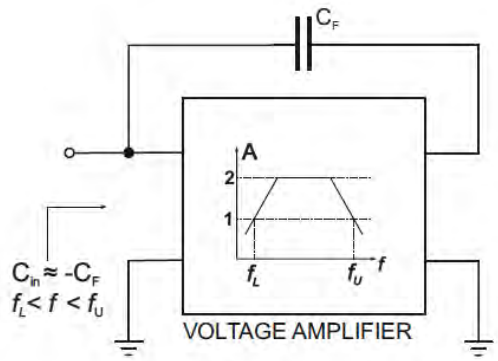

Figure 3-15 Implementation of a negative capacitor based on a voltage amplifier, using a 'bandpass' design that prevents occurrence of unstable 'DC pole'

The basic idea of avoiding occurrence of unstable 'DC pole' is to prevent the generation of negative capacitance for ω=0. Thus, the active element (modelled as a voltage amplifier in Figure 3-15) should have a frequency characteristic that is limited *for both high and low frequencies* (i.e. it should be of 'bandpass' type). More precisely, the gain should be lower than 1 at ω=0. For instance, it can be achieved by implementation of the amplifier transfer function A that has two time constants (τ_1 and τ_2):

$$A = \frac{A_0 s\tau_1}{(1+s\tau_1)(1+s\tau_2)}. \tag{3.28}$$

Here, s stands for a complex frequency ($s=\sigma+j\omega$). A straightforward derivation of input capacitance shows that it is positive for ω=0, preventing the existence of unstable 'DC pole'.

In the first step, the stability of proposed bandpass negative capacitor was investigated analytically. Again, it was assumed that a negative capacitor is shunted by external positive capacitor C_{EXT} and resistor R_{EXT}, and the system poles were sought. The derivation led to a cubic polynomial, the poles of which are enforced to reside in LHP of a complex plane by varying several system parameters. A rather representative sample of obtained results is shown in Figure 3-16 and Figure 3-17.

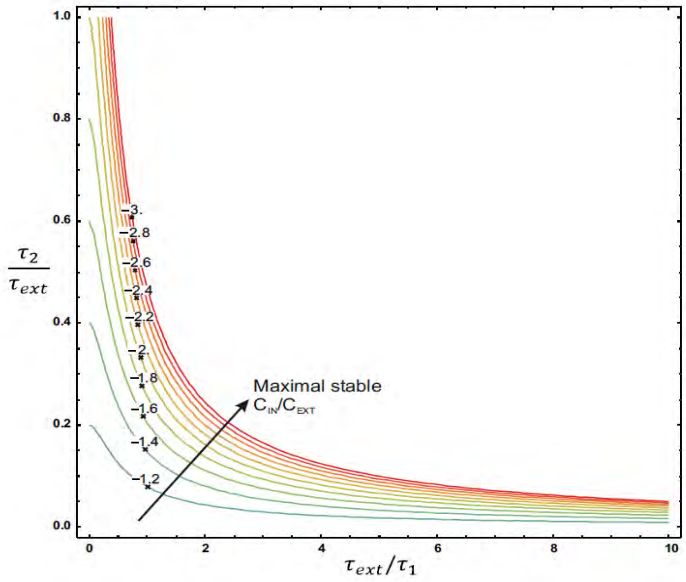

Figure 3-16 Bandpass negative capacitor – Contour plot of maximal stable normalized negative capacitance (obtained analytically)

It depicts a contour plot of maximal normalized negative input capacitance (C_{IN}/C_{EXT}) as a function of both amplifier time constants, normalized to the external time constant:

$$\tau_{ext} = R_{ext}\, C_{ext}. \tag{3.29}$$

There are several important properties that can be deduced from Figure 3-16. Firstly, it is possible to generate a stable overall negative capacitance that (for the given set of parameters) can be as large as $-3C_F$. In other words, in active metasurface applications, this approach can generate effective negative susceptance. This susceptance (again, for the given set of parameters) is equivalent to the slab bulk permittivity up to $-3\varepsilon_0$, ε_0 being the free-space permittivity. Thus, surface ENZ and MNZ phenomena are possible. At second, larger values of generated negative capacitance are possible by allowing higher losses in external circuit (i.e. by lowering R_{EXT}). At third, generated negative capacitance is inversely proportional to the amplifier bandwidth B (defined as $\omega_2/\omega_1=\tau_1/\tau_2$, $\omega_1$and ω_2 being lower and upper cut-off frequency, respectively).

The influence of the amplifier bandwidth on maximal generated negative capacitance can be understood in a more details with the help of Figure 3-17. It shows maximal stable normalized negative capacitance as a function of the amplifier bandwidth B, while the parameter τ_2/τ_{ext} is varied. It can be seen that higher values of normalized time constant enable larger absolute value of input negative capacitance. However, the increase of maximal absolute value of generated negative capacitance (in other words, a more pronounced ENG effect) is accompanied with the decrease of bandwidth. In a sense, this behavior appears to be similar to a well-known trade-off in passive metamaterials (constrained by Lorentz dispersion model, Chapter 1). Clearly, obtained 'negative' bandwidth in active structures is significantly larger than in passive ones, but the general behavior appears to be similar. It is worth mentioning that the theoretical studies that would support this hypothesis (to the best of Authors' knowledge) are not available in the literature.

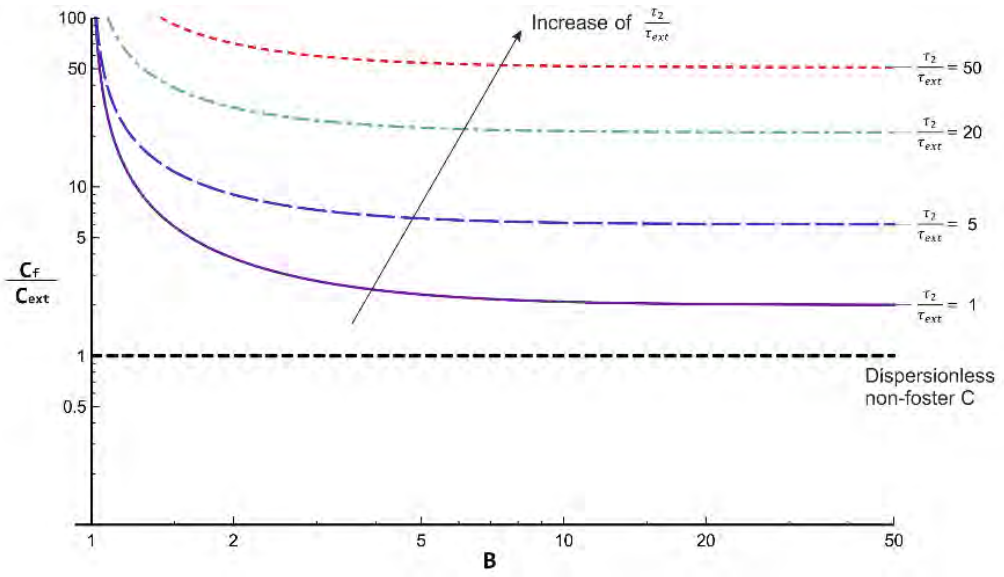

Figure 3-17 Bandpass negative capacitor - Maximal stable normalized negative capacitance as a function of amplifier bandwidth B with different values of τ_2/τ_{ext}

3.3.3. Band-pass negative capacitor: experimental RF demonstrator

In the second step, the proof-of concept bandpass negative capacitor operating in lower RF range (100 kHz to 100 MHz) was designed and manufactured. As in all the examples in this report, a very low frequency range was chosen due to ease of manufacturing ('hand-crafting'), the small influence of inevitable parasitic capacitances and very simple measurements. The design was based on THS4303 high-speed (> 1GHz) operational amplifier. The assembled band-pass capacitor is essentially a two-stage band-pass non-inverting amplifier. This amplifier has a frequency-dependent negative feedback that assures a band-pass behavior with two corner frequencies, at which voltage gain drops below 1 and a positive feedback responsible for negative capacitance effect. A schematic diagram of prototyped negative bandpass capacitor is depicted in Figure 3-18 and its physical appearance is shown in Figure 3-19.

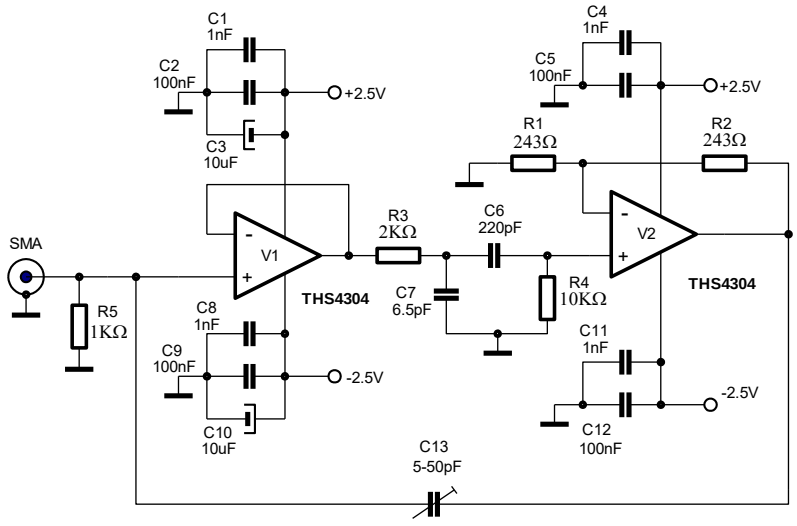

Figure 3-18 Schematic diagram of an RF demonstrator of stable negative band-pass capacitor

Figure 3-19 A photo of an RF demonstrator of stable negative band-pass capacitor

A Rohde Schwarz ZNC3 VNA was used for the measurement of input capacitance (with the help of standard extraction procedure that uses external stabilizing capacitor [2,51]). Comparison of analytical results, measured results, and SPICE simulations (Figure 3-20) revealed very good agreement.

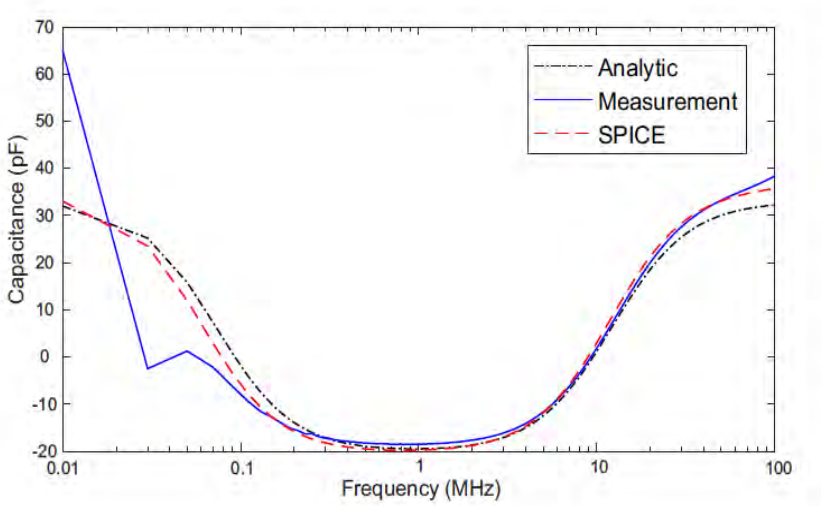

Figure 3-20 Extracted input capacitance of an RF demonstrator of bandpass negative capacitor (obtained analytically, numerically and experimentally)

Slight difference occurred due to limited VNA measurement accuracy at very low frequencies. Although there was no instability observed during VNA measurements, an additional testing was performed. Negative capacitor was loaded by shunt combination of a trimer capacitor and a trimer resistor. The values of loading capacitance and resistance were varied and eventual occurrence of instability was monitored by Anritsu S332E spectrum analyzer (weakly coupled to the circuit via a small loop antenna). Obtained results were found to be in very good agreement with both theory (Figure 3-20) and SPICE simulations, indicating

stability properties that are significantly better than those in the standard 'low-pass' design of a negative capacitor (Figure 3-10).

Finally, additional SPICE-base transient simulations were performed in order to test suitability of this approach for construction of active metasurface inclusions. A model comprised a voltage Thevenin's generator that excites a terminated transmission line that is loaded with a shunt band-pass negative capacitor. Both the internal resistance of a voltage generator and terminating resistance were chosen to be equal to the characteristic impedance of a transmission line. This model mimics realistic scenario of active metasurface with negative capacitive surface reactance, excited by a plane wave at normal incidence. The length of the 'connecting' transmission lines was varied from 0 to one λ, and no instability was observed.

Briefly, it can be concluded that all presented analytical, numerical, and experimental results show that the stability properties of a 'bandpass' negative capacitor are significantly better than those from classic design.

3.3.4. 'All-negative' unit cells: theoretical investigation

'All-negative' (generalized) non-Foster *lumped* networks, originally introduced in [51,77] and briefly reviewed in Chapter 1 comprise solely negative 'equivalent' elements. Physically, 'equivalent' elements are actually simple subnetworks (series or parallel combination) of several elements of different types (both positive and negative), the equivalent (net) quantity of which (resistance, capacitance, and inductance) *is negative number*. A simple example is a stable negative RLC tank circuit, originally introduced in [51], Figure 3-21, (a).

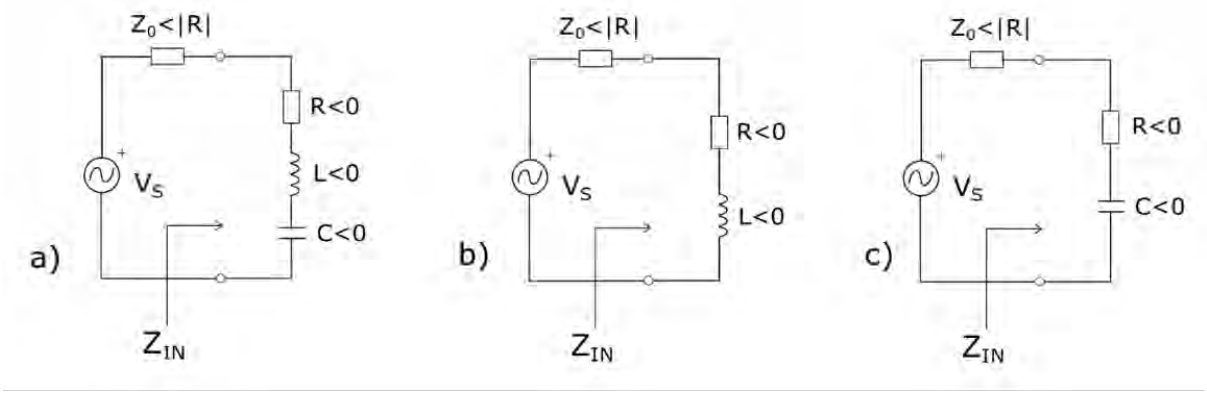

Figure 3-21 a) 'All-negative' stable RLC network, b) 'All-negative' stable RL network, c) 'All-negative' stable RC network

The stable operation of the circuit in Figure 3-21, (a) is achieved by choosing a generator internal (real) impedance Z_0 to be *lower* than the absolute value of the negative resistance R in the 'negative' RLC circuit ($Z_0 < |R|$). The overall resistance is $Z_0+R= Z_0 -|R|$, and this is a negative number ($Z_0 -|R| <0$). Since all other elements are also negative ($L<0$, $C<0$), the system is stable. Thus, the imaginary part of an input impedance Z (seen from the input port) will have non-Foster behavior ($\partial X/\partial\omega < 0$, X being a reactance). At the same time, the real part is negative, R<0. A standard circuit-theory analysis shows that the net power flow of the network in Figure 3-21, (a) *is reversed*, thus, the power flows *into the generator*. Actually, this network resembles a familiar reflection amplifier [19]. The main difference is the presence of negative

capacitor and inductor that contribute to the reactive part of reversed power flow. In the transient state, the energy first travels from the generator towards the RLC load, experiences reflection with amplification, travels back to the generator, experiences the second reflection, travels towards the RLC load etc. Hence, the steady-state reversed power flow is a sum of all partial re-reflections with amplification in time domain.

3.3.5. 'All-negative' unit cells: numerical analysis and experimental RF demonstrator

Above analysis [51] assumed ideal elements. Both preliminary experiments and the analysis with one-pole model of the NIC amplifier (similar to one from the Section 3.2) [51] reveals that it is possible to achieve stability with realistic non-Foster elements, as well. Apart from compensation of internal positive resistance of the generator (Z_0), the negative resistance (R) may be used for compensation of inherent loss in practical implementations.

In metasurface applications, it would be desirable to modify the network from Figure 3-21 (a) in way that avoids resonant behavior and provides pure negative inductive or negative capacitive surface admittance. This can be done by simple stable 'all-negative' RC and RL networks, depicted in Figure 3-21 (b) and Figure 3-21 (c), respectively. Stressing once again, the presence of negative resistance (R) is necessary in order to maintain stability. Using preliminary experiments from [51] as a 'recipe', we designed the electronic circuitry (NICs) that approximately behaves as networks from Figure 3-21. The example of designed negative RLC circuit and its physical appearance are given in Figure 3-22 and Figure 3-23, respectively. The prototype from Figure 3-22 is again based on the THS 4303 device. It is a wideband, fixed-gain amplifier that offers high bandwidth of 1.8 GHz at a nominal gain of 10, high slew rate (5500 V/μs), low noise, and low distortion. The gain of the amplifier itself (A=10) was lowered to A≈2 with an additional resistor (330 Ω) (Figure 3-22). The resonance of the RLC circuit in the positive feedback loop (R=470 Ω, L=100 nH, C=100 pF) was chosen to be approximately 55 MHz, which is well below the maximum frequency of the NIC inversion (700 MHz) that should assure stable operation. The positive feedback loop was modified to (R=470 Ω, C=100 pF) and (R=470 Ω, L=100 nH) in the 'all-negative' RC and RL versions, respectively. We performed ADS™ simulations of all three circuits, both using an ideal OPamp model as well as the THS 4303 SPICE model.

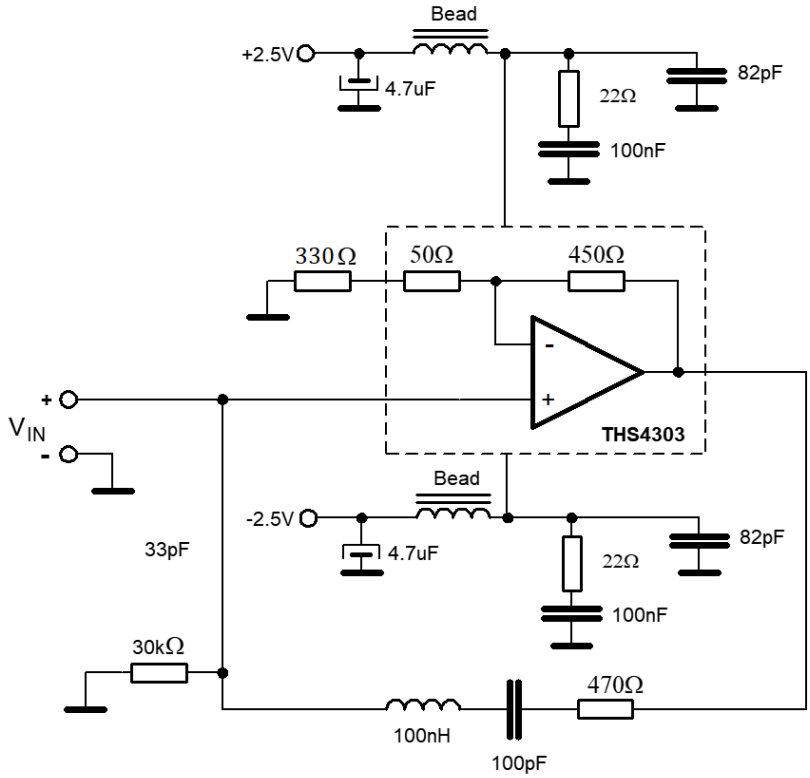

Figure 3-22 Schematics of 'all-negative' stable RLC circuit

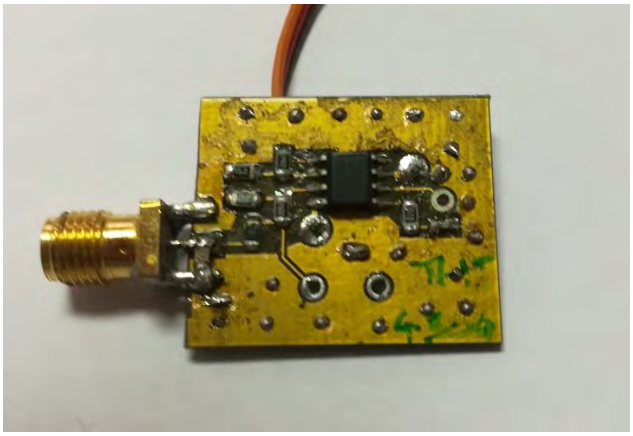

Figure 3-23 A prototype of 'all-negative' stable RLC circuit

In addition, the 'all-negative RLC' circuit was tested experimentally, by measurements of the input reflection coefficient and extraction of equivalent reactance and resistance values. The results are given in Figure 3-24, Figure 3-25 and Figure 3-26.

At first, it can be seen that the agreement between the simulation results obtained using an ideal OPamp model and a full SPICE model is very good up to frequency of 20 MHz and acceptable up to the frequency of 100 MHz. Furthermore, the measurements of 'all-negative' RLC circuit match the simulations well.

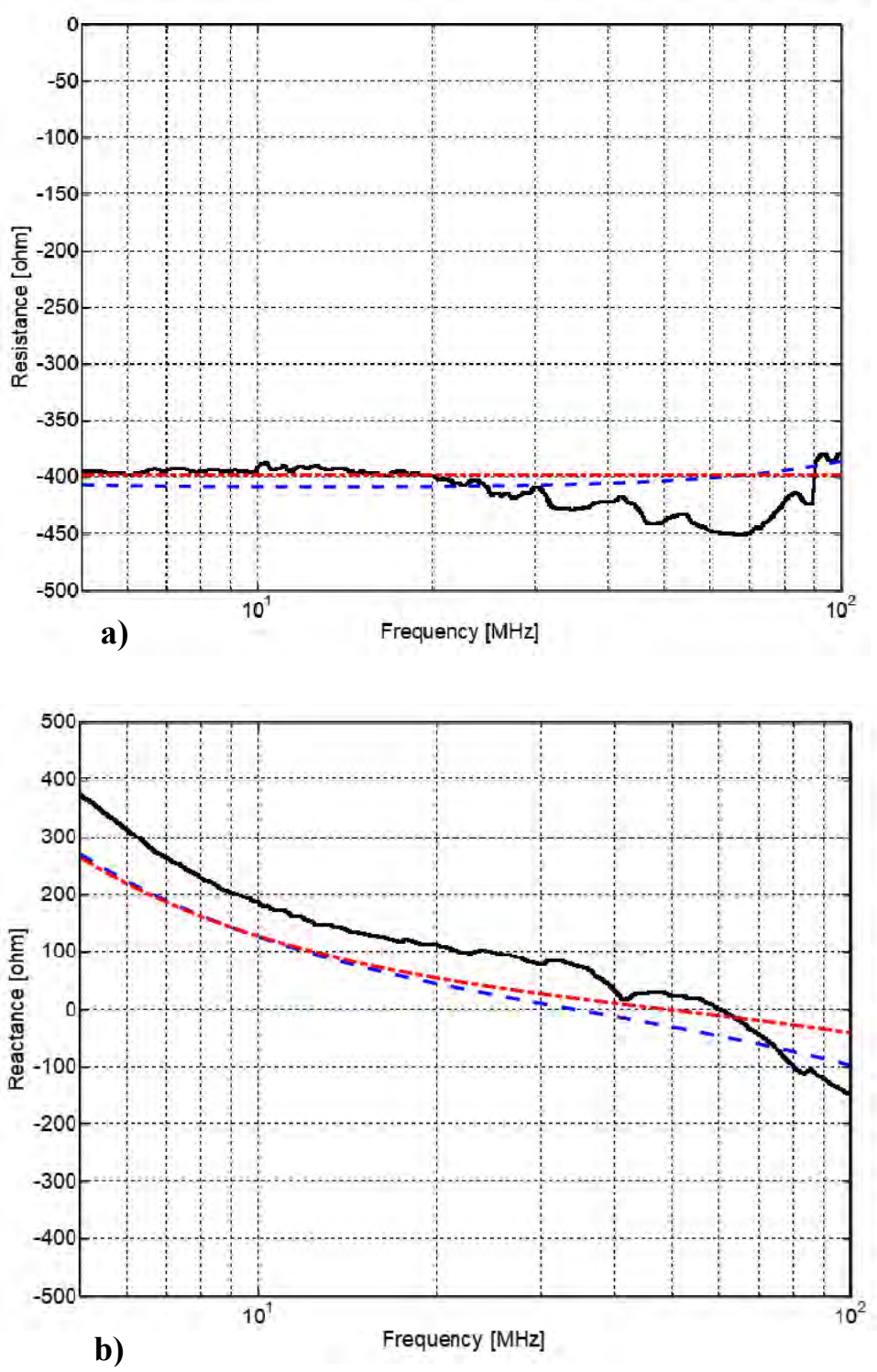

Figure 3-24 Input impedance of stable 'all-negative' RLC network, a) resistance, b) reactance. Solid: measurements, Dot-dashed (red) – model with ideal OPamp, Dashed (blue) – SPICE model of OPamp.

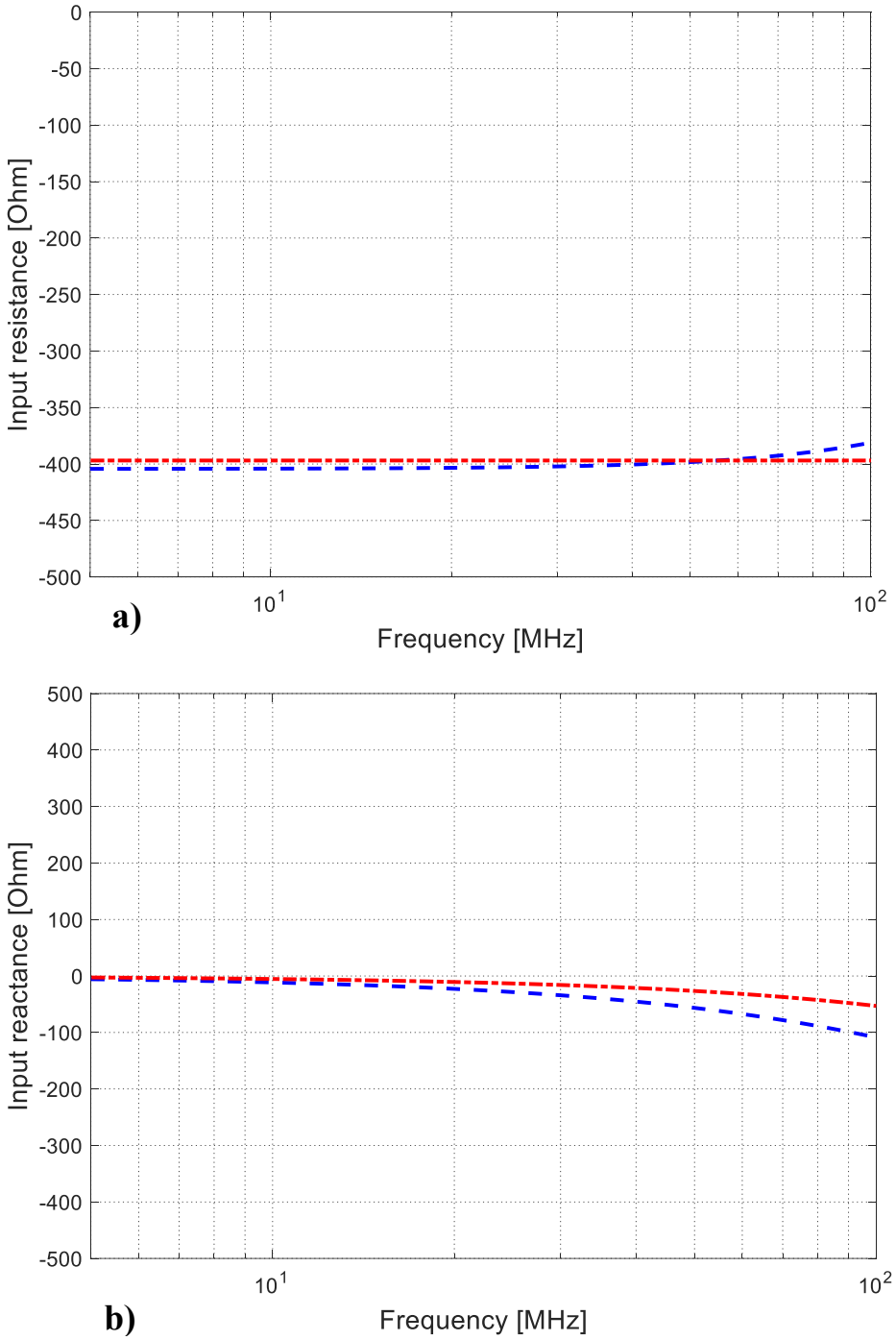

Figure 3-25 Input impedance of stable 'all-negative' RL network, a) resistance, b) reactance. Dot-dashed (red) – model with ideal OPamp, Dashed (blue) – SPICE model of OPamp.

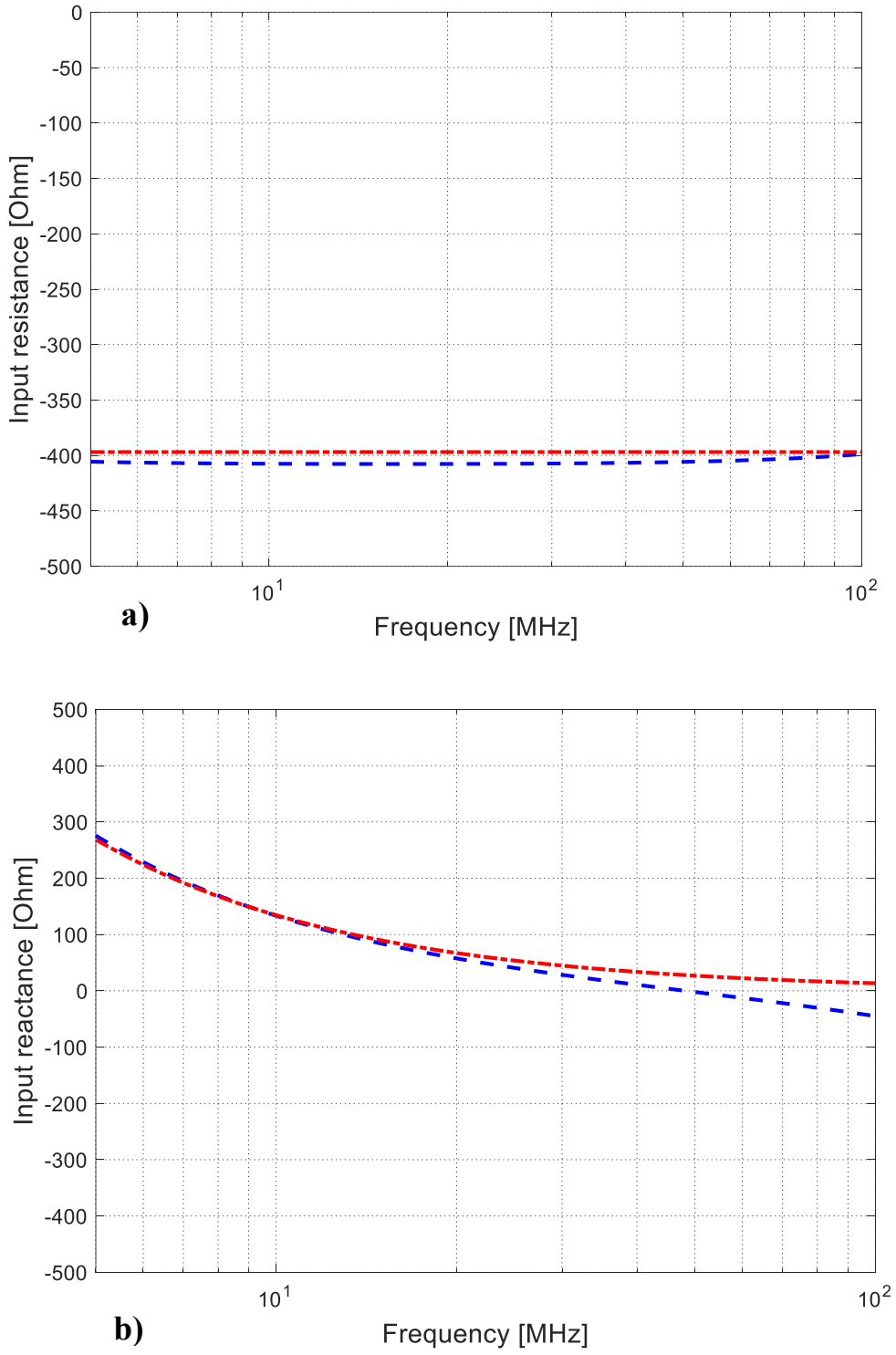

Figure 3-26 Input impedance of stable 'all-negative' RC network, a) resistance, b) reactance. Dot-dashed (red) – model with ideal OPamp, Dashed (blue) – SPICE model of OPamp.

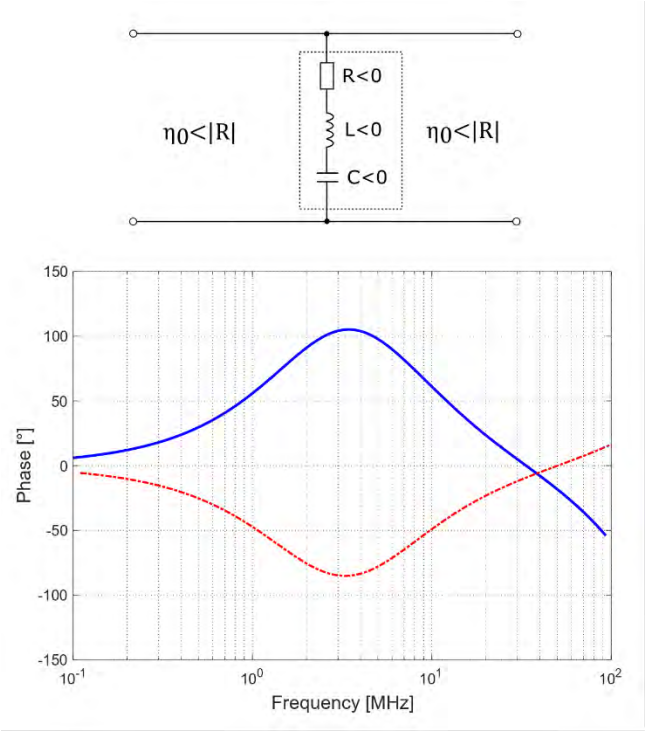

Figure 3-27 Simulated dependence of phase of transmission coefficient (S_{21}) on frequency for a transmission-line model of metasurface. Red: passive RLC inclusions, blue: active 'all-negative' RLC inclusions.

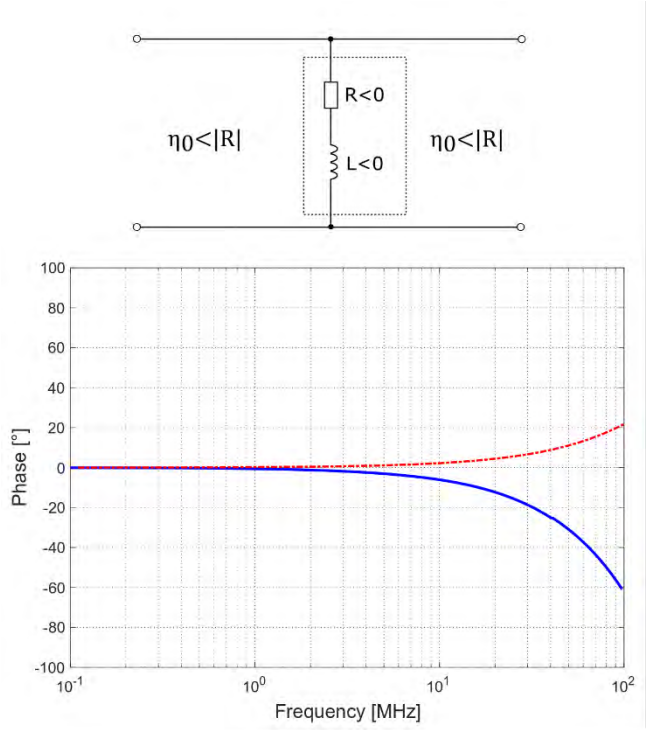

Figure 3-28 Simulated dependence of phase of transmission coefficient (S_{21}) on frequency for a transmission-line model of metasurface. Red: passive RL inclusions, blue: active 'all-negative' RL inclusions.

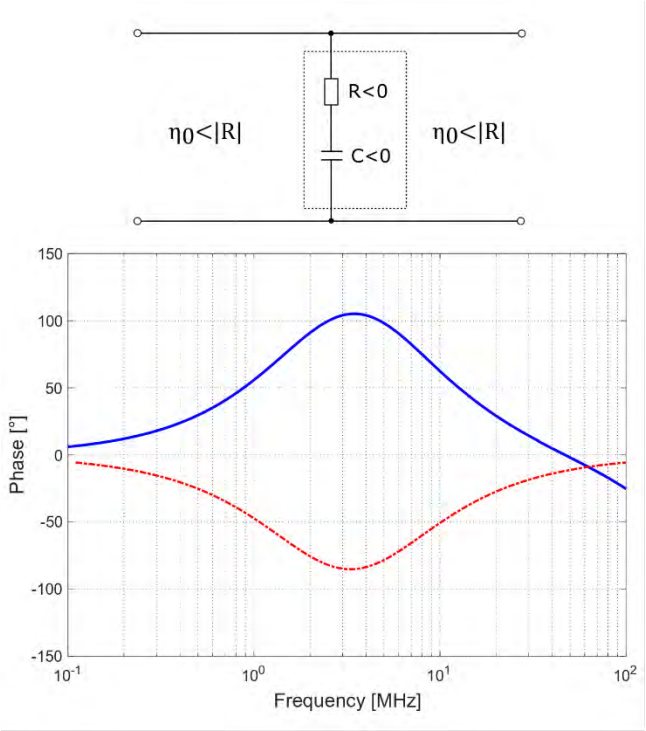

Figure 3-29 Simulated dependence of a phase of transmission coefficient (S_{21}) on frequency for a transmission-line model of metasurface. Red: passive RC inclusions, blue: active 'all-negative' RC inclusions.

The 'all-negative' networks were treated as one-port devices in above analysis. However, in MTM applications, they should work as two-port devices (Figure 3-13). Thus, in the last step, the simple transmission-line models of all three 'all-negative' networks were prepared in ADS^{TM} environment and the dependence of phase of transmission coefficient (S_{21}) on frequency was simulated. The results are given in Figure 3-27, Figure 3-28 and Figure 3-29. It is important to stress that the stable behavior was present in all three cases. Furthermore, the non-Foster behavior is clearly visible.

One concludes that 'all-negative' (generalized) non-Foster networks can assure stable operation even with interaction with the environment. The counter-intuitive reversed power flow (seen from 'outer world' does not appear as an obstacle. Thus, the 'all-negative' non-Foster networks can be used in active MTM applications.

3.4. Summary

Different methods of stability improvement of generalized non-Foster networks have been analyzed in Chapter 3. The most important issues are summarized below:

- The widely accepted stability criterion of positive 'mesh' capacitance fails for parallel combination of positive and ideal negative capacitor with connecting transmission line. Such a network is always unstable, regardless of the line length and capacitance values of positive and negative capacitor. However, the inherent dispersion of a realistic negative capacitor (usually considered as a drawback) can be tailored in a way that assures stable operation. Surprisingly, in some cases of lumped and mixed networks with realistic model of negative capacitor, stable operation is feasible even if overall capacitance is negative. All these findings have been verified both analytically and numerically.
- It is possible to significantly improve stability of a generalized non-Foster network by a 'band-pass' design that does not allow occurrence of unstable DC pole. A novel concept of a 'band-pass' negative capacitor has been introduced and investigated analytically and numerically. The measurements of manufactured RF demonstrator operating in the range 100 kHz – 100 MHz have shown stable operation and proven the validity of proposed design.
- A novel principle of 'all-negative' generalized non-Foster network for a unit cell in metasurface applications has been introduced. This is a network that comprises solely negative 'equivalent' elements and supports counter-intuitive reversed power flow. Analytical and numerical investigations showed that 'all-negative' non-Foster networks can assure stable operation. Measurements on the RF demonstrator operating in 100 kHz – 100 MHz have confirmed simulation results.

Chapter 4 GENERALIZED SOURCE-LOAD NON-FOSTER NETWORKS

Generalized source-load non-Foster networks

4.1 Linear non-Foster source

In Chapter 3, several different methods for improving stability properties of lumped and mixed lumped-distributed generalized non-Foster networks have been discussed. All these methods abandon description of idealized dispersionless non-Foster elements (defined by simple mathematical sign 'negation'). Instead, they use more realistic band-limited models that are physically sound [41], or even introduce new circuitry that behave similarly to hypothetical bandpass non-Foster elements [81]. Of course, a final goal is to prevent the occurrence of poles of a 'dead circuit' transfer function (i.e. the poles of natural response) in the right-hand-side of a complex plane [93]. As shown in several studies on non-Foster networks [2,41,51], it is absolutely necessary to test the stability before the analysis of transfer function otherwise the obtained results may not be physical. Only if the stability of natural response is assured, an active network may be thought of as a 'black box" with some inherent transfer function.

The transfer function of stable generalized non-Foster 'black box' excited by an external generator (Fig. 4-1) usually exhibits some kind of broadband phenomena not present in ordinary networks.

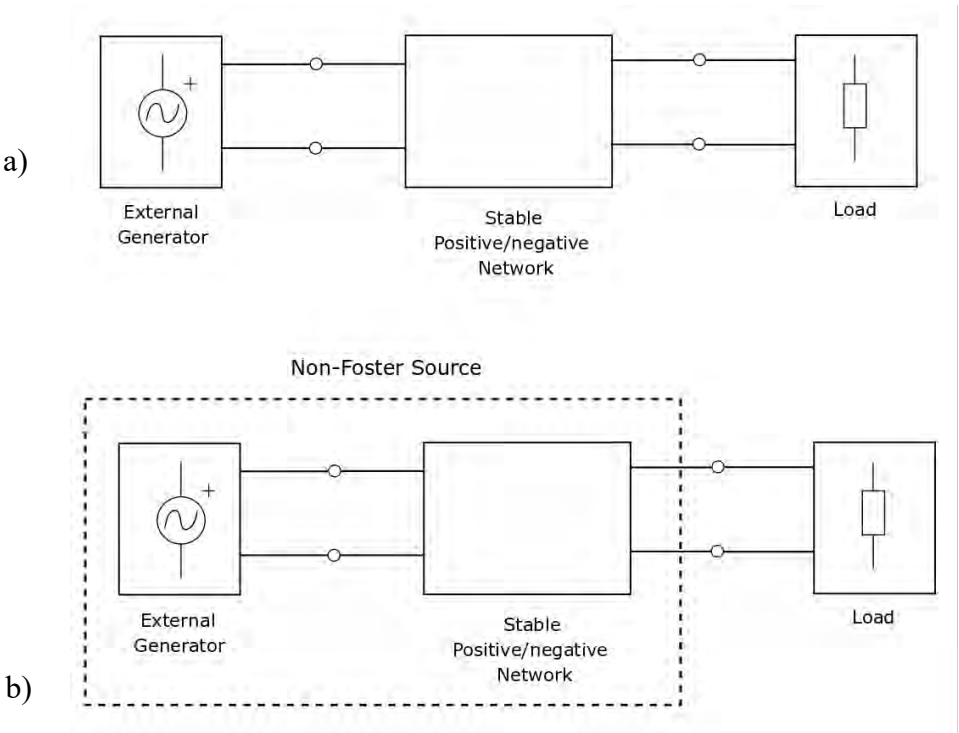

Figure 4-1 a) A system comprising stable generalized non-Foster network, external generator and load, b) Interpretation using a concept of non-Foster source

Prominent examples include ‘superluminal propagation’ in active broadband ENZ metamaterial [42,43], active broadband matching of an antenna to a receiver [60,61], broadband gain in distributed-amplifier/based devices [108] etc.).

Construction of aforementioned broadband systems presumes that the inclusion of external generator does not change stability properties of a given active network. Indeed, if the natural response of a linear network is stable, the forced response of the same network is stable, as well. This fact is one of the main properties of every linear network.

In some cases, it is simpler to look at the required output signal (signal at the load in Figure 4-1) instead of a system transfer function. Thus, one might think of a cascade of an external generator and generalized non-Foster network (or a part of it) as a new active one-port ‘black box’ (Fig. 4-1 b). This approach is discussed in the next paragraph.

4.1.1. Cascade of a generator and stable generalized non-Foster network

A dashed one-port ‘black box’ in (Fig. 4-1 b) can be thought of as a new equivalent source. Obviously, both the amplitude and internal impedance of a new source are different than those from original generator from Figure 4-1. Specifically, the internal impedance of a new source may have non-Foster properties ($\partial X/\partial\omega < 0$, X being an imaginary part of internal impedance, i.e. the reactance). It will be shown that this kind of source has several unusual properties and will be termed as a ‘non-Foster source’. As any other kind of source, the non-Foster source can be represented using well-known Thevenin’s and Norton’s models (Figure 4-2).

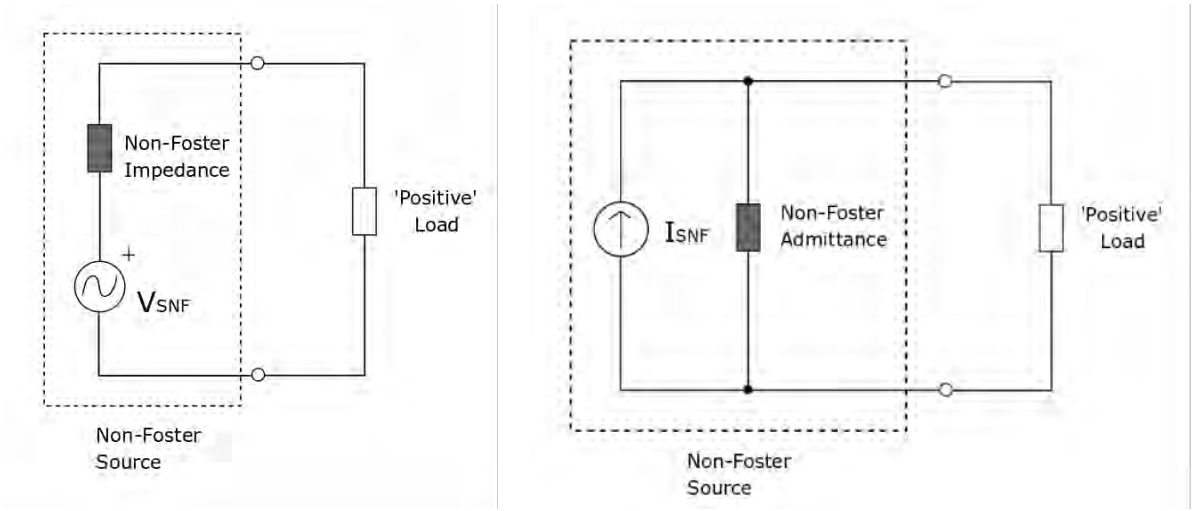

Figure 4-2 Non-Foster source a) Thevenin’s representation, b) Norton’s representation

As it is very well-known (and briefly reviewed in Chapter 1), the main idea of almost every potential application of non-Foster networks is the dispersion cancellation of a passive network in order to obtain some kind of broadband behavior. So, an external generator that is a part of a non-Foster source in Figure 4-2 is usually either inherently broadband *per se* (for instance, a receiving antenna that should be matched to a receiver across wide bandwidth, a transmitter with digital high data-rate modulation, a frequency hopping transmitter…) or it is a broadly tunable source (a transmitter that should be tuned to some particular channel).

Let us think of the architecture of non-Foster source for above applications. Obviously, one of the possible solutions may comprise an RF oscillator (with presumably real internal impedance) augmented with an additional active output network that assures non-Foster behavior. That additional network actually generates internal generator reactance of non-Foster

type and it is implemented by appropriate NIC circuit. The selection of appropriate configuration of the NIC depends on specific application, i.e. on the type of required non-Foster source.

There is a group of applications in which a non-Foster source should be able to deliver the power to highly reactive 'high-impedance' load (for instance, a transmitter that excites a short dipole antenna). According to the discussion in Section 3.3.3. and Linvill's original suggestion [26], it seems desirable to use an OCS NIC in this case. Such a voltage source augmented with OCS NIC is sketched in Figure 4-3.

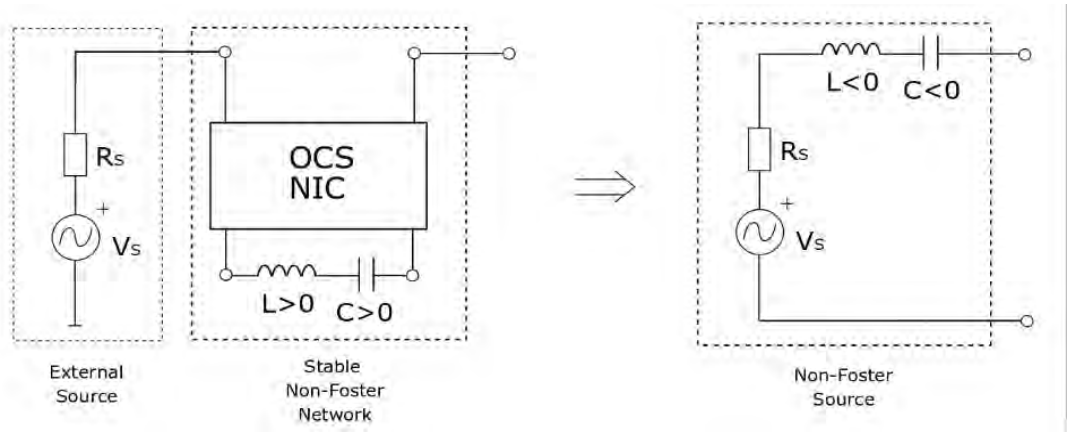

Figure 4-3 Possible implementation of non-Foster source intended for driving a high-impedance load

If the load is of a 'low-impedance' type (for instance, a small loop antenna), it appears to be more convenient to use a current non-Foster source with a SCS NIC (Figure 4-4).

Obviously, in both cases (Figure 4-3 and Figure 4-4) the frequency of the signal at the load is given by the excitation source, not by the active non- Foster network (the source is actually an oscillator with some kind of internal resonant circuit). It will be shown later (Section 4.1.3) that this is not the case in unstable generalized non-Foster networks that act as a non-Foster source.

As discussed in Section 3.1, above (traditional) choice of SCS or OCS NIC type is just a guidance that does not assure stability *a priory*. As noted before, if some system is SCS (or OCS) *it does not necessary mean* that it will be stable for some very low resistance (or some very low conductance). Thus, the stability of internal impedance of non-Foster sources in Figure 4-3 and Figure 4-4 should be tested beforehand for every particular load (for instance antennas). If a NIC is not designed carefully, its connection to the load might cause disturbing signals (i.e. instabilities) that would be superimposed to the signal of an external generator. Particularly inconvenient situation would arise if the amplitude of the signal is high enough to drive the NIC into non-linear regime. It would cause very complicated intermodulation process between driving and disturbing signals. Clearly, potential instability of the NIC that should assure non-Foster behavior of a generator internal reactance might be a problem in practical applications. Thus, it appears that implementation of a simple non-Foster source that comprises just stable general non-Foster network and an external generator, is challenging.

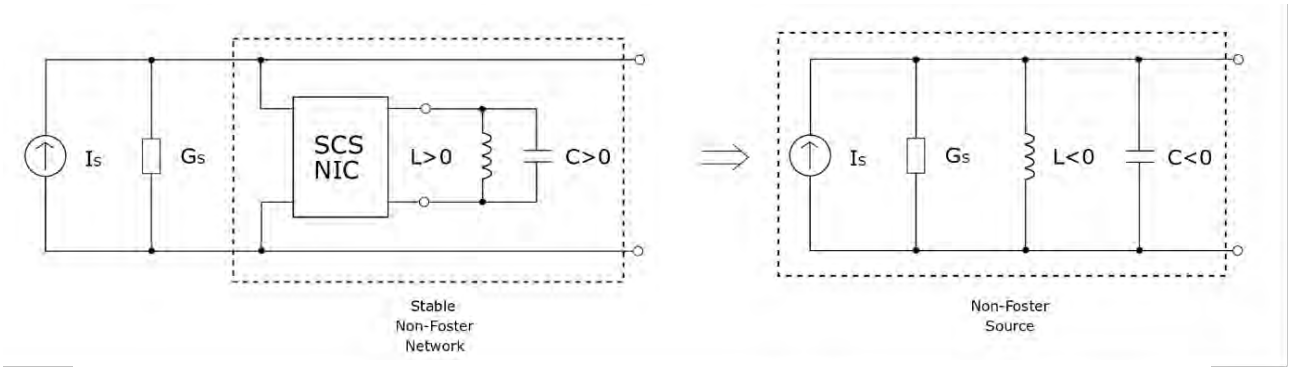

Figure 4-4 Possible implementation of a non-Foster source intended for driving a 'low-impedance' load

4.1.2. Similarity between non-Foster source and active matching of transmitting antenna

As mentioned in Chapter 1, one among popular applications of generalized non-Foster elements is active antenna matching. While active matching of small receiving antenna has been developing slowly and gradually over a couple of decades [50,51,58,59,60,61] there are a very few papers regarding transmitting applications [59]. One may say that the non-Foster matching of transmitting antenna is still in infant phase.

It is instructive to investigate the similarity between non-Foster matching of transmitting antenna and concept of a non-Foster source. As it can be shown later, by applying this similarity it is possible to develop a novel perfectly-matched broadband transmitting system.

A typical implementation of a classical non-Foster matching is sketched in Figure 4-5. Transmitting antenna is represented as a complex impedance (here R_A (ω) stands for the antenna radiation resistance while X_A (ω) is the antenna reactance). The antenna is connected to a transmitter (modelled as a Thevenin generator with signal amplitude Vs and the internal resistance Rs) via series active circuit (NIC) that exhibits non-Foster reactance (-X_A(ω)). Thus, the antenna reactance (X_A (ω)) is (theoretically) completely cancelled by a series non-Foster reactance -X_A(ω) leaving matching properties solely determined by the real part of antenna and generator impedance (R_A and R_S). Furthermore, if R_A=R_S the whole amount of generator (transmitter) available power ($\frac{V_S^2}{4R_S}$) will be delivered to the antenna. Due to inverse dispersion characteristics of antenna reactance and non-Foster reactance, the spectrum of transmitting signal can span very broad (theoretically infinite) bandwidth with perfect matching.

There are two important problems that significantly deteriorate this optimistic scenario in practice: the design of an efficient NIC that can sustain high-power levels needed for transmitting applications and the assurance of a stable operation without unwanted oscillations [113].

Now, let as think of a non-Foster impedance generated by the NIC in active matching network, as the internal part of a transmitter. Thus, the transmitter (V_S), its internal resistance (R_S) and the non-Foster reactance (-X_a) form the non-Foster source. At first sight, the 'integration' of a non-Foster impedance into the transmitter block might look as just a matter of convenience (clearly, two equivalent circuits in Figure 4-5 are identical). However, practical implementation of the transmitter with integrated non-Foster impedance (instead of use of an external matching) offers two advantages. Firstly, the NIC and transmitter circuitry can be optimized together. This might lead to a more robust design and significantly simpler assurance of stable operation. Secondly, the non-Foster network is now part of the transmitter. Thus, it is easier to construct it in a way that assures required high-power operation.

It is worth mentioning that there are some silent details presumed in Figure 4-5. As it is well known, the radiation resistance of a small antenna is extremely small. Therefore, the non-Foster matching almost always requires an additional network that transforms a small radiation resistance to the transmitter internal resistance. For the sake of clarity, this additional network is not shown in Figure 4-5. Furthermore, it is well-known that the perfect cancellation of antenna reactance by non-Foster element is impossible in the case of ideal elements because such a system is inherently unstable. In order to maintain stability, it would be necessary to assure the existence of some 'residual' reactance (susceptance) of ordinary Foster type (residual positive capacitance or positive inductance). As it was noted recently, perfect cancellation (within some bandwidth) with stable operation is possible in the case of realistic elements [93]. All these details complicate practical realization of non-Foster matching of the transmission antenna. Nevertheless, if the given implementation is stable, it can (formally) be thought of as a network with non-Foster source.

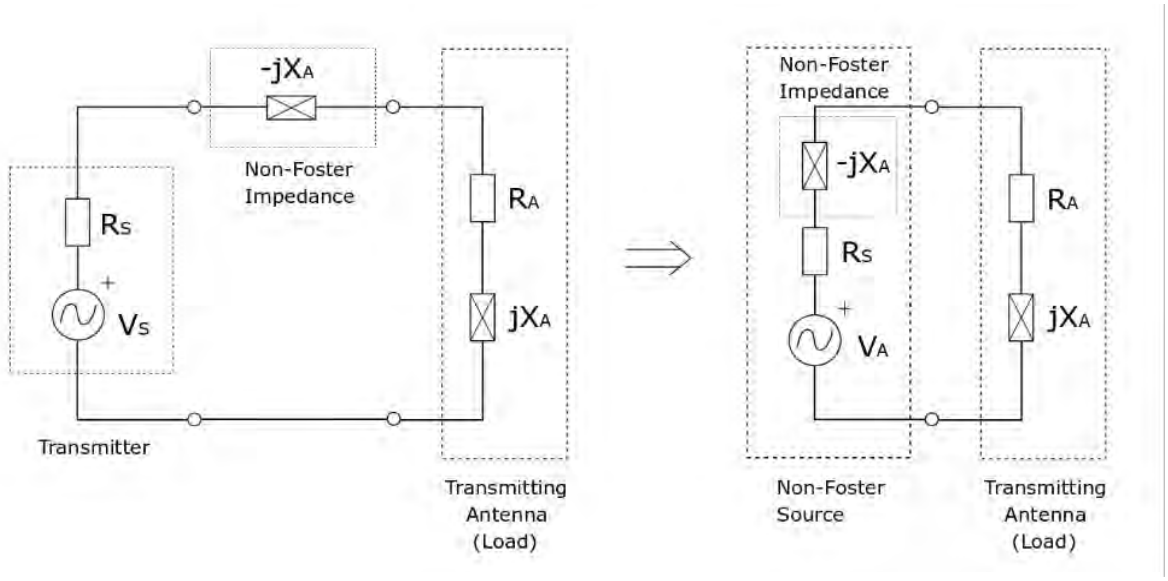

Figure 4-5 Interpretation of active matching of transmitting antenna using a concept of non-Foster source

4.1.3. Unstable generalized non-Foster network as a non-Foster source

Concepts discussed in the previous section presume inherent stability of a generalized non-Foster network excited by an external generator. Recently, there have been several practical examples that show that is indeed possible to achieve stable operation of different generalized non-Foster networks of both lumped and lumped-distributed type by careful design [2,47,49,51,52,63,67,68]. On the other hand, there is an additional problem with sensitivity of active network components' tolerance, temperature change etc. A standard way of softening this problem is the use of negative feedback. However, the NIC' circuits inevitably employ positive feedback. Therefore, the NICs are much more sensitive to aforementioned changes than standard electronic circuitry [2,51]. Furthermore, it is often very challenging to assure that non-idealities never 'push' active network into the unstable mode.

Instead of controlling non-idealities, one could think in a completely different way. Let us suppose that some (generalized) non-Foster network is unstable in such a way that it behaves as a non-Foster source *per se*. So, all the energy of an unstable signal is transferred to some

external load (antenna, for instance) with perfect matching. If feasible, this idea would certainly be very convenient for many practical applications.

To investigate the background physics of this idea, let us suppose that a linear generalized non-Foster network shows instability of oscillating type (Figure 4-6).

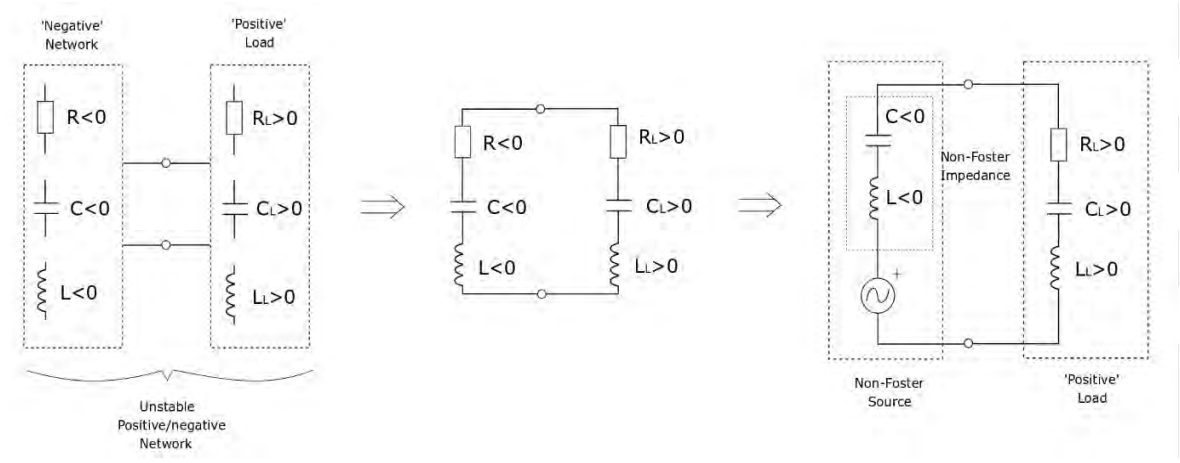

Figure 4-6 Interpretation of an unstable generalized non-Foster network as a system with voltage non-Foster source

From linear theory point of view, the stability means that there is at least one complex pole in the RHS of a complex plane). With the help of standard theory of microwave oscillators [19] such a system can always be decomposed into at least one positive (passive) subnetwork and one negative (active) subnetwork. If those networks contain many elements, their equivalent input impedance may be a very complicated rational function with many poles.

For the beginning, let us assume the simplest case of subnetworks that contain only three elements: positive/negative resistor, positive/negative capacitor, and positive/negative inductor. This is a simple the case of a generalized series RLC circuit with positive/negative elements, analyzed in [2,114]. Oscillations in this system are sustained only if a real part of net impedance (equivalent resistance) has opposite sign that overall inductance and overall capacitance [2,114] (Table 4-1).

Sign of equivalent overall R	**Sign of equivalent overall C**	**Sign of equivalent overall L**	**Type of equivalent Thevenin sinusoidal source**
-	+	+	**Foster**
+	-	-	**non-Foster**

Table 4-1 Types of equivalent Thevenin source of unstable generalized non-Foster network that can be reduced to series RLC circuit

In the first case (the first row in Table 4-1), a net impedance contains overall negative resistance ($R+R_L<0$), overall positive capacitance ($C+C_L>0$), and overall positive inductance ($L+L_L>0$). In this case, the whole system behaves as a familiar negative-resistance oscillator (a negative resistance R generates RF energy that is absorbed by a positive resistance R_L while a positive LC circuit determines the frequency of oscillations). In the second case (the second

row in Table 4-1), net impedance contains overall positive resistance ($R+R_L>0$), overall negative capacitance ($C+C_L<0$), and overall negative inductance ($L+L_L<0$). In this case, the RF energy is generated by the negative capacitance and the negative inductance and dissipated at the positive resistance. The energy generation by reactive elements such as negative capacitor and negative inductor looks counter-intuitive, but it is possible due to the fact that they are active devices. Actually, it is very difficult to find an appropriate physical explanation of reactive energy for non-Foster elements. One notices that this energy flows *outward from* the series negative LC combination during a positive period of a voltage signal. Thus, the negative LC combination indeed performs as a generator. In this case, the frequency of oscillations is determined by the negative LC circuit. It may be said that this system is a 'non-Foster' oscillator (in analogy to familiar negative-resistance oscillator), [114]. It behaves as a voltage source with internal non-Foster impedance (a voltage non-Foster source, Figure 4-7). Similarly, this unstable active network can be interpreted as a Norton's current source (current non-Foster source), as shown in Figure 4-7.

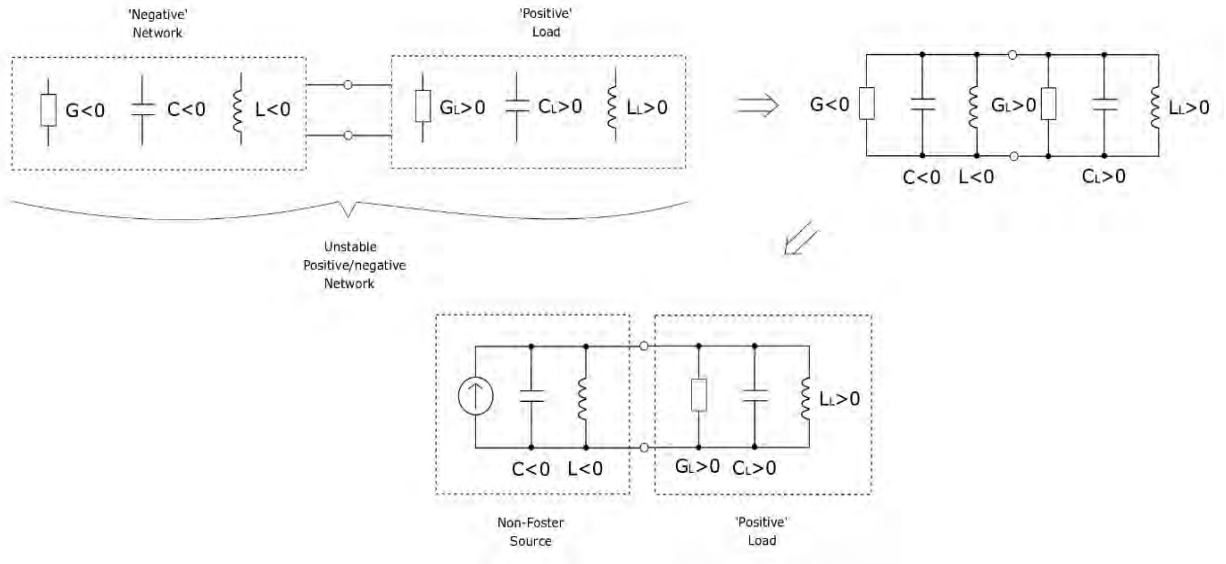

Figure 4-7 Interpretation of an unstable generalized non-Foster network as a system with current non-Foster source

The active network in above examples comprised only three ideal positive/negative elements. In the case of larger number of elements, the equivalent input impedance can again be modelled as RLC circuit, but with dispersive elements. Mathematical analysis is more complicated than one presented in [2] but the condition for sustained oscillations is the same: a real part of net impedance (equivalent resistance) should have a sign that is opposite to overall inductance and overall capacitance [114].

As reviewed in Chapter 1, all realistic generalized non-Foster elements are dispersive and can be modelled with active elements, a gain function of which has one, two, or three poles. Therefore, the same equivalent circuit (series or parallel RLC circuit with dispersive elements) can again be used for modelling of input impedance of realistic network. Only difference is that the dispersion function will be different than the dispersion function from an ideal case. Thus, above discussion is valid for realistic active networks, as well.

As it was already mentioned, presented properties of a linear non-Foster source resemble traditional small-signal (linear) one-port negative-resistance oscillator. Therefore, a brief discussion of similarities and differences between a non-Foster source and a small-signal negative-resistance oscillator are given in the next section.

4.1.4. Linear non-Foster source versus small-signal negative-resistance oscillator

The internal (active) admittance of an unstable generalized non-Foster network in Figure 4-7 is a non-Foster negative RLC circuit. Since the circuit is oscillating, it is obvious that the load admittance is a negative 'mirror image' of the admittance of active network (Y_{load}= -Y_{active}). Actually, this is very well-known condition for the existence of oscillations in small signal negative-resistance oscillator [19]. But, there is one crucial difference. In ordinary oscillator, the condition is met at only one frequency, which is determined by some kind of a resonant circuit. On the contrary, in the case of discussed generalized non-Foster network, this condition is met at every frequency. The signal waveform will be determined solely by the initial conditions of the circuit in Figure 4-8. In addition, the *whole RF power* generated within the active network is delivered to the load resistance (conductance) *without any reflection*. So, the load is perfectly matched to the source within a very broad (theoretically infinite) bandwidth. In the sense, this circuit is similar to the 'white noise' generator with infinite spectrum, but with correlated type of generated signal. This is the property of perfectly matched non-Foster source (Figure 4-8).

Furthermore, if one adds a tuning (resonant) circuit, it will be possible to tune the frequency of oscillations at any frequency, within (theoretically) infinite bandwidth and with the perfect load matching. Ordinary oscillator connected to a load (for instance, a transmitter that feeds an antenna) does not have this attractive property. Such tunable perfectly-matched non-Foster source can be represented either as a series or a parallel circuit (Figure 4-9 and Figure 4-10).

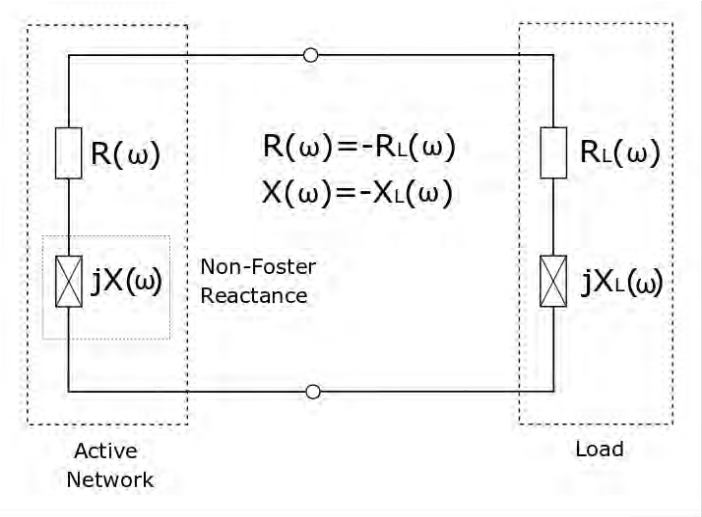

Figure 4-8 Concept of a broadband perfectly-matched non-Foster source

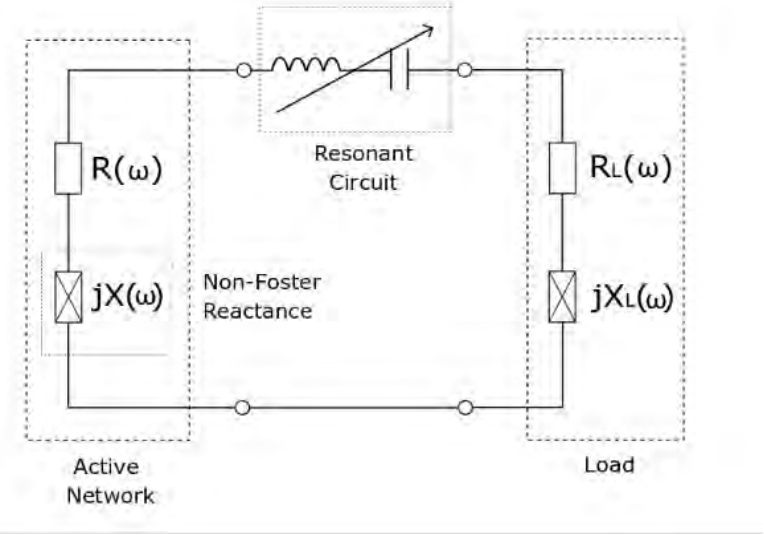

Figure 4-9 Tunable perfectly-matched non-Foster source represented as a series circuit

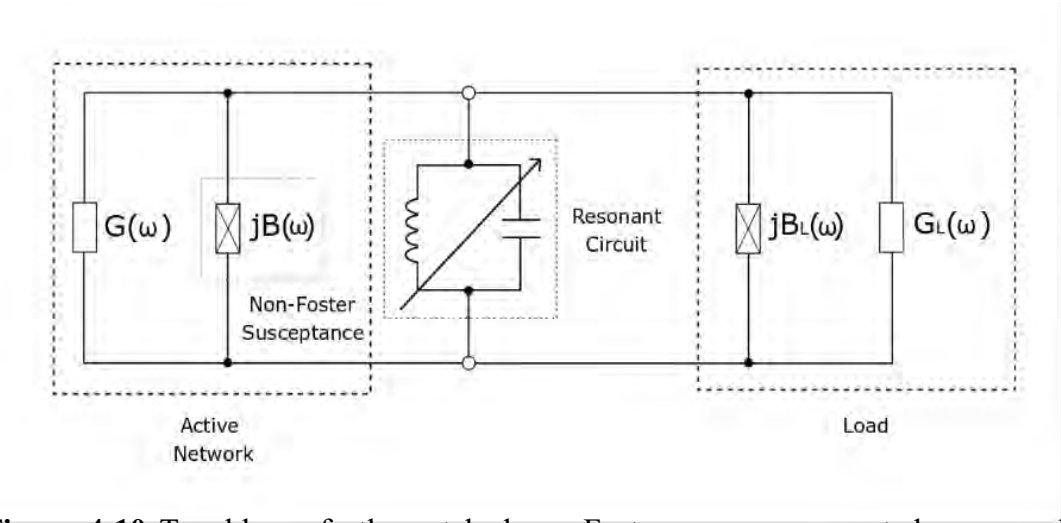

Figure 4-10 Tunable perfectly-matched non-Foster source represented as a parallel circuit

The fact that a combination of Foster and non-Foster elements, in which reactive and resistive elements have different signs, gives rise to oscillation has been known for a long time [103]. Nowadays, it is used as a basic principle of negative-impedance (non-Foster) microelectronic oscillator that is gaining popularity in wireless applications [114].

However, an idea of a broadband non-Foster source perfectly matched to the load has been proposed just very recently by our group [82,83]. It should be stressed that this approach turns inherent instability of practical non-Foster reactance (usually considered as a serious drawback that prevents widespread application of non-Foster elements) into a very useful feature.

4.2 Non-linear non-Foster source

In the previous section, the unstable generalized non-Foster linear network with oscillating response was interpreted as a linear non-Foster source. Due to linearity, it is possible to use the Thevenin's representation (Figure 4-6) or the Norton's representation (Figure 4-7), and either of them gives the same results.

Clearly, linearity is only an approximation since all non-Foster elements (just as all active circuits) inevitably enter non-linear regime at high levels of input signal. Unfortunately, possible non-linear properties of non-Foster elements are analyzed very rarely in the literature [115,116,117]. Therefore, it is convenient to briefly revise a standard theory of negative-resistance microwave oscillators [19] and extend it to non-linear non-Foster source. It is well-known that oscillator can be considered as being linear only for a very low amplitude of the generated signal. In addition, such a system has low efficiency. Indeed, the signal generated in any efficient oscillator inevitably enters the non-linear region of voltage-current characteristics of an active element. The amplitude grows up to the point at which the generated power equals the power dissipated at the load [19]. This process can be described by the well-known negative conductance/resistance properties of so-called N and S curves (Fig. 4-11, [19,103]).

Briefly, all negative elements with real impedance can be classified into a voltage-driven type ('N' curve depicted in Figure 4-11 (a)) and a current-driven tape ('S' curve depicted in Figure 4-11 (b)). The 'bending' in the curves occurs because of saturation properties of a given element since. In other words, the voltage and current cannot grow above the values limited by feeding DC power source. Either maximum voltage across an active element or maximum current flowing through it, will be limited by saturation. In the case of 'N -type' element (Figure 4-11 (a)), it is convenient to connect it in a parallel with a load. Usually, there is also an additional parallel LC circuit that determines the frequency of oscillations (lower part of Figure 4-11 (a)). A quantity that is common for this parallel combination is the voltage, which gives only one (stable) operating point in current-voltage curve (the intersection between 'N' curve and the load line [19,103]). While the amplitude of oscillations grows up, it 'climbs' along the curve and enters the non-linear part. Due to the change of negative differential conductance, the growth stops when the generated power equals the power dissipated at the load (stable operating point). However, if the point is unstable, it will move over the 'hill top', enter the region with positive differential conductance and the oscillations will cease. If a series combination were used instead the parallel one, the common quantity would be the current and it would give two operating (unstable) points. Thus, the N element has SCS properties and it should be voltage-driven.

In the case of an 'S-type' element (Figure 4-11 (b)), the situation is exactly opposite. It is convenient to connect this element in series with a load. Here, a quantity that is common for this series combination is the current. It gives only one (stable) operating point in current-voltage curve (the intersection between 'S' curve and the load line [19,103]. Again, the operating point 'climbs' along the curve during the oscillations growth and enters the non-linear part. Due to the change of negative differential resistance, the growth stops when the generated power equals the power dissipated at the load (stable operating point). Similarly to the previous case, there is an additional series LC circuit that determines the frequency of oscillations (lower graph in Figure 4-11 (b)). If the point is unstable, it will move over the 'hill top', enter the region with positive differential conductance and again cause the oscillations diminishing. If a parallel combination were used, the common quantity would be voltage and it would give two operating (unstable) points. Thus, the 'S -type' element has the OCS properties and it should be current-driven.

Colloquially, both types of elements are called negative resistors. However, as emphasized in [103] it would be more correct to term ‘N -type’ element as a ‘negative conductor’ and ‘S -type’ element as a ‘negative resistor’.

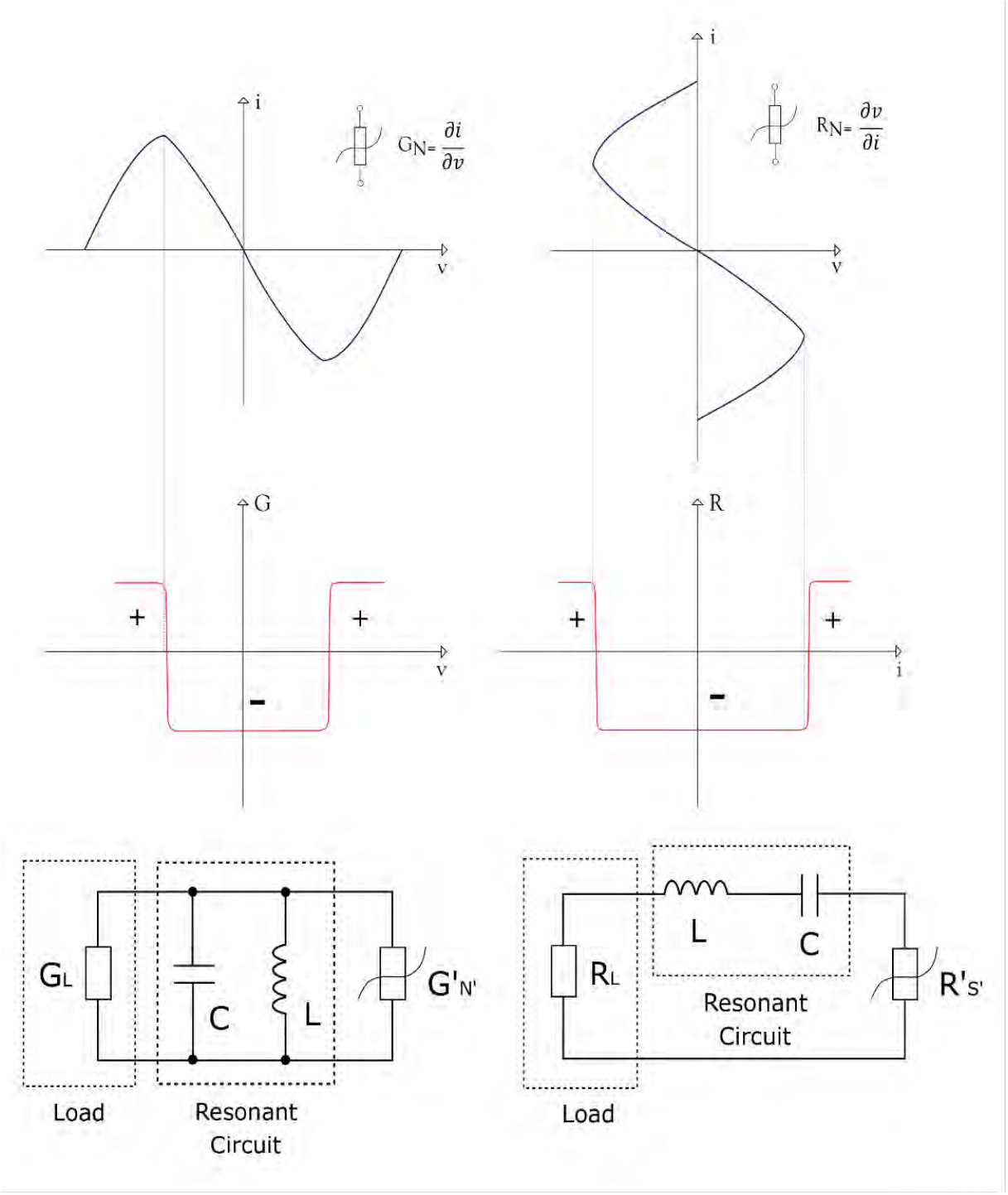

Figure 4-11 Voltage-current curves of negative conductance/resistance elements a) ‘N’ curve, b) ‘S’ curve

4.2.1. Extension of a concept of N and S curves to negative elements

As stressed before, the non-linear behavior of non-Foster networks is highly unexplored. Specifically, it is not clear how would non-linearity affect the operation of proposed non-Foster source. Therefore, it would be very convenient to extend the familiar concept of 'N' and 'S' curves to negative capacitance and negative inductance (non-Foster reactance) [78] (Figure 4-12). Keeping the current/voltage dependence for plotting does not seem to be appropriate since the current is a complex number over here (due to phase shift associated with negative capacitance/inductance). It would be better to define some new variable that is a real number ('effective quantity' [78]). We have chosen the differential electric charge and differential magnetic charge (magnetic flux) as effective quantities. They are related to capacitance and inductance by basic relations:

$$C(v)=\frac{\partial D}{\partial v}=\frac{\partial Q_e}{\partial v}\Rightarrow Q_e=\int C(v)dv \tag{4.1}$$

$$L(i)=\frac{\partial \phi}{\partial i}=\frac{\partial Q_m}{\partial i}\Rightarrow Q_m=\int L(i)di \tag{4.2}$$

Here D and ϕ are electric and magnetic fluxes while Q_e and Q_m stand for electric and magnetic charges, respectively. It is clear that all of these quantities would have their inherent physical meaning only in the case of some real negative non-linear capacitors and inductors (for instance in semiconductor technology and in inductors with ferromagnetic cores). In the case of electronic circuitry that emulate behavior of hypothetical negative capacitors and inductors (NICs) the effective quantities are primarily mathematical tools that simplify analysis. Using discussed approach it is possible to plot generalized N and S curves of non-linear negative capacitors and inductors (Figure 4-12 and Figure 4-13).

Quick analysis of Figure 4-12 and Figure 4-13 reveals that the use of non-linear negative

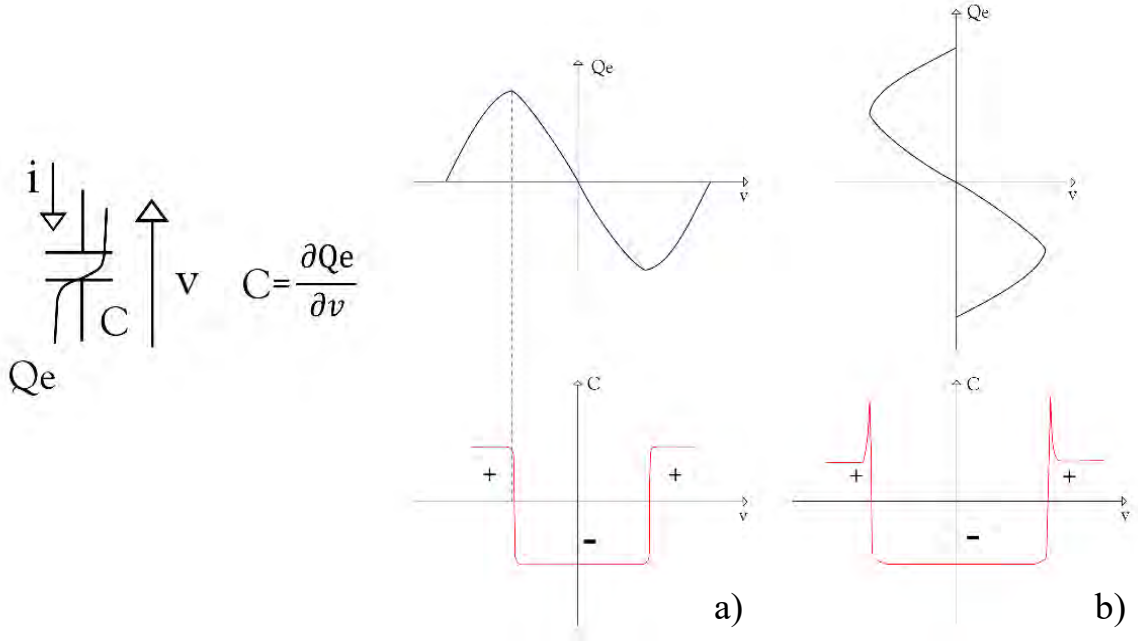

Figure 4-12 Generalized curves of non-linear negative capacitor a) 'N' curve, b) 'S' curve

capacitor in a parallel circuit and the use of non-linear negative inductor in a series circuit

assures smooth transition between positive and negative values at the ends of linear region of the operating curve ('hill top' points). On the contrary the use of non-linear negative capacitor in series circuits and the use of non-linear negative inductor in parallel circuits causes abrupt, pole-like change between positive and negative values at the ends of linear region of the operating curve.

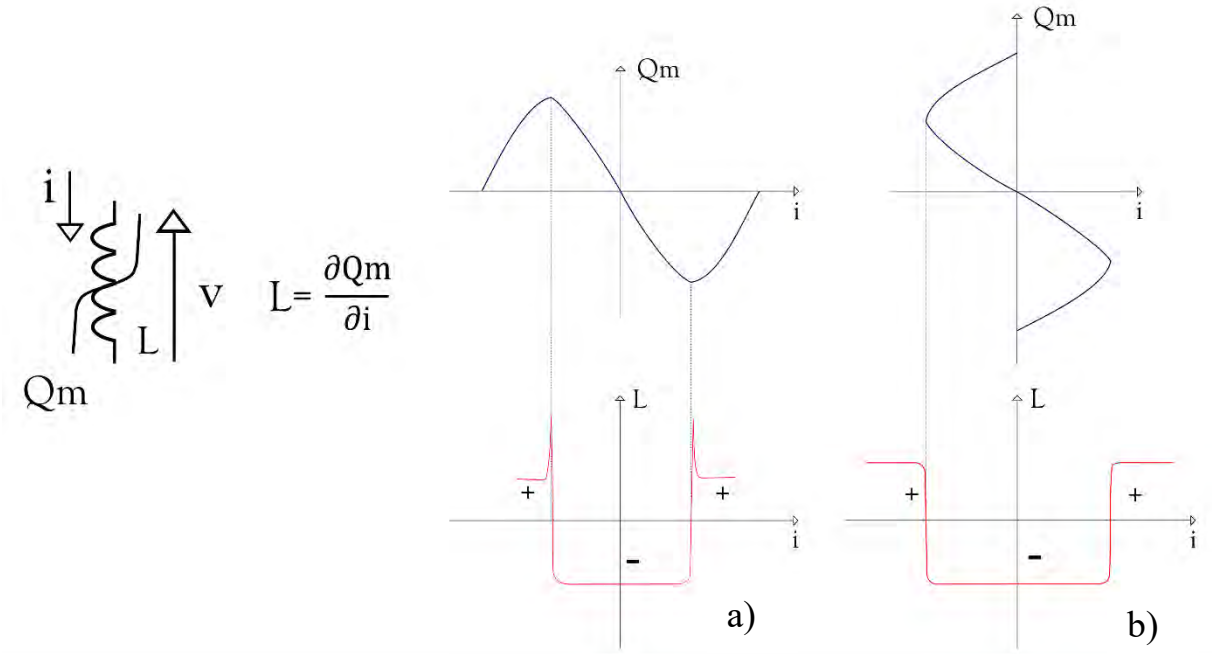

Figure 4-13 Generalized curves of a non-linear negative inductor a) 'N' curve, b) 'S' curve

Let us analyze the N and S curves of negative capacitors and negative inductors generated by NIC circuitry. There are two basic types of NIC circuits: the voltage-conversion type (VNIC) and the current-conversion type (INIC), sketched in Figure 4-14 (a) and, Figure 4-14 (b), respectively [2,51]. Briefly, they employ voltage-dependent and current-dependent sources (voltage and current amplifiers) with inverting loads in positive feedback loops. Simple analysis of circuits in Figure 4-14 (a) and, Figure 4-14 (b), yields well-known expressions for input admittance/impedance [2]:

$$Y_{inVNIC} = Y_L(1 - A_V), \quad Z_{inINIC} = \frac{Z_L}{1 - A_I}. \tag{4.3}$$

Here, $Y_{\text{in,VNIC}}$ and $Z_{\text{in,INIC}}$ are input admittance and impedance, Y_{L} and Z_{L} are associated loads, and A_{V} and A_{I} are voltage and current gain of associated amplifiers (active elements) used in VNIC and INIC circuits, respectively. Neglecting dependence of the gain on the frequency for the moment, one finds that both gains (A_{V} and A_{I}) decrease when the input signal drives circuit into a non-linear regime (this is a familiar phenomenon of gain compression, Figure 4-14 (c). The analysis of (4.3) in the region of compression shows that the input impedance/admittance change in a way described by generalized curves of non-Foster elements (Figure 4-12 and Figure 4-13). This difference (for the case of a capacitive load) is sketched in Figure 4-15. The VNIC has the 'N' type non-linearity and, according to (4.3), the input capacitance smoothly changes from negative to positive values with the increase of input signal level, crossing zero-capacitance for A_{V}=1. On the other hand, the INIC has the 'S' type non-linearity, in which (4.3) yields divergent behavior of input capacitance with a pole at the frequency for which A_{I}=1 (Figure 4-16).

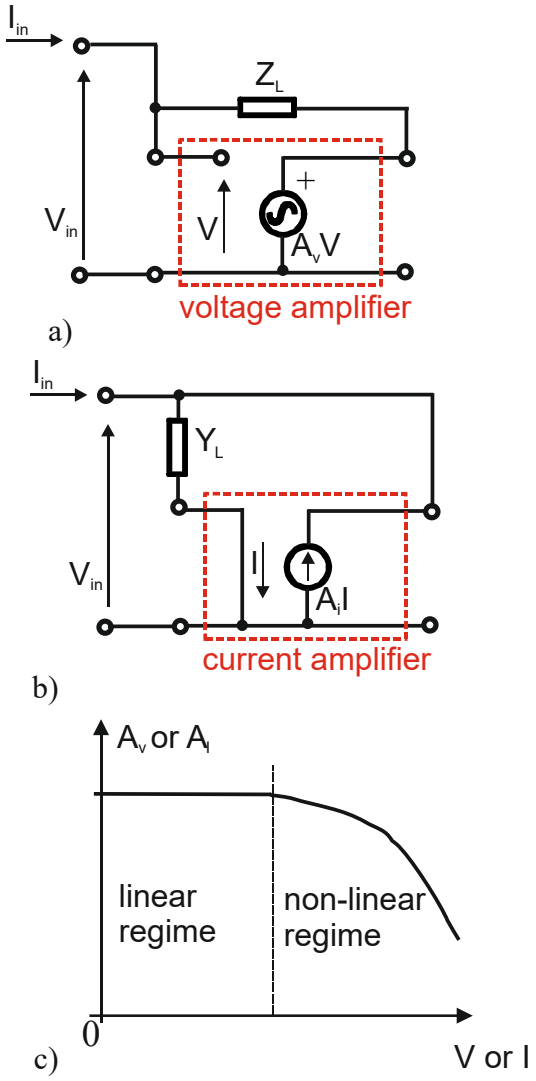

Figure 4-14 Non-linear properties of different types of NIC circuits
a) Basic design of Voltage inversion NIC (VNIC)
b) Basic design of current inversion NIC (INIC)
c) Gain-input characteristic of active element (amplifier) of realistic VNIC or INIC circuit

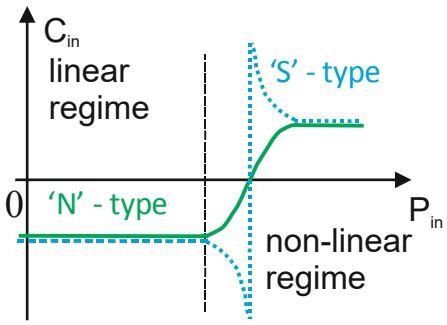

Figure 4-15 Dependence of input capacitance on input signal for VNIC and INIC ('N' and 'S' NIC)

Let us briefly discuss possible practical realization of demonstrators of non-linear non-Foster sources. As it was done in the case of 'all-negative' circuits and 'band-pass' non-Foster elements, in Section 3.3, the high-speed OPamps have been chosen for practical realization. They are very simple for prototyping and allow 'hand-crafting' of appropriate NIC circuits up to several hundred MHz, which is enough for proof-of-concept demonstrations. Extension to microwave regime would be possible by the use of microelectronic technology.

Hence, at this point it is convenient to briefly review the OPamp implementations of N (SCS) an S type (OCS) of NIC circuits.

The N-type NIC is actually an amplifier that uses a non-inverting input for the input impedance port (Figure 4-16).

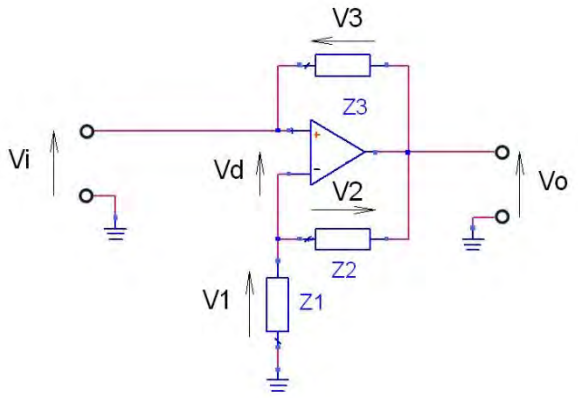

Figure 4-16 N-type of OPAMP-based NIC

KCL and KVL equations for the circuit in Figure 4-16 are:

$$Vi - Vd - i_2 \cdot Z_1 = 0, \tag{4.4}$$

$$Vi - i_i \cdot Z_3 - Vo = 0, \tag{4.5}$$

$$Vo - i_2 \cdot (Z_1 + Z_2) = 0, \tag{4.6}$$

$$Vd - i_i \cdot Z_3 - i_2 \cdot Z_2 = 0, \tag{4.7}$$

$$Vo = A(f) \cdot Vd. \tag{4.8}$$

By solving the system of equations (4.4-4.8) one finds an expression for input impedance:

$$Z_i = \frac{Vi}{i_i} = \frac{(Z_1 + A(f)\cdot Z_1 + Z_2)\cdot Z_3}{Z_1 + Z_2 - A(f)\cdot Z_2}. \tag{4.9}$$

If one neglects amplifier's dependence on the frequency (as it can be done for the frequencies significantly lower than the frequency of the first pole [2]) and providing that a modulus of open-loop gain $|A(f)|$ is large enough, (4.9) can be simplified to:

$$Z_i = -Z_3 \frac{Z_1}{Z_2}. \tag{4.10}$$

By choosing Z_1 and Z_2 to be simple resistors ($Z_1 = R_1, Z_2 = R_2$,) the ratio R_2/R_1 determines the NIC gain and, therefore, the impedance conversion factor.

By exchanging the roles of inverting and non-inverting input terminals, on gets the S-type NIC (Figure 4-17).

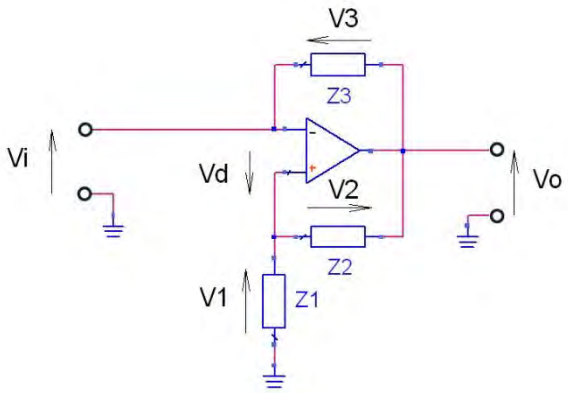

Figure 4-17 S-type of OPAMP-based NIC

By applying very similar analysis as one in the previous case, one obtains the expression for the input impedance:

$$Z_i = \frac{Vi}{i_i} = \frac{(Z_1 - A(f)\cdot Z_1 + Z_2)\cdot Z_3}{Z_1 + Z_2 + A(f)\cdot Z_2}. \tag{4.11}$$

Again, by applying simplifications of neglected frequency response of OPamp and a large modulus of open-loop gain $|A(f)|$ one gets:

$$Z_i = -Z_3 \frac{Z_1}{Z_2}. \tag{4.12}$$

The expressions (4.10 and 4.12) are identical, but they are valid only for very low frequencies. Associated original equations that do not neglect amplitude/phase frequency dependence (4.9 and 4.11) *are different*. Thus, it is expected that the non-linear behavior against frequency *is different* for N and S-types of OPamp-based NICs. Along this line, we performed a slightly more complicated analysis, which takes into account the gain dependence on the

frequency given by (4.9 and 4.11). The result, for the case of negative capacitors is shown in Figure 4-18. It can clearly be seen that the increase of the input power decreases the 'negative' bandwidth smoothly in the case of N-type NIC. On the contrary, there is a 'pole-like' abrupt change in the case of S-type NIC. This behavior is fully consistent with proposed generalized N and S curves in Figure 4-12 and Figure 4-13.

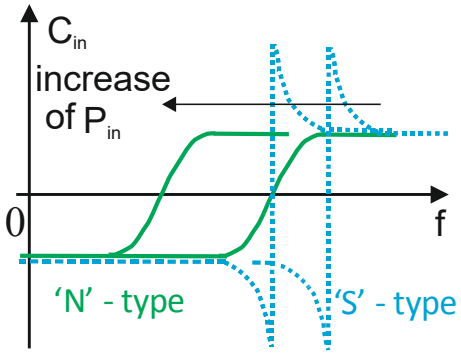

Figure 4-18 Dependence of input capacitance bandwidth on input signal for VNIC and INIC ('N' and 'S' NIC)

So far, the discussion on non-linear behavior of general non-Foster elements and associated NIC circuits has been purely analytical and it used simplified models of active elements (OPamps). It is known that practical OPamps are more complicated than simple idealized models with controlled voltage and current sources. Therefore, we proceeded with numerical analysis using Large Signal S-parameter Simulations (LSSP) within the ADS™ environment. Basic N and S types NIC' schematics from Figure 4-16 and Figure 4-17 have been used, with the SPICE model of THS 4304 high-speed OPamp.

4.2.2. Input impedance and bandwith of non-linear 'N'-type NIC

The first set of simulations deals with the N-type NIC. Three different cases of NICs with several representative loads were simulated:

- N-type NIC with a capacitance (C) in the positive feedback loop (Figure 4-19, Figure 4-20, Figure 4-21 and Figure 4-22)
- N-type NIC with a conductance (G) in the positive feedback loop (Figure 4-23, Figure 4-24, Figure 4-25, and Figure 4-26)
- N-type NIC with a series resistor-capacitor network (RC) in the positive feedback loop (Figure 4-27, Figure 4-28, Figure 4-29, and Figure 4-30)

Two different effects were studied:

- Dependence of input impedance on frequency with input power as parameter
- Dependence of input impedance on input power with frequency as parameter

In all above simulations, a particular attention was paid to the assurance of a 'low-impedance' driving generator, consistent with the suggested SCS use.

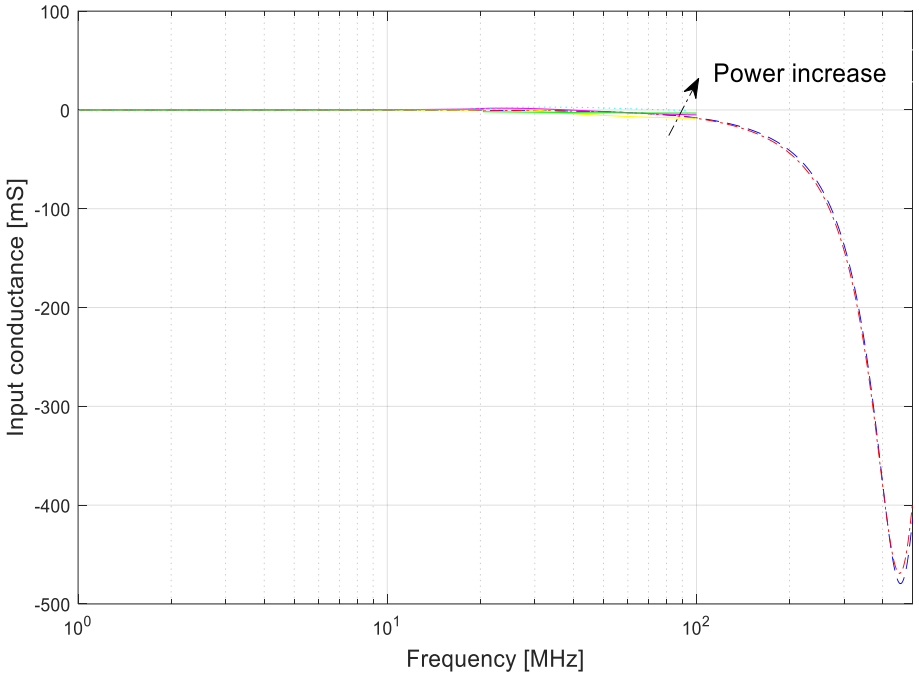

Figure 4-19 Dependence of input conductance of N-type NIC (with capacitance C=50pF in the feedback) on the frequency for several different input power levels (sequentially: 30, 32, 34, 36, 38, and 40 mW)

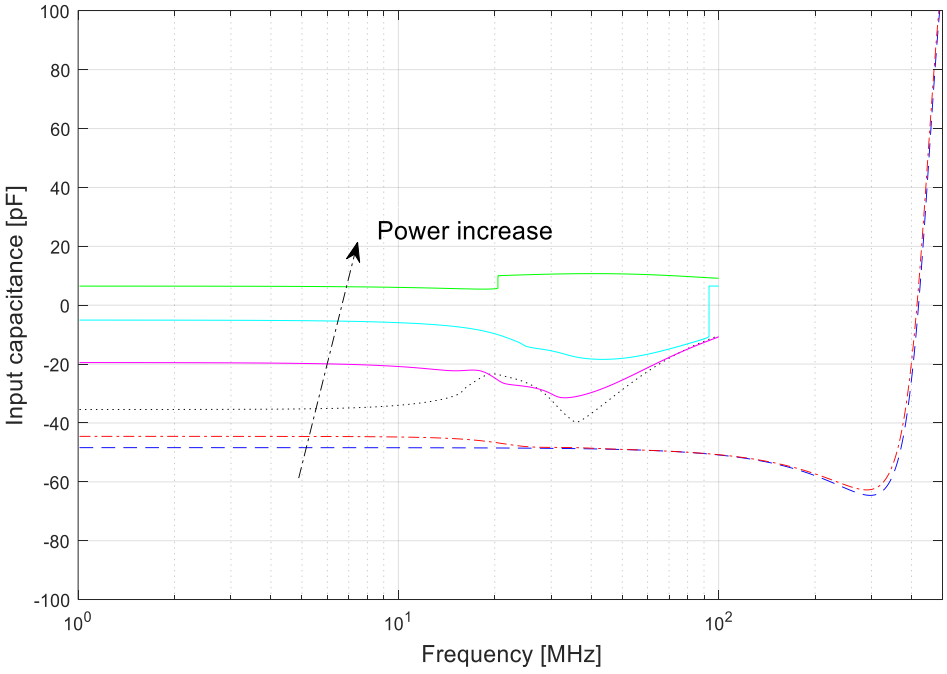

Figure 4-20 Dependence of input capacitance of N-type NIC (with capacitance C=50pF in the feedback) on the frequency for several different input power levels (sequentially: 30, 32, 34, 36, 38 and 40 mW)

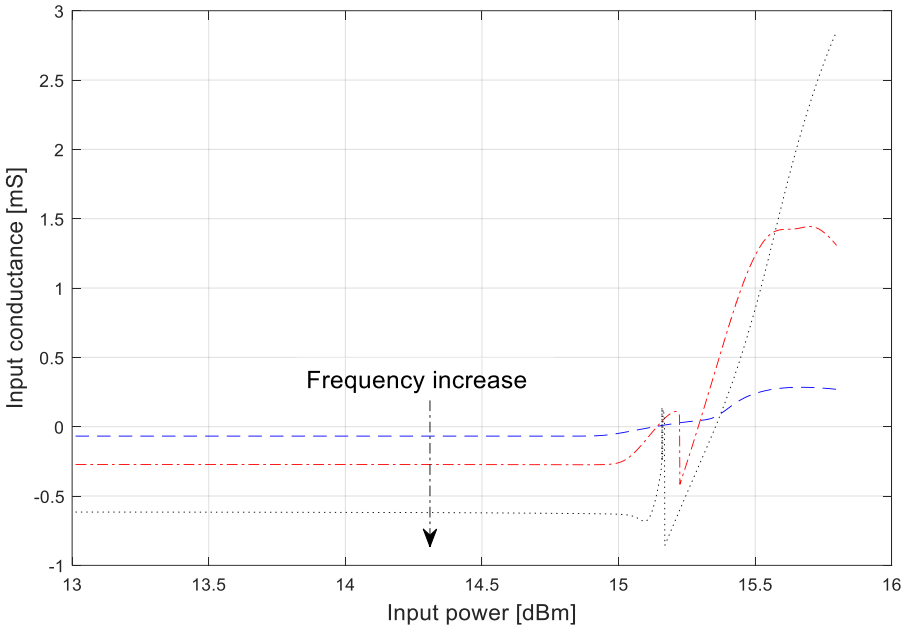

Figure 4-21 Dependence of input conductance of N-type NIC (with capacitance C=50pF in the feedback) on input power at 3 different frequencies (10, 20 and 30 MHz)

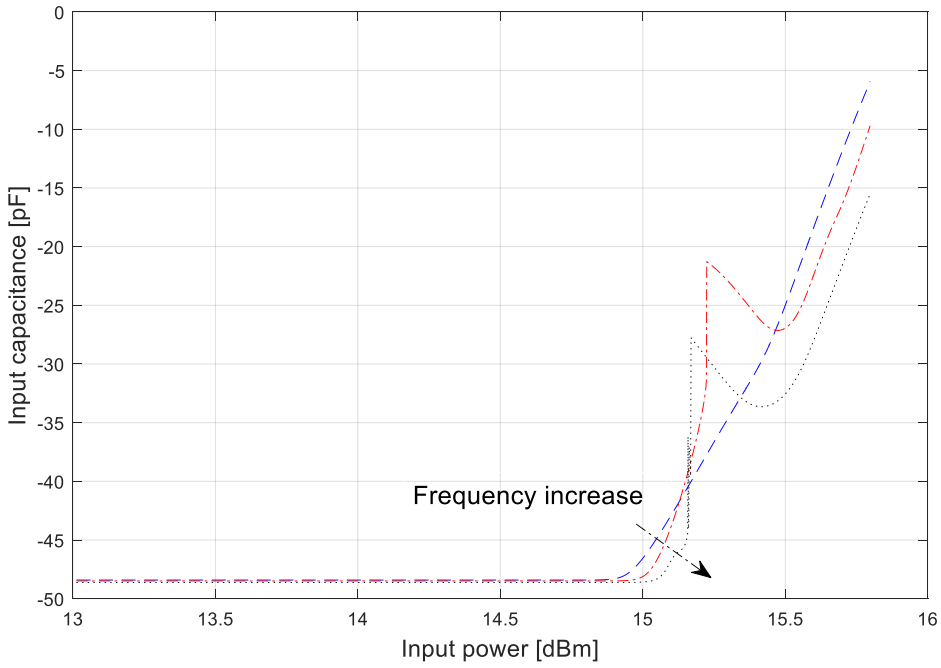

Figure 4-22 Dependence of input capacitance of N-type NIC (with capacitance C=50pF in the feedback) on input power at 3 different frequencies (10, 20 and 30 MHz)

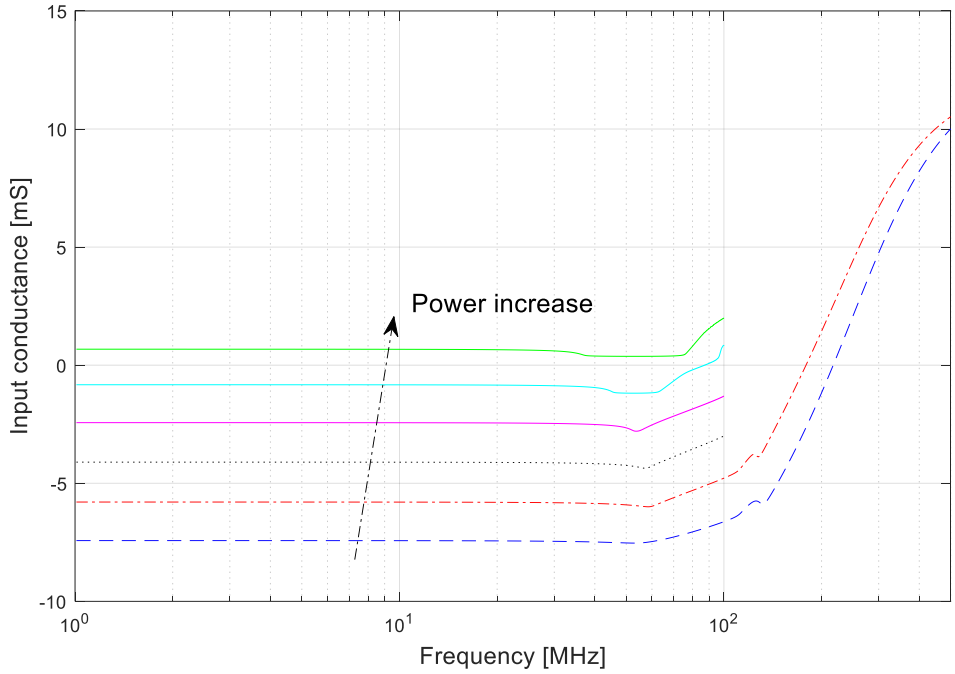

Figure 4-23 Dependence of input conductance of N-type NIC (with conductance G=10mS in the feedback) on the frequency for several different input power levels (sequentially: 30, 32, 34, 36, 38 and 40 mW)

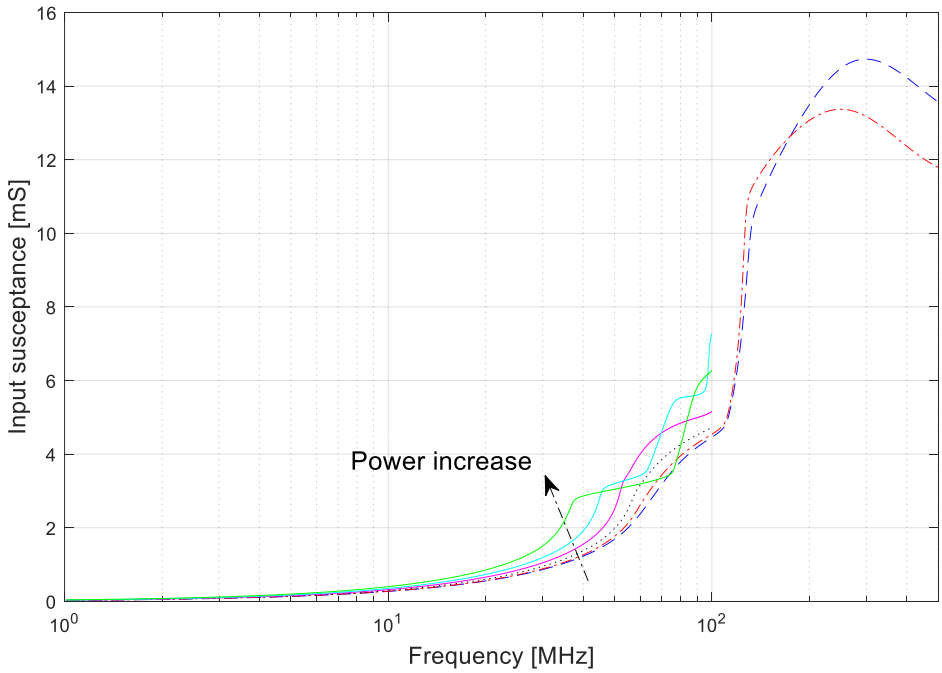

Figure 4-24 Dependence of input susceptance of N-type NIC (with conductance G=10mS in the feedback) on the frequency for several different input power levels (sequentially: 30, 32, 34, 36, 38 and 40 mW)

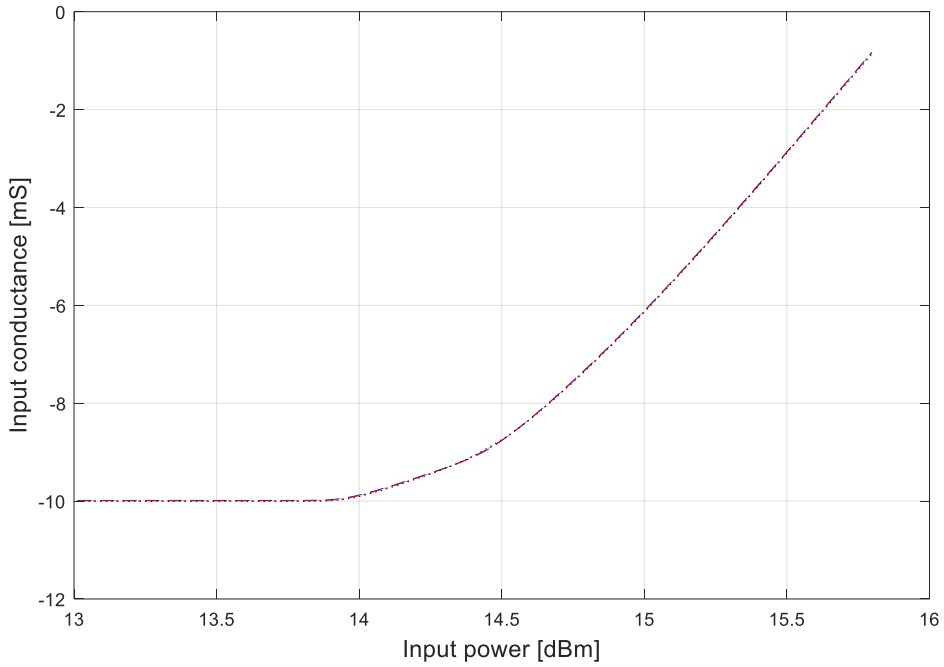

Figure 4-25 Dependence of input conductance of N-type NIC (with conductance G=10mS in the feedback) on input power at 3 different frequencies (10, 20 and 30 MHz)

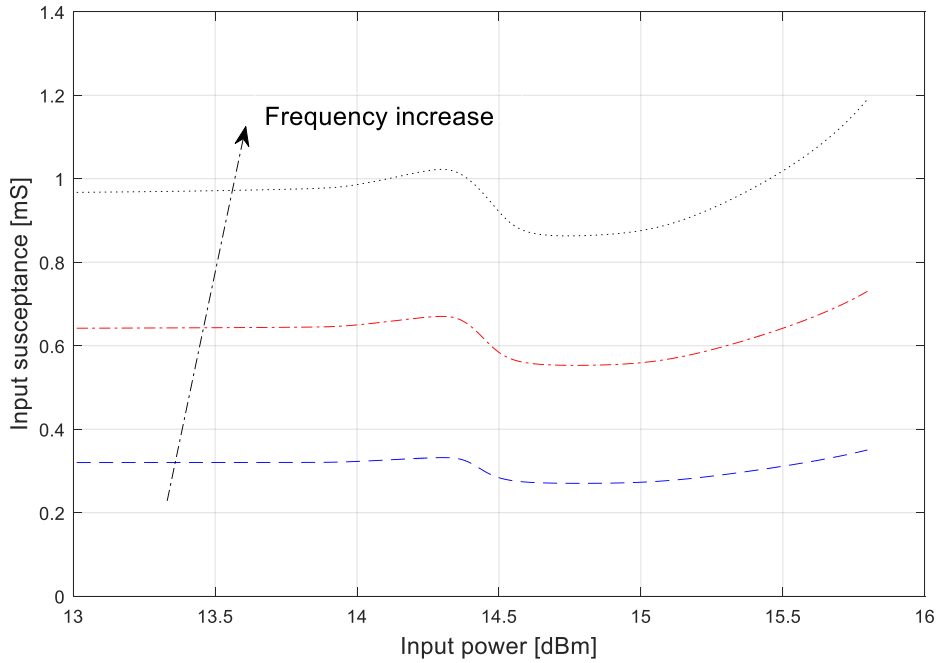

Figure 4-26 Dependence of input susceptance of N-type NIC (with conductance G=10mS in the feedback) on input power at 3 different frequencies (10, 20 and 30 MHz)

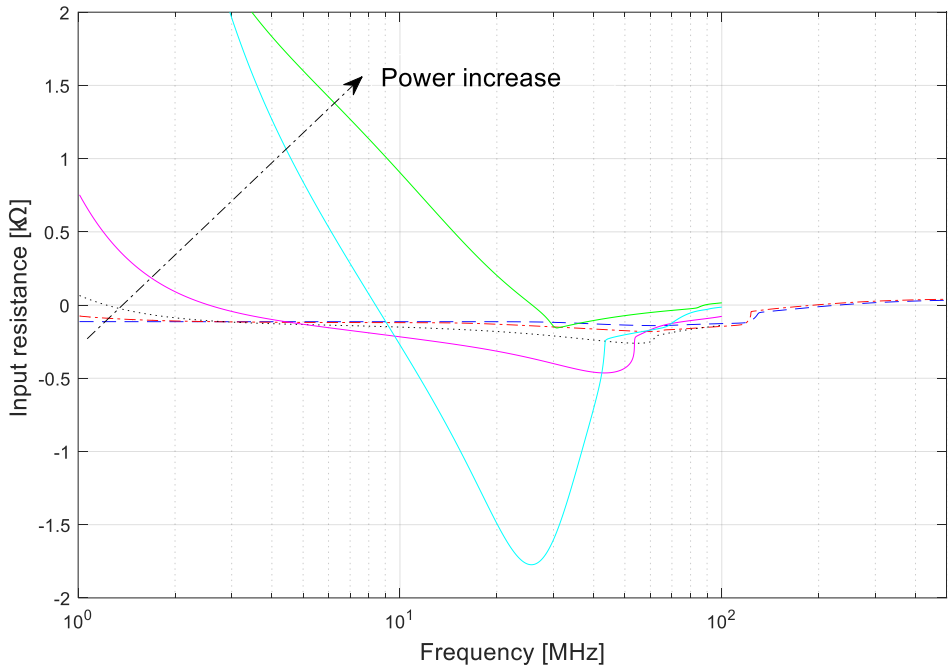

Figure 4-27 Dependence of input resistance of N-type NIC (with series RC combination, R=100Ω, C=50pF, in the feedback) on the frequency for several different input powers (sequentially: 30, 32, 34, 36 and 38 mW)

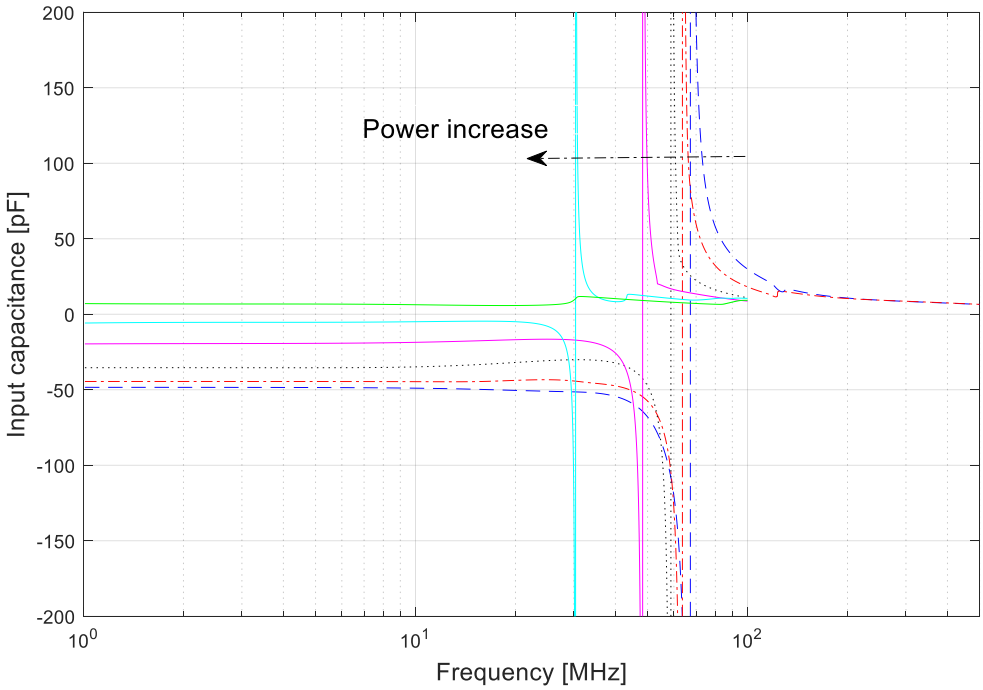

Figure 4-28 Dependence of input capacitance of N-type NIC (with series RC combination, R=100Ω, C=50pF, in the feedback) on the frequency for several different input powers (sequentially: 30, 32, 34, 36 and 38 mW)

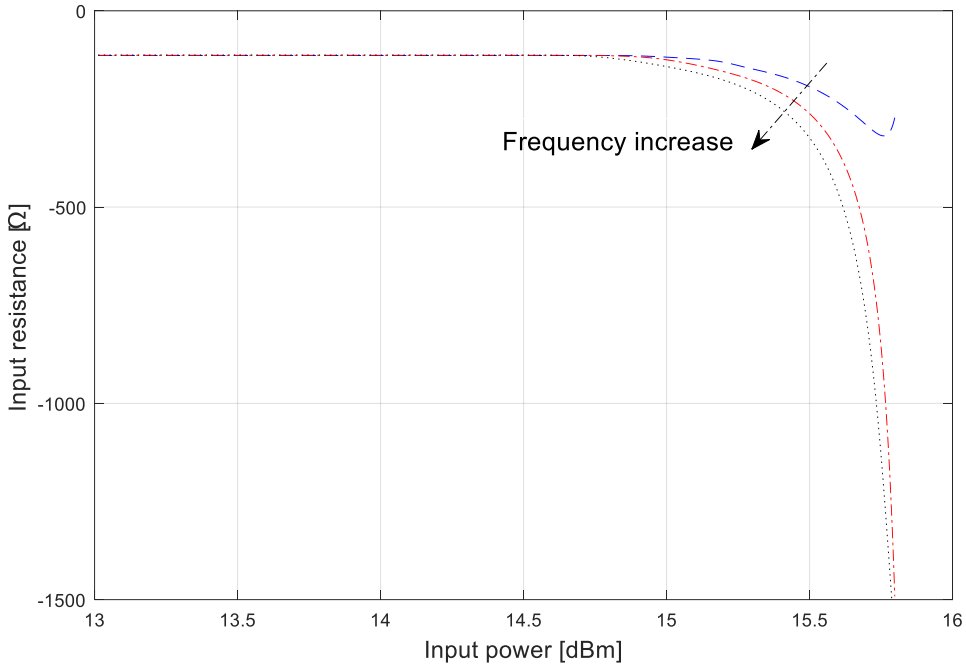

Figure 4-29 Dependence of input resistance of N-type NIC (with series RC combination, R=100Ω, C=50pF, in the feedback) on input power at three different frequencies (10, 20 and 30 MHz)

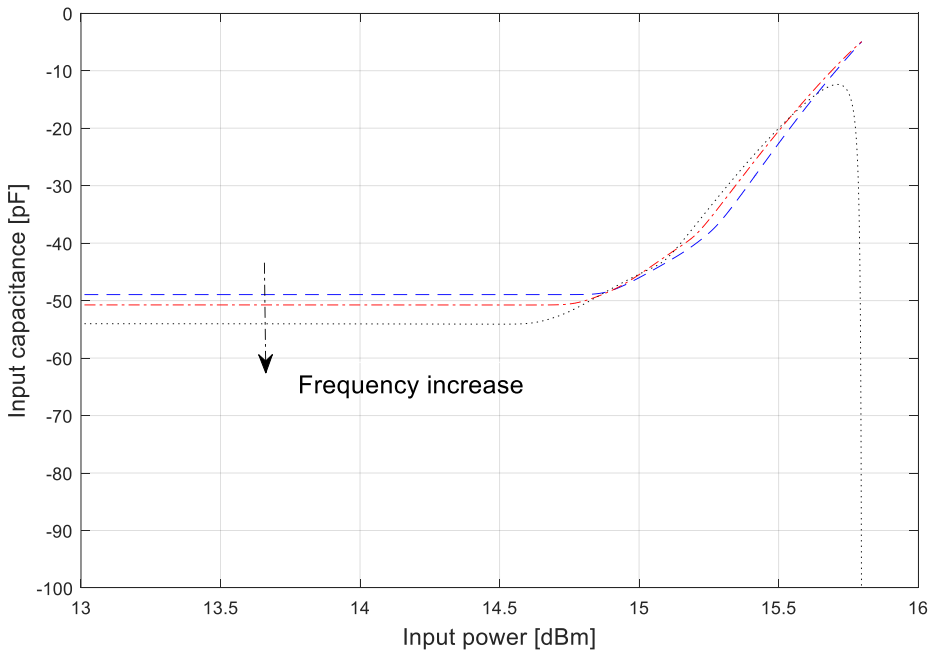

Figure 4-30 Dependence of input capacitance of N-type NIC (with series RC combination, R=100Ω, C=50pF, in the feedback) on input power at three different frequencies (10, 20 and 30 MHz)

There are several important conclusions that can be drawn from the results of the large signal S-parameters analysis of the N-type NIC circuit based on THS 4304 OPamp. At first, the results are mostly in agreement with those from analytical investigations in the Section 4.2.1. In the cases in which the frequency was a parameter, the slight differences occur ('crossing' of the curves) at the higher frequencies (Figure 4-21, Figure 4-22). It might be attributed to the fact that the maximum output current of the amplifier decreases with the frequency, causing sooner occurrence of non-linear effects. In the cases in which the power level was a parameter, the differences generally occurred at higher power levels. This might be associated with the use of simplified models in the Section 4.2.1 and the validity of SPICE models for higher power levels. Somehow unexpected result was obtained for the case of the NIC with series RC circuit in the feedback loop at lower frequency (Figure 4-27). The explanation for this difference might be attributed to the specific OPamp model we used. From the datasheet [118] of THS 4304 one can notice that the resistance of each input node to the ground is only 100 kΩ, which is relatively low for our application. At the frequencies where reactance of the impedance in the positive feedback is much larger than its resistance (below 1 MHz), and also comparable to input resistance of OPamp, the conversion error of real part due to non-linearity is certainly not negligible. Finally, it was noted that, generally, the N-type NIC with the RC circuit in the positive feedback loop introduces a notable error in the impedance conversion if the load is highly reactive (a large ratio between imaginary and real part of the load impedance). These unwanted effects will be analyzed in more details in Section 4.3.

In spite of observed differences, it can be concluded that the non-linear behavior of N-type NIC circuit is quite robust on load variation and no instability problems were noted.

4.2.3. Input impedance and bandwith of non-linear 'S'-type NIC

The second set of simulations deals with S-type NIC. Although it was planned to run the same cases of NICs with representative loads as with the N type, that was not found possible. Many different cases of input generator network (designed in order to simulate a current source in order to meet the OCS condition) have been teste. It was found that the S type NIC is sensitive to load, and in many cases was unstable. Thus, we managed to simulate the following cases:

- S-type NIC with a resistance (R) in the positive feedback loop (Figure 4-31, Figure 4-32, Figure 4-33, Figure 4-34)
- S-type NIC with a capacitance (C) in the positive feedback loop (Figure 4-35, Figure 4-36)
- S-type NIC with a series resistor-capacitor network (RC) in the positive feedback loop (Figure 4-37, Figure 4-38)

As in the previous analysis, following effects were studied (for some cases only one effect could be considered):

- Dependence of input impedance on frequency with input power as parameter (only for the case with a resistance (R) in the positive feedback loop)
- Dependence of input impedance on input power with frequency as parameter

Analysis of the obtained results shows predicted behavior at lower input power levels. However, at higher levels (above 40 mW), the occurrence of instability was observed. Thus, it seems that the S–type OPamp-based NIC is rather sensitive on both load and source impedance variation and, therefore, less appropriate for the construction of a non-Foster source.

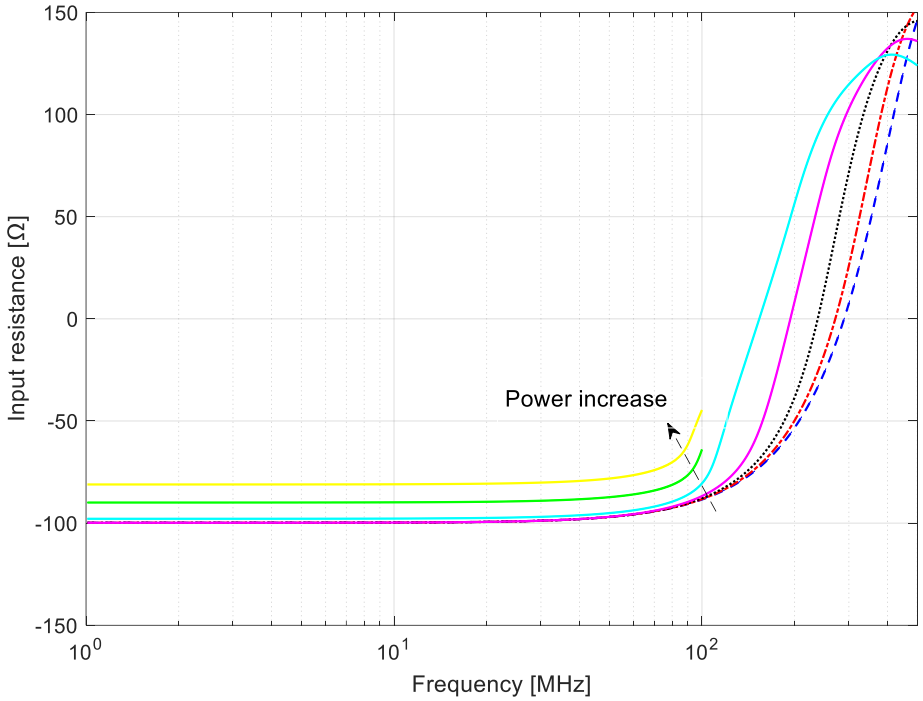

Figure 4-31 Dependence of input resistance of S-type NIC (with resistance R=100Ω in the feedback) on the frequency for several different input power levels (sequentially: 36, 39, 42, 45, 48, 49 and 50 mW)

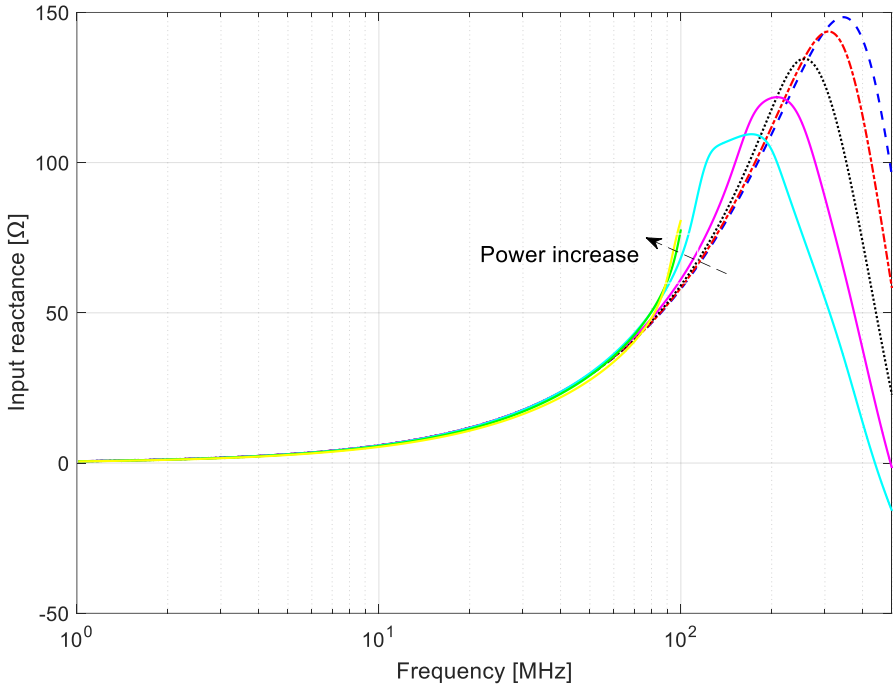

Figure 4-32 Dependence of input reactance of S-type NIC (with resistance R=100Ω in the feedback) on the frequency for several different input power levels (sequentially: 36, 39, 42, 45, 48, 49 and 50 mW)

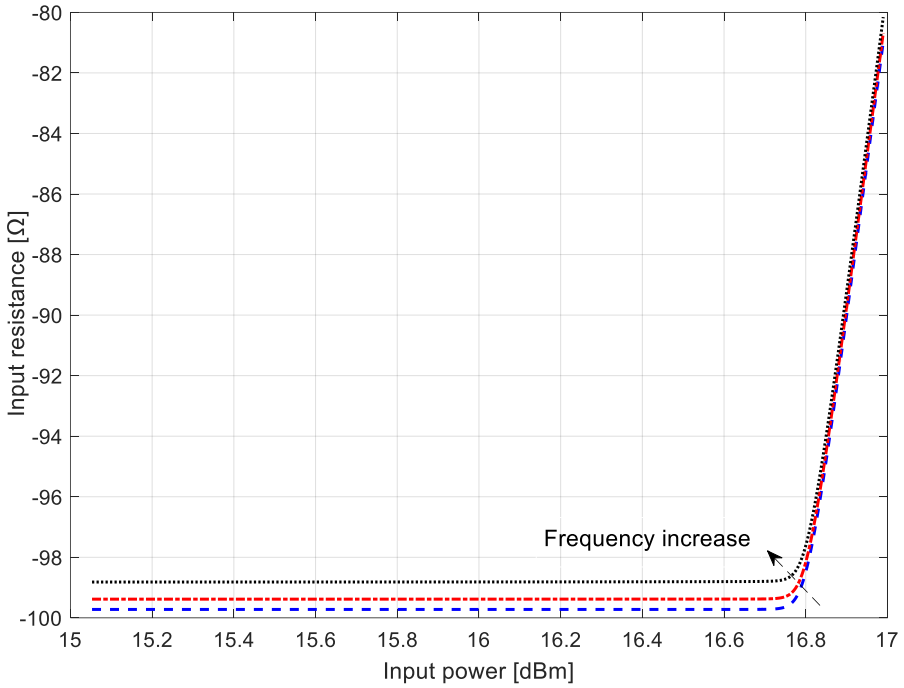

Figure 4-33 Dependence of input resistance of S-type NIC (with resistance R=100Ω in the feedback) on input power at three different frequencies (10, 20 and 30 MHz)

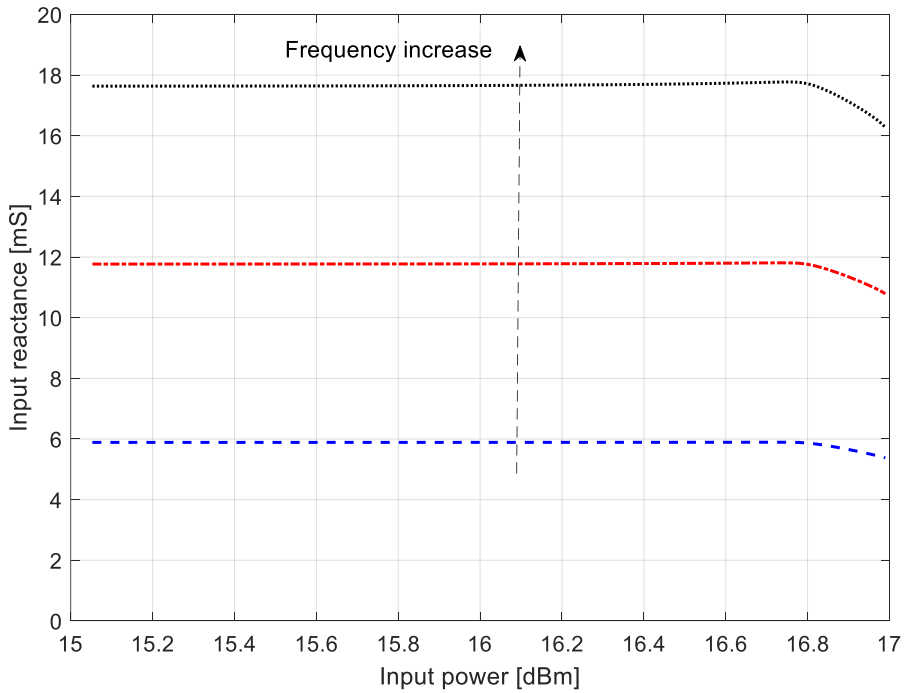

Figure 4-34 Dependence of input reactance of S-type NIC (with resistance R=100Ω in the feedback) on input power at three different frequencies (10, 20 and 30 MHz)

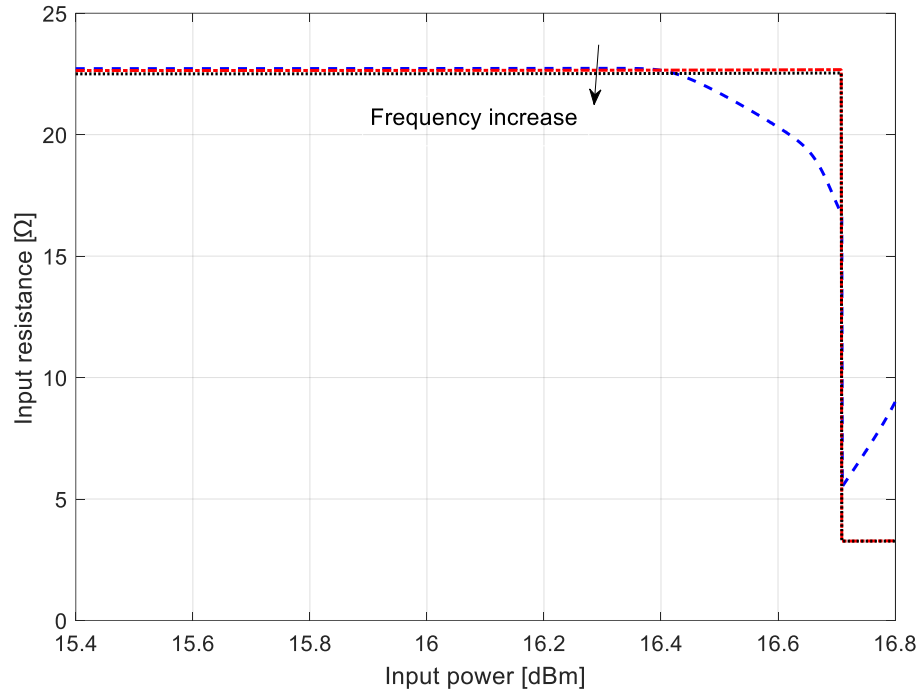

Figure 4-35 Dependence of input resistance of S-type NIC (with capacitance C=50pF in the feedback) on input power at three different frequencies (10, 20 and 30 MHz)

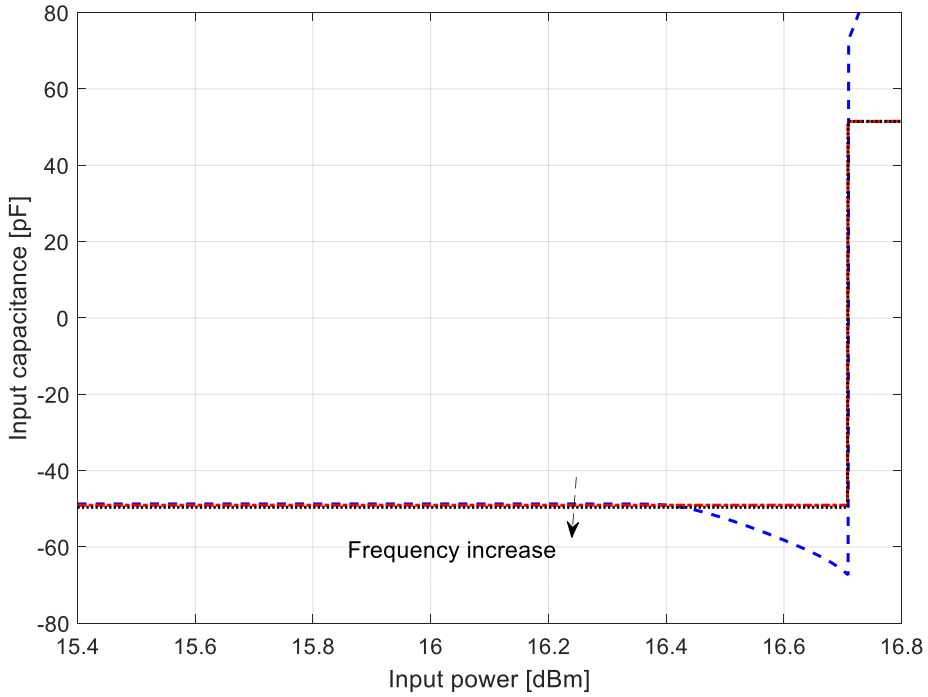

Figure 4-36 Dependence of input capacitance of S-type NIC (with capacitance C=50pF in the feedback) on input power at three different frequencies (10, 20 and 30 MHz)

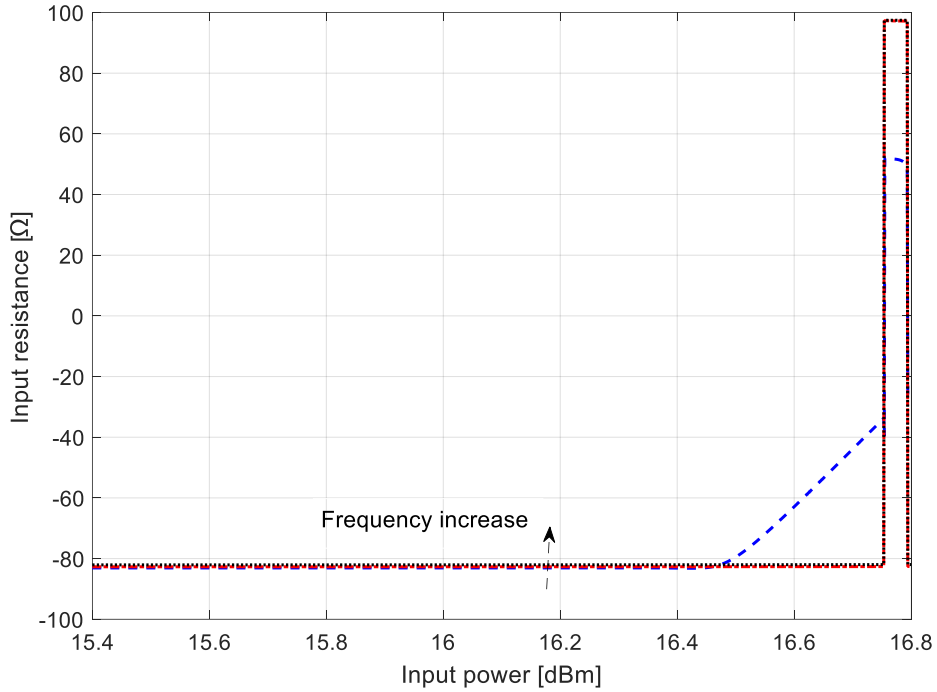

Figure 4-37 Dependence of input resistance of S-type NIC (with series RC combination, R=100Ω, C=50pF, in the feedback) on input power at three different frequencies (10, 20 and 30 MHz)

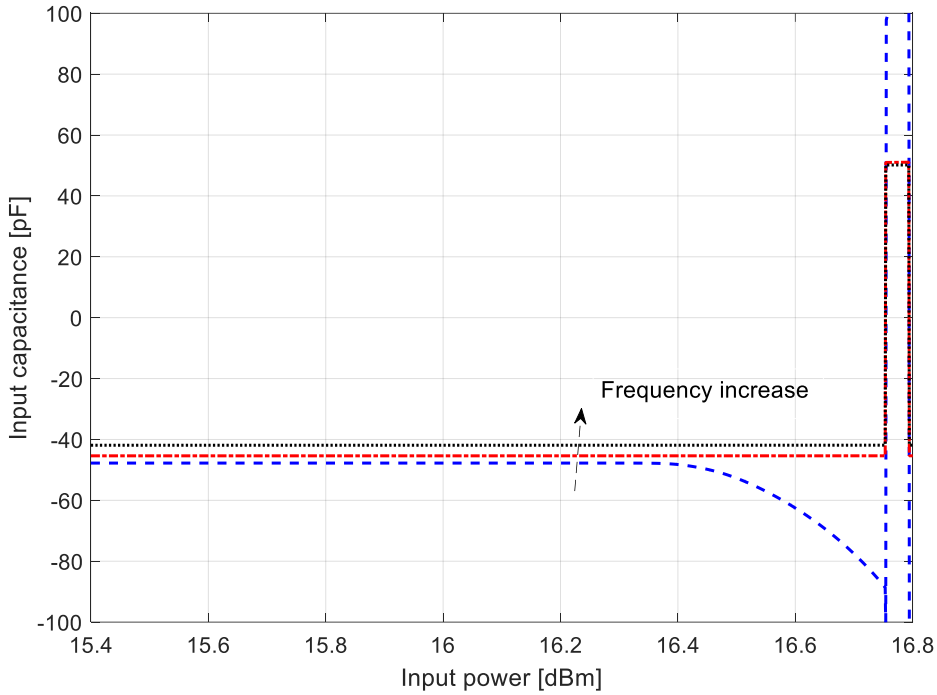

Figure 4-38 Dependence of input capacitance of S-type NIC (with series RC combination, R=100Ω, C=50pF, in the feedback) on input power at three different frequencies (10, 20 and 30 MHz)

4.2.4. Non-linear non-Foster source versus large-signal negative-resistance oscillator

The analysis of non-Foster source in the Section 4.1. pointed out that the main difference between a linear non-Foster source and a classical small signal negative oscillator is in the tuning and matching bandwidth. In ordinary oscillator, the oscillation condition of 'mirror image' impedances of active and passive parts is met at only one frequency, determined by some kind of a resonant circuit. In the case of a non-Foster source (Figure 4-9, Figure 4-10) this condition is met at every frequency, with perfect matching. Furthermore, the inclusion of the tuning resonant element assures a very broad (theoretically infinite) tuning bandwidth. In this section, this comparison is extended to the large-signal (non-linear) behavior.

The case of a classical large-signal N-type negative-resistance oscillator that comprises active element (Y_A), load (Y_L) and a parallel resonant LC circuit (Y_{RES}) [19] is briefly reviewed in Figure 4-39 (a). The oscillator dynamics is described by the admittance loci of the active element and the resonant circuit in the complex plane (Figure 4-39 (b), with standard approximation, in which the active impedance is considered only amplitude dependent). After the onset of oscillations (caused by the noise), locus of the 'mirror image' of real part of active negative impedance ($-Y_A$), grows until it intersects the load-line (a parallel combination of Y_{RES} and Y_L). This intersection (point 'P') represents stable operating point. If the resonant frequency of an LC circuit changes, the intersection will occur at a new stable operating point P. Usually, the tuning bandwidth is small ($\Delta\omega/\omega_0 \ll 1$) and it depends on the part of the active element admittance curve that can be intersected by a load line.

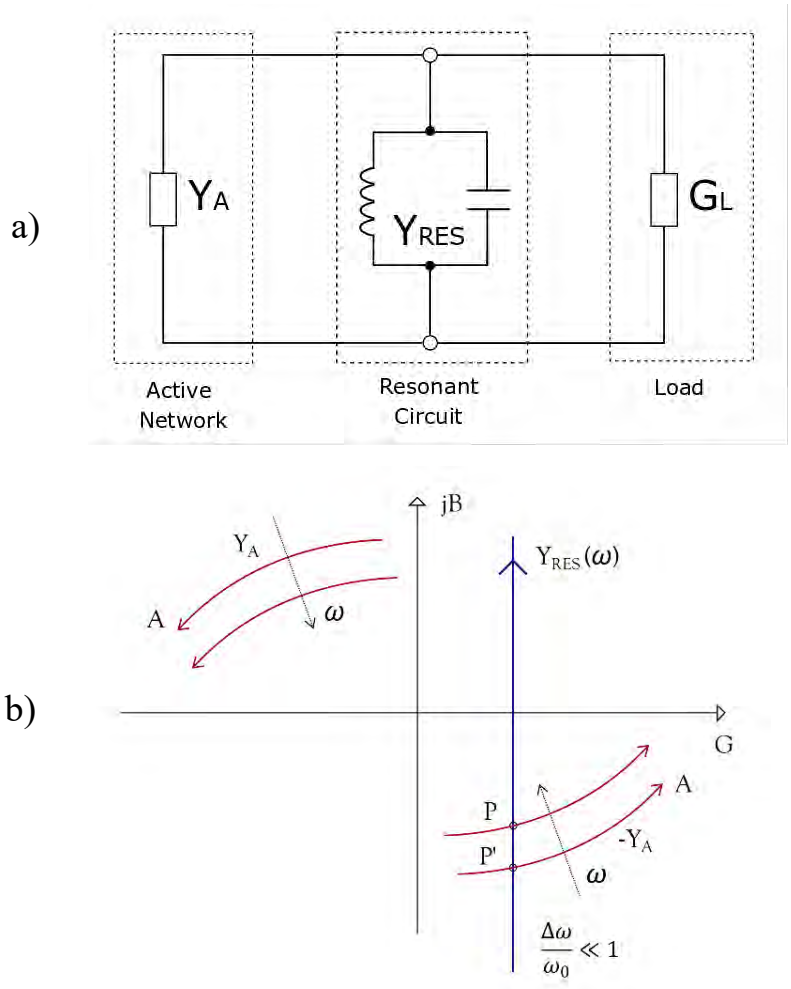

Figure 4-39 Classical large-signal 'N'-type negative-resistance oscillator a) equivalent circuit b) Admittance loci of active element, load, and the resonant circuit

a)

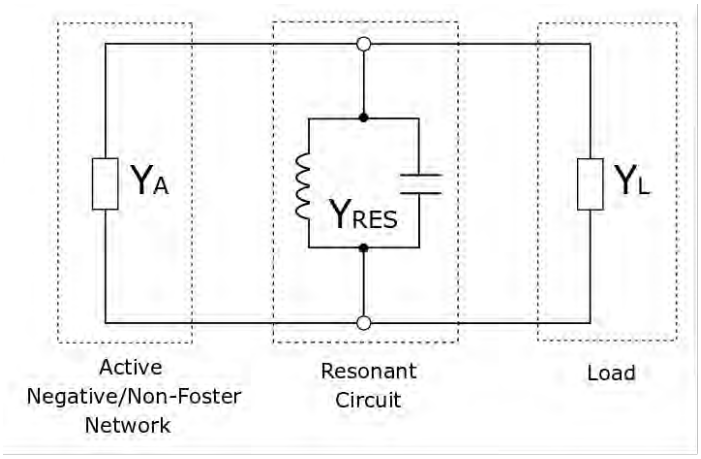

b)

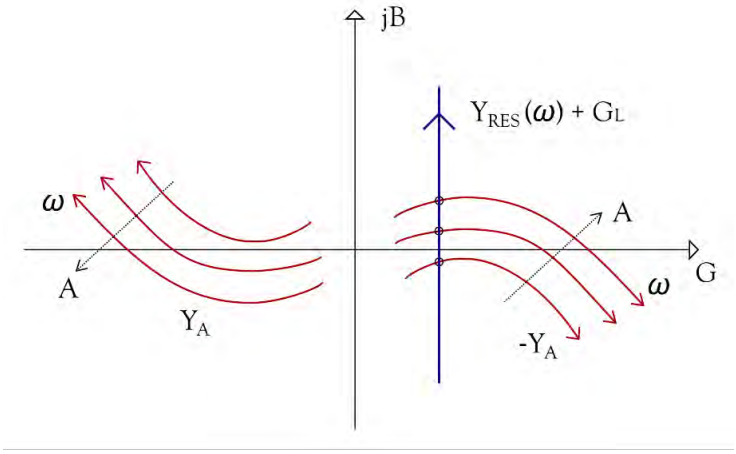

c)

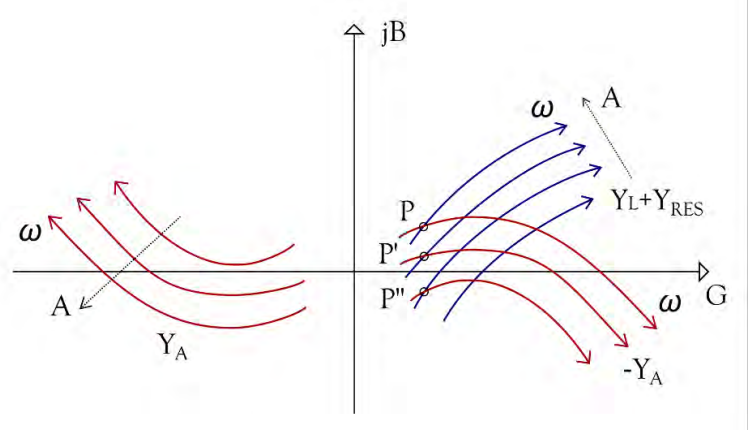

Figure 4-40 a) Non-linear 'N'-type non-Foster source equivalent circuit b) Admittance loci of active element, resistive load, and resonant circuit c) Admittance loci of active element, general complex load, and resonant circuit

Situation is rather different in the case of the non-linear non-Foster source (Figure 4-40 (a)). In the case of a simple resistive load, the operation is very similar to the one in ordinary negative -resistance oscillator (Figure 4-40 (b), except that the tuning range may be larger). The main difference occurs in the case of a general complex load (Figure 4-40 (c)), for which the tuning bandwidth can be significantly larger. The bandwidth will be very broad if the locus of active admittance (approximately) follows the locus of a passive element. If the active element is constructed with the help of NIC that inverts the impedance that is identical to a load impedance (Section 4.4), the tuning bandwidth is (theoretically) infinite.

4.3 Non-Foster antenna-transmitter

Discussion in Section 4.2. showed that a non-linear non-Foster source can be thought of as a perfectly-matched and broadly tunable oscillator. In this section, we investigate possibility of combining the non-Foster source and an antenna into a (nearly) perfectly matched and broadly tunable radiating system. This system is termed as a 'Non-Foster antenna-transmitter'.

4.3.1. Basic concept

Classical realization of any transmitting system comprises three building blocks: an RF source, a guiding structure (transmission line or a waveguide) with matching network and a transmitting antenna (Figure 4-41 (a)). One of the greatest challenges in such a design is matching of a small antenna. It is well known that impedance of a small antenna is inevitably highly reactive, which significantly limits the achievable matching bandwidth [60, 120]. Quite often, a passive matching network cannot achieve an acceptable impedance match within a full desired bandwidth. The typical fractional bandwidth, defined as useful bandwidth divided by its center frequency, achievable using a passive matching of a small antenna ranges between 10 to 15 %. On the other hand, non-Foster networks can be used to realize significantly wider matching bandwidths. However, as detailed in Section 4.1.2, this approach is still very limited due to problems of the proneness to instability and (sometimes) not acceptable poor efficiency of the NIC. Similar problems may occur in application of a simple non-Foster source that contains an external generator and non-Foster impedance (Section 4.1.1. and Section 4.1.2.).

Recently, we proposed a quite unusual approach of managing stability issue of active non-Foster matching in transmitting applications [82]. It is a self-oscillating non-Foster matching network connected to a short dipole antenna (a dipole antenna shorter than $\lambda/10$), (Figure 4-41 (b)). Thus, the whole transmitting chain (from Figure 4-41 (a)) is replaced with a new single-element system: Antenna-transmitter. This is actually a non-linear non-Foster source (Section 4.2), a load of which is a transmitting antenna.

One may argue that a system in Figure 4-41 (b) is nothing more than a well-known concept of active antennas [119]. However, there is one important difference between classical active antenna [119] and a non-Foster antenna-transmitter: a non-Foster source can assure perfect matching of the antenna across extremely broad bandwidth. Let us discuss this issue in more details. The system in Figure 4-841 (b) depicts a simple case of a 'negative' (*-R-C*) circuit (obtained by the negation of series 'positive' *RC* circuit via an ideal NIC). If such a negative impedance is connected to the short dipole antenna (again modelled as a simple positive RC circuit) the overall system will be unstable. Actually, the system operates as a perfectly-matched non-Foster source (Figure 4-841) and the presence of *negative resistance* supports a *real power flow* that causes radiation with perfect matching (the antenna radiation resistance 'absorbs' the

RF energy generated by its 'negative image' (-R)). At the same time, imaginary part of the antenna impedance is compensated with –C. In order to assure the sinusoidal oscillations, one follows 'a recipe' from Figure 4-9 and Figure 4-10 and add the tuning LC circuit of series or parallel type. This completes the concept of a non-Foster transmitter, sketched in Figure 4-42.

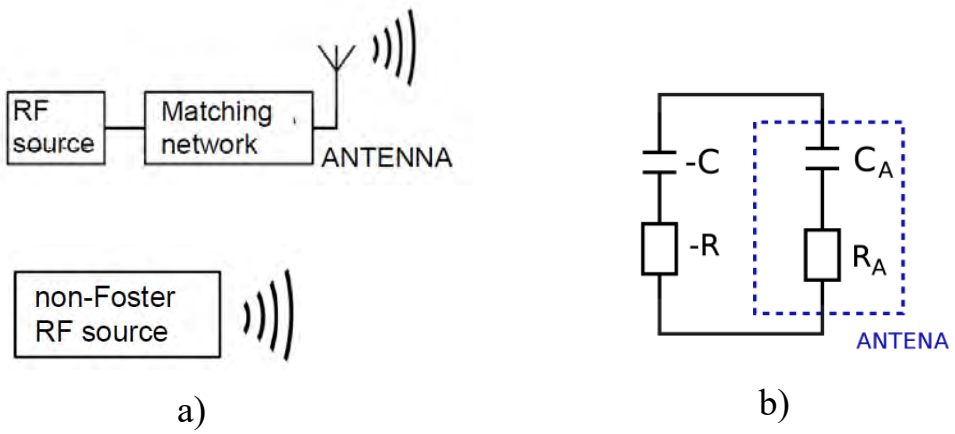

Figure 4-41 Basic concept of a non-Foster antenna-transmitter
a) Comparison between usual implementation of negative elements for use in antenna matching networks and a non-Foster source which consists of antenna and transmitter integrated in one system
b) Simplified schematic of a non-Foster antenna-transmitter network

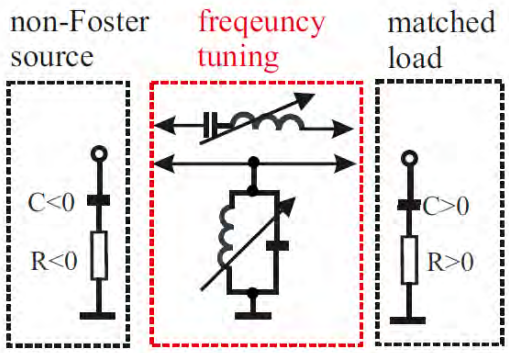

Figure 4-42 A simplified block diagram of a tunable non-Foster antenna-transmitter

As a first step in investigation of the correctness of proposed idea, we decided to perform extensive numerical analysis of the system from Figure 4-42.

4.3.2. Numerical investigation

The model of antenna transmitter system contained the N-type OPamp-based NIC discussed in Section 4.2, Figure 4-16, two passive RC networks and a parallel tuning LC circuit (Figure 4-43). The THS 4304 device was again chosen as the active device and it was described by the SPICE model provide by manufacturer. The NIC conversion ratio was adjusted by resistors R_1 and R_2, while the antenna was modelled as a simple $R_F C_F$ combination.

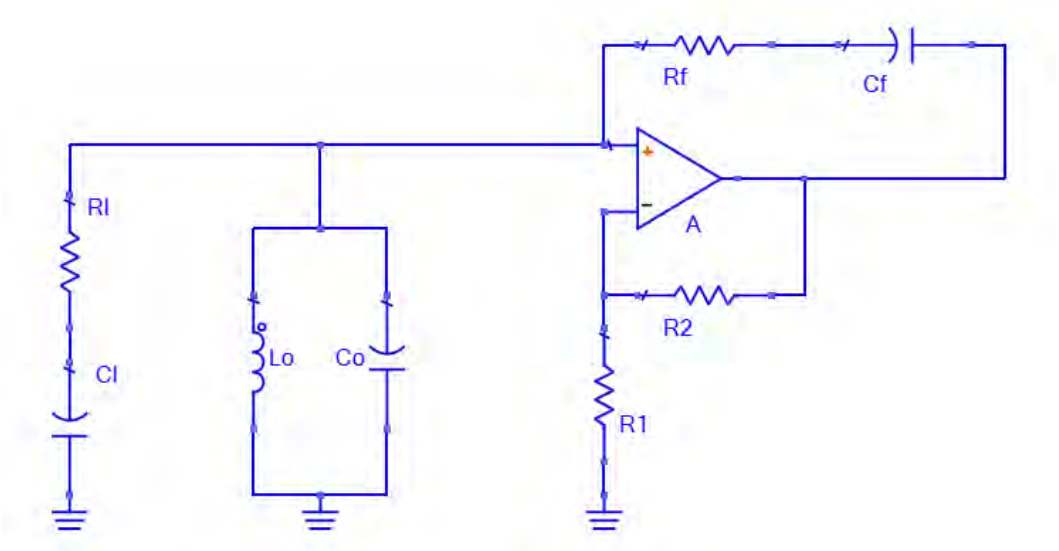

Figure 4-43 Simplified schematic of N-type non-Foster antenna-transmitter implemented using operational amplifier with antenna-emulating network (R_L, C_L). The frequency of oscillations is adjusted by L_0C_0 tank circuit

For the beginning, the NIC conversion factor in SPICE model was set to 1 (A=2, R_1=R_2=243Ω). Two different antenna models (given by the values of R_L and C_L) were used: a model of a short dipole antenna (l ≈λ/10, l being the antenna length, R_L=2.2Ω, C_L=3.9pF), and a model of dipole antenna operating slightly below resonance, with l being slightly less than λ/2 (R_L=60Ω, C_L=220pF), l being the antenna length. The appropriate values of L_0, C_0, needed to tune the oscillations at the predetermined frequency, were chosen accordingly.

Transient simulations in the ADS™ environment were used for investigation of the NIC input impedance/admittance. An external disturbing pulse was used to initiate the oscillations. The input impedance was calculated by dividing Fourier transforms of voltage and current signals at first harmonic, once the steady state is achieved (at the NIC input terminals). Clearly, this approach takes into account the NIC non-linearity. Therefore, it should give more realistic results than a simplified analytical approach used in the previous discussion. Simulated input impedance was compared to the analytically determined input impedance of an ideal NIC and the measurements on assembled RF demonstrator (hardware details of this demonstrator will be described in Section 4.3.4.). The results are given in Figure 4-44, Figure 4-45, Figure 4-46, and Figure 4-47.

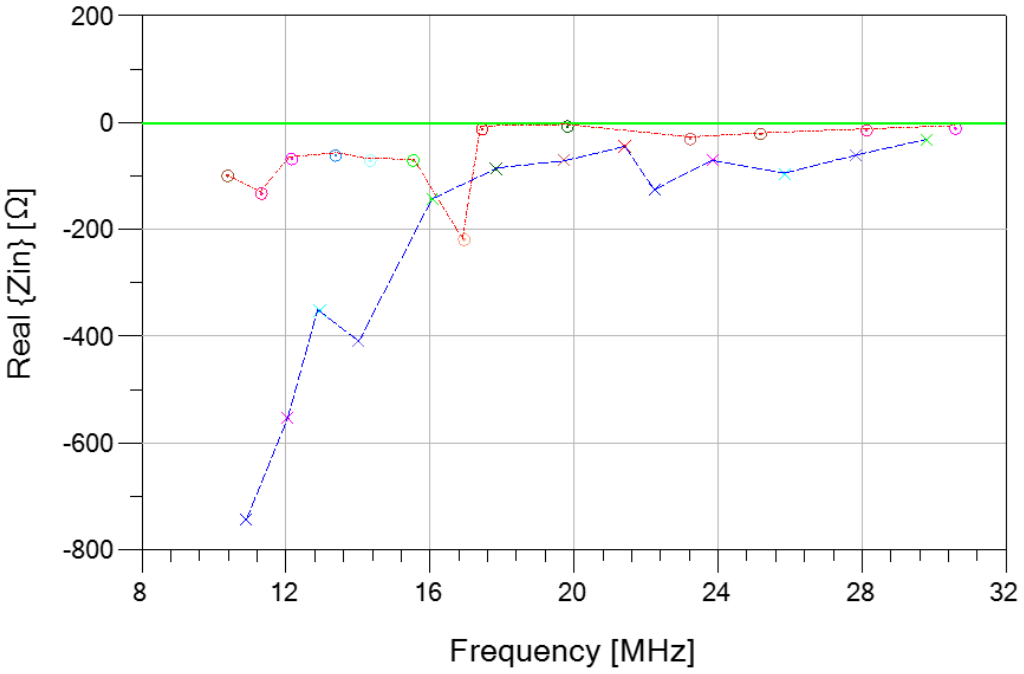

Figure 4-44 Real part of input impedance of N-type antenna-transmitter with series RC combination, mimicking short antenna $l \approx \lambda/10$ (R_L=2.2Ω, C_L=3.9pF), a comparison between ideal negative RC (green solid line), transient simulation (red dotted) and measurements on experimental demonstrator (blue dashed).

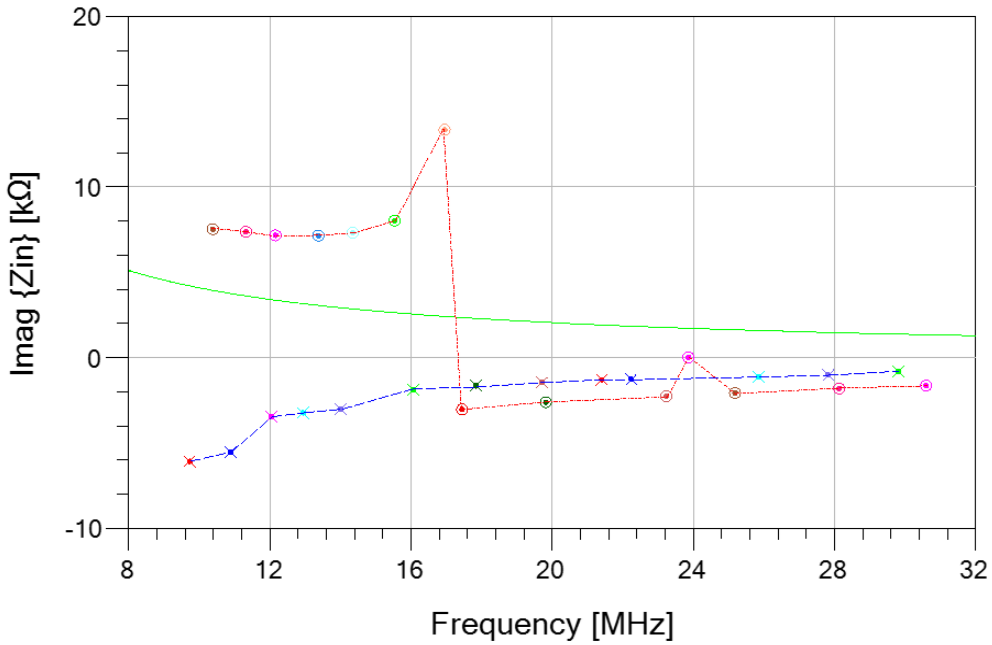

Figure 4-45 Imaginary part of input impedance of N-type antenna-transmitter with series RC combination, mimicking short antenna $l \approx \lambda/10$ (R_L=2.2Ω, C_L=3.9pF), a comparison between ideal negative RC (green solid line), transient simulation (red dotted) and measurements on experimental demonstrator (blue dashed)

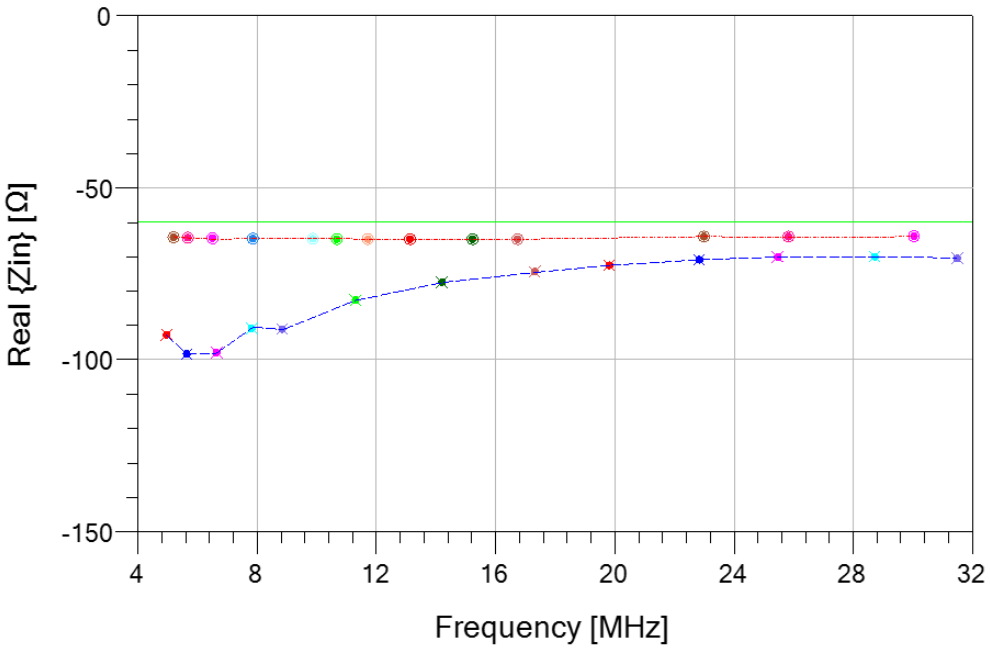

Figure 4-46 Real part of input impedance of N-type antenna-transmitter with series RC combination, mimicking resonant antenna $l \approx \lambda/2$ (R_L=60Ω, C_L=220pF), a comparison between ideal negative RC (green solid line), transient simulation (red dotted) and measurements on experimental demonstrator (blue dashed)

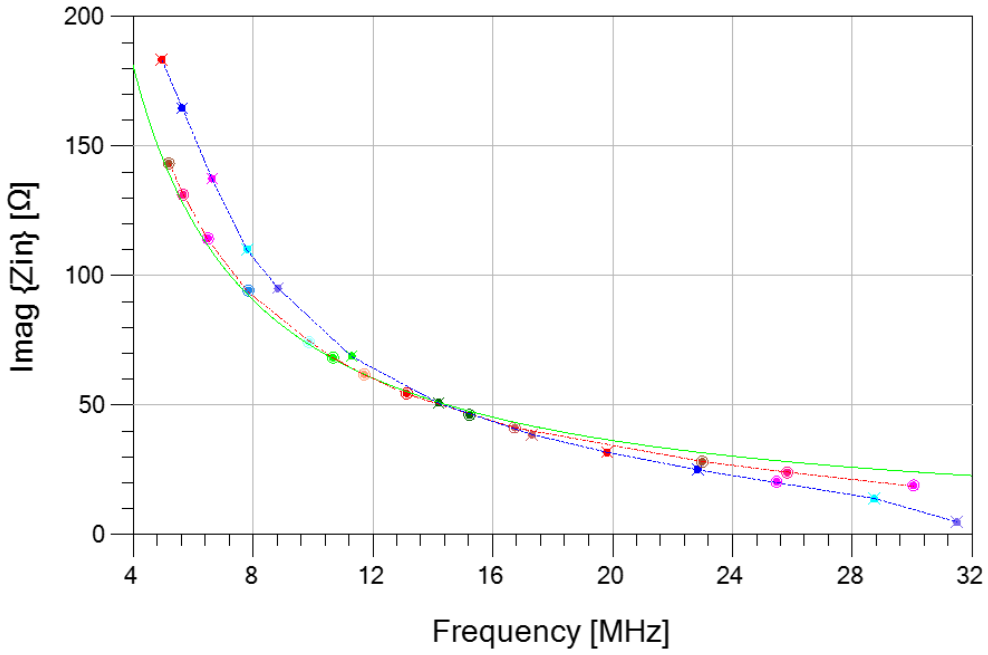

Figure 4-47 Imaginary part of input impedance of N-type antenna-transmitter with series RC combination, mimicking resonant antenna $l \approx \lambda/2$ (R_L=60Ω, C_L=220pF), comparison between ideal negative RC (green solid line), transient simulation (red dotted) and measurements on experimental demonstrator (blue dashed)

At first, it should be stressed that both models gave stable oscillations and could be tuned in the frequency range of approximately 1:8 (4 MHz – 32 MHz) for the RC combination mimicking resonant antenna, and approximately 1:4 (8 MHz – 32 MHz) for the RC combination mimicking short antenna. That was achieved by variation of the elements of tuning LC circuit (*L*o and *C*o were varied from 1μH to 4 μH, and 5 to 250 pF, respectively). Secondly, it can be seen that the real part of NIC input impedance matches the ideal case and the measurements with acceptable accuracy for the frequencies above 20 MHz. Above this frequency, the error in conversion ratio occurs. However, the difference between simulations, ideal case and measurements is much more pronounced for the imaginary part of input impedance. In some cases, even the sign of the imaginary part predicted by simulations was incorrect (Figure 4-45). There are two possible reasons for occurrence of this phenomenon. The first reason deals with the NIC conversion error associated with inevitable phase shift of OPamp. This effect is pronounced for highly reactive loads of RC type (loads with a large ratio of imaginary and real part). The second effect is associated with non-linearity and the change of NIC conversion ratio with the level of input signal. Both of these effects will be discussed in details later.

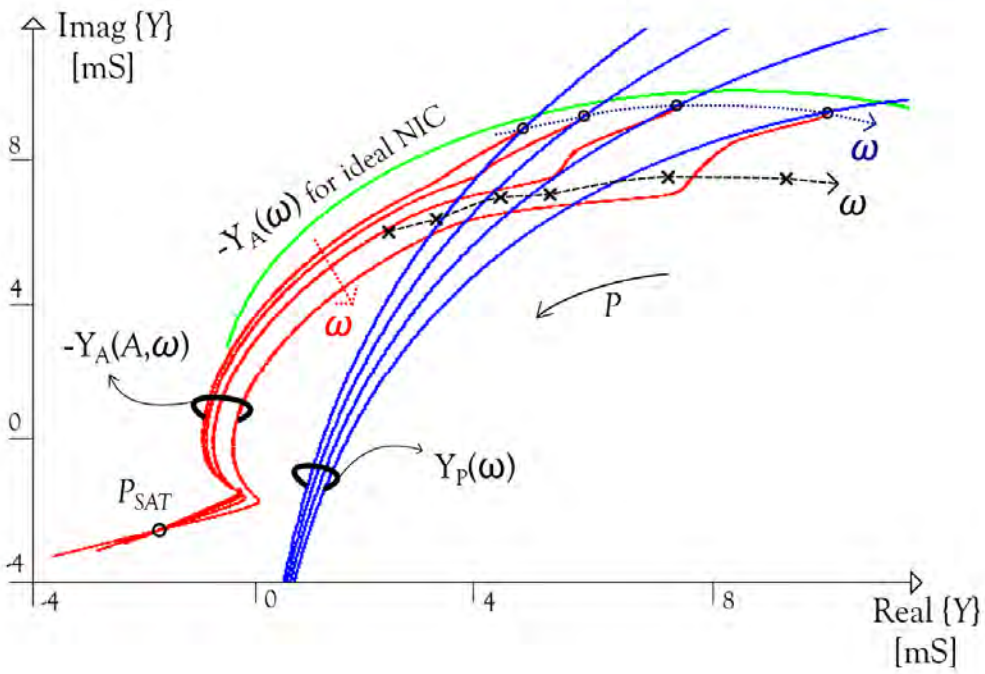

Figure 4-48 Comparison of admittance loci of linear model (green solid line), numerical (SPICE-based) non-linear model (red curves with circles, representing oscillating frequencies, 7.6, 8.7, 10.4 and 13.9 MHz, increasing from left to right) and measurements on a prototyped N-type non-Foster oscillator with the load network that emulates a resonant antenna (R_L=60 Ω, C_L=220 pF) (crosses, frequencies 5.6, 6.6, 7.8, 8.8, 11.3 and 14.2 MHz, increasing from left to right). The power levels were varied from 20 mW to 36 mW, increasing from right to left.

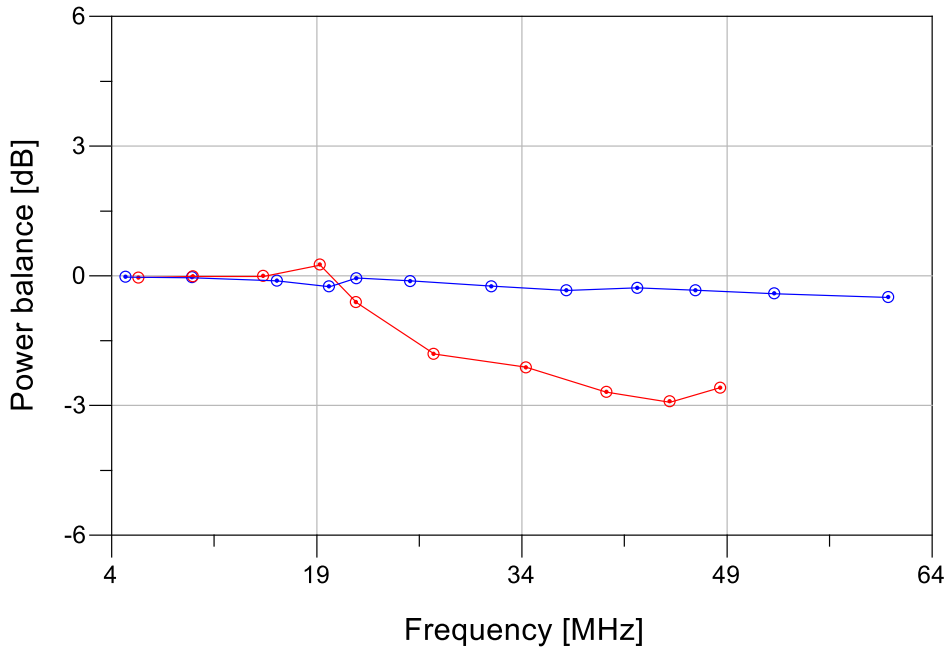

Figure 4-49 Power balance representing ratio (in dB) between the power absorbed by antenna emulating load (R_L, C_L) and the power dissipated in the feedback for N-type oscillator with antenna-emulating network, comparison between short antenna ($l \approx \lambda/10$, red curve, R_L=2.2Ω, C_L=3.9pF) and the resonant antenna ($l \approx \lambda/2$, blue curve, R_L=60Ω, C_L=220pF)

In order to understand the non-linear effects in the antenna-transmitter, the admittance loci of active and passive parts were calculated from the simulation results. A sample of obtained results is presented in Figure 4-48. It can be seen that higher levels of signal move operating point along the generalized N-curve and cause change of NIC conversion ratio and, therefore, the NIC input impedance. These results are in good agreement with analytical approach presented in Section 4.2.1. and the results from numerical analysis in Section 4.2.2. Furthermore, we calculated the ratio of the power radiated at the antenna (dissipated in the R_L in R_L-C_L model) and power dissipated at the feedback 'impedance inverting' network (R_F), (Figure 4-49). It can be seen that these two power levels are rather similar (within the difference of 0.5 dB) for the case of resonant antenna. However, this difference increases up to 3dB at higher frequencies, in the case of short antenna. This phenomenon again indicates a possible existence of errors in NIC conversion ratio for highly reactive loads.

Due to several observation of errors in NIC conversion ratio (Figure 4-44, Figure 4-45, Figure 4-46, Figure 4-47) it was decided to investigate this effect analytically. To this end, we used a simple one-pole model of the OPamp (3.19), the basic expression for NIC input impedance (4.3), and assumed the load as a series RC circuit:

$$Z_F = R + jX_C \tag{4.13}$$

Using (3.19, 4.3, and 4.13), one derives new expressions for real and imaginary parts of NIC input impedance:

$$Real(Z_{IN}) = \frac{R(1-Ao)+R(\frac{\omega}{\omega_p})^2+AoX\frac{\omega}{\omega_p}}{(1-Ao)^2+(\frac{\omega}{\omega_p})^2} \tag{4.14}$$

$$Im(Z_{IN}) = \frac{X\frac{\omega^2}{\omega_p^2}-(1-Ao)X-AoR\frac{\omega}{\omega_p}}{(1-Ao)^2+(\frac{\omega}{\omega_p})^2} \tag{4.15}$$

For $A_o = 2$ and $(\omega/\omega_p) << 1$, (4.14 and 4.15) simplify to:

$$Real(Z_{IN}) = -R - \frac{2}{\omega_p C} \tag{4.16}$$

$$Im(Zin) \approx \frac{1}{\omega C} \tag{4.17}$$

Quick inspection of (4.16) shows that the 'parasitic' part of input resistance depends both on the frequency of the first pole and the value of feedback capacitance. Now, the observed errors in NIC conversion ratio at low frequencies are clear. At these frequencies, the antenna is highly reactive and the second term in (4.16) is significant. With the frequency increase, the antenna becomes less reactive and the influence of the second term in (4.16) is less pronounced.

Deeper physical insight into this effect can be gained by the analysis of amplifier delay by the phasor plots depicted in Figure 4-50, Figure 4-51 and Figure 4-52. The realistic amplifier with a series RC circuit in the positive feedback and with a phase shift ϕ (caused by a finite delay) is sketched in Figure 4-50, (a). By assigning the potentials to the left and right terminal of the feedback impedance (A and B, respectively), it is possible to sketch the phasors of all the voltages and currents in the network (Figure 4-50, (b)). Analysis of the phasors at the amplifier input clearly shows that the phase shift ϕ introduces an error in NIC input impedance (the angle between voltage and current phasors at the input (V_{IN}, I_S) is not equal to the angle between voltage and current phasors at the load (V_{AB}, I_S)). Further analysis shows that this error is not pronounced for the case of a load impedance with similar values of its real and imaginary part (Figure 4-51). On the contrary, if the imaginary part is significantly larger than the real part (the case of a short dipole antenna), the error in conversion ratio increases (Figure 4-52).

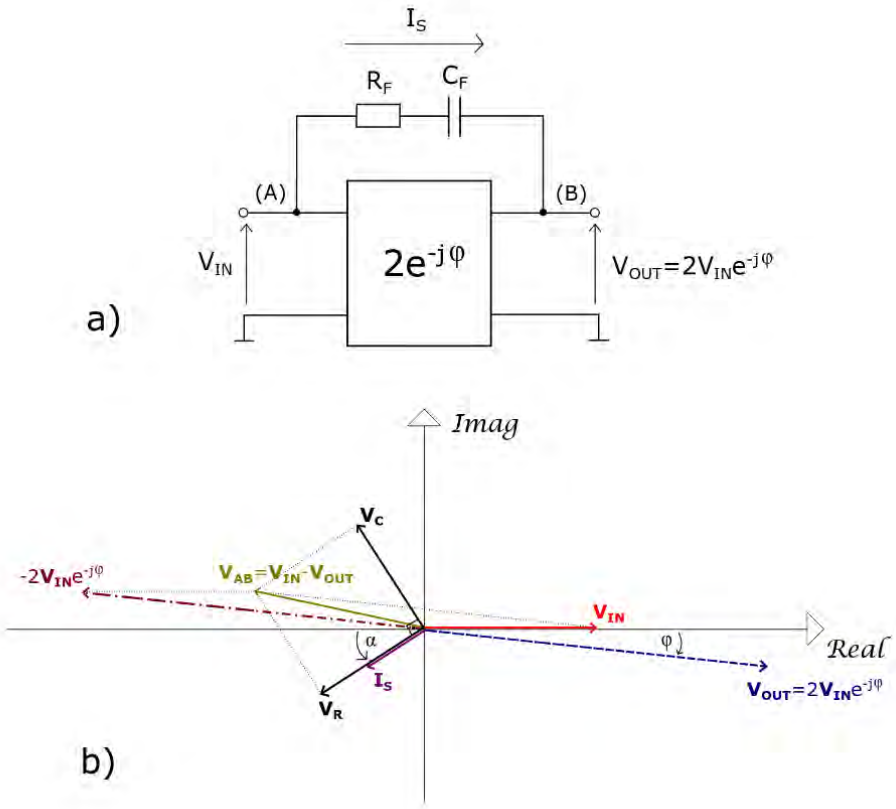

Figure 4-50 Influence of amplifier delay on NIC impedance conversion, a) Block diagram of a negative impedance converter implemented using realistic OPamp with series RC combination in the feedback, b) Phasor diagram of a NIC from part a)

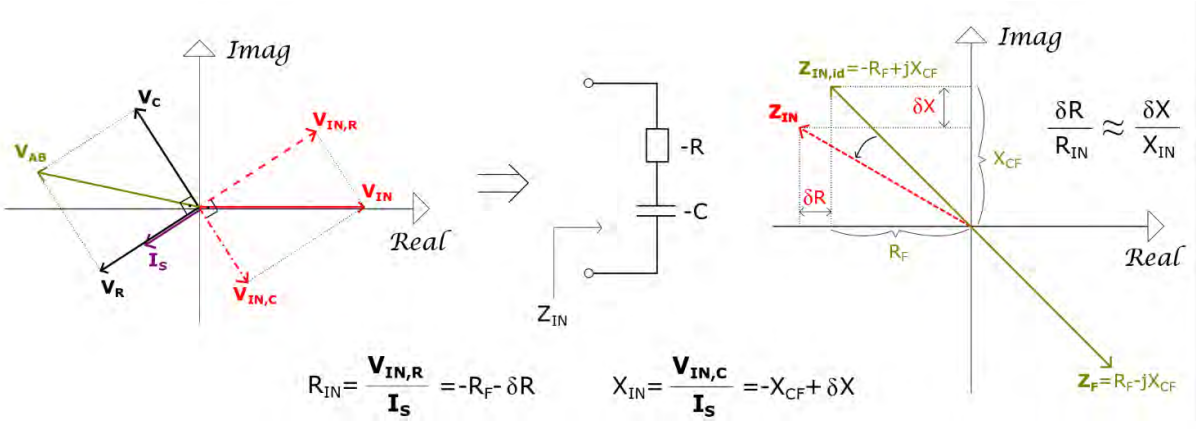

Figure 4-51 Phasor diagram of a NIC with series RC combination in the feedback: the case in which $\mathrm{Im}(Z_F)/\mathrm{Re}(Z_F)\approx 1$,
(left) Decomposition of input voltage to the components at equivalent resistance and capacitance, (right) Impedance diagram displaying relative errors in real and imaginary parts of NIC input impedance

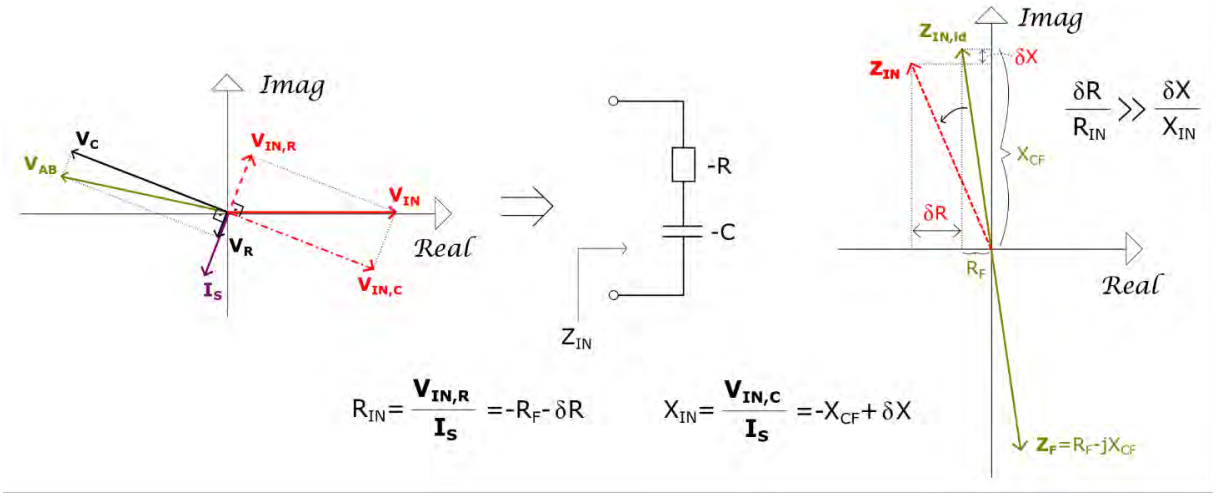

Figure 4-52 Phasor diagram of a NIC with series RC combination in the feedback, the case in which $\mathrm{Im}(Z_F)/\mathrm{Re}(Z_F)>>1$,
(left) Decomposition of input voltage to the components at equivalent resistance and capacitance, (right) Impedance diagram displaying relative errors in real and imaginary parts of NIC input impedance

Please note that above mechanism does not explain unexpected sign change of imaginary part of NIC input impedance (Figure 4-45). Our hypothesis was that the sign change of imaginary part of NIC input impedance occurs due to the non-linear effect (the gain compression). More precisely, if the gain $|A_0|$ in (4.3) decreases below 1, there will be no effects of negative impedance anymore. In order to test this hypothesis, we analyzed the transient state of the antenna-transmitter (obtained by ADS™ simulations). The non-Foster antenna-transmitter design details were those from Figure 4-45. We investigated the non-linear effects both in the time domain and in the frequency domain (Figure 4-53, Figure 4-54).

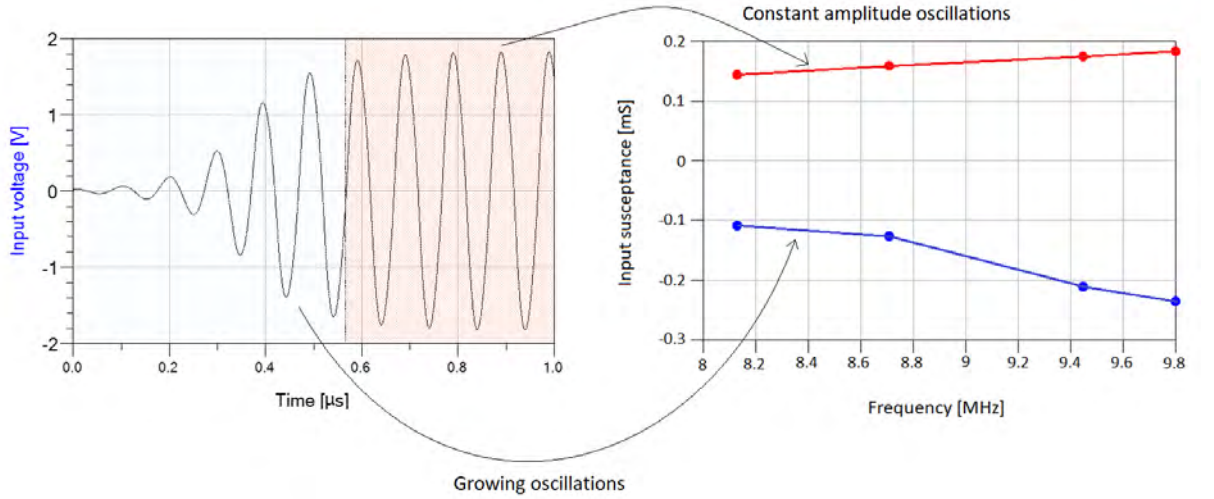

Figure 4-53 Transient state of a non-Foster oscillator
(left) Transition from growing oscillations to constant amplitude oscillations in time domain (right) Non-Foster behavior during amplitude growth vs. Foster behavior during steady state

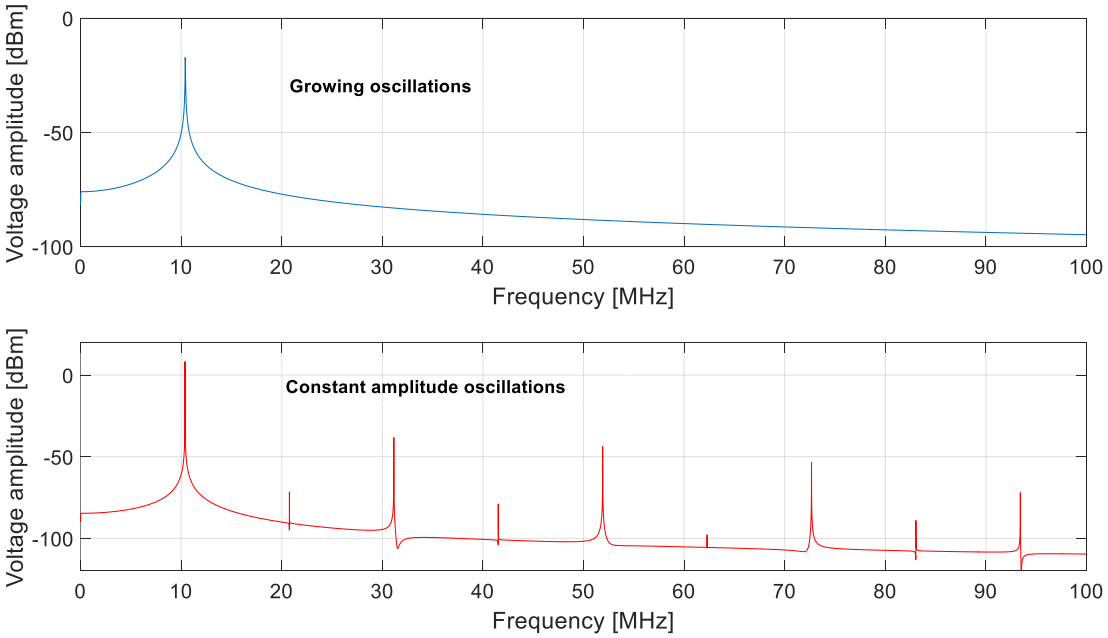

Figure 4-54 Comparison of spectra obtained using Fourier transform of voltage at NIC's input during the amplitude growth and the steady state

It can clearly be seen that in the low-signal (linear) regime there is expected non-Foster behavior due to gain modulus that is higher than 1. However, with the increase of the signal amplitude, the gain compression occurs. When the gain modulus decreases below 1, the non-Foster effects cease (Figure 4-54). The non-linear effects associated with the gain compression cause harmonic distortion visible in the spectrum of generated signal (Figure 4-54). One concludes that the control of the amplitude of the oscillating signal, in order to prevent the cease of non-Foster effects, is an important task in the construction of a non-Foster antenna-transmitter.

4.3.3. Experimental RF demonstrator

After numerical investigation, a simple demonstrator of a non-Foster antenna-transmitter in lower RF range (operating up to 100 MHz) was prototyped. As described in previous section, it was based on THS 4304 high-speed OPamp, configured as the N-type NIC, antenna emulating network (R_L, CL), inverting impedance network (R_F, C_F) and a tuning circuit (L_0, C_0), (Figure 4-43). The passive part and active part were prototyped on separate PCBs and equipped with SMA connectors. When those two parts are connected, it is possible to monitor the spectrum of oscillating signal by a spectrum analyzer coupled via small loop antenna. After the frequency is measured, the passive part can be disconnected and its impedance measured by VNA. This impedance is a 'mirror image' of the NIC input impedance. This procedure was used for measuring of the large-signal NIC input impedance, already compared with the ideal case and the simulations in Figure 4-44, Figure 4-45, Figure 4-46, and Figure 4-47.

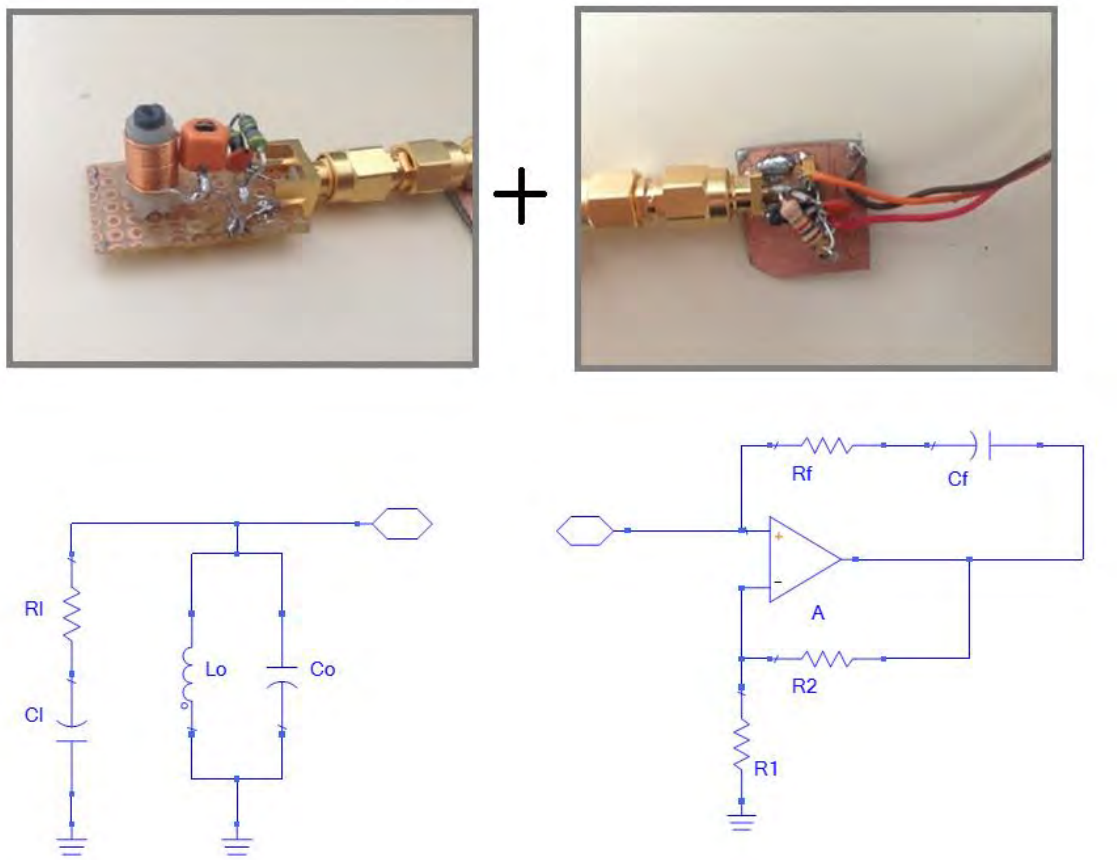

Figure 4-55 Experimental demonstrator of N-type non-Foster antenna-transmitter with antenna-emulating network (upper) and associated simplified schematics (lower), the component values are R_F=R_L=2.2Ω, C_L=C_F=3.9 pF, R_1=R_2=243Ω, L_o is tunable from 1μH to 3.8μH, C_o is tunable from 5 to 60 pF

In the next step, the spectrum of oscillating signal was measured. The suppression of the spurious signals was found to be better than 25 dBc (Figure 4-56) and the tuning bandwidth was slightly larger than 1:3 (9 to 30 MHz) (Figure 4-57). It is important to stress that this tuning bandwidth was constrained only by available tuning elements. The simulations showed that the tuning bandwidth larger than 1:10 can be achieved by using different tuning elements. Finally, the power level flatness of a generated signal was found to be within 3 dB (Figure 4-57).

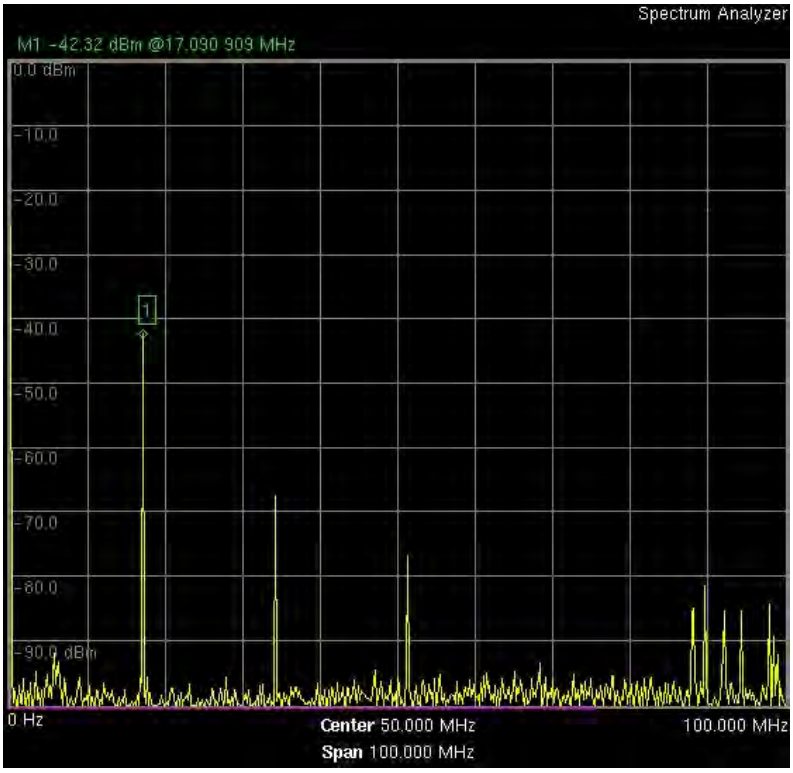

Figure 4-56 A sample of measured spectrum of prototyped N-type non-Foster antenna-transmitter with antenna-emulating network

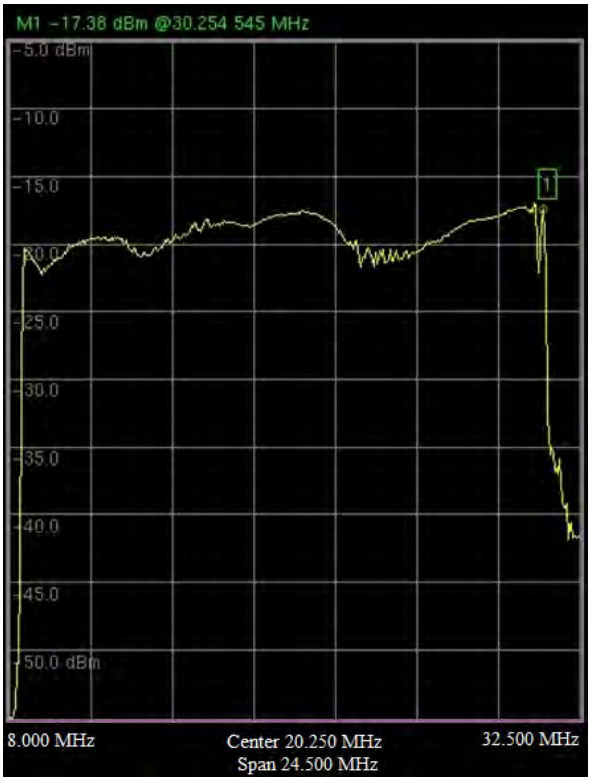

Figure 4-57 Measurements of generated signal power of prototyped N-type non-Foster antenna-transmitter with antenna-emulating network operating within 9 to 30 MHz bandwidth

In the last step, it was attempted to prototype the RF demonstrator of a non-Foster antenna–transmitter that includes the transmitting antenna (instead of the antenna-emulating network used so far). The manufactured prototype is shown in Figure 4-58 .

Active part was very similar to one shown in Figure 4-43. The used OPamp was THS4303 device, the gain of which was adjusted to approximate value of two by the selection of external resistor of 330 Ω (the gain-setting network was identical to the one in 'all-negative' RLC circuit, Figure 3-23). The tuning network was slightly more complicated than in the previous case and it included a double trimmer capacitor with extended tuning range. The active part was connected to a simple, short, top-loaded monopole (the length of λ/15 at the highest frequency). The monopole (Figure 4-58) was mounted above the large ground plane (metallic mesh) and equipped with the *LC* tuning circuit (a 'resonator'). The active part of the system (a NIC-based non-Foster source) was located below the ground plane and connected to a monopole. A special near-field probe (similar to a tapered transmission line used in TEM cell) was terminated with a spectrum analyzer and used for monitoring of radiated signal.

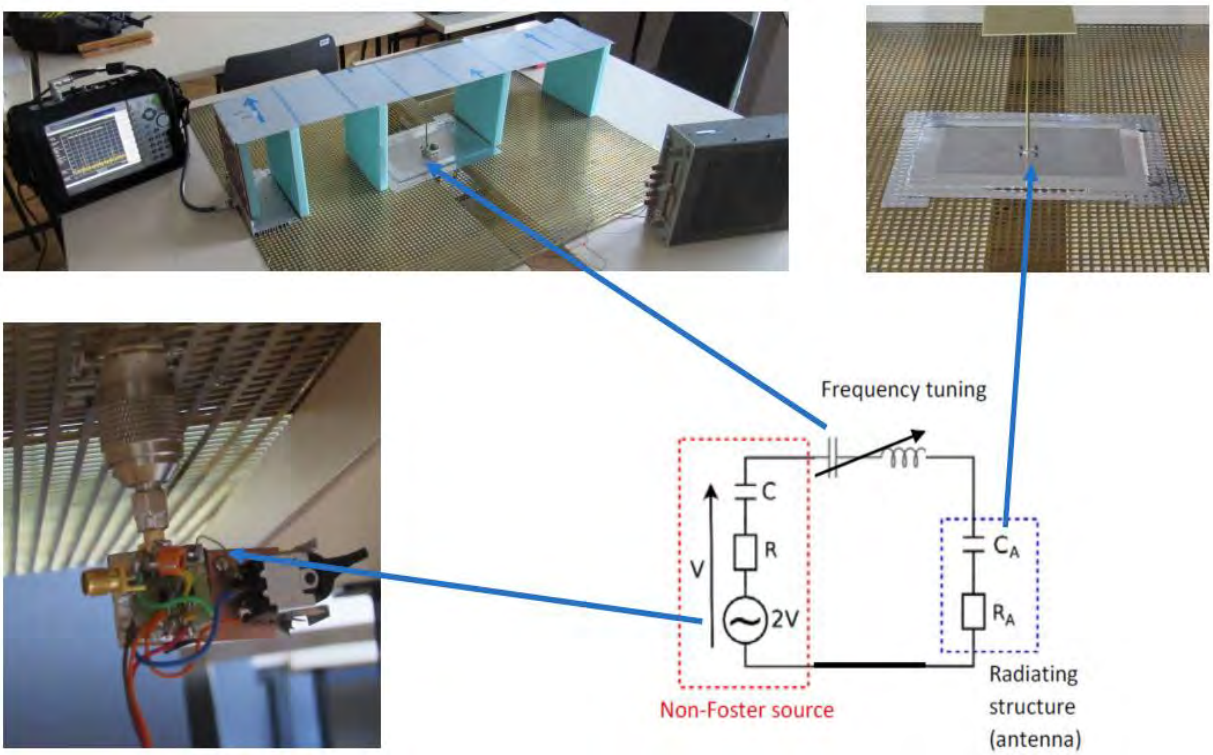

Figure 4-58 N-type non-Foster antenna-transmitter prototype (bottom left) with a monopole antenna on a conducting plane (top right), tunable from 1 to 10 MHz
(top left) Measurement setup
(bottom right) Simplified block-diagram of a tunable non-Foster antenna-transmitter

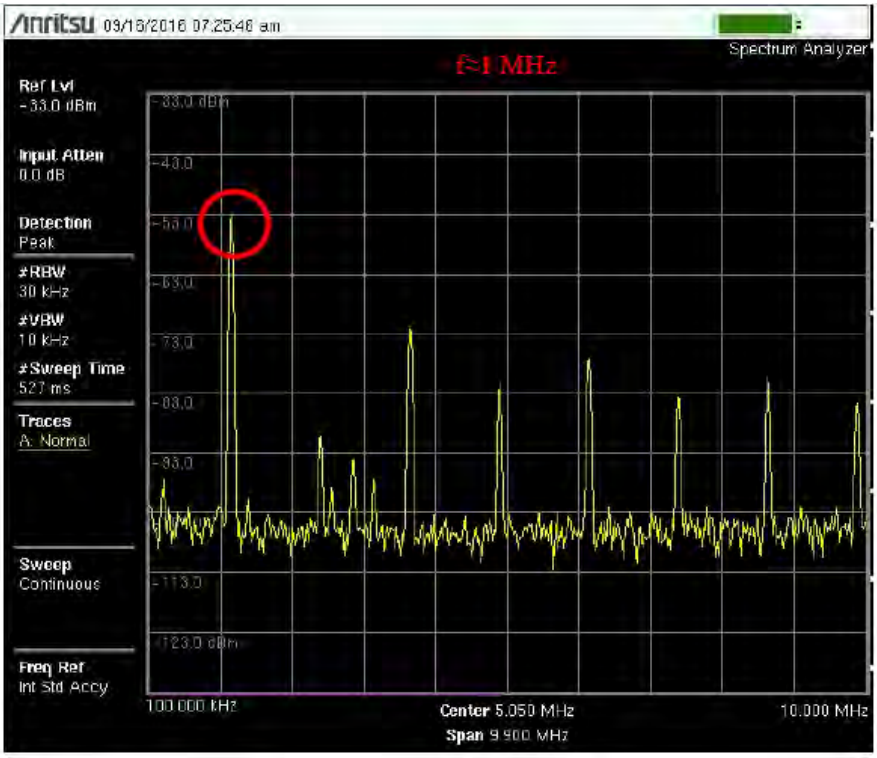

Figure 4-59 Measured spectrum of a non-Foster antenna-transmitter prototype with a short monopole antenna at the lowest frequency (1MHz)

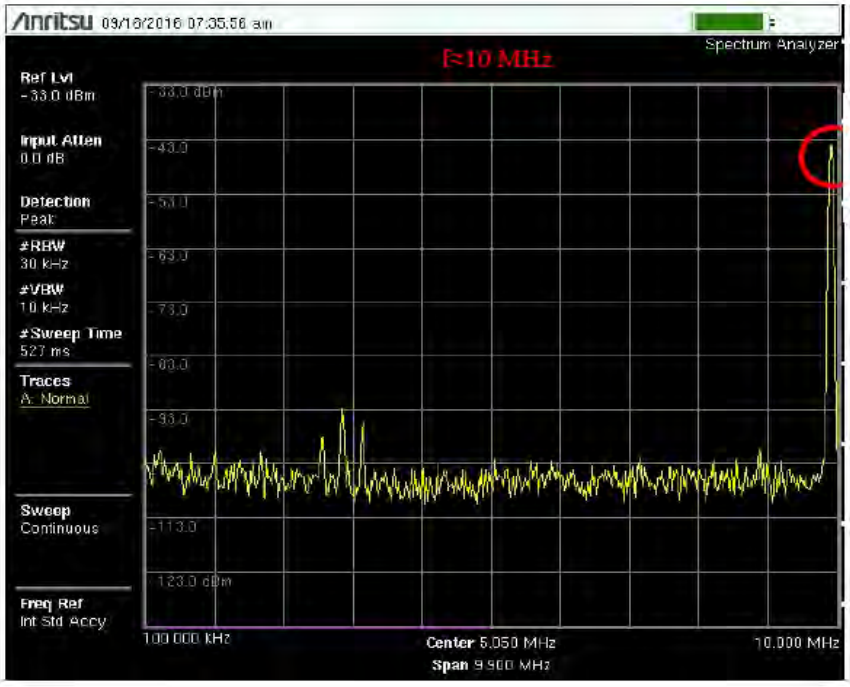

Figure 4-60 Measured spectrum of a non-Foster antenna-transmitter prototype with a short monopole antenna at the highest frequency (10MHz)

Figure 4-61 Measured normalized radiated power of prototyped N-type non-Foster antenna-transmitter with a short monopole antenna on a conducting plane at 1 to 10 MHz bandwidth

A sample of measured spectrum of radiated signal (showing oscillations at 1 MHz) is given in Figure 4-59. It can be seen that there are both harmonic and non-harmonic spurious signals caused by non-linear operation of a non-Foster device. The maximum relative power of the spurious components was -20 dBc. One should note that no methods of amplitude stabilization were included in the design of this preliminary system. Furthermore, it was attempted to tune the oscillations frequency. Measured spectra (Figure 4-59 and Figure 4-60) showed stable oscillations with amplitude flatness of approximately +- 2 dB, within the 1:10 tuning range (1MHz – 10 MHz), (Figure 4-61). The power delivered to the antenna was also calculated from the measured RF voltage (at antenna terminals) and compared to the measured RF voltage at the lumped-element-based antenna replica. The estimated return loss was better than 15 dB across the whole band.

One can conclude that these experimental results verify the correctness of a basic idea of the non-Foster antenna transmitter.

4.4 Non-Foster antenna-transmitter array

Detailed analytical, numerical and experimental investigation presented in Section 4.3. showed that a non-linear non-Foster source, the internal impedance of which is a simple negative RC circuit can be used as a non-Foster antenna transmitter (Figure 4-62, (a)). That system uses a simple short dipole antenna as a radiator. Measurements on two prototyped demonstrators in lower RF range (< 100 MHz) revealed the tuning bandwidth between 1:2 to 1:10 (depending on the construction of a tuning circuit), with an equivalent return loss of 15 dB.

Naturally, above system has also some limitations. Firstly, a dipole mimicking network that comprises only one resistor and only one capacitor is a very crude approximation, only valid within the narrow bandwidth. A standard extension is associated with letting the radiation resistance to be proportional to the square of frequency. However, the analysis in Laplace domain shows this widely used dispersive RC equivalent model is (surprisingly!) unstable [87]. This is obviously a non-physical artifact (a passive antenna system is always stable) and it shows that this model (although widely used in steady-state analysis) is not physically correct.

Furthermore, due to inevitable antenna imperfections, the impedance of the antenna in a realistic transmitting scenario cannot be predicted accurately. Thus, it would be necessary to measure the impedance of used short dipole antenna beforehand and, using measured data, to design a dedicated RC network used as the NIC load. This is impractical as each antenna requires a specially designed NIC load and does not allow a simple use of different antennas in different applications.

Secondly, the RF power dissipated in a resistor of antenna mimicking network obviously does not contribute to radiation. This fact lowers the system efficiency.

In this section, we propose improved design that overcomes aforementioned problems.

4.4.1. Basic concept

A basic idea of proposed improvement is sketched in Figure 4-62 (b).

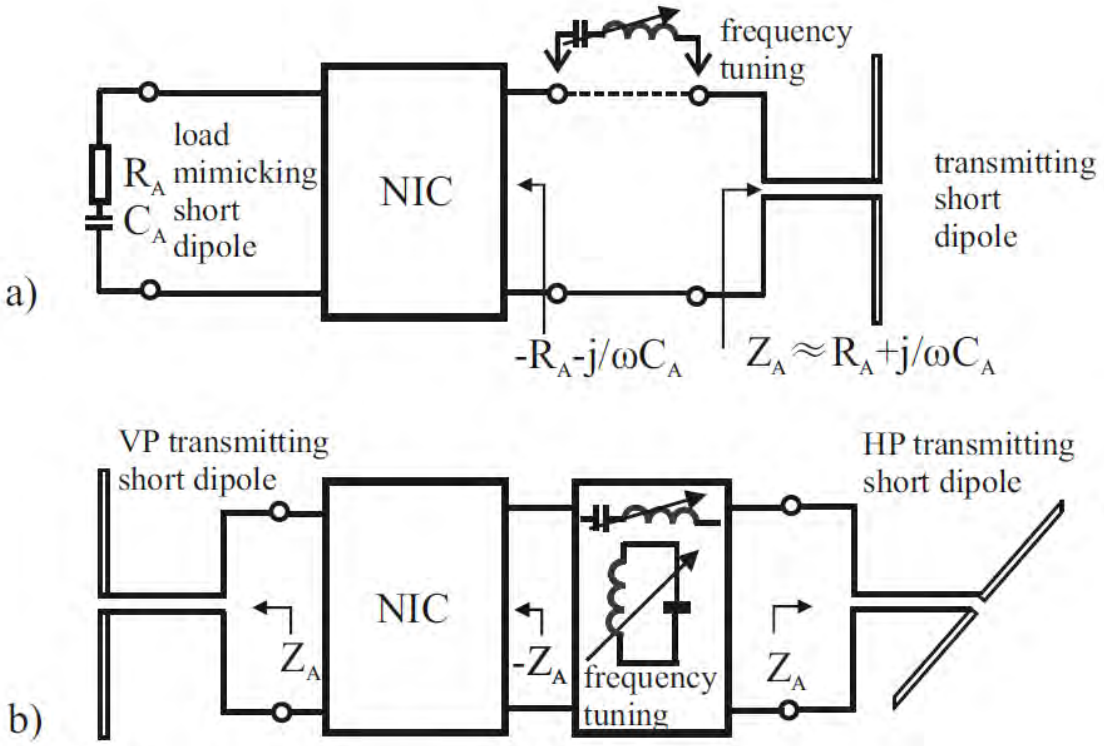

Figure 4-62 Evolution of non-Foster radiating systems
a) The first design with one transmitting antenna and negative antenna-emulating network
b) New design with two orthogonal transmitting antennas

Here, the load mimicking antenna impedance is replaced with a second antenna (located on the left side) that is identical to the original transmitting antenna. By doing so, the NIC input

impedance at any frequency would be (approximately) equal to the negative image of the input impedance of the first antenna (located on the right side in Figure 4-62 (b)). Thus, the tuning bandwidth would not depend on antennas, but only on the properties of used NIC. Furthermore, the voltage (or current, depending of the type of used NIC) at the second antenna is equal to the one at the first antenna. Due to this, both antennas contribute to radiated power that is (theoretically) 3dB higher comparing to the previous design with one antenna. In principle, two identical antennas of any kind can be used. Actually, the system in Figure 4-62 (b) behaves as a nearly perfectly matched, broadband antenna-transmitter array.

Of course, a proposed principle presumes that there is no mutual coupling between two antennas. There are several ways of approaching this idealized scenario in practice. For instance, one could use crossed dipoles with orthogonal polarizations, as depicted in Figure 4-62 (b). In practice, it is possible to achieve isolation between dipoles better than 20 dB.

4.4.2. Numerical investigation

As the first step in verification of presented idea, a circuit model of a system in Figure 4-62 (b) was developed and tested in ADS^{TM} simulation environment (Figure 4-63).

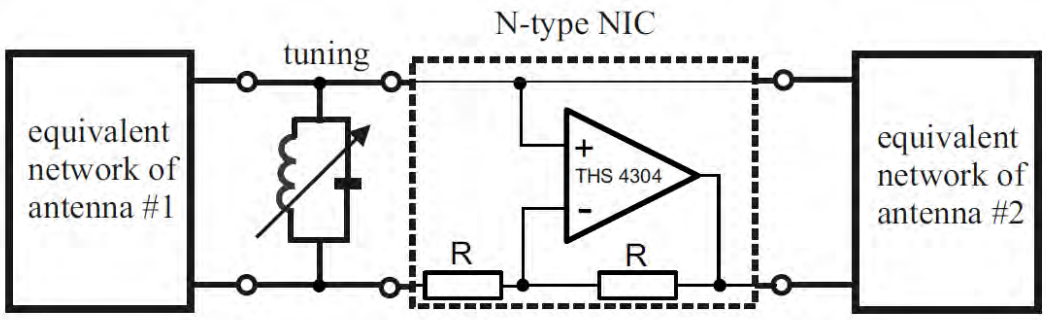

Figure 4-63 Simulation model of two element non-Foster antenna-transmitter array based on N-type NIC

Particular attention was paid to antenna modelling. There are several models of simple linear antennas in the literature, as reviewed in [87]. Here, we used a numerical five-element Stearn's model that is very accurate both for short and resonant antennas, with the length up to λ, (Figure 4-64, [87]).

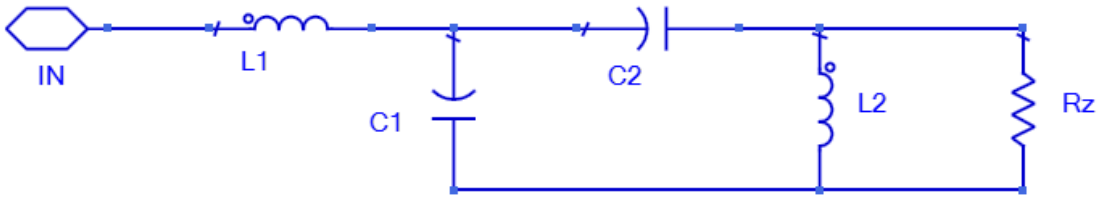

Figure 4-64 Stearn's broadband five-element dipole antenna model. The values of L_1, C_1, C_2, L_2 and R_z have been developed by the network synthesis with expansion coefficients obtained from full-wave simulation, [87]

Stearn's antenna model has been incorporated into the model of active part that comprises the N-type OPamp-based NIC with THS 4304 device (Figure 4-65) and simulations in ADS^{TM} environment were performed. The following parameters have been extracted from simulations: NIC input admittance (Figure 4-66 and Figure 4-67), a ratio of power level at the first antenna and at the second antenna (Figure 4-68), and the total relative radiated power (Figure 4-69).

It can be seen that the real part of input admittance (conductance) matches idealized case quit well (Figure 4-66). On the contrary, the imaginary part of input admittance (susceptance) shows pronounced difference from the ideal case, even including the incorrect sign (Figure 4-67). This happens due to problems with non-linearity, discussed in Section 4.2.2. Non-linearity also causes pronounced unbalance in radiated power at the antennas, varying from 1 dB at lower frequencies, up to 8 dB at higher frequencies (Figure 4-68). Although this difference is pronounced, it affects only the polarization angle and not the total radiated power. As expected, the radiated power increases with frequency (Figure 4-69).

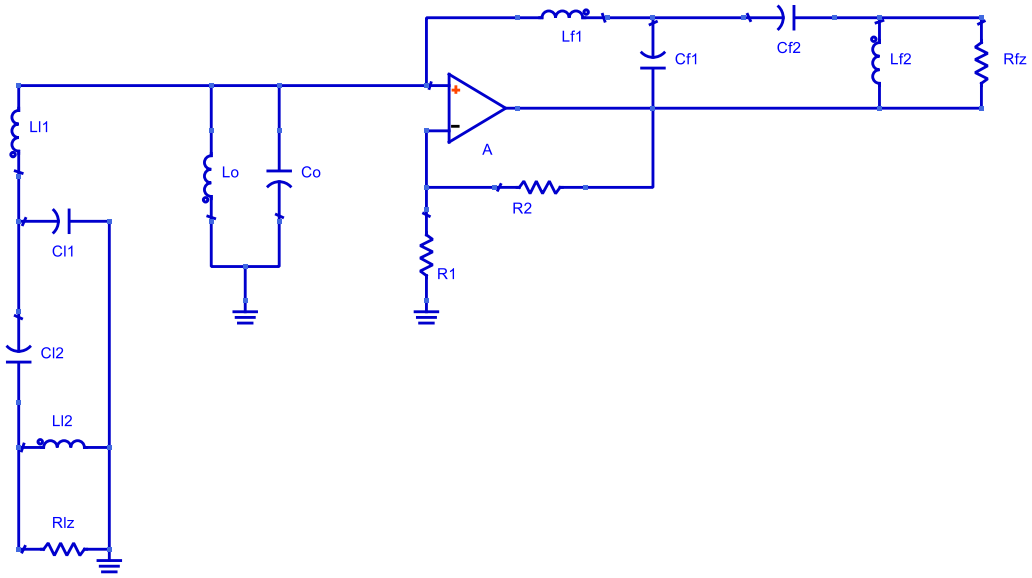

Figure 4-65 Simplified simulation model of N-type non-Foster antenna-transmitter array with Stearn's numerical 5-element dipole antenna model. Element values (for antenna length l = 1.5m): L_1=47.25nH, C_1=0.625pF, C_2=1.95pF, L_2=1.335µH, R_z=8992Ω, R_1=R_2=243Ω

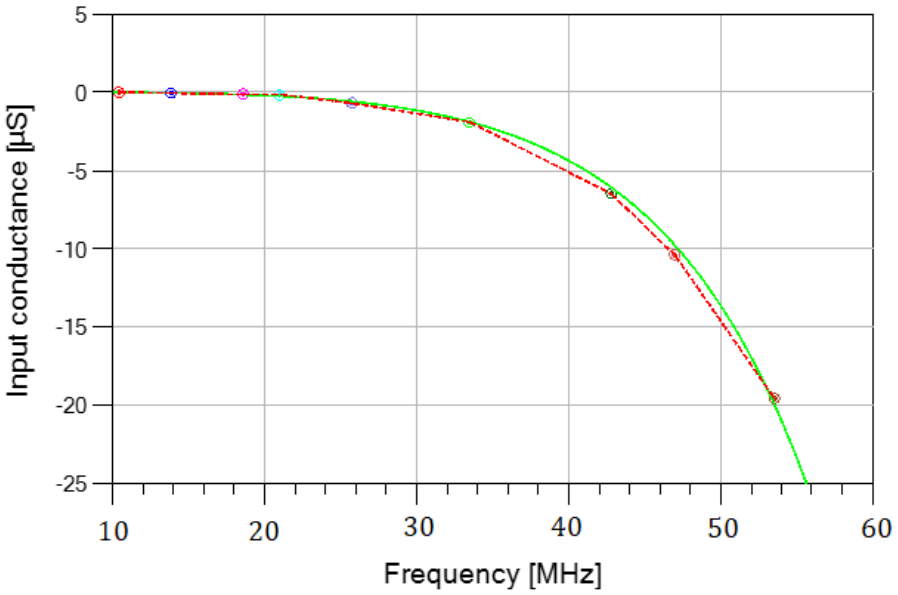

Figure 4-66 NIC's input conductance for N-type non-Foster antenna-transmitter array with Stearn's five -element dipole antenna model [87], a comparison between ideal negative antenna (green solid line), and SPICE-based transient simulation (red dashed)

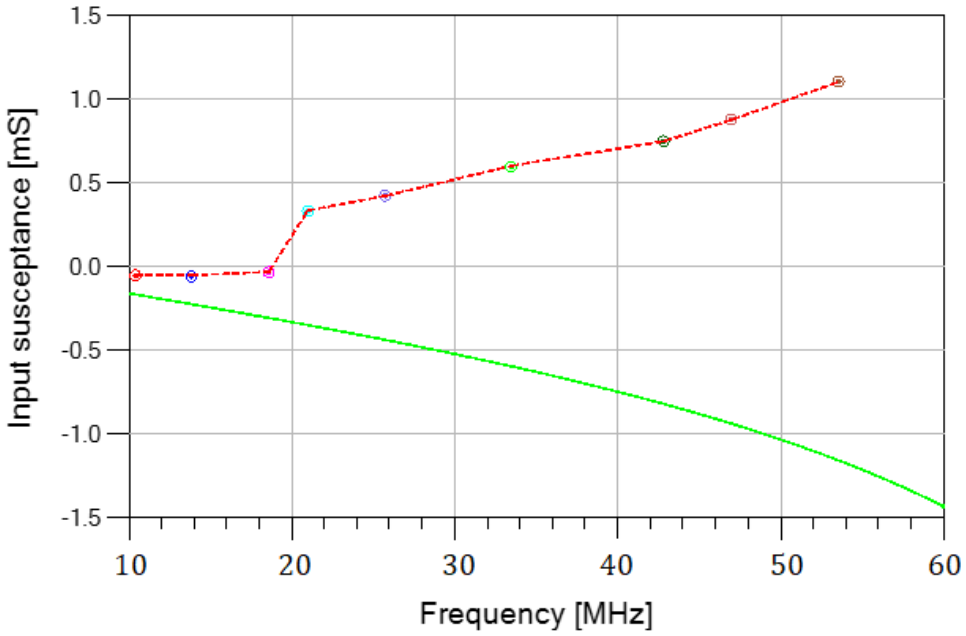

Figure 4-67 NIC's input susceptance for N-type non-Foster antenna-transmitter array with Stearn's five-element dipole antenna model [87], a comparison between ideal negative antenna (green solid line), and SPICE-based transient simulation (red dashed)

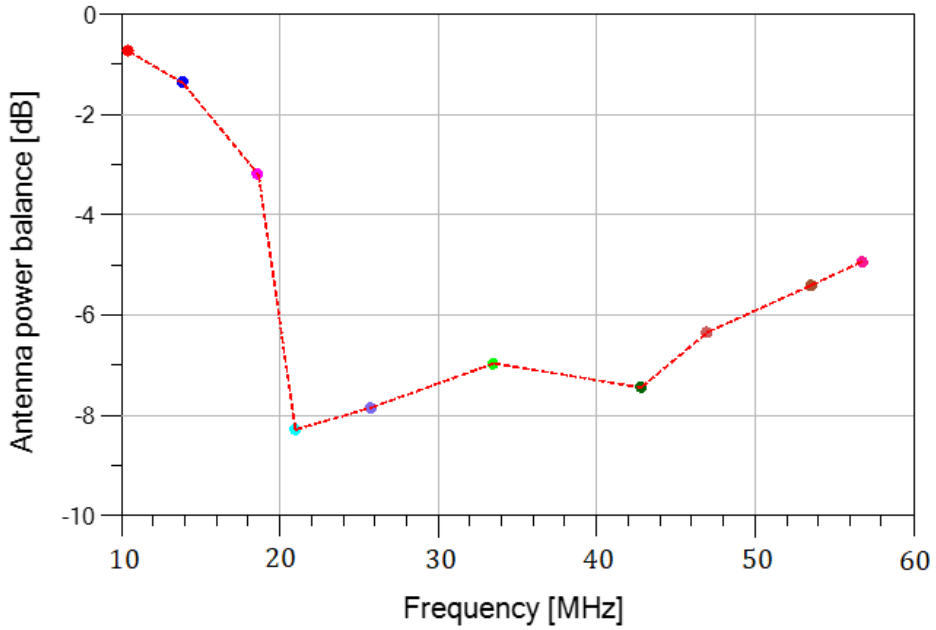

Figure 4-68 Simulated antenna power balance for N-type non-Foster antenna-transmitter array with Stearn's five-element dipole antenna model [87], in the frequency range 10 MHz - 60 MHz.

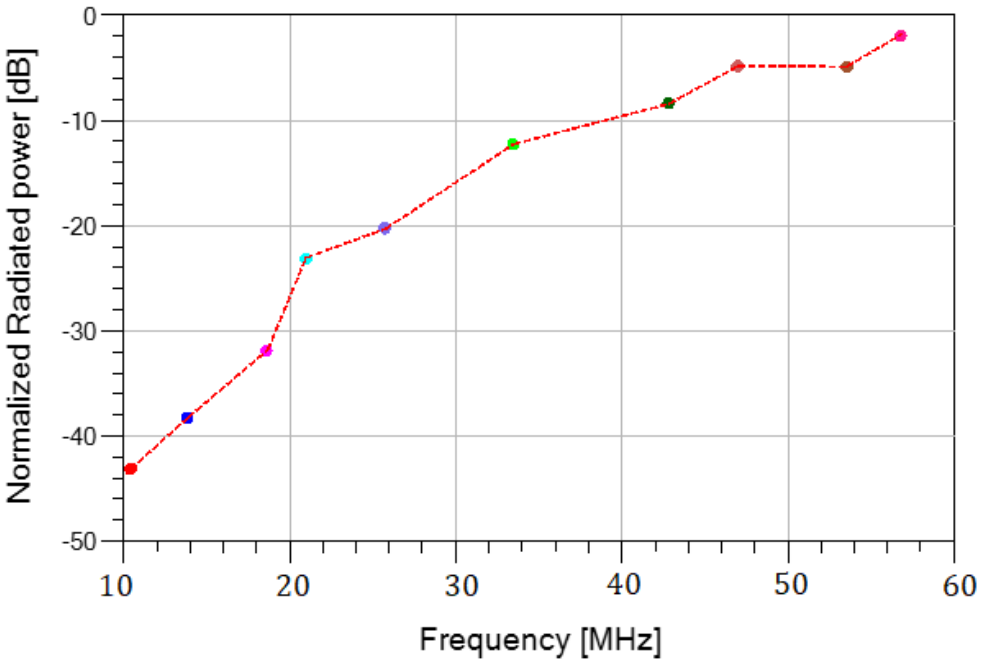

Figure 4-69 Simulated normalized total radiated power of N-type non-Foster antenna-transmitter array with Stearn's five-element dipole antenna model [87], in the frequency range 10 MHz - 60 MHz.

In the next step, it was attempted to decrease the influence of non-linearity on NIC input admittance by adding the diode limiter. It was expected that diode limiter would prevent the movement of the operation point above the 'hill-top' of the generalized N-curve and a decrease of the gain below unity. To this end, a new ADS model of the antenna-transmitter array was prepared (Figure 4-70). The limiter was designed using two HP HSMS2805 Schottky barrier diodes, connected in the familiar anti-parallel fashion.

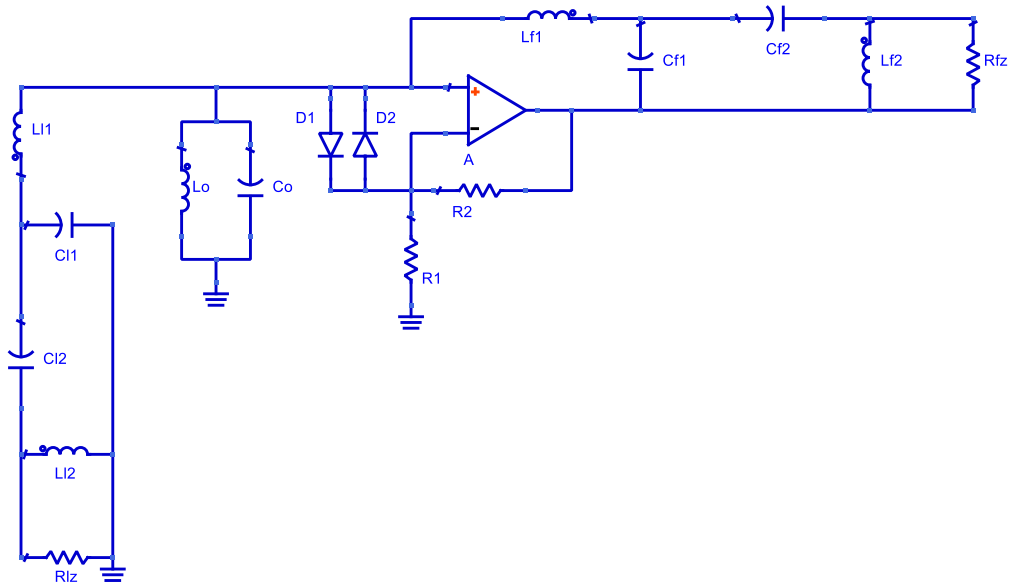

Figure 4-70 Schematic diagram of a non-Foster antenna-transmitter array based on Stearn's antenna model [87] with diodes for amplitude stabilization, values of Stearn's elements are the same as in previous example, diodes used in simulations are SPICE model of HP HSMS2805 Schottky barrier diodes with 410 mV forward voltage

As in the previous case, several parameters have been extracted from simulation: the NIC input impedance (Figure 4-71 and Figure 4-72), a ratio of power level at the first antenna and at the second antenna (Figure 4-73), and total relative radiated power (Figure 4-74)

It can be seen that the real part of input impedance (resistance) deviate from the idealized case (Figure 4-71), which is caused by the highly reactive nature of the load. This deviation does not seem to be very important since it only affects generated power. At the same time, it can be seen that the imaginary part of input impedance (reactance, Figure 4-67) now has a correct sign. Generally, the NIC input impedance matches the ideal case much better than in the previous case (without limiter). It also can be seen that the balance in radiated power is improved by 2 dB. Thus, one concludes that the inclusion of a limiter significantly improves the properties of antenna-transmitter array.

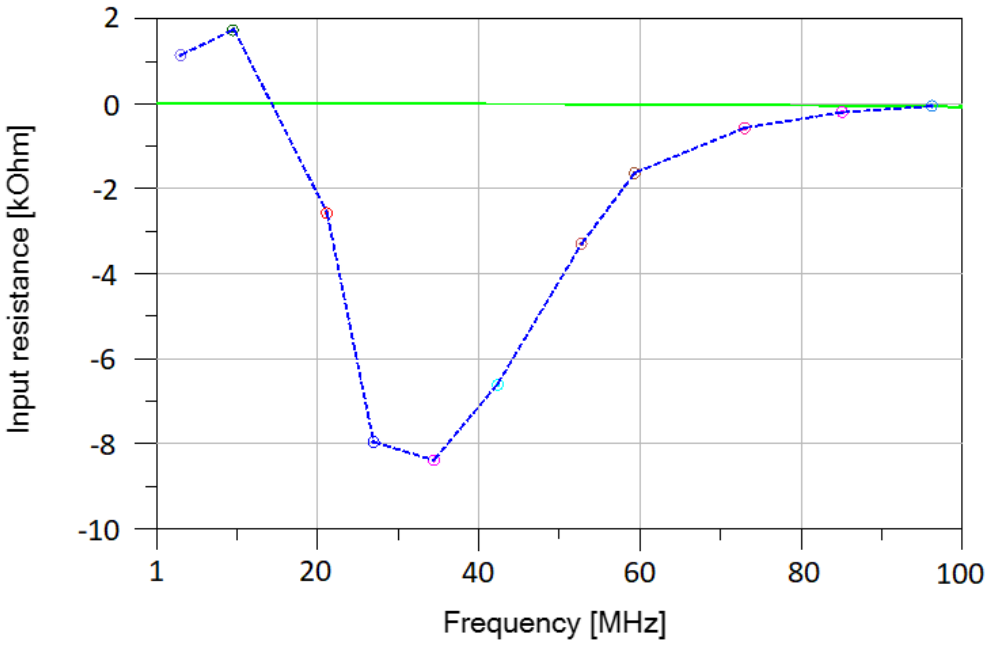

Figure 4-71 NIC's input resistance for N-type non-Foster antenna-transmitter array based on Stearn's antenna model [87] with diodes for amplitude stabilization, comparison between ideal negative antenna (green solid line), and SPICE-based transient simulation (blue dashed)

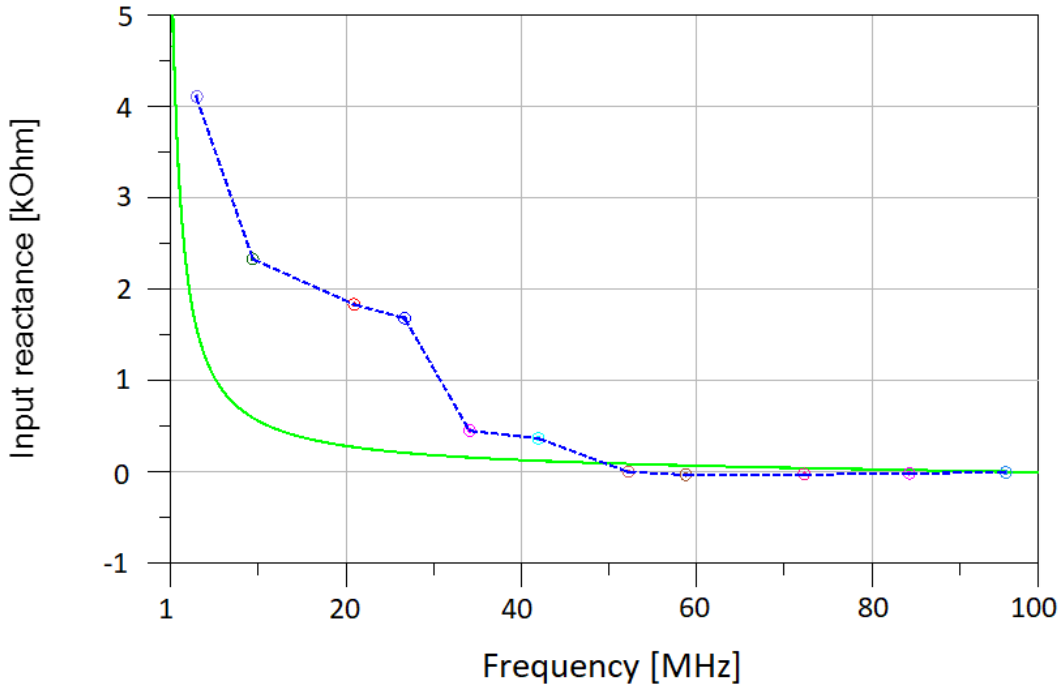

Figure 4-72 NIC's input reactance for N-type non-Foster antenna-transmitter array based on Stearn's antenna model [87] with diodes for amplitude stabilization, comparison between ideal negative antenna (green solid line), and SPICE-based transient simulation (blue dashed)

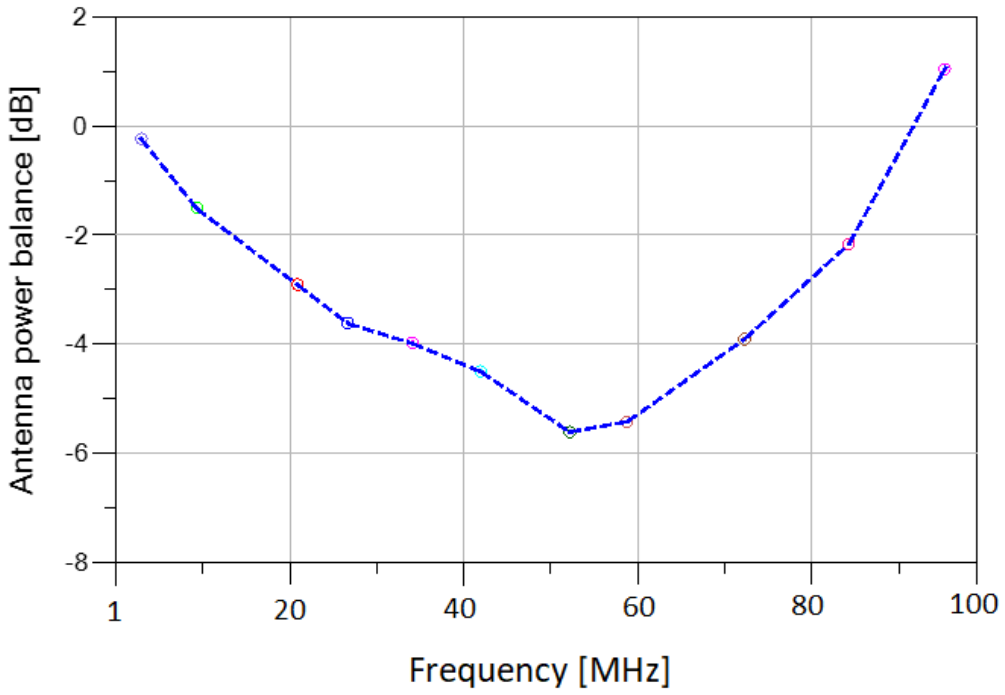

Figure 4-73 Simulated antenna power balance for N-type non-Foster antenna-transmitter array based on Stearn's antenna model [87] with diodes for amplitude stabilization at 4 to 100 MHz frequency range

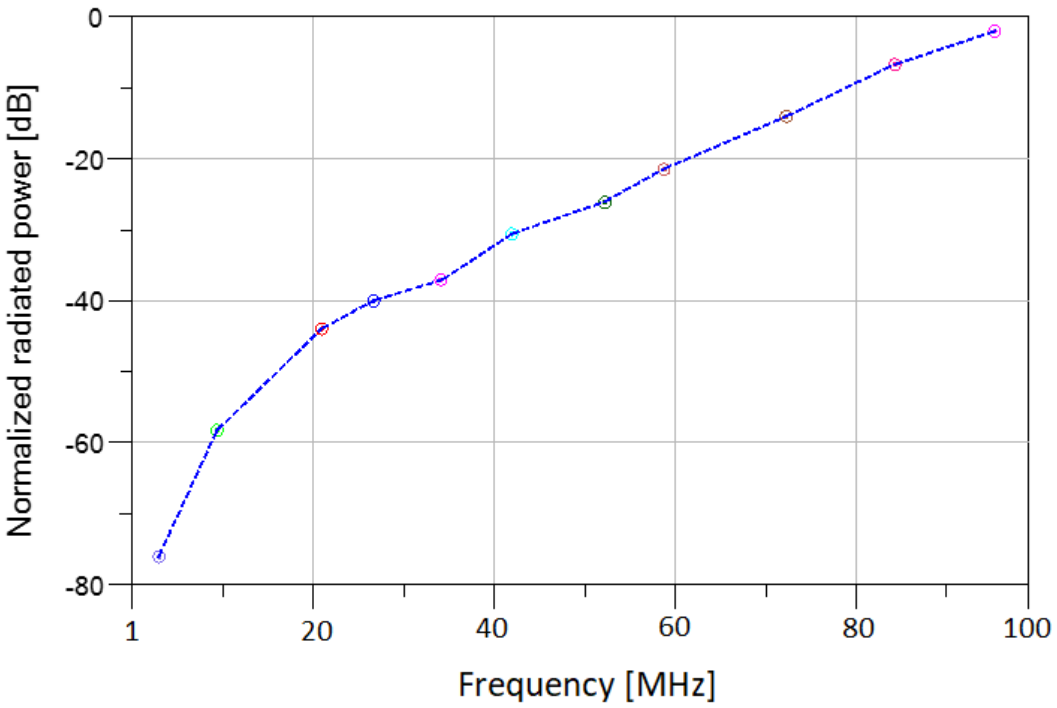

Figure 4-74 Simulated total radiated power of N-type non-Foster antenna-transmitter array based on Stearn's antenna model [87] with diodes for amplitude stabilization, normalized to a maximum of 0 dB at 4 to 100 MHz frequency range

In the last set of simulations, it was attempted to investigate the injection-locking of antenna-array transmitter without a resonant tuning element. This is basically a different idea from a standard injection locking, in which the locking range is constrained by the Q factor of the resonator [121]. Our hypothesis was that the locking range of antenna-transmitter array without a resonant tuning element will be broader than the case of standard oscillator with a resonator. This hypothesis comes from the comparison of a perfectly matched non-linear non-Foster source and an ordinary negative-resistor oscillator (sections 4.1 and 4.2).

Therefore, the appropriate ADS^{TM} simulation model was prepared (Figure 4-75). In this model, the LC circuit was removed, and external locking oscillator was simply modelled by a voltage source. A sample of simulation results is presented in Figure 4-76. It can be seen that the locking range of 1:2 (10 MHz -20 MHz) was achieved. Actually, the locking range is constrained only by the NIC imperfections. However, it can be seen that harmonic distortion (the presence of harmonics) is rather pronounced. Thus, the correctness of the basic idea has been proven, but the appropriate method of decreasing distortion effects should be found. This needs further investigation.

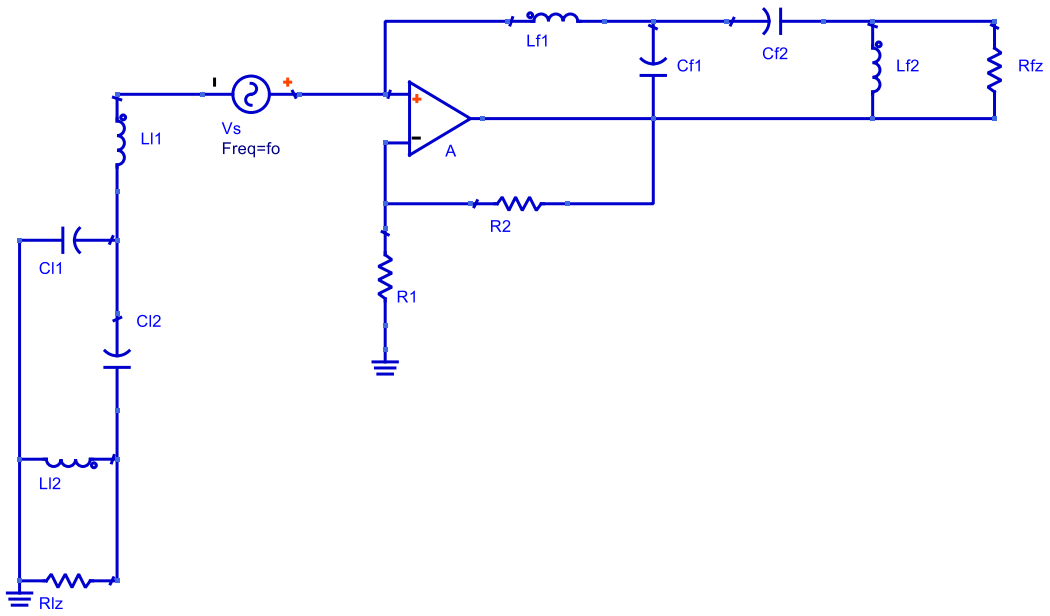

Figure 4-75 Simplified simulation model for injection locking of N-type antenna-transmitter array with Stearn's 5-element antenna model (l = 1.5m, L_1=47.25nH, C_1=0.625pF, C_2=1.95pF, L_2=1.335μH, Rz=8992Ω, Vs=0.1V, f_o is a frequency of an external locking source.

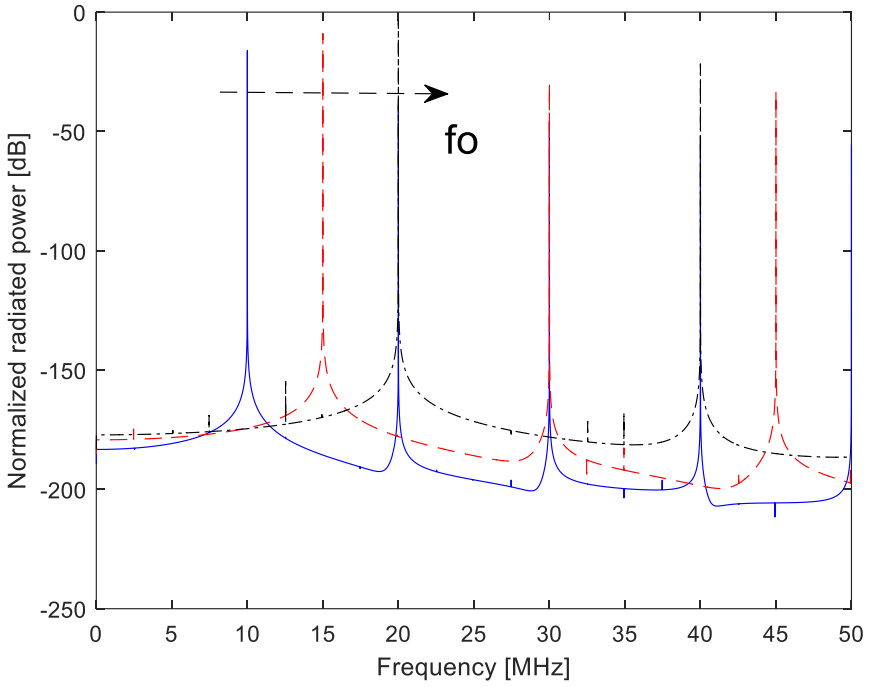

Figure 4-76 The spectra of N-type antenna-transmitter array with Stearn's 5-element antenna model [87], injection-locked with an external source. The frequency of locking source: f_o=10 MHz (solid blue), f_o=15 MHz (dashed red), f_o=20 MHz (dot-dashed black)

4.4.3 Experimental RF demonstrator

In the final step, an experimental demonstrator of a non-Foster antenna-transmitter array was designed and manufactured. It comprised two crossed dipoles with the length of 1.5m, made out of brass tubes with 6 mm diameter (Figure 4-77). The dipole feeding points were connected to the THS 4304-based NIC input and output ports, instead of previously connected antenna emulating networks from Figure 4-65. The close-up view of the connection between the active part and dipoles is shown in Figure 4-78. Dipoles have one common connecting point (non-inverting input node of the OPamp), which should operate as 'AC' ground. Therefore, the battery set was used in order to assure floating DC biasing. Construction of both the NIC circuit and the *LC* tuning network was identical to that from the previous experiments in Section 4.3.3. Antennas operate at very low frequency and associated far-field boundary extends to several hundred meters. Measurements in the far-field are fairly impractical, so very simple measurements in the near field were performed with the help of several small dipole antennas and a spectrum analyzer (Figure 4-79). At first, it was found possible to tune the oscillations within the range of at least 1:2 (16 MHz – 32 MHz). This tuning range is lower than one from Section 4.3. (1:10). This difference solely comes from the available tuning elements. Simulations showed that the tuning bandwidth larger than 1:10 can be achieved by using different tuning elements. The measurement of the spectrum of oscillating signal showed that the amplitude of the spurious components was better than -20 dBc (Figure 4-80).

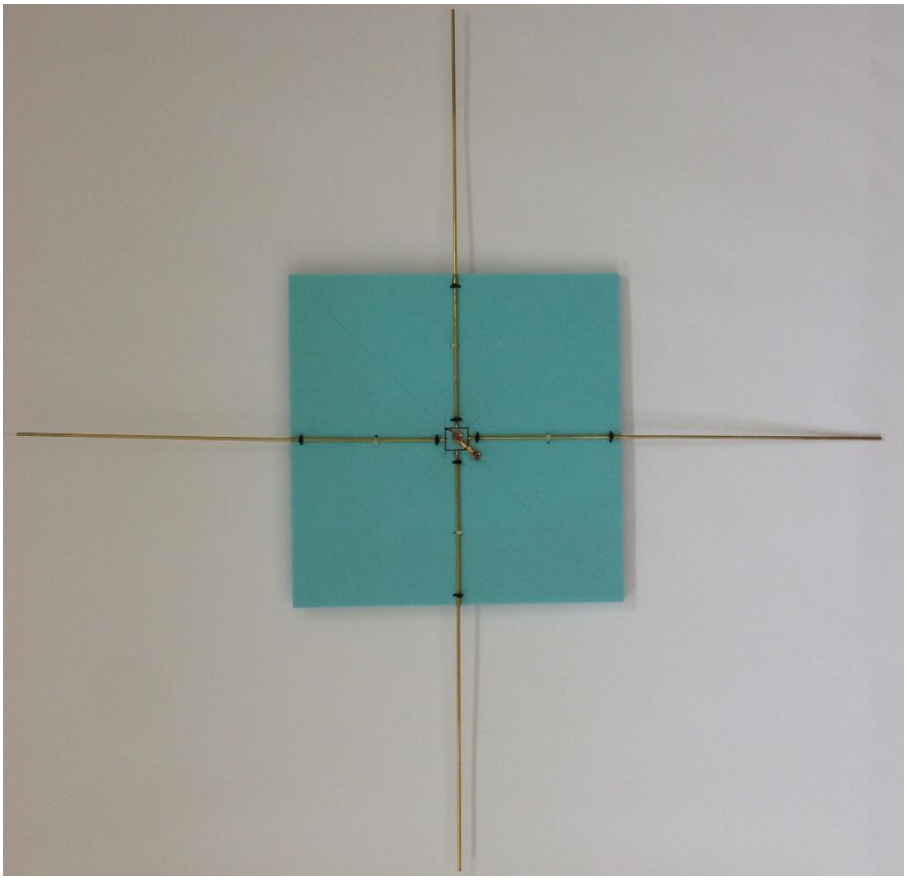

Figure 4-77 Photo of the antenna-transmitter array experimental demonstrator with two crossed dipoles (l = 1.5m)

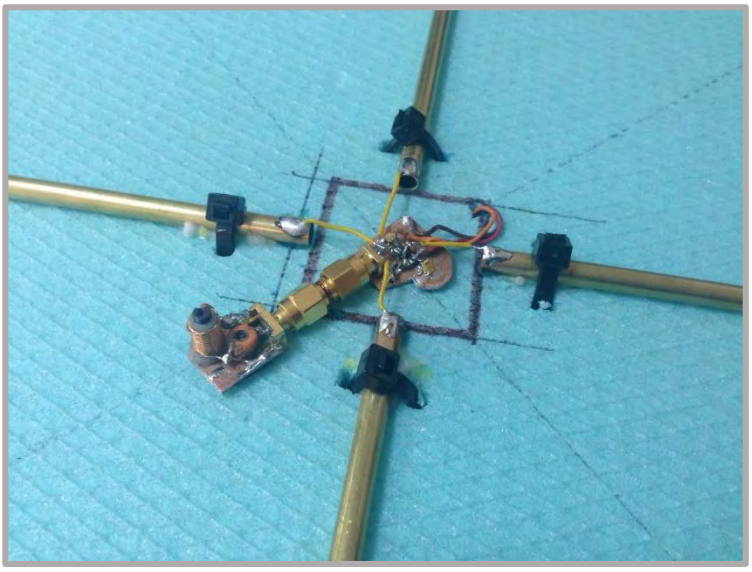

Figure 4-78 Experimental demonstrator close-up

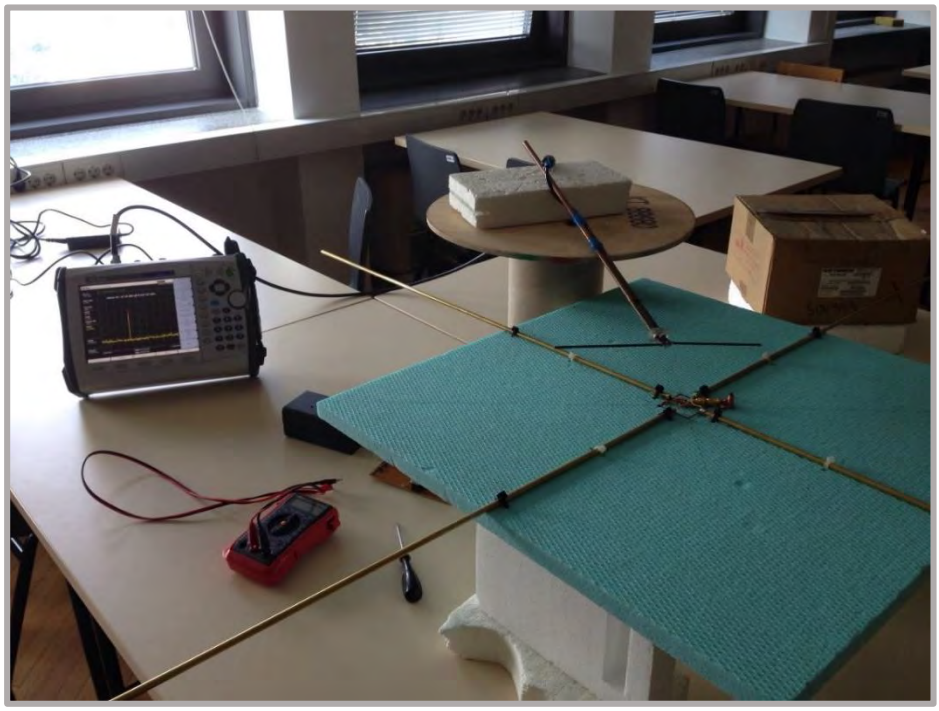

Figure 4-79 Power and spectrum measurement setup

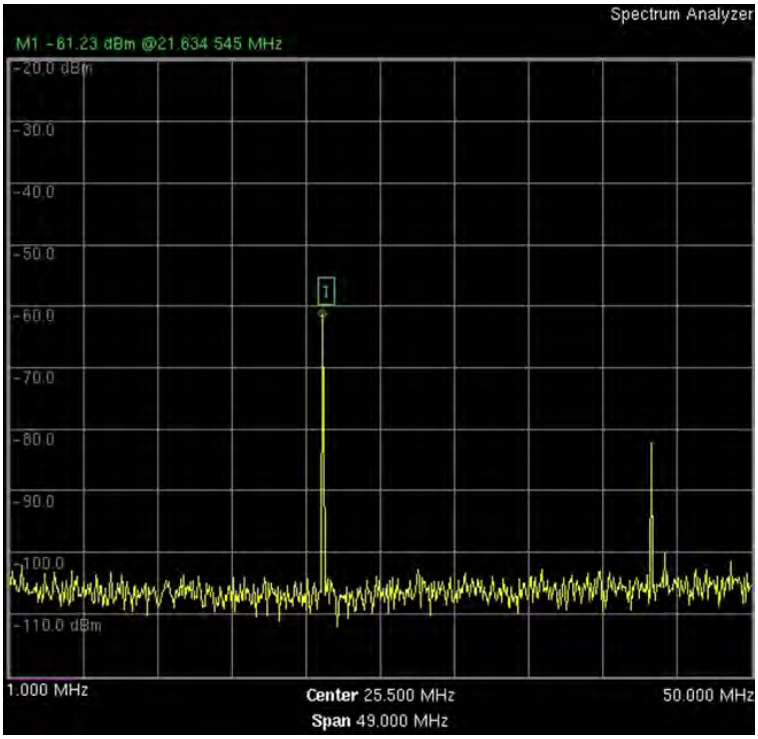

Figure 4-80 A sample of measured spectrum of the oscillating signal of antenna-transmitter array (tuned to f=21 MHz)

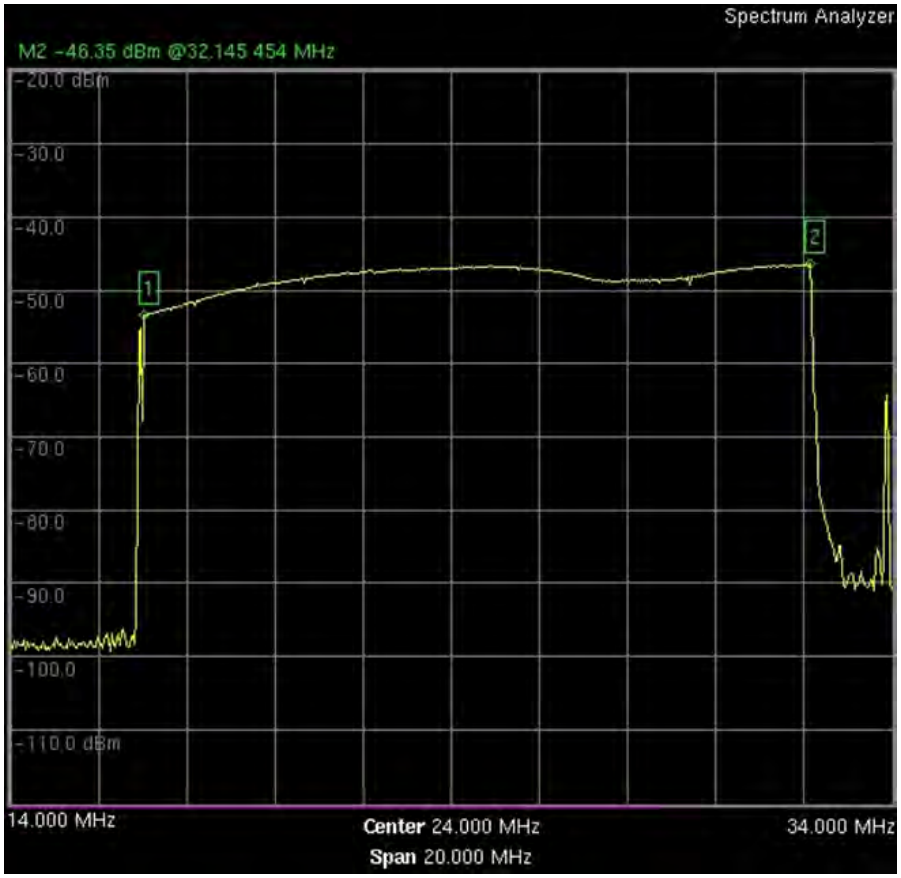

Figure 4-81 Measured relative output power of prototyped antenna-transmitter array within a tuning range of 16 MHz – 32 MHz

The flatness of output power was measured using spectrum analyzer 'max-hold' function and the result is presented in **Figure 4-81**. It can be seen that variation of the output power was up to 5 dB within a tuning range 16 MHz – 32 MHz.

Finally, the classical injection-locking experiments [121] were performed in the last set of measurements. They were done with the help of small external dipole antenna fed by synthesized RF generator. It was found possible to lock the antenna-transmitter array within the fractional bandwidth of approximately 2%. A sample of obtained familiar spectra of locked oscillator, the low frequency boundary, and the high frequency boundary of the lock-in range are given in Figure 4-82, Figure 4-83 and Figure 4-84, respectively.

Unfortunately, it was not found possible to test the idea of injection-locking of the antenna-transmitter array without the resonant LC circuit due to DC biasing problems. Looking at the basic schematic diagram (Figure 4-65), one finds that the DC return path of the non-inverting input was assured via the inductor of the tuning LC circuit. If the LC circuit were removed, the non-inverting input would not have the DC return path. One could use the RF choke, but its inductance should be very large due to low operating frequency. Therefore, the principle of a broadband injection-locking of the antenna-transmitter array has been tested only numerically while the experimental verification needs additional efforts.

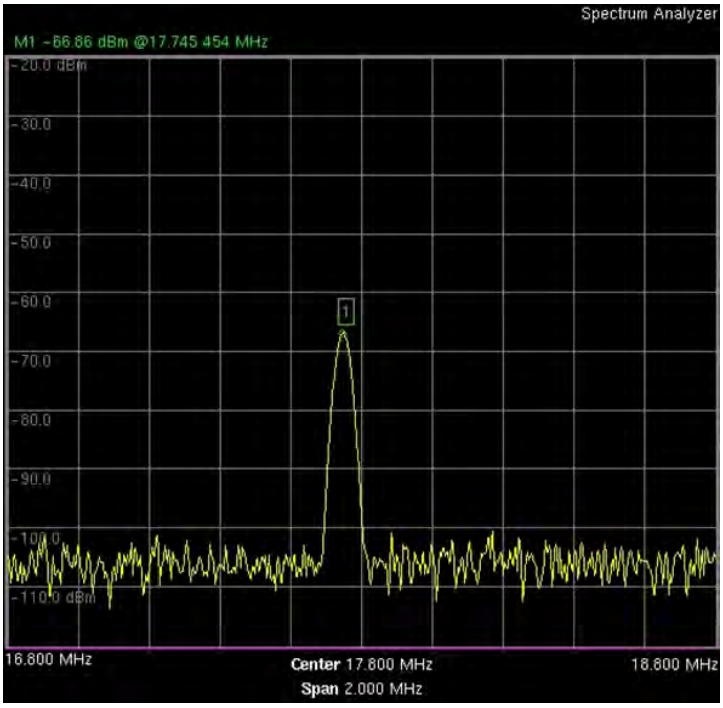

Figure 4-82 Injection locking of a non-Foster antenna-transmitter array, f_o=17 MHz, locked signal

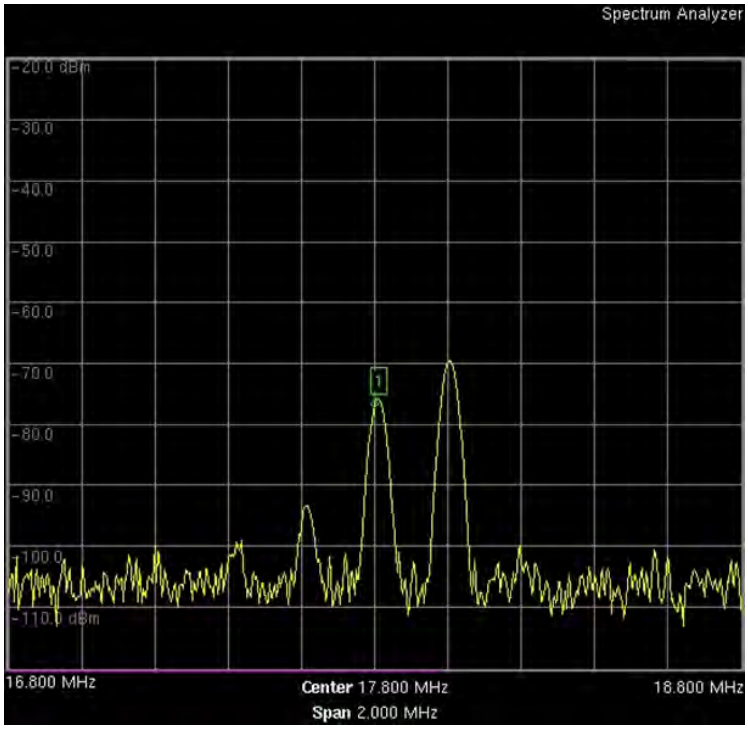

Figure 4-83 Injection locking of a non-Foster antenna-transmitter array, f_o=17.82 MHz, upper lock-in boundary

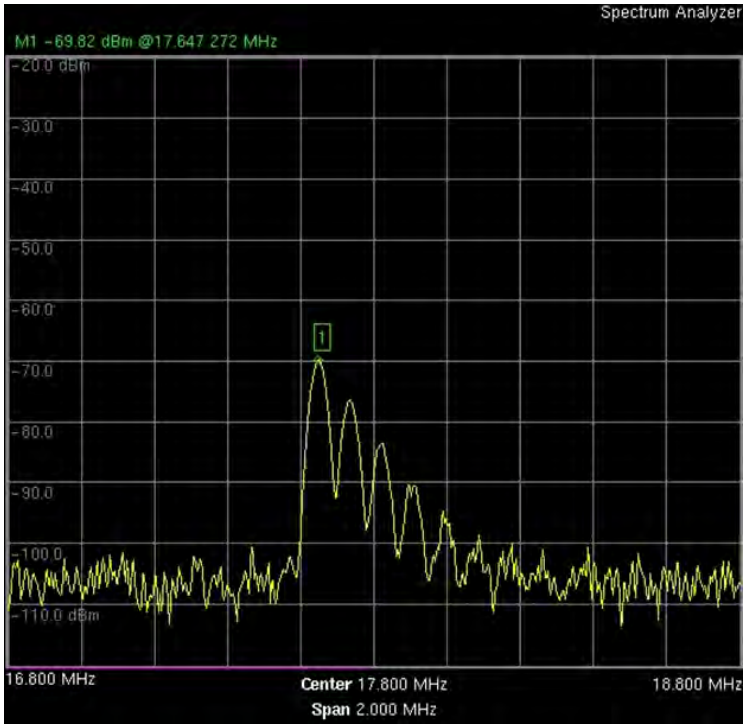

Figure 4-84 Injection locking of a non-Foster antenna-transmitter array, f_o=17.62 MHz, lower lock-in boundary

4.5 Non-Foster Fabry-Perot antenna-transmitter

(*The part of the results presented in Section 4.5 was achieved with the help of Borna Vukadinovic, who is a graduate student at University of Zagreb, Faculty of Electrical Engineering and Computing).

The Fabry-Pérot (FP) antenna is well known and different kinds of it have been investigated in many papers [122]. The main idea behind FP antenna is to make use of successive reflections of electromagnetic waves in order to enhance radiated electromagnetic signal through constructive interference. That is achieved using a partially reflective surface (PRS), and a perfect electric conductor (PEC) sheet that form a cavity (Figure 4-85). A PRS is usually constructed as a capacitive artificial structure that consists of a thin dielectric slab with printed conductive patches. The cavity is excited by a small point source (small horizontal electric dipole). Since the electric field vector is parallel to the PRS, it gives rise to charge accumulation on the patch edges (Figure 4-85), and therefore the surface has capacitive character [123]. The wave emanated from the point source travels to the PRS, where it is partially transmitted through the slots between neighboring patches (radiated into free space, Figure 4-85) and partially reflected back from the patches themselves. That reflected wave travels back across the cavity, experiences total reflection from the PEC, and again travels back to the PRS. At the PRS, the wave is again partially reflected and partially radiated. Thus, there is an infinite number of zig-zag travelling paths and associated waves, which build-up the interference pattern. This interference pattern should be of constructive form (i.e. there should be an enhancement of the wave radiated from the cavity). The radiation enhancement will occur if the path difference Δ_d satisfies:

$$\Delta_d = N \cdot \lambda \tag{4.18}$$

where N is an integer and λ is the wavelength of the electromagnetic wave. The path difference can also be expressed in terms of associated phase shift:

$$\Delta_p = N \cdot 2\pi. \tag{4.19}$$

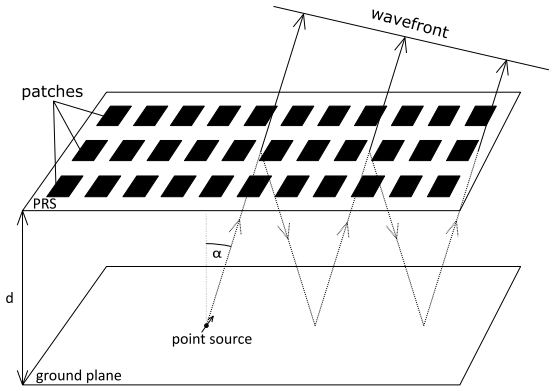

Figure 4-85 Structure of a general Fabry-Pérot antenna

The phase difference is a result of a phase shift of the EM wave upon reflections and travelled distance. This difference is given by [124]:

$$\Delta_p = \Psi - \pi - \frac{2\pi}{\lambda} \cdot 2d \cdot cos(\alpha). \tag{4.20}$$

It can be seen that the phase difference depends on the angle of reflection coefficients of PRS and PEC (ψ and π, respectively), and the distance which wave travels across the cavity ($2d \cdot \cos(\alpha)$). Since the PRS has capacitive character, its surface reactance decreases with frequency (approaching 0), and therefore, ψ decreases with frequency, as well (approaching -180°). That is a direct consequence of a Foster theorem, which requires that $\partial X/\partial\omega>0$ and $\partial B/\partial\omega>0$ (X and B being reactance and susceptance, respectively) [3]. Therefore, for any passive structure, the decrease in ψ (caused by change of frequency) cannot be compensated by the third term in (4.20). In other words, if frequency changes, (4.19) is not fulfilled any more. Thus, the standard FP antenna is inevitably a very narrow-band device. The FP antenna bandwidth is usually defined as normalized frequency range within the directivity drops by 1 dB (comparing to the directivity at central frequency, for which $\Delta_p = \pi$). Typical FP antenna parameters are -1 dB bandwidth of around 2% and 20 dB directivity [125].

4.5.1. Basic concept

So far, there have been several attempts to increase the FP antenna bandwidth. In [126] the authors increased bandwidth up to 5.4% by changing the PRS structure. A few central patches were joined to form a larger patch in order to achieve photonic band-gap resonance. In [127], the bandwidth was further increased to 12%, also by slightly changing the PRS structure. Specifically, the patches were rearranged to be closer to one another in the middle of the PRS.

All these approaches used passive elements, therefore their bandwidths are constrained by Foster theorem.

Here we propose use of the concept of non-Foster source presented in Section 4.1., towards construction of a broadly tunable FP antenna-transmitter.

For the sake of simple analysis, it is convenient to use one-dimensional equivalent circuit of FP antenna (Figure 4-86 (a)). Within the frame of this model, the two-dimensional cavity is reduced to one dimension, represented with a transmission line. Of course, this corresponds to one direction of propagation of electromagnetic wave.

The PEC (ground plane) is represented by a short circuit in equivalent circuit (Figure 4-86 (b)). The FP cavity is represented by a transmission line, length of which depends on the angle of propagation of electromagnetic wave. For a wave travelling upwards (from PEC towards PRS) this angle is equal to zero, and the transmission line length is equal to the cavity width. The PRS itself can be modelled as a parallel combination of a resistor and a capacitor. The resistor represents the intrinsic impedance of free space, while the capacitor is added because the PRS has capacitive character, as explained before.

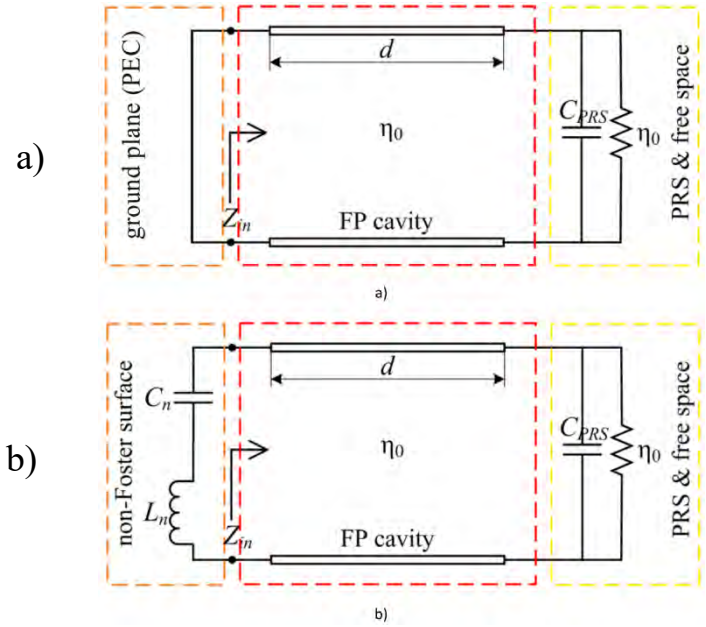

Figure 4-86 a) 1D model of ordinary Fabry-Pérot antenna, b) 1D model of non-Foster-based Fabry-Pérot antenna (taken from [124])

In order to approach (ideal) condition needed for constructive interference (4.19) within a broad frequency range, the PEC may be replaced with an artificial surface (additional lumped reactance in 1D equivalent circuit, Figure 4-86 (b)). The purpose of this artificial surface is a broadband compensation of the overall phase shift caused by reflection from PRS and by propagation across the cavity [124,125]. It can be shown that required phase of reactance of artificial surface should decrease with frequency, thus, it should show a non-Foster behavior [124,125]. As explained in [3,5], the appropriate non-Foster element is a series combination of negative capacitor and negative inductor ('negative LC circuit'). For the simple demonstration of proposed principle, one may use realization of negative LC circuit with OPamp-based N-type NIC (Section 4.2). The basic idea is sketched in Figure 4-87. Actually, it is again a special kind of non-liner non-Foster source (Section 4.3), based on a 'mixed' lumped-distributed network (Section 3.2).

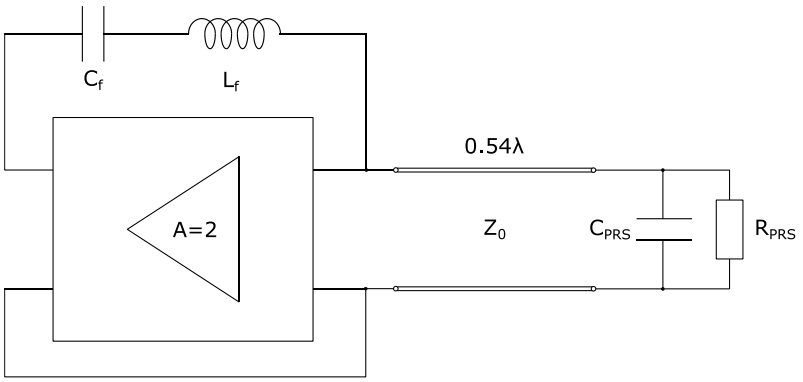

Figure 4-87 1D model of FP antenna with a PEC plane replaced with negative LC artificial surface (negative LC circuit).

4.5.2. Numerical investigation

In order to test this basic idea of a non-Foster FP antenna-transmitter, the first step would be to build-up one-dimensional experimental demonstrator. Such a demonstrator should operate in lower RF regime (instead in microwave regime, which should be the operating band of actual active FP antenna), in order to minimize parasitic capacitances and inductances. Thus, the operating frequency of approximately 10 MHz was chosen. If the oscillating frequency is tunable, the system will inherit broadband behavior of a non-Foster-based FP antenna from [124] (it should be possible to tune the system to any desired CW operation point within -1dB bandwidth). Hence, it is important to determine which part of the system primarily determines the oscillating frequency. The main resonant element of the system is a cavity (which corresponds to a transmission line segment in equivalent circuit). This cavity is coupled to the second resonant element (negative LC circuit). Obviously, instead of changing the cavity thickness in order to change the frequency, it would be more practical to change negative capacitance of non-Foster LC circuit.

In order to investigate oscillation properties, we proceeded with linear analysis of natural frequencies of the system. To this end, one-dimensional model (Figure 4-87) was described by a voltage transfer function, defined as a ratio of voltage at two ends of the transmission line. The transfer function (in Laplace domain) is given by [93]:

$$H(s) = \frac{Z_1 \cdot Z_0}{\frac{(Z_2+Z_1)\cdot Z_0}{(Z_2 \cdot Z_1+Z_0^2)}+\mathrm{th}\left(\frac{s\cdot l}{c}\right)}. \tag{4.21}$$

Here, Z_1 and Z_2 are given with (4.22) and (4.23), respectively:

$$Z_1 = \frac{s\cdot L_f+\frac{1}{s\cdot C_f}}{1-A(s)} \tag{4.22}$$

$$Z_2 = \frac{R}{1+s\cdot R\cdot C} \tag{4.23}$$

The symbol $s=\sigma+j\omega$ is a complex frequency. The symbols R and C denote resistivity and capacitance of the PRS, while L_f and C_f stand for inductance and capacitance in the feedback loop, respectively. In addition, symbols c, l and Z_0 stand for speed of light, length of the transmission line and characteristic impedance, respectively. As before, the symbol A(s) stands

for the gain function of used amplifier. This function was modelled using a three-pole model [51]:

$$A(s) = \frac{A_0}{(1+s\cdot\tau_1)\cdot(1+s\cdot\tau_2)\cdot(1+s\cdot\tau_3)} \tag{4.24}$$

Here τ stands for pole time constant (an inverse of pole angular frequency, $\tau_i = \frac{1}{\omega_{p,i}}$). Of course, the presence of amplifier poles decreases the gain at higher frequencies, which is consistent with causality and model's behavior of real-world amplifier.

Natural frequencies of the system can be calculated by equating denominator of (4.24) to zero. For natural frequencies, the real part of which is negative (σ<0), associated time domain response decays exponentially and (after some time) dies out. Therefore, these natural frequencies do not influence the oscillating behavior of the system (they present stable poles). The complex frequencies, the real part of which is either equal to zero (σ=0) or greater than zero (σ>0) determine the oscillating frequency of the system (they present marginally stable and unstable poles). In order to investigate the influence of the different parameters of the system (e.g. feedback capacitance, feedback inductance) on oscillating frequency, a time-efficient method for finding poles of the system was developed. The (4.24) is a transcendent equation and its solution cannot be found analytically. Of course, one can use some of numerical root finding algorithms. However, due to presence of hyperbolic function, is difficult to find the initial searching area. Thus, associated numerical method is rather slow. This makes real time visualization of poles movement (as a function of some design parameter) hardly feasible. Therefore, we used a Taylor expansion of hyperbolic function. It leads to polynomial equation, the roots of which that can (numerically) be solved very quickly. Analysis of the pole locations revealed that the change of feedback capacitance has predominant effect on frequency of oscillations (Figure 4-88 (a)). At first, it can be seen that a system has infinite number of stable poles located close to imaginary axis. These poles are associated with periodic behavior of a transmission line. In addition, there are several complex (both stable and unstable) poles. However, it can also be seen that the influence of a transmission line on oscillating frequency (i.e. on unstable poles located in the right-hand-side of complex plane) is very small.

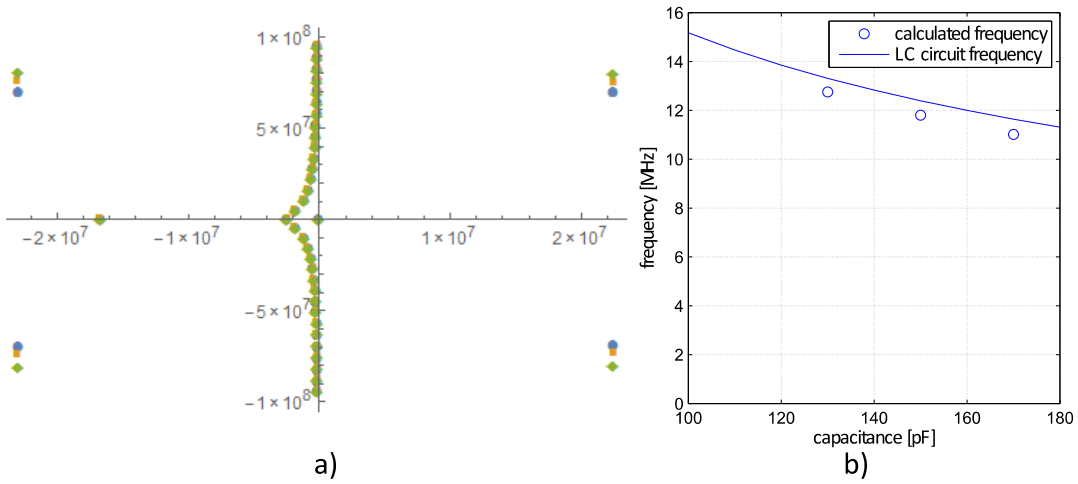

Figure 4-88 a) Loci of system poles for several feedback capacitances (blue circle - 170 pF, orange square - 150 pF, green rhombus - 130 pF), b) Frequency of oscillations compared to a resonant frequency of LC circuit in the positive feedback

This can be explained by the fact that the transmission line length is approximately equal to λ/2. Hence, the PRS equivalent impedance is transformed into a similar impedance at the other end of transmission line. This leaves the LC negative circuit in feedback loop (in other words, a negative LC circuit generated by negative impedance converter) as the element that predominantly determines oscillating frequency.

It is clear that presented linear analysis cannot predict spectral properties of oscillating signal. Within the linear model, the amplitude of the signal (caused by instability) will grow to infinity. Of course, in reality, the nonlinear effects will limit the amplitude and introduce both harmonic and non-harmonic spectral components. Thus, we proceeded to non-linear analysis using the SPICE model of ADA4860 (high-speed OPamp chosen for practical realization). Using this OPamp one might construct experimental demonstrator that would operate at several hundreds of MHz (the frequency of the ADA4860 dominant pole is approximately 500MHz). However, the central oscillating frequency was chosen to be only 10 MHz, in order to decrease the unwanted influence of parasitic capacitances and inductance, as explained before. The feedback capacitance and inductance were chosen in a way that assures needed frequency of oscillations (230 pF and 1.1 μH). After analysis of the results of transient simulation, the frequency of oscillations was found to be very similar (the discrepancy smaller than 1%) to that obtained in linear analysis based on location of system poles. Also, it was found possible to tune the oscillating frequency (by changing capacitance in positive feedback loop) across at least 20% bandwidth. Thus, the tuning bandwidth can be made equal to intrinsic 1dB bandwidth of original FP antenna [125].

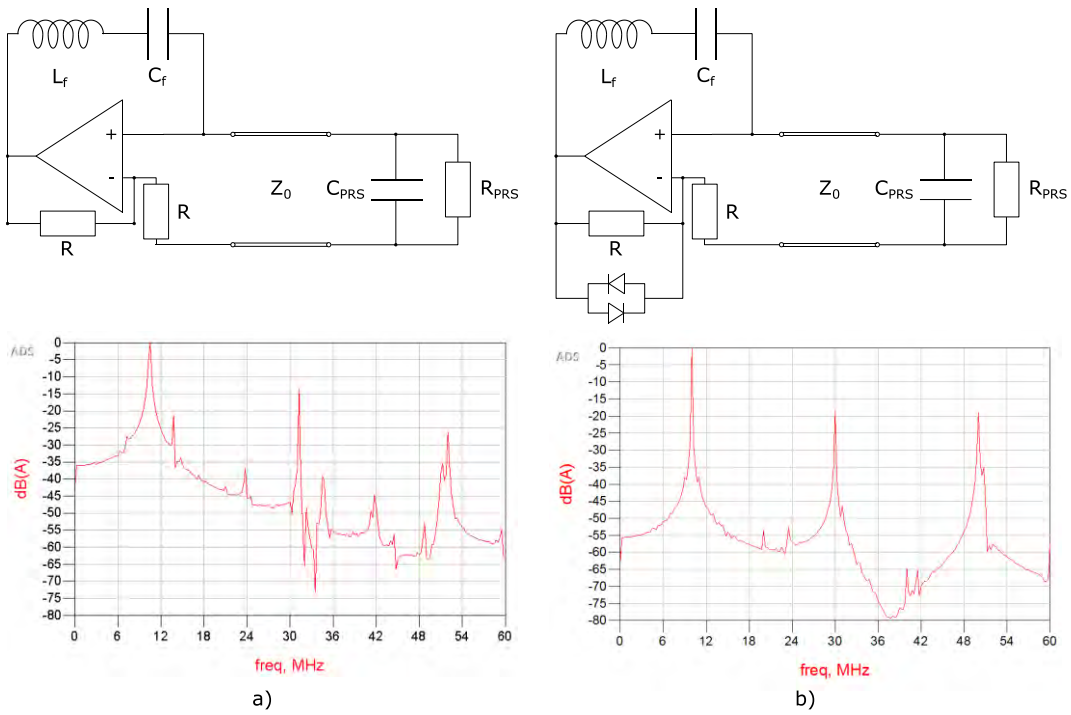

Figure 4-89 a) 1D model with negative LC circuit and associated signal spectrum b) 1D model with negative LC circuit with added diode limiter and associated signal spectrum

In the next step, the time-domain response was transformed into the frequency domain and the spectrum of oscillating signal was investigated. A typical spectrum is shown in lower part of Figure 4-89. It can be seen that higher harmonic components (second and third harmonics) were lower than -15 dBc, which is satisfactory for the proof-of-concept demonstration. Further increase of suppression of the spurious components can be achieved by automatic gain stabilization using well-known approach based on diode limiter as shown in Figure 4-89 (upper part). Simulation of this case showed 5 additional dB of suppression of spurious components (all higher harmonics are lower than -20 dBc, Figure 4-89 (b), lower part).

4.5.3 Experimental RF demonstrator

An experimental demonstrator was built in order to test the basic idea and to cross-check the validity of developed models. It comprised a negative LC circuit based on ADA4860, a transmission line (RG 58U coaxial cable with the length of 10 meters), and a parallel RC circuit that models the PRS. Clearly, the characteristic impedance of used coaxial cable (50 Ω) is different than intrinsic impedance of free space (377 Ω). Thus, the values of R and C from [124] were scaled in such a way that retains the required reflection coefficient ($R = 50\Omega, C = 1.2\ nF$). Coaxial cable was used instead of air transmission line in order to shorten the required length. The central frequency was 13 MHz (determined with elements in the feedback loop $L = 1\mu H, C = 150pF$). As noted before, at such low frequency the parasitic inductances and capacitances can be neglected, which is important for clear testing of proof of concept. The physical appearance of assembled demonstrator is shown in Figure 4-90.

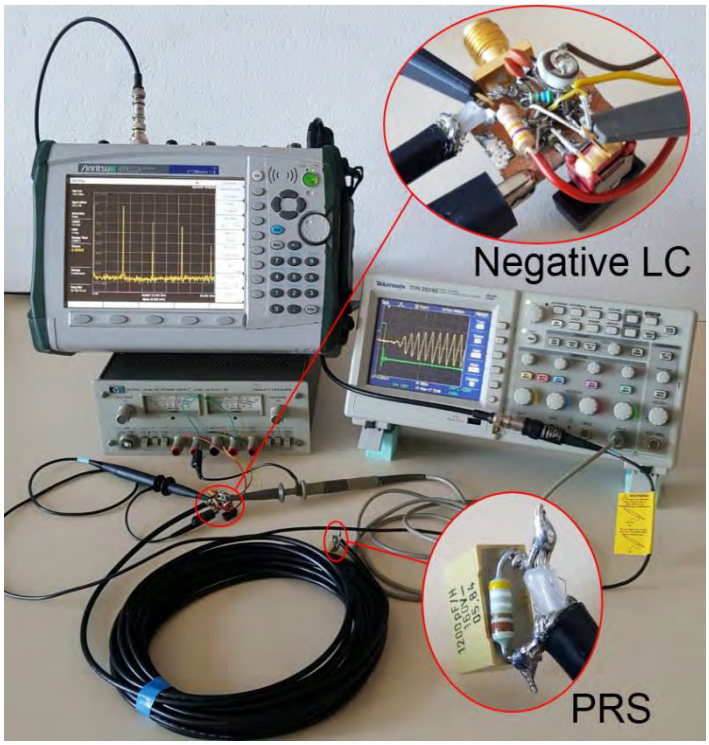

Figure 4-90 Photo of the experimental demonstrator and measurement setup

The measurements were performed both in the time and frequency domain and, as expected, they revealed oscillating behavior. This indeed proves idea of FP antenna-transmitter system. At first, the transient behavior of the system (the onset of oscillations) was investigated using a digital scope and a sample of the measurements is shown in Figure 4-91 (a). Obtained results were found to be in good agreement with simulations. It was possible to tune the oscillating frequency using a trimmer capacitor (120 pF-180 pF) and the tuning bandwidth was approximately 10%. By use of a trimmer capacitor with higher tuning range, the 20% bandwidth (the -1dB bandwidth of a FP antenna, per se) can be covered easily. The frequency of oscillations approximately matched the predicted frequency (within 10%) and observed difference is a consequence of tolerances of used elements. The frequency-domain measurements revealed suppression of higher harmonics of approximately 25 dBc (Figure 4-91 (b)). This result is again in a good agreement with non-linear analysis.

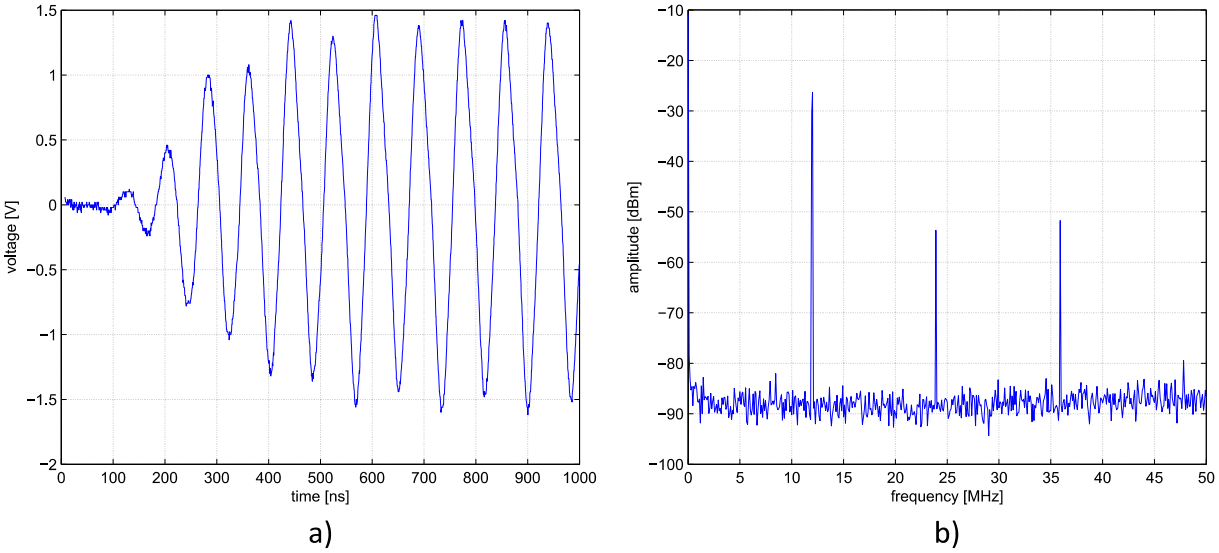

Figure 4-91 Measured onset of oscillations of the experimental demonstrator, b) measured spectrum of steady-state oscillating signal

One concludes that numerical and experimental results presented in this section proved the correctness of basic idea of a broadband active self-oscillating FP antenna (antenna-transmitter system). This system has -1 dB bandwidth of 20% and it can be tuned at any frequency within this band.

4.6. Technological issues and possible extension to microwave active metasurfaces

Up to now, a couple of novel ideas regarding possible use of non-Foster source-load networks and metasurfaces have been presented. Apart from theoretical and numerical investigation, several experimental demonstrators have been designed and tested:

a) Experimental demonstrator of a band-pass non-Foster capacitor (CH 3.3.3)
b) Experimental demonstrator of an 'all negative' RLC metasurface unit cell (CH 3.3.5)
c) Two experimental demonstrators of a non-Foster antenna transmitter (CH 4.3.4)
d) Experimental demonstrator of a non-Foster antenna-transmitter array (CH 4.4.3)
e) Experimental demonstrator of non-Foster Fabry-Perot antenna-transmitter (CH 4.4.3)

All these demonstrators used cheap OPamp technology and operated in the lower RF range (< 100 MHz). The reason for choosing such a low frequency is a lack of microelectronic technology at University of Zagreb. As detailed in [51], the microelectronic technology is needed in order to extend non-Foster approach into microwave frequency regime. This is a direct consequence of the fact that operating frequency of non-Foster negative capacitors and inductors should be approximately one tenth of the frequency of the first pole of used active device [2,51]. Specifically, it was shown in [51] that the use of standard 65 nm CMOS technology offers possibility of increase the highest operating frequency into the microwave

regime (above 5 GHz). Since the 27 nm CMOS technology is nowadays widely available, even higher frequencies could become possible, as well. Furthermore, as recently reviewed in [20], several examples of specially design non-Foster integrated circuits operating above 30 GHz have been demonstrated recently. Of course, all these studies show very preliminary results, but, they definitely indicate that extension of non-Foster negative elements into microwave regime is, at least in principle, feasible.

The next question is whether the devices proposed in this report can also be integrated, and therefore, their frequency of operation pushed into microwave regime. Devices a) an b) are stable networks with negative capacitors, inductors, and resistors, that work in the linear regime. Almost all examples of microelectronic realization of non-Foster device recently reviewed in [20] operate in linear regime. Therefore, it appears that there are not some fundamental problems in microelectronic realization of devices a) and b) in microwave regime. On the contrary, the situation with devices c), d) and e), which work in non-linear regime, is not clear. One should perform detailed physical-level simulations of microelectronic realization in order to make some feasibility estimation.

Additional problem with devices c) and d) is that they use NICs with highly reactive loads (short dipole antennas). As discussed in Section 4.3., this sometime introduces problems with error in NIC conversion ratio. It was shown that in the case of NIC based on OPamps (or more generally on a simple non-inverting amplifier, Figure 3-10), conversion error can be kept within acceptable limits. However, microelectronic realizations of non-Foster circuits are usually based on Linvill's cross-coupled floating circuit [2, 26]. It is not clear whether the same behavior of NIC conversion ratio is valid in that case. In order to tackle this issue, we performed a very simple S-parameter simulation of such a floating NIC. We have selected HRL H3-150 HEMT microelectronic transistor and imported the S parameters (available from the manufacturer [128]) into the ADS^{TM} simulator. The simulation of the $S_{21}|$ parameter has shown that the frequency of a first pole is approximately 10 GHz (Figure 4-92).

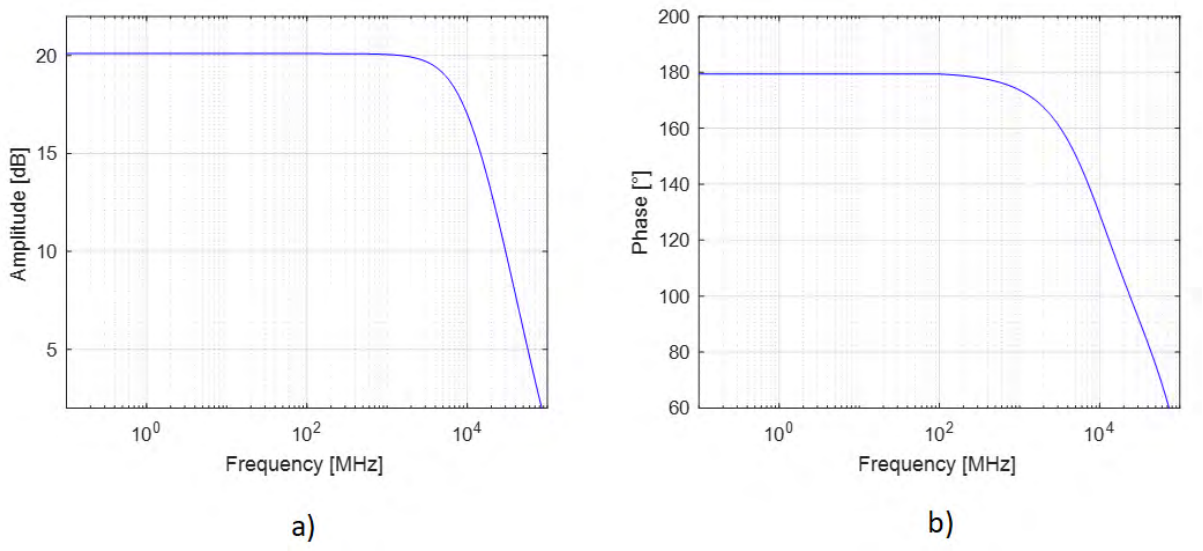

Figure 4-92 Frequency dependence of a) amplitude and b) phase of S_{21} of HRL H3-150 HEMT transistor

In the second step, we designed a model of a non-Foster antenna-transmitter, similar to the RF demonstrator from 4.4., (Figure 4-93). Since we are interested primarily in the AC behavior of the circuit, the biasing and coupling networks were idealized using large values of

associated inductors (L_B) and capacitors (C_B). The performed ADS^{TM} simulations were very similar to those from Section 4.3. and a sample of the results that show comparison of NIC input impedance with the idealized case is given in Figure 4-94. It can be seen that the behavior is very similar to that one obtained in the case of OPamp-based demonstrator in Section 4.3. Thus, one concludes that the realization of non-Foster antenna transmitter in microwave regime might be feasible.

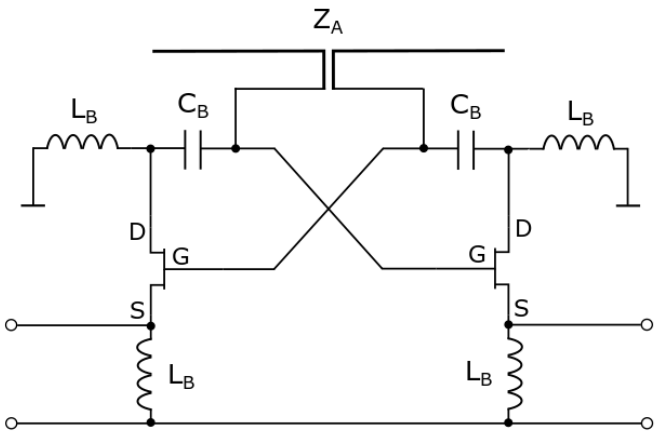

Figure 4-93 Simplified schematics of a non-Foster antenna-transmitter based on HRL H3-150 HEMT transistor ($L_B = 1\mu H$, $C_B = 1$ nF). The dipole antenna in the feedback ($l = 5$cm) is modelled as a Stearn's 5-element network [87]

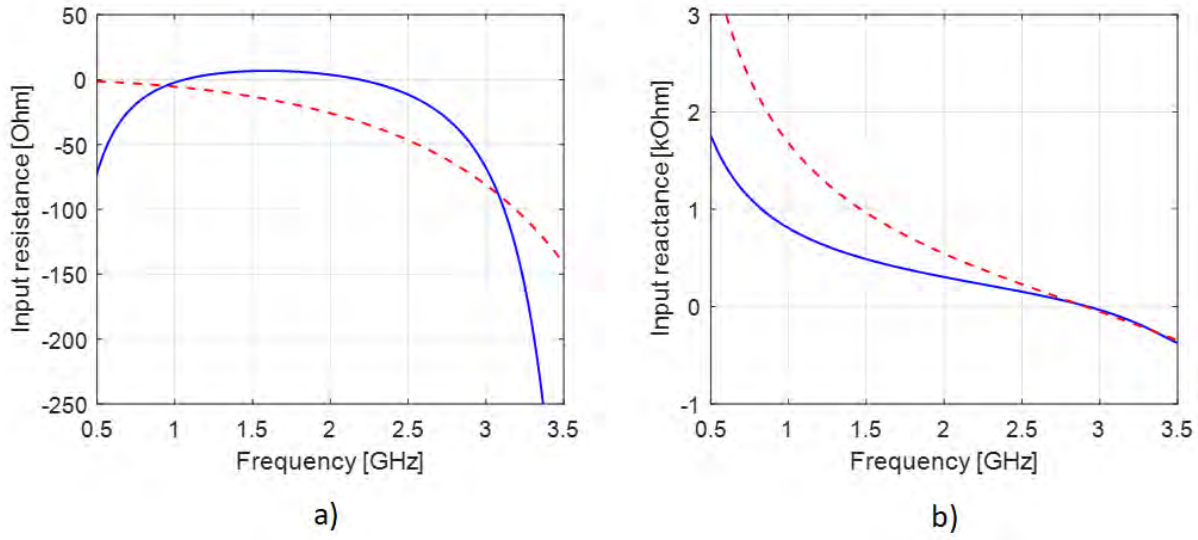

Figure 4-94 Dependence of a) input resistance and b) input reactance of the non-Foster antenna-transmitter based on HRL H3-150 HEMT transistor on the frequency, a dipole antenna in the feedback ($l = 5$cm) is modelled as a Stearn's 5-element network [87]

What kind of novel applications will become possible once the microwave version of devices demonstrated in this report (in RF regime) are available? Certainly, one of the most interesting electromagnetic systems are active metasurfaces. All the devices proposed so far (a, b, c, d, e)

can be thought of as the metasurface unit cells. Particularly attractive would be an active self-oscillating metasurface that contains an array of non-Foster antenna-transmitter subarrays (Figure 4-95).

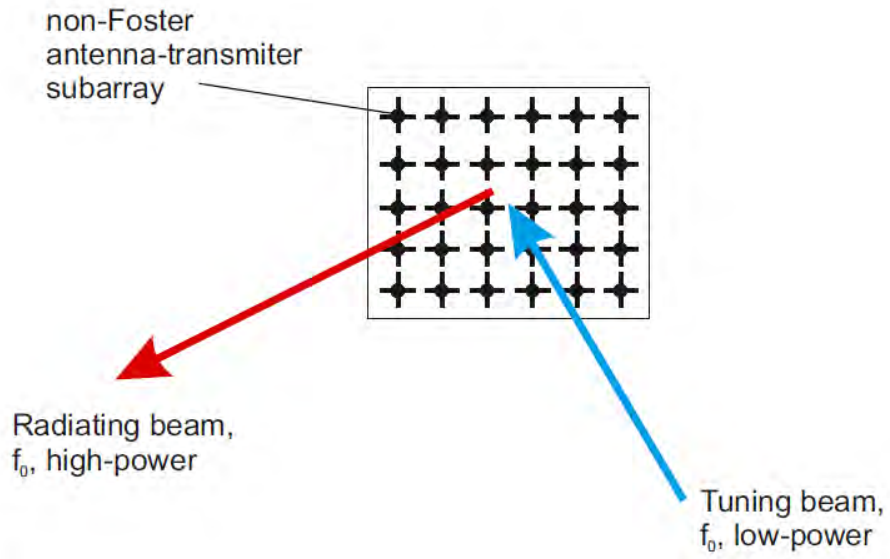

Figure 4-95 Envisaged extension of a non-Foster antenna-transmitter unit cell to a self-oscillating non-Foster metasurface

Each subarray contains NIC and two crossed dipoles *without* a resonant circuit. The whole array is injection-locked by an external tuning beam. Such a self-oscillating metasurface could be tunable within 1:10 frequency range.

4.7. Summary

A novel concept of generalized source-load non-Foster networks has been analyzed thoroughly in this chapter, and several potential applications have been proposed. The brief summary of presented discussion is given below:

- An idea of a broadband linear non-Foster source perfectly matched to the load has been proposed. It can be constructed either by using an external generator and additional stable generalized non-Foster network or by unstable generalized non-Foster network. The latter turns the inherent instability of practical non-Foster reactance (usually considered as a serious drawback that prevents widespread application of non-Foster elements) into a very useful feature.

- It has been shown that the voltage-conversion and the current-conversion negative impedance converters have fundamentally different properties in non-liner regime. Furthermore, it has been shown that these non-linear properties can be analyzed using generalized N and S curves of non-linear negative capacitance and inductance. In addition, it has been shown that non-linear non-Foster source is in a sense similar to the large-signal negative resistance oscillator. The most important difference is that non-

Foster source offers (theoretically) infinite tuning bandwidth with nearly perfect matching.

- It has been shown that a non-linear non-Foster source, the internal impedance of which is a simple negative RC circuit can be used as a non-Foster antenna transmitter. That system uses a simple short dipole antenna as a radiator. Measurements on two prototyped demonstrators in lower RF range (< 100 MHz) revealed the tuning bandwidth that varies from 1:2 to 1:10 (depending on the construction of a tuning circuit), with equivalent return loss of 15 dB.

- A concept of 'non-Foster antenna-transmitter' has been extended to 'non-Foster antenna-transmitter array. Comparing to the previous design based on a self-oscillating single short dipole, the array offers much broader tuning and matching bandwidth, it enables use of any type of small antenna, and it has up to 3 dB higher radiated power. The simulation results and associated proof-of-concept demonstrator verified correctness of the proposed approach. An experimental RF demonstrator based on two crossed dipoles and has been constructed and measurements revealed oscillations that can be tuned within 16 - 32 MHz bandwidth. It is important to stress that this tuning bandwidth was constrained only by available tuning elements. The simulations showed that the tuning bandwidth larger than 1:10 can be achieved by using different tuning elements.

- A concept of an active self-oscillating non-Foster Fabry-Pérot antenna has been proposed theoretically, with potential to increase 1 dB bandwidth for ten times (compared with ordinary passive Fabry-Pérot antenna). One dimensional model of such a system was analyzed using both simple linear model and SPICE-based non-linear model. An RF experimental demonstrator operating in 10 MHz range was constructed and measured. Experimental results proved the correctness of basic idea of a broadband active self-oscillating FP antenna (antenna-transmitter system). This system has -1 dB bandwidth of 20% and it can be tuned at any frequency within this band.

Chapter 5 CONCLUSIONS AND FUTURE WORK

Conclusions and future work

This study reports 24-month research effort undertaken towards two basic goals:

1. To significantly suppress stability problems in *the most common applications* of non-Foster elements (*the non-Foster metamaterials and the non-Foster matching*) by novel design of non-Foster elements and/or applying concept of 'all-negative' stable networks
2. To propose a novel concept of *'non-Foster' source* that turns instability of non-Foster network into a useful feature, convenient for use in transmitting applications

This research is novel and unique since so far it has been believed that the construction of stable non-Foster SNG/DNG transmission lines/metamaterials/metasurfaces is not feasible. In addition, the idea of turning the instability of non-Foster element into a useful feature in the form of non-Foster source and transmitter-antenna system has not been presented yet.

Our research efforts have been divided into two mean streams.

In the first stream, we re-examined basic stability properties of non-Foster elements (negative capacitors and negative inductors) with additional third element: a negative resistor. We have shown that these *generalized non-Foster elements* supplemented with a transmission line form a 'mixed' network with novel and counter-intuitive stability properties. Furthermore, we found possible to construct a stable system with ENG/MNG properties by modifying a dispersion characteristic of the generalized non-Foster elements or letting all the elements to be negative. We have proven the correctness of proposed approach by construction and measurements of two experimental demonstrators in a lower RF range (<100 MHz).

In the second stream, we examined unstable non-Foster networks and found that, in some case they me be modelled as non-Foster source. This source is actually an oscillator that offers perfect matching to its load and (theoretically) infinite tuning bandwidth. By choosing a short dipole antenna as a load, we created broadly tunable non-Foster radiating system .We have proven the correctness of this approach by construction of two experimental demonstrators of non-Foster antenna-transmitter systems and one experimental demonstrator of non-Foster antenna-transmitter array. As in the previous case, aforementioned demonstrators operate in lower RF range (<100 MHz)

All achieved results clearly show that a novel concept of improving the stability properties of generalized non-Foster networks, as well as a novel concept of a non-Foster source and associated non-Foster antenna transmitter are correct. Finally, we have argued that these new concepts could be extended into microwave regime and pave a way towards manufacturing of stable non-Foster metasurfaces for manipulation of electromagnetic waves. Yet another future application would be non-Foster-based self-oscillating metasurfaces with a tuning bandwidth ten times larger than the existing transmitting systems. .

As a short summary, the realized outcomes of the project are:

- We have shown that the widely accepted stability criterion of positive 'mesh' capacitance fails for parallel combination of a positive and ideal negative capacitor with connecting transmission line. Such a network is always unstable, regardless of the line length and capacitance values of positive and negative capacitor. However, the inherent dispersion of a realistic negative capacitor (usually considered as a drawback) can be tailored in a way that assures stable operation. Very similar conclusion applies for a series combination of positive and ideal negative inductor with connecting transmission line. We have also shown a rather surprising fact that in some cases of lumped and mixed networks with a realistic model of negative capacitor, stable operation is feasible even if overall capacitance is negative.

- We have found that a concept of unstable 'mixed lumped-distributed network' can be used in active self-oscillating non-Foster Fabry-Pérot antenna. Theoretical investigation predicted increase of 1 dB bandwidth for ten times (compared with ordinary passive Fabry-Pérot antenna). One dimensional model of such a system was analyzed using both simple linear model and SPICE-based non-linear model. An RF experimental demonstrator operating in 10 MHz range was constructed and measured. Experimental results proved the correctness of basic idea.

- We have developed a novel topology of a 'bandpass' non-Foster capacitor intended for use in active metamaterials/metasurfaces and antennas. We have developed appropriate experimental demonstrator based on high-speed OPamp, operating in low RF range (< 100 MHz). Measurements have shown stable operation although the overall capacitance is negative and the results match analysis and simulations very well. We believe that this is the first demonstration of a stable 'bandpass' negative capacitor.

- We have performed analytical and numerical investigation of counterintuitive physics of 'all-negative' stable lumped network with 'reversed power flow' and found that such a network is indeed stable if equivalent 'mesh elements' are negative. It was found possible to design active RC, RL, And RLC networks that might find application as unit cells of active metasurfaces. All analytical results were verified by circuit simulations that used a realistic SPICE model of commercial OPamp and measurements on negative RLC demonstrator operating in 100 MHz RF range.

- We have investigated an idea of non-Foster source ('non-Foster antenna-transmitter') based on negative series RC circuit and found that it indeed offers (theoretically) infinite tuning bandwidth. We constructed an experimental demonstrator operating in a lower RF range (300 kHz – 10 MHz). The demonstrator comprised an OP-amp based negative RC circuits connected to a simple, short top-loaded monopole (the length of $\lambda/15$ at the highest frequency). Measurements revealed stable oscillations with amplitude flatness of approximately +- 2 dB, within the range 1MHz – 10 MHz. We believe that this is the first demonstration of a 'non-Foster antenna-transmitter'.

- We have extended the concept of 'non-Foster antenna-transmitter' to 'non-Foster antenna-transmitter array. Comparing to the previous design based on a self-oscillating single short dipole, proposed approach offers much broader (theoretically infinite) tuning and matching bandwidth, it enables use of any type of small antenna, and it has up to 3 dB higher radiated power. The simulation results and associated proof-of-concept demonstrator verified correctness of the proposed approach. We have

constructed an experimental demonstrator based on two crossed dipoles and verified oscillations that can be tuned within 16 – 32 MHz bandwidth. It is important to stress that this tuning bandwidth was constrained only by available tuning elements. The simulations showed that the tuning bandwidth larger than 1:10 can be achieved by using different tuning elements.

Finally, we have examined feasibility of extension of proposed concepts and devices into microwave range and found that it should be possible using a microelectronic technology. It would enable construction of active metasurfaces with broadband phase-shifting properties as well as self-oscillating metasurfaces that are broadly tunable by an external beam.

Chapter 6 BIBLIOGRAPHY

Bibliography

[1] L. D. Landau, E. M. Lifshits, "Electrodynamics of Continuous Media", 2nd edition, Buttterwoth Heinmann, Oxford, 2002

[2] S. Hrabar, I. Krois, I., Bonic, A., Kiricenko, E. U. Munoz, "Broadband Epsilon-Near-Zero (ENZ) and Mu-Near-Zero (MNZ) Active Metamaterial", *Final Report for Contract FA 8655-10-1-3030, EOARD/AFRL*, August 2011

[3] R. M. Foster, "A reactance theorem", *Bell Labs Syst. Tech. J.,* Vol. 3, No. 2, pp. 259-267, 1924

[4] N. Engheta, R. Ziolkowsky, (ed.), "Metamaterials: Physics and Engineering Explorations", Wiley 2006

[5] G. V. Eleftheriades, K.G. Balman, (ed.), "Negative Refraction Metamaterials: Fundamental Principles and Applications", Wiley 2005

[6] C. Caloz, T. Itoh, "Electromagnetic Metamaterials: Transmission Line Theory and Microwave Applications", Wiley 2006

[7] S. Hrabar, "Application of Wire Media in Antenna Technology", *Metamaterials and Plasmonics, Fundamentals, Modeling, Applications*, (ed. S. Souhdi, A. Sihvola, A.P. Vinogradov), *NATO Science for peace and security*, Springer, 2009

[8] D. Smith, J. Willie, et. al., "A Composite Medium with Simultaneously Negative Permeability and Permittivity", *Physical Rev. Lett.*, Vol. 84, No. 18, pp. 4184-4187, May 2000

[9] S. Hrabar, J. Bartolic, et. al., "Experimental Investigation of Subwavelength Resonator based on Backward-wave Meta-material", *Proc. on. IEEE Antenna and Propagation & URSI Symposium 2004*, pp. 2568-2571, Monterey, 2004

[10] S. Hrabar, J. Bartolic, et. al., "Waveguide Miniaturization Using Uniaxial Negative Permeability Metamaterial", *IEEE Tran. on Antennas and Propagation*, Vol. 53, No. 1, pp. 110-119, January 2005

[11] S. Hrabar, J. Bartolic, Z. Sipus, "Reply to Comments on `Waveguide Miniaturization Using Uniaxial Negative Permeability Metamaterial'", *IEEE Tran. on Antennas and Propagation*, Vol. 55, pp. 1017-1018, May 2007

[12] S. Hrabar, D. Zaluski, "Subwavelength Guiding of Electromagnetic Energy in Waveguide Filled with Anisotropic Mu-Negative Metamaterial", *Electromagnetics*, Vol. 28, No. 7. pp. 494-512, October 2008

[13] J. B. Pendry, "Negative Refraction Makes a Perfect Lens", *Physics Review Letters,* Vol. 85, pp. 3966-1 - 3966-4, 2000

[14] A. Grbic, J. Eleftheriades, "Overcoming the Diffraction Limit with a Planar left-Handed Transmission-line lens", *Physical Review Letters*, Vol. 92, No.11, pp.117403-1 – 117403-4, November 2004

[15] A. Alu, N. Engheta, "Achieving Transparency with Metamaterial and Plasmonic Coatings", *Physical Review E*, Vol. 72, No. 1, pp. 16623-1 - 16623-3, July 2005

[16] D. Schurig, J. Mock, et. al., **"**Metamaterial Electromagnetic Cloak at Microwave Frequencies", *Science*, pp. 977 -980, November 2006

[17] B. Ivsic, Z. Sipus, et. al., "Analysis of Uniaxial Multilayer Cylinders Used for Invisible Cloak Realization", *IEEE Tran. on Antennas and Prop.*, Vol. 57, No. 5, pp. 1521-1527, April 2009

[18] M. J. Freire, R. Marques, L. Jelinek, "Experimental demonstration of a $\mu = -1$ metamaterial lens for magnetic resonance imaging", *Applied Physics Letters*, Vol. 93, pp. 231108-1 - 231108-3, December 2008

[19] D.M. Pozar, "Microwave Engineering", Willey, 1998
[20] S. Hrabar, "First Ten Years of Active Metamaterial Structures with 'Negative' Elements", accepted to *EPJ Applied Metamaterials Journal,* 2018
[21] H.-T. Chen, A. J. Taylor, N. Yu, "A review of metasurfaces: physics and applications", *Reports on progress in physics*, Vol. 79, No. 7, pp. 1-40, 2016
[22] J. Vehmas, S. Hrabar, S. Tretyakov, "Transmission lines emulating moving media", *N. J. Phys.,* Vol. 16, 093065, pp. 1-20, 2014
[23] D. Zaluski, S. Hrabar, D. Muha, "Practical realization of DB metasurface", *Appl. Phys. Lett.*, Vol. 104, No. 23, 234106-1~234106-5, 2014
[24] Q. Tang, "Active Metamaterial: Gain and Stability, and Microfluidic Chip for THz Cell Spectroscopy", PhD thesis, The University of Arizona, 2017,
[25] J. L. Merrill, "Theory of the negative impedance converter", *Bell System Technical Journal*, Vol. 30, No. 1, pp. 88–109, 1951
[26] J. G. Linvill, "Transistor negative impedance converters", *Proc. IRE*, Vol. 41, pp. 725-729, June 1953
[27] L. Verman, "Negative circuit constants", *Radio Eng. Proc. Inst.*, Vol. 19, No. 4, pp. 676–681, 1931
[28] B. van der Pol, "A new transformation in alternating-current theory with an application to the theory of audition", *Radio Eng. Proc. Inst.*, Vol. 18, No. 2, pp. 220-230, 1930
[29] A. K. Perry, "Broadband antenna systems realized from active circuit conjugate impedance matching", AD-769 800, Naval Postgraduate School, Monterey, September 1973
[30] F. Auzanneau, R. W. Ziolkowski, "Theoretical study of synthetic bianisotropic materials", *J. Electromag. Waves,* Vol. 12, No. 3, pp. 353-370, 1998
[31] R. W. Ziolkowski, "The design of Maxwellian absorbers for numerical boundary conditions and for practical applications using engineered artificial materials", *IEEE Trans. on Antennas and Propagation,* Vol. 45, No. 4, pp. 656-671, 1997
[32] S. A. Tretyakov, T. G. Kharina, "The perfectly matched layer as a synthetic material with active inclusions", *Electromagnetics*, Vol. 20, No. 2, pp. 155-166, 2000
[33] F. Auzanneau, R. W. Ziolkowski, "Artificial composite materials consisting of nonlinearly loaded electrically small antennas: Operational-amplifier-based circuits with applications to smart skins", *IEEE Tran. on Antennas and Propagation,* Vol. 47, No. 8, pp. 1330-1339, 1999
[34] S. Tretyakov, "Meta-Materials with Wideband Negative Permittivity And Permeability", *Microwave Opt. Technol. Lett.*, Vol. 31, No. 3, pp. 163-165, 2001
[35] S. Hrabar, I. Krois, B. Ivsic, D. Zaluski, G. Pavlaković, "Active Dispersionless 'Plasmonic' Metamaterial - a Step Towards Broadband Cloaking", *Proc. of the 2008 IEEE AP-S International Symposium and USNC/URSI National Radio Science Meeting*, pp. 203-20, San Diego, 2008
[36] S. Hrabar, "Active non-Foster Metamaterials: From Intriguing Background Physics to Real-world Applications", A plenary talk*, Proc. on Metamaterials Congress*, pp. 601-603, Sankt Petersburg, 2012
[37] S. Hrabar, "Active radiofrequency metamaterial structures — Pros, cons and future trends", *Proc. on Metamaterials Congress,* pp. 418, Oxford, 2015
[38] S. Hrabar, "Active Dispersionless Metamaterials - a Path towards Broadband Cloaking", *Proc. on 2009 REME Workshop*, pp. 108, Madrid, 2009
[39] S. Hrabar, I. Krois, A. Kiricenko, "Towards Active Dispersionless ENZ Metamaterial for Cloaking Applications", *Metamaterials*, Vol. 4, No. 2-3, pp. 89-97, August-September 2010
[40] B. Okorn, S. Hrabar, I. Krois, "Investigation of basic physics of non-Foster negative capacitance in time domain", *Proc. on ELMAR*, pp. 373, Zadar, 2011
[41] B. Okorn, S. Hrabar, I. Krois, "Physically sound model of a non-Foster negative capacitor",

Automatika: Journal for Control, Measurement, Electronics, Computing and Communications, Vol. 55, No. 2, pp. 244-252, 2017

[42] S. Hrabar, I. Krois, I. Bonic, A. Kiricenko, "Negative Capacitor Paves the way to Ultra-broadband Metamaterials", *Appl. Phys. Lett.*, Vol. 99, No. 25, 25403~25403-4, 2011

[43] S. Hrabar, I. Krois, I. Bonic, A. Kiricenko, "Ultra-broadband simultaneous superluminal phase and group velocities in non-Foster epsilon-near-zero metamaterial", *Appl. Phys. Lett.*, Vol. 102, No. 5, 05408-1~05408-5, 2013

[44] P. Y. Chen, C. Argyropoulos, A. Alù, "Broadening the cloaking bandwidth with non-Foster metasurfaces", *Phys. Rev. Lett.*, Vol. 111, 23-6, 233001-1~233001-5, 2013

[45] J. C. Soric, A. Alù, "Wideband tunable and non-Foster mantle cloaks", *presented at USNC-URSI Nat Radio Sci Meeting*, Boulder, CO, USA, January 8–12, 2014

[46] S. Hrabar, Z. Sipus, I. Malcic, "Broadening of cloaking bandwidth by passive and active techniques", *A chapter in 'Transformation Electromagnetics and Metamaterials'*, D. Werner, D. Kwon (editors), Springer, London, 2013

[47] J. Long, M. Jacob, D. Sievenpiper, "Broadband fast-wave propagation in a non-Foster circuit loaded waveguide", *IEEE Trans. Microw. Theory Techn.*, Vol. 62, No. 4, pp. 789-798, 2014

[48] A. Niang, A. de Lustrac, S. N. Burokur, "Superluminal wave propagation in a non-Foster negative capacitor loaded transmission line", *Electronic Letters*, Vol. 53, No. 8, pp. 547-549, 2017

[49] J. Long, "Non-Foster Circuit Loaded Periodic Structures for Broadband Fast and Slow Wave Propagation", PhD Thesis, University of California, San Diego, 2015

[50] S. Hrabar, I. Krois, I. Bonic, A. Kiricenko, "Non-Foster elements - new path towards broadband ENZ and MNZ metamaterials", *Proc. on EUCAP*, pp. 2674, Prague, 2011

[51] S. Hrabar, I. Krois, I. Bonic, A. Kiricenko, D. Muha, "Active Reconfigurable Metamaterial Unit Cell Based on Non-Foster Elements", *Final Report for Contract FA8655-12-1-2081, EOARD /AFRL*, October 2013

[52] O. O. Tade, "Negative impedance converter for antenna matching", PhD thesis, University of Birmingham, 2014

[53] C. R. White, J. W. May, J. S. Colburn, "A variable negative-inductance integrated circuit at UHF frequencies", *IEEE Microw. Wireless Compon. Lett.*, Vol. 22, No. 1, pp. 35-37, 2012

[54] S. Saadat, H. Aghasi, E. Afshari, H. Mosallaei, "Low-power negative inductance integrated circuits for GHz applications", *IEEE Microw. Wireless Compon. Lett.*, Vol. 25, No. 2, pp. 118-120, 2015

[55] S. E. Sussman-Fort, "Gyrator-Based Biquad Filters and Negative Impedance Converters for Microwaves", *International Journal RF and Microwave CAE*, Vol. 8, No. 2, pp. 86-101, 1998

[56] S. Kolev, B. Delacressonniere, J. Gautier, "Using a Negative Capacitance to Increase the Tuning Range of a Varactor Diode in MMIC Technology", *IEEE Tran. on Microw. Theory and Tech.*, Vol. 49, No. 12, pp. 2425-2430, 2001

[57] D. S. Nagarkoti, Y. Hao, D. P. Steenson, L. Li, E. H. Linfield, K. Z. Rajab, "Design of broadband non-Foster circuits based on resonant tunneling diodes", *IEEE Ant. Wirel. Propag. Lett.*, Vol. 15, pp. 1398-1401, 2015

[58] G. Skahill, R. M. Ruish, et. al., "Electrically Small, Efficient, Wide-Band, Low-Noise Antenna Elements", *Proc. on the 1998 Antenna Applications Symposium* (in AFRL-SN-RS-TR-1999-86 Final Technical Report), UMAS 1998, pp. 214- 213

[59] J. Aberle, R. Lomak, "Antennas with non-Foster Matching Networks", Morgan & Claypool, 2007

[60] S. E. Sussman-Fort, "Matching Network Design Using Non-Foster Impedances", Presentation slides

[61] S. E. Sussman-Fort, "Non-Foster Impedance Matching of Electrically-Small Antennas", *IEEE Trans. Antennas and Propagation*, Vol. 57, No. 8, pp. 2230-2241, August 2009
[62] S. E. Sussman-Fort, "Matching Network Design Using Non-Foster Impedances", *International Journal RF and Microwave CAE,* Vol. 16, No. 2, pp. 135-142, March 2006
[63] N. Zhu, R. W. Ziolkowski, "Broad-bandwidth electrically small antenna augmented with an internal non-Foster element", *IEEE Ant. Wirel. Propag. Lett.,* Vol. 11, pp. 1116-1120, 2012
[64] N. Zhu, R. W. Ziolkowski, "Broad bandwidth, electrically small, non-Foster element-augmented antenna designs, analyses, and measurements", *IEICE Tran. on Comm.*, Vol. 96, No. 10, pp. 2399-2409, 2013
[65] F. Albarracín-Vargas, V. Gonzalez-Posadas, F. Javier Herraíz-Martinez, D. Segovia-Vargas, "Design Method for Actively Matched Antennas with Non-Foster Elements", *IEEE Tran. Ant. Prop.*, Vol. 64, No. 9, pp. 4118-4123, 2016
[66] H. Mirzaei, G. V. Eleftheriades, "A resonant printed monopole antenna with an embedded non-Foster matching network", *IEEE Trans. on Ant. and Prop.,* Vol. 61, No. 11, pp. 5363-5371, 2013
[67] J. Long, D. Sievenpiper, "Low-profile and low-dispersion artificial impedance surface in the UHF band based on non-foster circuit loading", *IEEE Trans. Ant. and Propag.*, Vol. 64, No. 7, pp. 3003-3010, 2016
[68] J. Mou, Z. Shen, "Design and experimental demonstration of non-Foster active absorber", *IEEE Trans. Ant. and Propag.*, Vol. 65, No. 2, pp. 696-704, 2017
[69] J. Mou, Z. Shen, "Broadband and thin magnetic absorber with non-Foster metasurface for admittance matching", *Scientific Reports*, Vol. 7, pp. 1-9, 2017
[70] M. Barbuto, A. Monti, F. Bilotti, A. Toscano, "Design of a non- Foster actively loaded SRR and application in metamaterial inspire components", *IEEE Trans. Ant. and Propag.*, Vol. 61, No. 3, pp. 1219-1227, 2013
[71] D. F. Sievenpiper, "Superluminal Waveguides Based on Non-Foster Circuits for Broadband Leaky-Wave Antennas", *IEEE Ant. and Wirel. Prop. Lett.,*Vol. 10, pp. 231-234, 2011
[72] D. Muha, S. Hrabar, I. Krois, I. Bonic, A. Kiricenko, D. Zaluski, "Design of UHF Microstrip Non-Foster Leaky-wave Antenna", *Proc. on ICECOM* (Dubrovnik, 2013), pp. 134.
[73] S. Hrabar, "Leaky-wave Antenna based on Non-Foster Metamaterial - Is Stable Operation Feasible?", *Proc. on IWAT* (Seoul, 2015), pp. 7
[74] H. Mirzaei, G. V. Eleftheriades, "Realizing non-foster reactive elements using negative-group-delay networks", *IEEE Trans. Microw. Theory Techn.*, Vol. 61, No. 12, pp. 4322-4332, 2013
[75] H. Mirzaei, "Negative-group-delay and non-Foster electromagnetic structures", PhD dissertation, Dept. Elect. Comput. Eng., Toronto Univ., Toronto, ON, Canada, 2015
[76] H. Mirzaei, G. V. Eleftheriades, "Arbitrary-angle squint-free beamforming in series-fed antenna arrays using non-Foster elements synthesized by negative-group-delay networks", *IEEE Trans. Ant. and Propag.*, Vol. 63, No. 5, pp. 1997-2010, 2015
[77] S. Hrabar, **"**Is Stable Dispersionless non-Foster DNG Metamaterial Indeed Impossible?"**,** *Proc. on Metamaterial Congress* (Copenhagen, 2014), pp. 13.
[78] S. Hrabar, "Metamaterial Structures based on 'Negative' Elements - What Do We Know After a Decade of Research?", *Proc. on Metamaterial Congress* (Rome, 2017), pp. 197
[79] Y. Fan, "Research and Design of Non-Foster Active Metamaterials", PhD Thesis, Queen Mary University, United Kingdom, 2013
[80] S. Saadat, M. Adnan, H. Mosallaei, E. Afshari, "Composite metamaterial and metasurface integrated with non-Foster active circuit elements: A bandwidth-enhancement investigation", *IEEE Trans. Ant. and Propag.*, Vol. 61, No. 3, pp. 1210-1218, 2013
[81] S. D. Stearns, "Stable Band-pass Non-Foster Circuits", *Proc. on IEEE APS/URSI*

(Vancouver, 2015), pp. 1386
[82] S. Hrabar, A. Kiricenko, "Towards broadband tunable non-Foster radiating systems", *Proc. on Metamaterial Congress* (Crete, 2016), pp. 133
[83] S. Hrabar, A. Kiricenko, I. Krois, "Antenna-transmitter based on Non-Foster Source", *Proc. on IEEE APS/URSI* (San Diego, 2017), pp. 875
[84] J. Loncar, S. Hrabar, A. Kiricenko, "Stability of Metasurface-Based Parity-Time Symmetric Systems", *Proc. on Metamaterial Congress* (Crete, 2016), pp. 738
[85] Y. Ràdi, D. L. Sounas, A. Alù, S. A. Tretyakov, "Parity-Time Symmetric Teleportation", *Phy. Rev. B*, Vol. 93, 235427-235434, 2016
[86] E. Ugarte-Muñoz, S. Hrabar, D, Segovia-Vargas, A. Kiricenko, "Stability of Non-Foster Reactive Elements for use in Active Metamaterials and Antennas", *IEEE Tran. on AP-S*, Vol. 60, No. 7, pp. 3490-3494, 2012
[87] S. D. Stearns, "Counterintuitive Aspects of Non-Foster Networks", Presentation slides, *Adelphi Antenna Workshop on Electrically Small Antennas*, Clarksville, MD, July 8-9, 2010
[88] S. D. Stearns, "Non-Foster Circuits and Stability Theory", *Proc. on IEEE APS/URSI* (Spokane, 2011), pp. 1942-1945
[89] S. D. Stearns, "Incorrect Stability Criteria for Non-Foster Circuits", *Proc. on IEEE APS/URSI* (Chicago, 2012), pp. 1
[90] S. Tretyakov, S. Maslovski, Veselago Materials: "What is Possible and Impossible about the Dispersion of the Constitutive Parameters", *IEEE Ant. and Prop. Mag.*, Vol. 49, No. 1, pp. 37-43, 2007
[91] Q. Tang, H. Xin, **"**Stability Analysis of Non-Foster Circuit Using Normalized Determinant Function", *IEEE Tran. Microw. Theory and Techn.*, Vol. 65, No. 9, pp. 3269-3277, 2017
[92] S. R. Rengarajan, C. R. White, "Stability analysis of superluminal waveguides periodically loaded with non-Foster circuits", *IEEE Anten. and Wireless Prop. Lett.*, Vol. 12, pp. 1303-1306, 2013
[93] J. Loncar, S. Hrabar, D. Muha, "Stability of simple lumped-distributed networks with negative capacitors", *IEEE Tran. on Ant. and Prop.*, Vol. 65, No. 1, pp. 390-395, 2017
[94] K. Z. Rajab, Y. Hao, D. Bao, C. G. Parini, C. Vazquez, J. Philippakis, M. Philippakis, "Stability of active magnetoinductive metamaterials", *J. Appl. Phys.*, Vol. 108, No. 5, 054904-1~054904-6, 2010
[95] G. Eleftheriades, "Analysis of bandwidth and loss in negative-refractive-index transmission-line (NRI–TL) media using coupled resonators", *IEEE Microw. Wireless Compon. Lett.*, Vol. 17, No. 6, pp. 412-414, 2007
[96] D. Gregoire, C. White, J. Colburn, "Wideband Artificial Magnetic Conductors Loaded With Non-Foster Negative Inductors", *IEEE Ant. and Wirel. Prop. Lett.*, Vol. 10, pp. 1586-1589, 2011
[97] D. J. Gregoire, C. R. White, J. S. Colburn, "A coaxial TEM cell for direct measurement of UHF artificial magnetic conductors", *IEEE Ant. and Prop. Mag.*, Vol. 54, No. 2, pp. 251-259, 2012
[98] J. Vehmas, S. Hrabar, S. Tretyakov, "Omega transmission lines with applications to effective medium models of metamaterials", *J. of App. Phys*, Vol. 115, No. 13, 134905-1~934905-1, 2014
[99] J. D. Brownlie, "On the Stability Properties of a Negative Impedance Converter", *IEEE Trans. CT-13*, pp. 98-99, March 1966
[100] R. F. Hoskin, "Stability on Negative Impedance Converters", *Elec. Lett. 2*, *3U1*, September 1966
[101] A. F. Schwarz, "On the Stability Properties of a Negative-Immittance Converter", *IEEE Trans. CT-1*, 77, March 1967
[102] C. K. Kuo, "Realization of negative-immittance converters and negative resistances with

controlled sources", PhD Thesis, Georgia Institute of Technology, December 1967
[103] A. F. Schwarz, *Tijd8chr. ned. Elektronica Radio Genoot.,* Vol. 32, No. 45, 1967, Doctoral dissertation, Delft University of Technology, 1969
[104] S. D. Stearns, "Circuit Analysis of the Stability of a Two-Element Non-Foster Impedance Matching Network", *Proc. on IEEE APS/URSI* (San Diego, 2017), pp. 1
[105] S. Keum-Su, R. G. Rojas, "Electrically small wire monopole antenna with Non-Foster impedance element", *Proceedings of the Fourth European Conference on Antennas and Propagation (EuCAP),* pp. 1-4, 12-16, April 2010
[106] Z. Ning, R. W. Ziolkowsky, "Design and measurements of an electrically small, broad bandwidth, non-Foster circuit-augmented protractor antenna", *Appl. Phys. Lett*. Vol. 101, No. 2, 024107, 2012
[107] L. Batel, L. Rudant, J. F. Pintos, A. Clemente, C. Delaveaud, K. Mahdjoubi, "High directive compact antenna with Non-Foster elements", *International Workshop on Antenna Technology (iWAT)*, Seoul, Republic of Korea, 4-6 March 2015
[108] A. Ghadiri, K. Moez, Ghadiri, "Gain-Enhanced Distributed Amplifier Using Negative Capacitance", *Circuits and Systems I: Regular Papers, IEEE Transactions on,* pp. 2834–2843, Vol. 57, Issue: 11, November 2010
[109] G. Metzger, J. P. Vabre, "Transmission Lines with Pulse Excitation", Academic, New York, 1969
[110] J. Loncar, D. Muha, S. Hrabar, "lnfluence of Transmission Line on Stability of Networks Containing ldeal Negative Capacitors", *Proceedings on Antenna and Propagation Society International Symposium (IEEE APSURSI)*, Vancouver, July 2015
[111] T. P. Weldon, K. Miehle, R. S. Adams, K. Daneshvar, "A wideband microwave double-negative metamaterial with non-Foster loading", *Proceedings of IEEE SoutheastCon*, pp. 1-5, 15-18 March 2012
[112] www.ti.com
[113] M. W. Yung, D. A Hitko, "Non-Foster Impedance Power Amplifier", US patent 8,374,561 B1
[114] Y. Kwisung, M. Mohammed, et. al., "Negative impedance circuit and its application to inductorless resonant oscillators", *Pro. Int SOC Conference in Seoul,* pp. 13-16, 2007
[115] M. M. Jacob, L. Jiang, D. F. Sievenpiper, "Nonlinear effects of non-Foster matching networks", *Proc. of the 2015 IEEE AP-S USNC/URSI,* pp. 1248–1249, 2015
[116] M. M. Jacob, D. F. Sievenpiper, "Non-Foster matched antennas for high-power Applications", *IEEE Tran, on Antennas and Propagation*, Vol. 65, pp. 4461-4469, 2017
[117] H. Khoshniyat, A. Abdipour, G. Moradi, "Nonlinear modeling, time-domain analysis and simulation of non-Foster elements", *International Journal of Microwave and Wireless Technologies*, Vol. 9, No. 4, pp. 1-9, September 2016
[118] http://www.ti.com/lit/ds/symlink/ths4304.pdf
[119] K. Chang, et. al., "Active integrated antennas", *Trans. Microwave Theory Tech.*, Vol. 50, pp. 937-944, March 2002
[120] W. L. Stutzman, G. A. Thiele, "Antenna Theory and Design", Willey, 2012
[121] B. Razavi, "A Study of Injection Locking and Pulling in Oscillators", *IEEE Journal of Solid-State Circuits*, Vol. 39, No. 9, September 2004
[122] Z. G. Liu, "Fabry-Perot resonator antenna", *Journal of Infrared, Millimeter, and Terahertz Waves*, Vol. 31, No. 4, pp. 391-403, 2010
[123] T. Debogovic, J. Perruisseau-Carrier, J. Bartolic, "Partially reflective surface antenna with dynamic beamwidth control", *IEEE Antennas and Wireless Propagation Letters*, Vol. *9*, pp. 1157-1160, 2010
[124] T. Debogović, S. Hrabar, J. Perruisseau-Carrier, "Broadband Fabry-Pérot radiation based on non-Foster cavity boundary", *Electronics letters*, Vol. 49, No. 4, pp. 239-240, 2013

[125] S. Hrabar, T. Debogovic, "Broadband Fabry-Pérot antenna with non-Foster metasurface - how to test the basic idea?", *Antennas and Propagation & USNC/URSI National Radio Science Meeting, 2015 IEEE International Symposium,* pp. 798-799, July 2015

[126] Y. Qian, D. Sievenpiper, V. Radisic, E. Yablonovitch, T. Itoh, "A novel approach for gain and bandwidth enhancement of patch antennas", *Radio and Wireless Conference, RAWCON 98. 1998 IEEE,* pp. 221-224, August 1998

[127] Z. Liu, W. Zhang, D. Fu, Y. Gu, Z. Ge, "Broadband Fabry- Perot resonator printed antennas using FSS superstrate with dissimilar size", *Microwave and Optical Technology Letters*, Vol. 50, No. 6, pp. 1623-1627, 2008

[128] www.hrl.com